WIND – HYDROGEN ENERGY SYSTEMS FOR REMOTE AREA POWER SUPPLY

Thesis submission in accordance with the regulations of the degree of Doctor of Philosophy

AKRAPHON JANON

School of Aerospace, Mechanical and Manufacturing Engineering
RMIT University
Melbourne, Australia

January 2009

ACKNOWLEDGEMENTS

Through out the period of this research I have received support from many people. This supports has come in various forms and without it this project would not have been possible. Firstly, I would like to give thanks to my mum and dad: Bhirom and Abhon Janon, who have lent support to me from my first school class up until now. Their love, encouragement and mental support are the most vital ration that has come in a constant supply. Yet they have always given me enough independence for me to feel confident and strong on my own. In addition, I must thank Hyo Jin Kim who has been a constant source of power, inspiration and most of all comfort throughout these years.

Secondly, I would like to thank to the Royal Thai Government for this opportunity to study abroad and for almost ten years of financial support during my bachelor and PhD degree programs, I am completing a PhD degree that otherwise would not be possible. Even though my allocated fund was initially only for five years, I have been allowed to continue on to further my studies well beyond this period. For this student who came from a farming background and could only dream of such opportunity, I feel grateful.

I also would like to give praise to Dr John Andrews, who has supervised me on this project. His directions and advice are invaluable, and have enabled me to carry out this project successfully. Moreover, I must give special thanks to Dr Andrea Bunting, my second supervisor and a friend, for my first renewable energy class at RMIT University, which inspired me to pursue this field.

I like to thank RMIT workshop staff for technical help and tools. They are Don Savvides, David Goodie, Gil Atkin, Patrick Wilkins, Peter Tkatchyk and Sebastiano Naselli and also Ashley who give free advices on electrical work. For an engineer who still has things to learn about engineering drawing and techniques, I have certainly been impressed by your help. I was even trusted to borrow some expensive tools and was given a special permission to use some of your non-student tools. In addition, I could not go by without saying thanks to RMIT Bundoora East administrative staff for helping with documents and I have been very impressed by the level of service, which goes beyond that provided on other campuses. They are Lina Bubic, Marjory Leitch, Emilija Simic and Sandy.

Lastly, I would like to thank friends at RMIT post grad for all the sporting games and making the time there enjoyable. They are Weng-Yew Chan, Lok-Tin Choi, Krishna Mohanarangam, Kiao Inthavong, Huafeng Li, Dr. Zhaofeng Tian, Dr. Sherman Chi-Pok Cheung, Dr. Edsil Dilla, Thau Do, Yoshiki Sato and Wentian and Simin Wang.

DECLARATION

I, Akraphon Janon, hereby submit the thesis entitled "Wind – Hydrogen Energy System For Remote Area Power Supply" for the degree of Doctor of Philosophy by Research and certify that except where due acknowledgement has been made, the work is that of the author alone; the work has not been submitted previously, in whole or in part, for any other academic award and that the content of the thesis is the result of work that has been carried out since the official commencement of the program.

Akraphon Janon
12th January 2009

TABLE OF CONTENTS

LIST OF ABBREVIATIONS

P_{wind}	power available in the wind (W)
ρ	air density (kg/m^3)
A	aerogenerator's turbine swept area (m^2)
v	wind speed (m/s)
P_{aero}	power captured by aerogenerator (W/m^2)
P_{gen}	electrical power output by aerogenerator (W)
P_{load}	power used by load (W)
h_{theory}	single-cell theoretical hydrogen production rate (kg/s)
i^{cell}	current input of a single cell (A=C/s)
F	Faraday constant, 96 485 C
η_f	Faraday efficiency
h_{actual}	single-cell actual hydrogen production rate (kg/s)
$E_{hydrogen}$	energy stored in the form of hydrogen gas (J)
$E_{electric}$	electrical energy input (J)
η	overall energy efficiency
n	number of moles of hydrogen gas produced
V^{cell}	single cell voltage (V)
HHV	High heating value (hydrogen is 285840 J/mol)
N	number of cells connected in series in an electrolyser branch
M	number of branches connected in parallel in an electrolyser stack
H_{actual}	stack actual hydrogen production rate (kg/s)
I	total current drawn by the electrolyser bank (A)
m^{cell}	slope of a straight-line approximation of an electrolyser single-cell characteristic curve
$V^{cell}_{cut\text{-}in}$	Cut-in voltage of a straight-line approximation of an electrolyser single-cell characteristic curve
V^{cell}_{max}	maximum allowable cell voltage of electrolyser single-cell
i^{cell}_{max}	maximum allowable cell current of electrolyser single-cell
p_{in}	power input of an individual electrolyser cell
W	work done (J)
Δh_f	enthalpy of formation of the products in chemical reaction (kJ/mol)
Δg_f	Gibbs free energy (kJ/mol)

$H_{consumption}$	hydrogen consumption rate for fuel cell stack (kg/s)
μ_f	hydrogen fuel utilisation coefficient
$\eta_{fuelcell}$	fuel cell energy efficiency
P	pressure (Pa)
T	temperature
h_1	height 1
h_2	height 2
v_1	wind speed at h_1
v_2	wind speed at h_2
α	ground surface friction coefficient
$P_{transloss}$	power transfer loss (W)
P_{MPP}	power production at the maximum power point (W)
P_A	power production at an point A (W)
η_{trans}	power transfer efficiency
MPP	maximum power point
MPC	maximum power curve
v_i	mean wind speed in wind speed range i (m/s).
$P_{MPP}(v_i)$	maximum power from maximum power point at i wind speed range (W)
$P_{elec}(v_i)$	power transfer at i wind speed range (W)
$P_{transloss}(v_i)$	power transfer loss at i wind speed range (W)
$E_{transloss}$	accumulated energy transfer loss over a year (J)
E_{trans}	accumulated energy transfer over a year (J)
N	total number of ranges of wind speeds
t	time interval (s)
f_i	frequency of wind speed readings within wind speed range i
$P_{theoretical}$	theoretically estimated power (W)
$P_{corrected}$	theoretical estimated power transfer after application of correction factor
$E_{corrected}$	theoretical estimated energy transfer after application of correction factor
T_{net}	net torque (Nm)
J	moment of inertia (kg m^2)
θ	angular displacement (rad)
ω	angular velocity (rad/s)

T_{aero}	aerodynamic torque generated (Nm)
T_{mec}	mechanical torque (Nm)
C_p	power coefficient
λ	tip speed ratio
R	aerogenerator radius (m)
v	wind speed (m/s)
ρ	air density (kg/m^3)
β	pitch angle of the rotor blades
C_q	torque coefficient
$P_{in}(generator)$	generator power input (W)
$P_{out}(generator)$	generator power output (W)
η_{gen}	generator efficiency
W	number of turns of copper per coil in the winding
B	average flux density (Tesla)
u	peripheral speed in m/s
l	stack length (m)
N	number of stator slots
m_g	generator RPM and voltage output linear relationship graph slope
C_g	generator constant value where its RPM and voltage output linear relationship cuts the y-axis at
V_a	phase-to-neutral voltage output of a generator phase a (V)
V_b	phase-to-neutral voltage output of a generator phase b (V)
V_c	phase-to-neutral voltage output of a generator phase c (V)
V_o	DC voltage
I_o	DC current
V_{ac}	RMS value of the voltages V_a, V_b and V_c
P_{dc}	DC power
η_{rec}	rectifier energy efficiency
P_{actual}	actual power output (W)
$P_{in}(rectifier)$	power input of rectifier (W)
$P_{out}(rectifier)$	power output of rectifier (W)
m_r	rectifier voltage input and voltage output linear relationship graph slope
C_r	rectifier constant value where its voltage input and voltage output linear relationship cuts the y-axis at

m_e	slope of the electrolyser stack V-I characteristic
C_e	intercept of the electrolyser stack V-I characteristic on the y-axis
$P_{in}(electrolyser)$	power input of electrolyser (W)
Δt	intervals of time
J_{blade}	moment of inertia of a blade of an aerogenerator (kg m^2)
J_{hub}	moment of inertia of aerogenerator hub (kg m^2)
J_{rotor}	moment of inertia of aerogenerator rotor (kg m^2)
M_{hub}	aerogenerator hub mass
R_{disk}	aerogenerator disk radius
R_{shaft}	aerogenerator shaft radius
ρ_s	Stainless steel density
V_{shaft}	volume of aerogenerator shaft (m^3)
V_{disk}	volume of aerogenerator rotor disk (m^3)

LIST OF FIGURES

LIST OF TABLES

EXECUTIVE SUMMARY

This project has investigated wind – hydrogen energy systems for remote area power supply (RAPS) applications. The particular focus of the study has been theoretical and experimental work to assess the potential for direct coupling of the aerogenerator and PEM electrolyser in a wind- hydrogen energy system to reduce overall unit costs of the electricity produced.

The threats of global warming due to greenhouse gas emissions from utilisation of fossil fuels, and concerns about the availability and price of conventional fuels, have increased the need for developing sustainable energy sources based on renewable energy and low or zero emission energy conversion technologies. Renewable energy sources in general are intermittent and variable by nature. Hence there is a need for a medium to store surplus renewable energy at times of high supply, for reuse later at times of lower or zero supply. Hydrogen is a prime contender for this role as an energy storage and carrier for renewable energy.

In a stand-alone wind – hydrogen energy system for RAPS, an aerogenerator is used to produce electricity that is either fed directly to the load or to an electrolyser to produce hydrogen for storage. From an energy efficiency perspective the best arrangement is for the aerogenerator to meet the final demand directly to the maximum extent possible, with only the electricity produced exceeding user demand being fed into the electrolyser for hydrogen generation. The hydrogen produced is stored for later feeding to fuel cell to produce electricity at times when the demand cannot be met by the wind turbine alone.

The present project concentrates on wind – hydrogen energy systems for RAPS applications such as remote stations or homesteads, remote communities, mining facilities, islands, and telecommunications facilities, which are prime early markets for such systems. Such systems employing proton exchange membrane (PEM) electrolysers and PEM fuel cells are studied theoretically, using computer modeling and experimentally.

A key question addressed is how the hydrogen production efficiency of a PEM electrolyser might be affected by the intermittent, unpredictable and highly fluctuating nature of the electrical input from a wind turbine. Another related question investigated is how an

intermittent electrical input for an aerogenerator might affect the longevity of a PEM electrolyser. Most wind–hydrogen systems to date have employed expensive electronic systems to match the voltage–current characteristics of the aerogenerator to those of the electrolyser over the range of operational wind speeds in order to achieve as high an energy transfer as possible. In the present project, the option of directly coupling the aerogenerator to the electrolyser using a suitable matching technique is studied both theoretically and experimentally.

Specifically the objectives of the project are thus to:

- Develop a computer – based mathematical simulation model of a wind – hydrogen energy system for remote power supply applications.
- Investigate both theoretically and experimentally ways to maximise the power transfer efficiency between a fixed-pitch variable-speed aerogenerator directly coupled to a PEM electrolyser, and hence the overall rate of hydrogen production
- Analyse any degradation in the performance of the electrolyser after extended operation subject to the variable electrical input from an aerogenerator as a result of wind speed fluctuations.
- Evaluate the unit costs of electricity produced by a wind – hydrogen energy system for RAPS, with a conventional electronic coupling unit and under direct coupling of the aerogenerator and electrolyser, and compare these costs against other RAPS options.

The research questions addressed by the investigations are:

1. What are the optimal design parameters of a wind – hydrogen system to meet a given remote area electrical demand in terms of lowest unit cost of energy on a lifecycle basis?
2. What matching procedures can be applied to maximise the power transfer efficiency between a fixed-pitch variable-speed aerogenerator directly coupled to a PEM electrolyser, and hence the overall rate of hydrogen production, without using an electronic converter/impedance matching unit?
3. How are the performance and longevity of the PEM electrolyser affected by the intermittent electrical input from an aerogenerator in the direct-coupled arrangement?

4. How do the unit costs of electricity produced by a wind – hydrogen energy system for RAPS, with a conventional electronic coupling unit and under direct coupling of the aerogenerator and electrolyser, compare with those for other RAPS options?
5. What are the most promising opportunities for cost reduction and improving competitiveness of wind-hydrogen energy systems?

The overall analysis of a wind – hydrogen energy system was conducted at the start of the project to evaluate and study system and component sizing. A specially-designed and constructed Visual Basic program was used to simulate a working wind – hydrogen energy system employing a fixed-pitch variable speed aerogenerator, a PEM electrolyser and PEM fuel cell. The main inputs to the program are hourly wind speed data, the aerogenerator power curve, the electrolyser and fuel cell characteristics, and the hourly load profile to be supplied. The main outputs from the program are a graph of hydrogen in storage throughout the year, and the required sizes of the aerogenerator, electrolyser, hydrogen storage, and fuel cell to enable the load to be met throughout the year, and sustainably from year to year.

The wind – hydrogen simulation model developed has been applied in a case study to meet the daily load of 5.9 kWh of a remote household located at a site in Kilcunda North, on the ocean coast near Melbourne, with an annual mean wind speed of 8.0 m/s. The model outputs suggested that in general the smallest practical storage capacity is found to be around 1 kg of hydrogen. The required aerogenerator size increases steeply as the smallest practical storage capacity is approached. The aerogenerator capacity should be between 3.4 to 4.2 kW and electrolyser should be between 0.7 to 1.5 kW. For a case where hydrogen storage is unconstrained, the aerogenerator capacity is 1.77 kW, electrolyser capacity is 1.42 kW, hydrogen storage capacity is 4.8 kg of hydrogen and fuel cell capacity is 0.35 kW. If hydrogen capacity is constrained at 3 kg of hydrogen, the required aerogenerator capacity is 2.0 kW, electrolyser capacity is 1.65 kW and fuel cell capacity is 0.35 kW.

The general relationships found between the required capacities of the main components of the system are the following:

- A reduction in hydrogen storage capacity increases the required aerogenerator size. This is because, as the hydrogen storage capacity gets smaller, a higher proportion of the annual load must be met directly by the aerogenerator. The system then relies less on the energy stored.

- A reduction in electrolyser capacity also increases aerogenerator size. This is because the hydrogen production is sometimes limited by as a result of setting the electrolyser capacity below the maximum surplus of wind power over the load. The system thus cannot rely so much on energy storage and the aerogenerator capacity has to be increased to meet more of the final load directly. A larger hydrogen storage does not help the situation since the amount of hydrogen produced has been cut back.

On the basis of the assumptions made about component costs and lifetimes, the most economic system has an average unit cost of electricity supplied over 25 years of US$ 0.66 /kWh, and employs a 2.6 kW aerogenerator, a 0.7 kW electrolyser, 1.9 kg of hydrogen storage, and a 0.35 kW fuel cell.

If the aerogenerator and electrolyser are suitably matched so that they can be directly coupled without electronic interconnection equipment, the unit cost of energy produced is reduced to US$ 0.57 /kWh, that is, 14% cut. In this case the optimal system comprises a 3.0 kW aerogenerator, a 0.7 kW electrolyser, and 1.5 kg of hydrogen storage. Hence it can be seen that direct coupling has the potential to reduce the cost of a wind – hydrogen energy system for RAPS applications significantly.

These unit costs are already very competitive with those for stand-alone wind – battery energy systems of the equivalent capacity, where unit energy costs are in the order of US$ 0.7/kWh, and diesel-battery systems, with costs at current diesel prices in the order of US$ 1.9/kWh. It is further reported that the approximate unit cost of energy for PV – hydrogen energy system is US$ 2.5/kWh, which is almost four times higher than that from the wind – hydrogen energy system investigated in this project (power electronics included) at a good wind site. A PV – battery energy system is estimated to produce electricity at a slightly higher cost (US$ 2.8/kWh), whereas a similar system with the addition of a diesel generator set is estimated to yield a unit electricity cost of US$ 2.3/kWh. Furthermore, a diesel-battery would generate electricity at the cost of US$ 1.9/kWh, already much higher than the estimated cost of a wind-hydrogen system even at current diesel prices, which are likely to rise in real terms in coming years.

In direct coupling, the matching of the V-I characteristics of an aerogenerator and PEM electrolyser has been utilised to achieve a high power transfer efficiency between a fixed-

pitch variable-speed aerogenerator directly coupled to a PEM electrolyser. This matching was done by altering the V-I characteristic of a bank of electrolysers so that it matched as closely as possible the maximum power point curve of the aerogenerator over its range of operating wind speeds. The connection configuration that gave the highest overall energy transfer over an annual period when directly coupled to the aerogenerator was then found using the known maximum power point curve of the aerogenerator and the annual frequency distribution of wind speeds at a particular site.

A case study of direct coupling for an AIR403 aerogenerator and PEM electrolyser bank at the Kilcunda North site has been conducted. A theoretical investigation of the annual energy transfer for 12 series-parallel configurations for the electrolyser bank, ranging from 16 to 27 cells in series in each branch, and up to three branches connected in parallel, has been carried out. The configuration found to yield the highest annual energy transfer to the electrolyser at this wind site was that three parallel branches each containing 25 cells in series. In this case, the predicted total energy transfer was 1371 kWh annually, only 3.8% less than the theoretical maximum energy transfer in which maximum power point tracking was assumed to be present at all times. Given that DC – DC voltage converters and maximum power point trackers typically have losses of 5 – 10%, the direct coupling promises at least as high an overall energy transfer, but without the cost of the electronic conversion equipment.

However, the direct coupling experiment conducted at RMIT University over a period of 51 days illustrated that in this particular case the energy transfer loss in direct coupling was substantially greater than that theoretically estimated even after factoring in possible sources error. The theoretically-estimated energy transfer was 4.85 kWh compared to the experimental result of 1.53 kWh. The theoretical estimate, based on a steady state model of aerogenerator performance, thus appeared to overestimate the overall energy transfer by as much as three times. Close inspection of data revealed that on many occasions the aerogenerator did not generate any power while the theoretical prediction suggested that power was being generated. Moreover, the intermittent and variable wind speeds hindered the ability of the aerogenerator to develop its maximum expected RPM at each recorded wind speed, so that much less power was generated than expected on the basis of the steady state response..

This discrepancy between theoretical prediction and experimental result warranted a new theoretical prediction approach, namely a dynamic state analysis. Consequently preliminary steps were taken within the present project to develop a dynamic model of the aerogenerator that takes into account the characteristics of its blades, electrical generator and moment of inertia. The dynamic model estimates the turbine RPM and output voltage according to the instantaneous and series of preceding wind speeds.

The dynamic model has been tested in a preliminary way by applying it to a limited period of 4 days, 23 hours selected from the 51 days of the entire experiment. The overall energy transfer estimated by the dynamic model was within 10% of the experimental value. A great deal of further testing of the model is, however, needed in a range of different cases in order to assess its predictive power and validity more generally.

In addition, the intermittent and variable wind speed creates highly variable current and voltage input to an electrolyser bank directly coupled to an aerogenerator. Measurements were made of V-I curves before and after the direct-coupling experiment to see if the performance of the PEM electrolysers degraded significantly as a result of being subjected to this variable power input.

It was found that four electrolysers in the experimental group did show some signs of performance degradation after being subject to the variable power input during the direct-coupling experiment. By contrast, electrolyser number 1 seemed to improve on performance, while the performance of electrolyser number 9 stayed constant.

Hence there was some indication from these results that the variable power input in itself did adversely affect the performance of some electrolysers. Clearly, however, additional experiments involving a larger number of electrolysers are needed before any firm conclusions can be drawn. The performance degradation needs to be measured at regular intervals over a longer period of usage than was possible in the experiment conducted in this project, both with constant power input and variable power input, to gain a better understanding of the practical lifetime of the electrolysers. A number of different designs of PEM electrolyser also need to be tested under similar conditions to see whether the degree of degradation differs from design to design. Such information is important since

maintenance of the performance of electrolysers over a long lifetime is critical to the viability and market competitiveness of wind – hydrogen energy systems.

From the overall findings and experience gained from this research project, the following recommendations are made:

- Further research and development is conducted into direct coupling of an aerogenerator and electrolyser in which the aerogenerator V-I curve is altered as well as the electrolyser characteristic to see if even better matching can be obtained. The aerogenerator characteristic can be modified by changing the permanent magnet or windings of the generator coils.
- The system and component sizing simulation model developed as part of the research program for this thesis is improved by:
    - The improvement of each submodel. For example, the net energy losses in the hydrogen storage system should be quantified. Options for storing as compressed gas or in metal hydrides of various kinds could be added.
    - Further automating the procedure for finding component sizes under different conditions, and minimum unit cost configurations.
- Further analysis, improvement, and testing against experimental values are conducted to check the predictive power and validity of the dynamic aerogenerator model in more general situations. The characteristic of the generator used (output voltage versus RPM) should be incorporated directly into the model
- Follow-up theoretical and experimental investigations are carried out into modifying the aerogenerator-electrolyser matching technique proposed in the present thesis for use:
    - with a dynamic model of aerogenerator performance rather than a steady state model
    - in the system configuration when only the surplus wind power over load is fed to the electrolyser, rather than all the wind power as examined here.

Further research and development is conducted into ways to maintain the performance and longevity of PEM electrolysers when subject to the intermittent and variable electrical input from a directly-coupled aerogenerator.

1 INTRODUCTION

1.1 GLOBAL WARMING, RENEWABLE ENERGY AND HYDROGEN

The threats of global warming due to greenhouse gas emissions from utilisation of fossil fuels, and concerns about the availability and price of conventional fuels, have increased the need for developing sustainable energy sources based on renewable energy and low or zero emission energy conversion technologies (Khan and Iqbal, 2005). Investment into low- emission technologies has been increasing in many countries, and much greater deployment of renewable energy systems is one of the central solutions to meeting global greenhouse gas emission reduction targets (IPCC, 2007).

Renewable energy sources in general are intermittent and variable by nature. The energy produced by renewable energy can be transmitted directly as electricity to users. But there is a need for a medium to store surplus renewable energy at times of high supply, for reuse later at times of lower or zero supply. Hydrogen is a prime contender for the role as an energy storage and carrier for renewable energy (Hoffmann, 2001). Hydrogen gas can be produced on site from renewable-energy electricity by electrsolysis of water or other process, and then transported or stored for use at times of low availability of the primary resource. The production of hydrogen by water electrolysis process in an electrolyser is very efficient (Larminie and Dicks, 2003). Hydrogen can be produced in large quantities at a large-scale plant associated with a commercial wind farm or solar energy installation (Bernal-Agustin and Dufo-Lopez, 2008, Jorgensen and Ropenus, 2008, Kelly et al., 2008). The hydrogen can be piped to users, or produced and used in a distributed manner in vehicles, homes, and industrial and commercial facilities. Hydrogen can be used in a fuel cell, internal combustion engine, jet engine, or burnt directly to meet all end-use needs in all sectors of the economy, hence the concept of the 'hydrogen economy' (Bockris, 2002). This distributed sustainable hydrogen system eliminates the dependence on centralised infrastructure, which allow for remote households.

Hydrogen could thus be the next energy carrier to replace fossil fuels across the entire economy in the future. Dougherty *et al*. (2008) suggest that there are three barriers slowing or preventing the completion of hydrogen transition:

- Existing infrastructures are geared toward fossil fuels

- Current hydrogen technology is not competitive in round trip energy efficiency and high energy production cost
- Consumers are facing "chicken-and-egg" problem, where the lack of infrastructure preventing consumers from purchasing devices and that lead to manufacturers not investing its infrastructure.

One attribute that may make hydrogen the best possible energy carrier to replace fossil fuels is that it can be made in many ways from a wide range of feed stocks such as water by electrolysis or photolysis, biomass (including from algae), and hydrocarbons (Holladay et al., 2008, Edwards et al., 2008). This diversity of feed stock and the flexibility of hydrogen in meeting end-use needs also enhances national and international energy security (Edwards et al., 2008).

Therefore, a wide range of renewable energy sources using hydrogen storage to provide a continuous supply energy offers one of the best prospects for a truly sustainable energy economy with zero greenhouse gas emissions and high energy security within each nation and internationally. Barbir (2005) argued the case for wider application of hydrogen energy in combination with renewable sources, including its use for storage on main grids to mitigate the intermittent and variable nature of renewable energy.

1.2 ENERGY SYSTEMS FOR REMOTE AREA POWER SUPPLY

1.2.1 Renewable Energy Sources and Energy Storage

Renewable energy in remote areas is economical and self-reliant compare to conventional energy systems due to the difficulties in transporting fuels or the cost of grid infrastructure (Department of the Environment Water Heritage and the Arts, 2008, Isherwood et al., 2000, Young et al., 2007). The locations play an important part in the type of renewable energy used. There could be a micro-hydro, aerogenerator or photovoltaic system or a combination of these. Apart from the electricity producing process, there must be an energy storage system. The most common are battery banks and fossil fuels. A battery bank energy storage could hold energy up to several days for use during a period of low primary energy resources. However, it is neither possible nor viable to store energy from

season to season using batteries, due to the high cost and limited charge holding capability of batteries (Ali and Andrews, 2006).

Other energy storage mediums also used are fossil fuels, for example, a diesel generator unit with diesel fuel tank could store energy as long as required although fuel transportation adds to the total cost. Another mean of energy storage is hydrogen.
Hydrogen could be stored under pressure in cylinders and will not degrade after time, which may enable a renewable energy system to store energy from season to season (Ali and Andrews, 2006).

1.2.2 Hydrogen energy storage in RAPS system

The use of renewable-energy hydrogen systems for Remote Area Power Supply (RAPS) applications offers an early market opportunity for deploying such systems and making the first moves towards a sustainable hydrogen economy more generally. Wind, solar and micro-hydro hydrogen systems have been designed, tested experimentally and to a more limited extent demonstrated in a number of RAPS applications. However, such systems are still in an early stage of development, generally have a high cost, and are not available commercially.

Renewable-energy hydrogen systems generally use surplus renewable energy during periods of abundant supply to produce hydrogen by electrolysis of water, which is then stored in gaseous form. At times when the primary energy source cannot adequately supply the demand, stored hydrogen gas is fed to fuel cells to regenerate electricity (Janon and Andrews, 2006).

Because components in hydrogen energy systems are still very expensive or not commercially available, the earliest market for these systems would be in the sector where the conventional systems and fuels are expensive and there is risk of supply interruptions. RAPS is thus a prime application where renewable-energy hydrogen systems may become competitive in the near future (Janon and Andrews, 2006, Young et al., 2007). In this case, dedicated standalone power systems are utilised to provide power to remote homes or stations. Due to their remote locations, convention energy systems that use fossil fuels must bear the high cost of fuel transportation and also the risks of supply failure. In

addition, the costs of connecting such locations to centralised energy infrastructure are also high, and the task would often be geographically challenging.

Conventional RAPS systems employ a diesel or petrol generator with battery bank energy storage. More recently photovoltaic (PV) and aerogenerator systems with battery storage, and often diesel generator back-up as well, have become increasingly popular. A potential key advantage of hydrogen storage over battery banks is that the hydrogen system will be able to store energy as long as is required with minimal energy losses, in particular from season to season as is frequently required with solar and wind energy.

Projects demonstrating the potential of such energy systems are currently being conducted by Ulleberg *et al*. (2008), Paul and Andrews (2008a) and Magill (2008). Ulleberg *et al*. (2008) show that with current equipment an autonomous wind – hydrogen energy system is possible and can supply energy reliably. Paul and Andrews (2008a) show possible cost cutting opportunities that will help a PV – hydrogen energy systems become competitive among other RAPS energy systems. On the other hand, Magill (2008) points out barriers such as work safety, lack of hydrogen standards, and problems in delivering and operating an unfamiliar and relatively untried energy system in a very remote place. Magill (2008) also exposed the common perception (as opposed to the reality) of hydrogen being more dangerous than other fuels. The experience gained from the project is very valuable and suggests that the technologies must also be supported by policy and educational work.

Young *et al*. (2007) suggests that RAPS is one of the first applications in which hydrogen energy systems could be viable. Their project examined the feasibility of wind, solar and hydro energy hydrogen systems in remote mountains of Bhutan, where grid electricity is not possible and diesel power is very expensive. A good case was made for a demonstration unit utilising hydrogen as energy storage. This point was also supported by Ali and Andrews (2006).

Dutton *et al*. (2000) conducted a preliminary analysis and experiment on the effects of variable wind speeds and electrical input to the electrolyser in a wind – hydrogen energy system. It is generally agreed that battery is not the suitable solution for long-term energy storage require for an autonomous energy system and that hydrogen could be the preferred energy carrier in such applications (Agbossou et al., 2001, Ali and Andrews, 2006).

Agbossou *et al*. (2001) investigated a system for supplying the electrical needs of a communications station based on an aerogenerator complemented by a PV system.

1.2.3 Wind – hydrogen energy systems for RAPS system

Among renewable energy sources, wind electricity in particular has become competitive in many markets around the world (Gipe, 1999). At sites with a relatively high mean wind speed wind power can thus generally offer the most economic renewable energy source within a renewable-energy hydrogen RAPS system.

In a wind – hydrogen system, an aerogenerator is used to produce electricity that is either fed directly to the load or to an electrolyser to split water molecules into hydrogen and oxygen gas. From an energy efficiency perspective the best arrangement is for the aerogenerator to meet the final demand directly to the maximum extent possible, with only the electricity produced exceeding user demand being fed into the electrolyser for hydrogen generation. The hydrogen produced is stored for later electricity production in a fuel cell, by the reverse process to that in the electrolyser, at times when the electricity demand cannot be met by the wind turbine alone. As a result, the hydrogen storage is the equivalent of a bank of batteries storing electric energy. Unlike batteries, hydrogen storage will not degrade over time so that relatively long-term energy storage is possible, and surplus energy during periods or seasons of the year when wind speeds are high can be stored for use much later in the year when wind speeds are low or zero.

The present project thus focusses on wind – hydrogen energy systems for RAPS applications such as remote stations or homesteads, remote communities, mining facilities, islands, and telecommunications facilities. Such systems currently exist in experimental and to a lesser extent demonstration form, and can be constructed using newly available hydrogen technologies. The aerogenerators used in such systems vary in their capacity (between 1 and 25 kW typically) and design, but are mature technologies and are readily available in the market. Examples of manufacturers of commercially available aerogenerators are Southwest Windpower (with models such as AIR 403 and AIR X), Bergey, Westwind and Wind Energy Solution Canada.

Alkaline electrolysers have in the past been the most common type used in wind-hydrogen energy systems. For example, Gammon *et al*. (2006) installed a renewable energy system that used a 36 kW alkaline electrolyser from Stuart Energy Systems producing hydrogen at 25 bar. The hydrogen is then compressed to 137 bar for storage in compressed gas cylinders. The system also includes 2 and 5 kW PEM fuel cells to supply the load using stored hydrogen. There are many other projects where alkaline electrolysers are used to produce hydrogen by electrolysis (Ulleberg et al., 2008, Aprea, 2008, Gazey et al., 2006).

However, solid-state PEM electrolysers are an emerging technology in water electrolysis and provide superior hydrogen gas purity (Barbir, 2005). Barbir (2005) and Magill (2008), for example, employ PEM 'HOGEN' electrolysers made by Proton Energy Systems.

The most developed hydrogen storage technology is compressed hydrogen gas storage, in metal hydrogen or composite cylinders at pressures now up to 350 bar (Aprea, 2008, Magill, 2008, Ulleberg et al., 2008). Liquid hydrogen storage technology is under development and has also been demonstrated in automotive applications by BMW (Hoogers, 2003), although requires a large amount of energy to cool, compress and hence liquefy hydrogen gas produced at ambient temperature. Liquid hydrogen is thus likely to have too low a net energy balance, and be too expensive for RAPS applications A considerable amount of research and development is going into solid-state hydrogen storages such as metal hydrides; here a key challenge is to achieve an acceptable gravimetric energy density, that is, a percentage of hydrogen stored to total system mass that is more than 1 – 2 % (Larminie and Dicks, 2003, Ali, 2007). Metal hydride canisters with weight percent hydrogen of around 1% are already available commercially, and could be suitable for wind-hydrogen systems. In stationary RAPS applications generally relatively low gravimetric and volumetric energy densities for the hydrogen storage are often not of inherent concern, because there are usually solid foundations and plenty of space available (Ali, 2007).

The fuel cell, which is the final component in a wind – hydrogen system, has similar technology to electrolysers, and the most promising type for RAPS applications is the PEM fuel cell, as evidenced by their increasing use in demonstration systems of this kind (Ulleberg et al., 2008, Magill, 2008, Gammon et al., 2006).

Because there is no turn-key wind – hydrogen energy system on the market, such a system must currently be designed and constructed for specific applications, including the required control system.

A key question that the present project will address is how the hydrogen production efficiency of a PEM electrolyser might be affected by the intermittent, unpredictable and highly fluctuating nature of the electrical input from a wind turbine. Unlike large grid-connected aerogenerators, smaller wind turbines used for RAPS do not generally have speed control mechanism to keep the generator speed constant as wind speed fluctuates. Hence, the effects of the transient electrical input to a PEM electrolyser may be greater than for larger-scale aerogenerators. It has been suggested that a fluctuating electrolyser's electrical input profile alters its hydrogen production rate, purity and its operating temperature, and hence its efficiency (Barbir, 2005). But these questions have yet to be examined in detail to obtain quantitative data in the magnitude of the effects, and search for practical ways to avoid a decreasing hydrogen production rate over time.

Another related question the project will investigate is how an intermittent electrical input for an aerogenerator might affect the longevity of a PEM electrolyser. Constant operating of a PEM electrolyser within its optimum performance range is practically difficult in this situation. As a result, deviations from ideal conditions may result in a faster rate of degradation of the electrolyser as well as of other ancillary components. Consequently, the electrolyser might have a shorter life span than anticipated, Currently there is a lack of information on the likely total number of operating hours at acceptable efficiency of PEM electrolysers in wind-hydrogen systems (Khan and Iqbal, 2005). Therefore, an investigation into their longevity is needed since the capital cost of the PEM electrolyser is a major component of the total capital cost of a wind-hydrogen RAPS system, so that the assumed lifetime of the electrolyser will have a significant bearing on the average unit cost of the power produced over the full lifecycle of the system

Most wind – hydrogen systems to date have employed expensive electronic systems to match the voltage–current characteristics of the aerogenerator to those of the electrolyser over the range of operational wind speeds in order to achieve as high an energy transfer as possible. However, the possibility exists of setting the V-I characteristics of these two components so that they can be directly coupled without any intervening electronic system. The direct coupling option, for example, has been examined in detail by Paul (2008) and

Paul and Andrews (2008b) for the case of a solar photovoltaic - hydrogen energy system. The present project will thus investigate the direct coupling option for a wind – hydrogen system, both theoretically and experimentally.

Overall the research project will aim to assist in improving the overall system efficiency and longevity of a wind – hydrogen energy system for RAPS. Improving the overall system efficiency will reduce the size of the system for a given power range. Secondly, improving the longevity and performance over the lifetime will reduce the unit cost of electricity generated over the system's life span. Hence wind hydrogen system could become competitive in the RAPS market, against, for example, diesel generators. Furthermore, the experiences and findings from this research may initiate or guide manufacturers of hydrogen technologies and RAPS systems into developing new or improved products.

The proposed program will make a significant and original contribution to knowledge of fact in a number of areas. This project will provide new experimental data on the performance of a PEM electrolyser subjected to variable power input from a fixed – pitch variable speed aerogenerator over an extended period. The research will also make a significant and original contribution to the theory relating to energy transfer between an aerogenerator and a PEM electrolyser, and the overall system efficiency of wind – hydrogen energy system for RAPS applications.

The experiment and numerical analysis in this research is unique and fill the gap by using PEM electrolysers and a fixed – pitch variable speed aerogenerator. The installation situates in RMIT University East Campus where wind speed data and other experimental data can be used to validate against results form numerical analysis. This project will also include financial analysis of the proposed energy system and then compared among its equivalent RAPS systems.

1.3 PROJECT OBJECTIVES

After due consideration of the current state of the art of wind – hydrogen systems for RAPS applications, the primary objectives of the present research project are to:

- Develop a computer – based mathematical simulation model of a wind – hydrogen energy system for remote power supply applications.
- Investigate both theoretically and experimentally ways to maximise the power transfer efficiency between a fixed-pitch variable-speed aerogenerator directly coupled to a PEM electrolyser, and hence the overall rate of hydrogen production
- Analyse any degradation in the performance of the electrolyser after extended operation subject to the variable electrical input from an aerogenerator as a result of wind speed fluctuations.
- Evaluate the unit costs of electricity produced by a wind – hydrogen energy system for RAPS, with a conventional electronic coupling unit and under direct coupling of the aerogenerator and electrolyser, and compare these costs against other RAPS options.

1.4 RESEARCH QUESTIONS

The specific research questions addressed in this thesis are the following:

1. What are the optimal design parameters of a wind – hydrogen system to meet a given remote area electrical demand in terms of lowest unit cost of energy on a lifecycle basis?
2. What matching procedures can be applied to maximise the power transfer efficiency between a fixed-pitch variable-speed aerogenerator directly coupled to a PEM electrolyser, and hence the overall rate of hydrogen production, without using an electronic converter/impedance matching unit?
3. How are the performance and longevity of the PEM electrolyser affected by the intermittent electrical input from an aerogenerator in the direct-coupled arrangement?

4. How do the unit costs of electricity produced by a wind – hydrogen energy system for RAPS, with a conventional electronic coupling unit and under direct coupling of the aerogenerator and electrolyser, compare with those for other RAPS options?
5. What are the most promising opportunities for cost reduction and improving competitiveness of wind-hydrogen energy systems?

1.5 SCOPE

The present thesis focuses on wind – hydrogen energy systems since wind energy is usually the most competitive renewable-energy option for electricity generation in a good wind area. These systems will be investigated particularly in relation to RAPS applications, because they are most likely to be economically competitive in the near term in remote applications where the costs of conventional fuels are very high. RAPS applications with a relatively low daily electrical energy demand are assumed in the case studies conducted.

The costs of the components of hydrogen system (electrolyser, hydrogen storage and fuel cell) for use with wind power are all high so that for such systems to become competitive the total system cost must be reduced. This project examines in detail one possible cost cutting measure: direct coupling of the aerogenerator and electrolyser to eliminating the need for and hence cost of expensive electronic coupling equipment. The implications of direct coupling for maintaining electrolyser efficiency over time and the overall practical lifetime of the electrolyser are investigated. These questions are addressed using theoretical analysis, computer modeling, and experimental work

The type of aerogenerator used is fixed-pitch with variable rotational speed, with a permanent-magnet synchronous generator. Aerogenerators whose blade pitch angle can be adjusted and employing other types of electric generator are outside of the scope of this study.

After a comparison of the experimental results for direct coupling of an aerogenerator to a PEM electrolyser with theoretical predictions, it was found that a steady-state model of aerogenerator performance at this site was inadequate. Hence preliminary work has been

undertaken on developing a dynamic model that seeks to take account of the turbine's moment of inertia and the finite time required to respond to changes in wind speed.

Only PEM electrolysers are covered in the present work, since these are becoming increasingly used in wind-hydrogen energy systems and have not been studied so much before in such applications. In addition, only PEM fuel cells are considered in the wind-hydrogen energy system modelling.

The experimental rig constructed for the direct coupling experiment in this study comprises just those parts of a wind – hydrogen energy system needed to investigate this option. A complete demonstration rig of a wind – hydrogen energy system, including hydrogen storage and a fuel cell, was outside of the scope of the project.

The system configuration used in the direct coupling experiment was that in which the entire output of the aerogenerator was at all times fed to the electrolyser. The alternative configuration, in which only the excess wind power over the end-use electrical load to be met is directed to the electrolyser, has not been able to be examined. It is very important, however, for the present work to be extended in the future to cover this second configuration, since it is likely to be preferable in most wind –hydrogen systems for RAPS.

The economic analysis of wind – hydrogen energy systems, and their comparison with commercially available RAPS systems such as diesel generator – battery, and PV battery systems, is conducted after system sizing simulations on the basis of the average unit cost of power delivered over the full lifetime of the system in present value terms. Further details of this costing methodology are given in chapter 3.

1.6 METHODOLOGY

The methodology that has been followed in order to meet the aims and address the research questions in this thesis is given in 1.4:

Step No.	Title of activity	Activity description & relation to research questions
1	Literature review	Review of renewable energy systems for RAPS, PV/wind – hydrogen energy system simulations and experiments, fuel cell and electrolyser and hydrogen technologies (addresses research questions 1 to 2)
2	Design and construction computer simulation program for a wind – hydrogen energy system	Review of previous simulations of wind power generation and hydrogen production and utilisation. Compiling wind data, aerogenerator data, household energy use and hydrogen system for construction of submodels. Construction of the computer model of a wind – hydrogen energy system in Visual Basic/Excel. (addresses research questions 1, 4 and 5)
3	AIR 403 aerogenerator modification and testing	Modification of the purchased AIR 403 aerogenerator and testing to obtain its V-I curve characteristic in a wind tunnel (addresses research question 2)
4	Theoretical investigation of direct coupling	Theoretical analysis of direct coupling between the AIR 403 aerogenerator and PEM electrolyser to find power and energy transfer (addresses research question 2)
5	Experimental testing of direct coupling	Setting up experimental rig for direct coupling experiment. Installation of AIR 403 aerogenerator at RMIT, aerogenerator control system, safety system and data collection equipment. (addresses research question 2 and 3)
6	Comparison of theoretical analysis of direct coupling	Results of theoretical analysis and experiment of direct coupling are compared. (addresses research question 2 and 3)

	with experimental results	
7	Improvement of theoretical prediction of direct coupling	Identifying the cause of discrepancy between the theoretical prediction of energy transfer in direct coupling and experimental results, and consequent improvement of the theoretical model. (addresses research question 2 and 3)
8	Thesis writing	Preparing and writing the thesis

1.7 OUTCOMES OF THE PROJECT

At the outset of this research work, the outcomes were expected to be the following:

- A simulation model predicting power output and hydrogen generation rate of a wind-hydrogen energy system for RAPS applications, validated by comparison with experimental data.
- Experimental data on the energy conversion efficiency for the wind power to hydrogen process in wind-hydrogen energy systems.
- A theoretical prediction of and experimental data on the energy transfer between an aerogenerator directly coupled to a PEM electrolyser
- Experimental data on the degradation in performance of PEM electrolysers subjected to variable input from wind power
- A small-scale demonstration of the aerogenerator – electrolyser part of a wind-hydrogen energy system.
- An assessment of the opportunities for improving the economics of wind- hydrogen systems, in particular by the direct coupling technique
- A triple bottom line comparison of a wind-hydrogen energy system and conventional RAPS systems.

1.8 STRUCTURE OF THE THESIS

The technical description of a wind – hydrogen energy system and a review of research done by others in this field are provided in Chapter 2.

Chapter 3 presents a theoretical analysis of a wind – hydrogen energy system, and a customised Visual Basic program for overall system simulation and its use for system and component sizing. A case study of the application of this program to the sizing of a wind-hydrogen energy system to supply electricity to a remote household at Kilcunda North on the ocean coast near Melbourne is described, as well as the economic evaluation of system and a comparison with conventional RAPS systems.

Chapter 4 is dedicated to a theoretical analysis of direct coupling of an aerogenerator and PEM electrolyser. It outlines a methodology for obtaining optimizing energy transfer under direct coupling, which is then applied to a case study.

The experimental investigation of direct coupling between an aerogenerator and PEM electrolyser that has been conducted as part of this project is presented in Chapter 5. It includes experimental rig design and construction at RMIT University East Campus.

In Chapter 6, the experimental results for direct coupling obtained are compared with a theoretical estimated using the procedure described in Chapter 4. The substantial difference found between the experimental and theoretically predicted results leads to the preliminary work presented in Chapter 7 on a dynamic model of the aerogenerator – electrolyser subsystem, as an alternative to the steady-state model used earlier.

Finally in Chapter 8 the answers obtained on the basis of all the theoretical and experimental work conducted to the research questions posed at the beginning of the thesis are presented. Overall conclusions are then drawn, and recommendations for future work on wind-hydrogen energy systems are put forward.

2 WIND – HYDROGEN ENERGY SYSTEMS FOR REMOTE AREA POWER SUPPLY

2.1 INTRODUCTION

2.1.1 Remote area power supply systems

Remote area power supply (RAPS) systems are not connected to conventional electricity grid networks due to their remote locations such as islands or mountainous areas (Department of the Environment Water Heritage and the Arts, 2008, Young et al., 2007). The cost of connecting to the grid can be very expensive, for example, in Australia up to AUD 10,000 per kilometre (Department of the Environment Water Heritage and the Arts, 2008). The majority of RAPS installations are for applications such as:

- Remote homesteads
- Remote farms such as in rural Australia
- Telecommunication towers
- Research stations
- Island or mountain communities
- Recreational boats and ships
- Households who wish to gain energy independence.

In some areas, part of the energy supply for RAPS systems comes from local renewable energy resources, although usually there is a back-up fossil-fuel system such as a diesel generator In the latter case, the diesel fuel must be transported to the destination, often at relatively high cost and with vulnerability to disruption. The local renewable energy resources may be a combination of wind, solar, hydro or thermal power, and hence offer the prospects of a zero-emission RAPS system if these can be relied upon exclusively.

2.1.2 RAPS technologies

A conventional energy system for RAPS normally consists of one or more primary energy sources, an energy storage device, and load management and power electronics. The principal renewable energy sources used in RAPS systems are photovoltaic (PV) arrays, aerogenerators, and micro hydro units. Energy storage units are used in remote locations to store energy at times when the primary energy sources are high in relation to the demand. The stored energy is then used later when the primary energy sources are low or not available. The most common energy storage units are batteries for storing electrical energy produced by the local renewable energy source at times of surplus power over demand, and diesel fuel used in a diesel-engine driven generator, where the diesel fuel must be imported usually at a high cost. The total load that is connected to an energy system determines the maximum power demand and hence the total electrical capacity (kW) of the RAPS system. Therefore the number of appliances to be supplied and their pattern of usage will primarily dictate the capital cost of the system.

The main components, including electronic devices, normally used in a renewable – energy RAPS systems are shown in Figure 1. The power control system and voltage regulator convert the output of the electrical generator into suitable current and voltage to be supplied to the load, and/or to the battery bank for electrical energy storage. If the output of the generator is alternating current (often 3-phase AC), this must be converted to the required AC mains voltage to supply the load, or to the required DC voltage if a DC supply system is used. In addition, any surplus power over the load must be converted to a DC voltage suitable for battery charging. Alternatively, and quite commonly, all the power input is fed to the battery, and the load is supplied totally from the battery, although this configuration is less energy efficient since all power supplied to the load from the renewable energy source suffers the energy loss due to the less than 100% roundtrip efficiency of the battery. The battery charger controls the charging of batteries, with the aim of maintaining their roundtrip energy storage performance and prolonging their lifetime. In the case of a PV system or aerogenerator, a maximum power point tracker is commonly used to ensure maximum power transfer from the supply system to the load or battery storage.

The power control system must also decide when to charge the batteries, supply energy directly to the load, or both, and when the diesel generator set is started. It is common that

all these power electronic functions are integrated into one or two physical items, such as Xantrex's XW Hybrid Inverter/Charger (Xantrex Technology Inc., 2008), or the VCS1.5 voltage regulator/charger and Selectronic Inverter that is used in a wind – battery energy system at RMIT University's Renewable Energy Laboratory (REL).

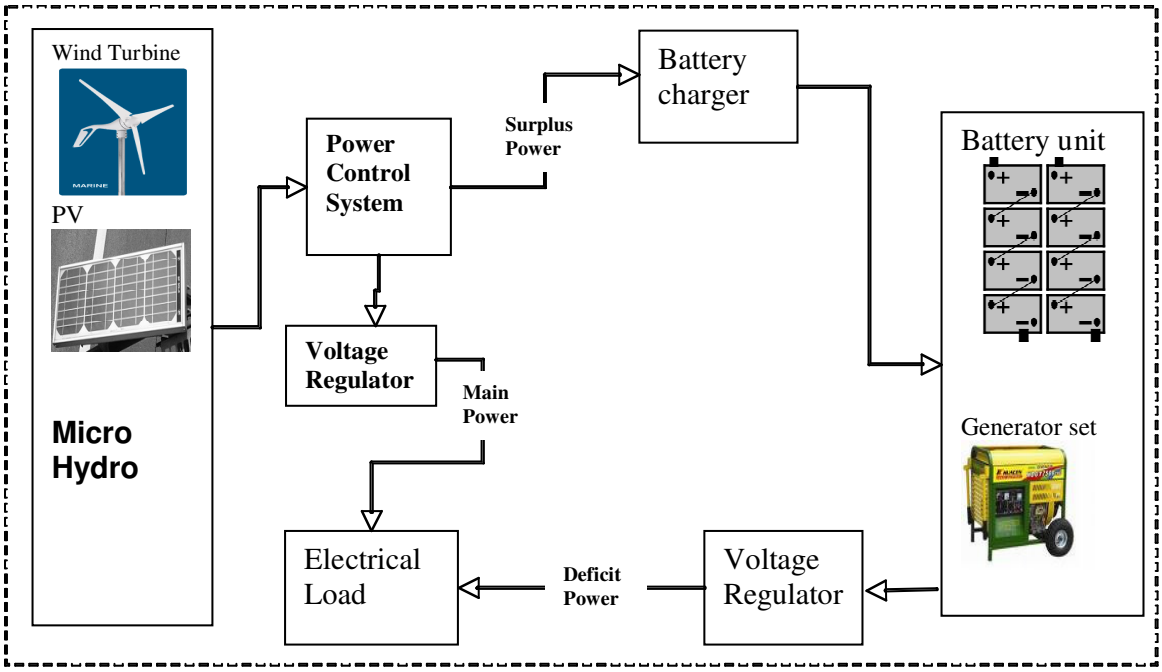

Figure 1: Schematic of a general RAPS system using three primary energy sources and batteries for energy storage with diesel generator as backup.

2.1.3 Renewable energy sources for RAPS

The selection of the most appropriate primary sources of renewable energy for a RAPS system depends very much on its location. A location with strong winds may have aerogenerators, a location with high solar radiation a PV array, or one with a large natural stream may use a hydro turbine generator. A combination of such renewable sources, each of which is inherently variable, can help to minimise the variation in the available input power to the system, and hence reduce the energy storage capacity required or reliance on a back-up diesel generator. For example, there might be weaker stream flow during summer but strong solar radiation could be utilised to supplement the power supply available. Therefore, a hybrid renewable – energy system is often preferable because it reduces vulnerability and reliance on fossil fuels.

There are many PV arrays available on the market, from suppliers such as BP, Kyocera, and Sharp. Installation of PV systems requires accredited installers and system components vary with capacity. Aerogenerators for use in RAPS systems are available from many manufacturers such as Southwest Windpower (with models such as AIR 403 and AIR X), Bergey, Westwind and Wind Energy Solution Canada.

2.1.4 Wind energy for RAPS

Aerogenerators are suitable for locations with relatively constant wind speeds such as coastal and hilly areas. Early wind energy systems in Australia were used extensively for water pumping. However, modern aerogenerators are increasingly being used to provide power to remote households and other facilities without easy access to grid electricity. Wind power at sites with high mean wind speeds is generally able to supply electricity at a significantly lower unit cost than solar options such as photovoltaic panels (Gipe, 1999).

The available wind energy is inherently intermittent and to a significant degree unpredictable, so some form of energy storage, commonly a battery bank in addition to a diesel generator, is essential for a standalone system. The ability of batteries to hold charge over a long period of time is limited, and this is a primary reason why a diesel generator also forms part of the system, despite the high cost of transporting diesel fuel to remote areas and the not inconsiderable maintenance requirements of diesel engines. To have a wind – energy RAPS system that truly had zero greenhouse gas emissions it would thus be preferable to have an energy storage that is capable of storing energy from season to season. There is increasing interest therefore in moving toward the use of hydrogen as energy storage medium for use with wind – energy RAPS systems.

2.2 WIND – HYDROGEN ENERGY SYSTEMS FOR RAPS

2.2.1 The basic wind – hydrogen system

A wind-hydrogen energy RAPS system is similar to a conventional wind-RAPS system but replaces the diesel generator and battery unit with a hydrogen energy-storage system. This hydrogen-based system must be able to produce hydrogen from surplus wind power over the load, store it for an extended period, and supply it to a fuel cell for conversion back into electricity and supply to the load at times of low or zero wind power. Hydrogen is produced from the surplus electricity by the electrolysis of water in an electrolyser. Hydrogen may be stored as compressed gas, liquefied hydrogen, or in solid form in materials such as metal hydrides. In a RAPS system the hydrogen is most commonly converted back into electricity in a fuel cell, but it can also be used in modified internal combustion engines, or combusted to produce steam for use in a steam turbine to generate power.

The key potential advantages of such a wind – hydrogen energy RAPS system are firstly its capability to store energy for a much longer period than a battery, indeed from season to season, so that a diesel generator is not needed at all; and secondly the minimisation of the capacity of the aerogenerator needed to guarantee supply for the whole year, because surplus wind energy during periods of high winds can be stored as hydrogen for extended periods to supplement supply at times of low wind.

From the perspective of a more general move to a hydrogen economy (Hoffmann, 2001), wind energy – hydrogen systems for remote area power supply (RAPS) are potentially an early niche market for zero-emission hydrogen energy technology because of the high costs of conventional energy sources in such applications (Isherwood et al., 2000).

2.2.2 System components and configuration

- The basic type of wind – hydrogen energy system for RAPS applications under investigation in the present thesis uses an aerogenerator as the primary energy source and replaces the battery unit of a conventional RAPS system with a

hydrogen energy system (Figure 2). The main components of the system are the followings:

- Aerogenerator (1): primary energy source to extract power from the wind.
- Power control system (2).
- Voltage regulator (3): performs conversion of AC to DC, DC to AC or DC/DC and controlling of voltage output.
- Electrolyser (4): production of hydrogen gas using surplus electricity
- Hydrogen storage (5): storage of hydrogen gas
- Fuel cell (6): production of electricity using hydrogen gas
- Load (7): household appliances and other electricity-consuming devices.

It is not uncommon that the power control system and power regulator are parts of the same physical unit.

The aerogenerator (1) produces electricity that is fed via a power control system and regulator (2) directly to the load (7) with any surplus over demand being directed to an electrolyser (4) for producing hydrogen for storage. The power control system switches the system to draw on the hydrogen from storage (5) for use in the fuel cell (6) to generate electricity to meet any demand deficit at times of insufficient wind energy.

The simplified system configuration in which all the power supplied by the aerogenerator is fed to the electrolyser for hydrogen production and subsequent use in the fuel cell to meet all the demand will be the primary one investigated when considering alternative coupling arrangements between the aerogenerator and electrolyser, because it is much easier to analyse both experimentally and theoretically. It is thus an important first step on the path to analysing the more complex configuration in which only the surplus aerogenerator power over the instantaneous load is supplied to the electrolyser.

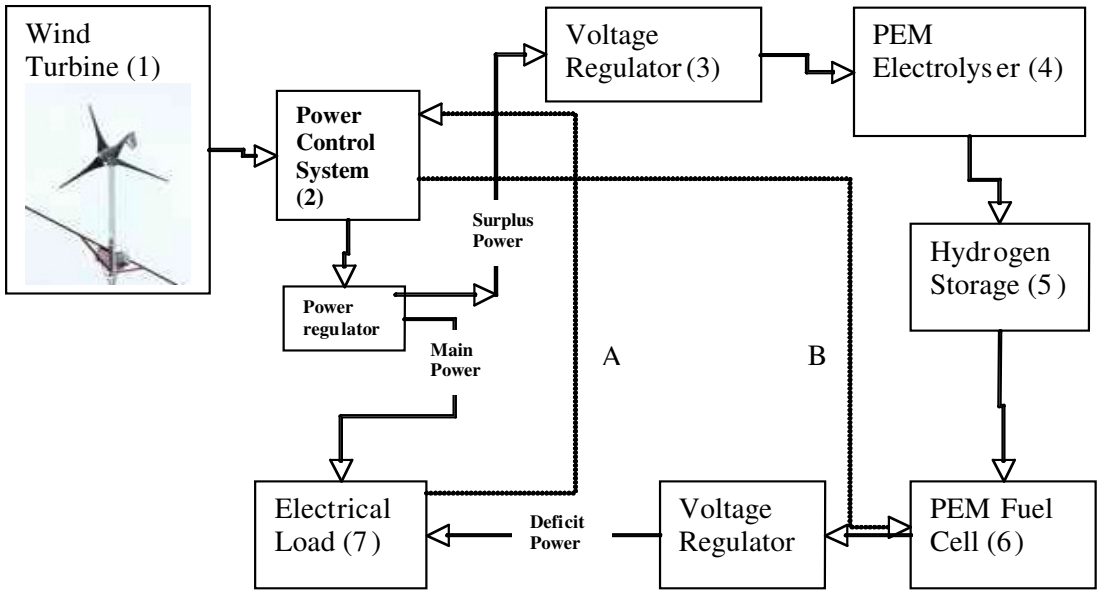

Figure 2: Schematic diagram of a wind – hydrogen energy system showing the aerogenerator as the primary energy source. The power from aerogenerator is directly fed to the load, with any excess over demand being used to produce hydrogen gas for storage and later reuse in the fuel cell to supplement supply at times of low or zero wind speed.

2.2.3 Aerogenerator

Aerogenerators are available in many sizes ranging from rated power outputs of a few kW for personal use to several MW in commercial wind farms. These turbines usually have a horizontal axis with three blades. The large aerogenerators used in wind farms have the ability to control their output and frequency because they need to feed power to the grid, which has specific standards. These turbines can be controlled by operators in almost every aspect such as turning on/off, yawing and blade angle.

The aerogenerators under consideration in the present project are relatively small, with rated power outputs of up to 20 kW. These turbines are normally used for RAPS due to their simple design and low maintenance requirements. They operate freely in the wind and most will furl or turn away from the wind to prevent damage in high wind. The power output is normally 3-phase AC, which is then rectified to DC power.

2.2.4 Electrolyser

Electrolysers use electrical energy in chemical reaction to produce hydrogen gas. There are two main kinds of electrolyser used in wind-hydrogen systems: alkaline and Proton Exchange Membrane (PEM) electrolysers.

Alkaline electrolysers employ an alkaline solution as the electrolyte, most commonly potassium hydroxide (KOH) solution (Divisek and Emonts, 2003). The working temperature of this type of electrolyser is under 100° C and the operating pressure varies from atmospheric up to 30 bar (Divisek and Emonts, 2003).

Proton Exchange Membrane (PEM) electrolysers use a solid polymer membrane, such as the proprietary material Nafion, a perfluorinated sulphonic acid polymer. The normal operating temperature is up to 85° C and pressures are usually only a little above atmospheric pressure. The solid electrolyte of the PEM electrolyser allows construction to be simpler than alkaline electrolysers. Even though the PEM electrolyser currently has a higher cost and there is a lack of information on its longer-term operating capabilities, it is expected over time to serve a wider range of applications (Barbir, 2005). The PEM electrolyser also produces high-purity oxygen and hydrogen, eliminating the need for a gas processing unit (Gazey et al., 2006). Therefore the PEM electrolyser is chosen as the focus for this project.

2.2.5 Fuel cell

Fuel cells that use hydrogen gas as fuel and produce electrical energy to supply load can be categorised into two groups according to their operating temperature range:

- Low temperature fuel cells:
  - The alkaline fuel cell is similar to an alkaline electrolyser explained in subsection 2.2.4 but it works in reverse. This fuel cell has a low operating temperature (50-200 °C (Larminie and Dicks, 2003)) and normally uses KOH or NaOH solutions for the electrolyte (Hoogers, 2003). The main problems affecting alkaline fuel cells are the presence of carbon dioxide in the electrolyte that reduce its conductivity, and the need for a circulation system to renew the electrolyte (Hamnett, 2003).

- The phosphoric acid fuel cell operates around 200°C and uses phosphoric acid as electrolyte (Hoogers, 2003).
- The PEM fuel cell uses a solid polymer for its electrolyte, as in PEM electrolysers, allowing transport of protons but not electrons from the hydrogen to oxygen electrodes. The low operating temperature leads to a relatively slow electrochemical reaction and the need for expensive catalysts such as platinum (Larminie and Dicks, 2003). The solid electrolyte must be hydrated to operate, which also dictates that the cell temperature must be less than 100°C. But the solid electrolyte and low operating temperature contribute to its simple construction and hence PEM fuel cells have strong potential for remote area power supply application (Ali, 2007). The low cell temperature also helps to reduce start-up time and makes the cell suitable for intermittent operation. As a result, the PEM fuel cell is the primary choice for other applications such as automotive and small-scale portable power sources. For these reasons, the PEM fuel cell is selected as the most suitable to be used in the present project.

- High temperature fuel cells:
  - The solid-oxide fuel cell is a high-temperature fuel cell that operates between 600-1000°C (Larminie and Dicks, 2003). Due to its high temperature, the chemical reaction within the cell is fast and hence does not require expensive catalysts. The feedstock can be methane or coal gas since the high temperature inside the cell allows in situ reforming to produce the required hydrogen gas, so that a separate reformer is not needed. However, the high cell temperature leads to material selection challenges, and high cost of these materials and the associated equipment.
  - The molten carbonate fuel cell is another type of high-temperature fuel cell operating in a similar temperature range to that of solid oxide cells, but with a liquid electrolyte. This type of fuel cell needs carbon dioxide in the air to work. Because of the high operating temperature both solid-oxide and molten carbonate fuel cells will take time start, and therefore they are more suitable for applications such as larger power plants (Hoogers, 2003) rather than RAPS.

2.2.6 Hydrogen storage

In RAPS applications relying on renewable energy, some form of energy storage is needed to overcome the variable energy input in both daily and seasonal cycles. The electrical energy from sources such as PV, aerogenerators and micro-hydro can be used to produce hydrogen gas in the type of system focused upon in this project. However, storing hydrogen gas, which has a very low density at atmospheric pressure (0.084 kg/m^3 at NTP), leads to a requirement for large storage volumes unless the gas is pressurised. In addition, special care must be taken to avoid leakage since the small size of the hydrogen molecule means that hydrogen gas is highly diffusive. The hydrogen storage methods available are:

Compressed hydrogen gas

This method of storing hydrogen gas is the most common and available in many industries. The hydrogen gas is compressed and put into cylinders, which can be metal or composite cylinders. The latter can operate at pressures up to 300 bar (or even 700 bar), and have a mass density of around 3.1% (kg of hydrogen/kg of storage) at 300 bar (Larminie and Dicks, 2003, Hoogers, 2003). The high gas pressure helps reduce the volume of the gas required for a given energy content, but the energy used in the compressing process of hydrogen has to be considered as well. The gravimetric or mass energy density of the system (that is, the net energy stored per unit total mass of the storage system, counting the container and the hydrogen itself) is also crucial for automotive and mobile applications. However, neither the volumetric nor gravimetric energy densities of hydrogen are such critical limiting factors in most RAPS systems where space is usually available as well as a solid base for a heavy storage system. Hence relatively low pressure, higher-volume storages for hydrogen may be considered for many wind – hydrogen RAPS systems so that parasitic energy losses for gas compression are minimised (Ali, 2007).

Liquefied hydrogen

When hydrogen gas is cooled to 22° K it turns into a liquid and can then be stored at relatively high volumetric and gravimetric energy densities. Liquefied hydrogen is already used in industries requiring large amounts of hydrogen. The liquid hydrogen must be heated and returned to gaseous form before feeding into a fuel cell. The cooling process of hydrogen is an energy-intensive one and in the best case the energy needed could be 25% of the equivalent heating energy of hydrogen stored (Larminie and Dicks, 2003). The gravimetric energy density of liquefied hydrogen (up to 14.2% mass percent) is five times

greater than that of a compressed gas system at 300 bar (Larminie and Dicks, 2003, Hoogers, 2003). In the case of tank failure, the liquid hydrogen will slowly evaporate into the atmosphere.

Metal hydrides

Hydrogen can also be stored in the solid state in certain metal hydrides, where there is a chemical reaction between the metal alloys and hydrogen gas molecules to form a weakly-bonded hydride. The reaction can be reversed by a combination of pressure reduction and heating (Larminie and Dicks, 2003, Sherif et al., 2005). Combinations of titanium, iron, magnesium, chromium and nickel have been used as the metals in such hydrides. Gravimetric energy densities in the range of 1 to 7.7% have been achieved depending on the type of alloy used (Hoogers, 2003). This method provides a very safe storage at relatively low pressures. In the event of leak or container failure the hydrogen can escape slowly at room temperature, which then reduces the overall temperature of the tank and hence slows down the rate of hydrogen release. Metal hydride storage is currently very expensive but may turn out to be the preferred storage method for wind – hydrogen RAPS systems in the future, especially where space is limited or there are risks of bushfires or thunderstorms.

Low-cost storage

Ali (2007) investigated a number of low-cost low-pressure storage systems for hydrogen gas in solar/wind - hydrogen RAPS systems, including composite cylinders (similar to those used for LPG), and fibre-reinforced plastic (FRP) tanks (originally designed for water storage using tow tanks at different levels and the standard water displacement method of gas storage in the lower tank. A 225 L tank was able to store hydrogen gas at a mass density of 0.4% (Ali, 2007).

A comparison of various hydrogen storage systems and conventional fuels was carried out by Hoogers (2003) with all options having an energy content equivalent to 50 L of gasoline or 1590 MJ of energy stored (Figure 3). With the same energy content, gasoline, diesel and propane have similar mass and volume, whereas the compressed hydrogen system at 300 bar has 12-13 times the mass and 18-20 times the volume (Hoogers, 2003, Sherif et al., 2005). It is apparent from this analysis that the mass of metal hydride is significantly greater than others among hydrogen storage methods for the same energy content of 1590 MJ.

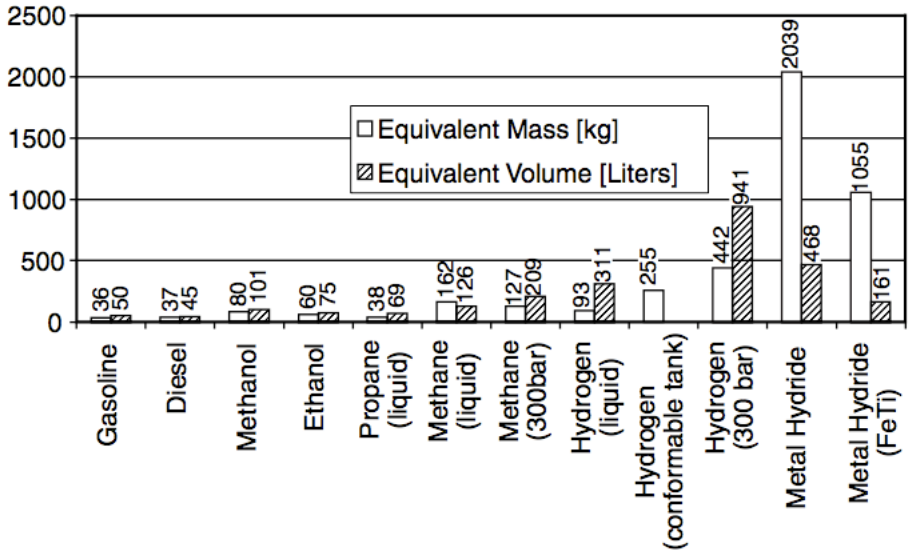

Figure 3: Comparison of different hydrogen storage options and conventional fuels in terms of the mass and volume required in each option such that its energy content is equivalent to 50 litres of gasoline or 1590 MJ of energy (Hoogers, 2003).

2.2.7 Power electronics and maximum power point tracker

Generally, power electronics such as a transformer, rectifier and voltage conversion unit, together with some means of variable impedance matching, are employed to achieve as close to optimal power transfer between the aerogenerator and the electrolyser as possible (Beukes and Moor, 2004). Such systems typically transfer around 80-95% of the maximum energy theoretically achievable (Dashlooty et al., 2004, Miland et al., 2006, Xantrex Technology Inc., 2008), but add significantly to the overall capital cost of the wind – hydrogen system. A combined inverter/charger from Xantrex suitable for a wind – hydrogen energy system may cost US$ 500-800/rated kW (Infinigi, 2008, Gogreensolar, 2008, Alter systems, 2008).

In an aerogenerator, the aerodynamic power and mechanical-electrical power conversion combine to give electrical output at a given wind speed. Since the aerodynamic power is free, the maximum power output from an aerogenerator is the priority over efficiency given that it operates within the safe wind speed range.

To extract the maximum electrical power from the wind at a wind speed, the load supplied by the aerogenerator must be varied to find the value at which the aerogenerator is working at its so-called maximum power point. There is only one maximum power value at a given wind speed and this corresponds to a single optimal value of the applied load. The maximum power points (on a V-I graph) of an aerogenerator operating at various wind speeds form a maximum power curve specific to that aerogenerator. An attempt was made by the National Renewable Energy Laboratory (NREL) in the USA to develop a commercial unit for a small aerogenerator (Corbus et al., 1999). However, at the present time, maximum power point trackers for small aerogenerators are not readily available in the market, unlike the case for PV systems.

A wind – hydrogen energy system for RAPS application has been simulated by Miland *et al*. (2006), where the primary objective was to test the model of the power electronics. A load control technique for coupling an aerogenerator to a PEM electrolyser stack was simulated in the mathematical model. The algorithm monitored aerogenerator output frequency and the rate of change of frequency, and then used this information to adjust the load and hence control the rotational speed of the generator and the frequency of its output voltage. This system adjusted the value of a dump load connected in parallel with the electrolyser to control the aerogenerator, rather than changing the electrolyser itself. The electrolyser provides the base load and the variable resistive load reacts to change in wind speed, where this heat could be used for heating. The study found that the system was able to respond adequately to intermittent wind speed inputs in a case study of a site on the north-east coast of England (Miland et al., 2006) and managed to couple an aerogenerator to a PEM electrolyser stack, but did not mention the power transfer efficiency.

Beukes and Moor (2004) used another coupling technique, varying the load itself rather than putting two load systems into the rig in the previous study. The load was varied according to the known instantaneous wind speed. To be able to apply the correct load to allow the aerogenerator to operate at its maximum power point, use was made of a previously measured power-load-wind speed relationship. Two methods of measuring the instantaneous wind speed were compared: anemometer measurement and calculation from the electrical output frequency of the generator (Beukes and Moor, 2004). In the first method, the anemometer was used to determine the wind speed at an instant, and then a simulated maximum power point tracker will determine the optimal V-I combination from a look-up table in the system. In the second method, an electrical output frequency was

related to rotor RPM of a synchronous generator and thus the maximum power for that RPM found from the generator characteristic. The two approaches gave similar results in the computer modelling and they both track the expected power output calculated from the wind speed as the reference output (Beukes and Moor, 2004). However, there was no experimental measurement of these methods applied to an actual system. A similar simulation presented by Nakamura (2002) of a small aerogenerator with a simple wind speed profile showed that the turbine rotational speed in response to wind speed changes has a lagging effect due to component inertia as shown in Figure 4, thus differing from the simulation results of Beukes and Moor (2004) that did not allow for any lag in response.

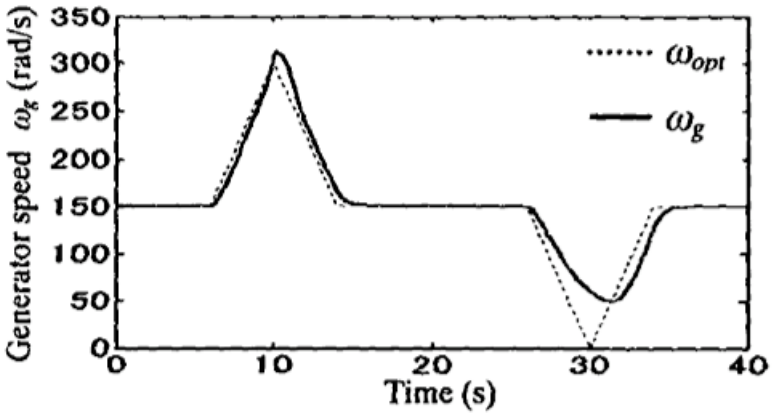

Figure 4: The solid line shows the turbine rotational speed (rad/s) in respond to wind speed as represented in dotted line. The turbine speed responds to the change in wind speed with a lag and does not reach the same amplitude due to its inertia (Nakamura, 2002).

2.2.8 Experimental and demonstration wind – hydrogen energy systems

A small number of demonstration wind-hydrogen energy systems have been built and tested for technical performance evaluation and for estimating economic viability, although none as yet are truly commercial installations. For example, a demonstration wind – hydrogen energy system at ENEA's Casaccia Research Centre in Italy was described by Dutton *et al*. (2000), which tackled the issue of power input fluctuation from the aerogenerator, hydrogen and oxygen production and other practical issues, but did not mention the type of electrolyser used.

The Hydrogen and Renewables Integration (HARI) project, comprising an aerogenerator, PV and hydro generator coupled to a hydrogen energy system, was set up by the Centre for Renewable Energy System Technology (CREST) at West Beacon Farm, Leicestershire, UK (Gammon et al., 2006). Prior to the project there was an existing RAPS system using a battery bank for energy storage. The hydrogen system installed employs a 36 kW electrolyser, compressed hydrogen storage system at 137 bar, and 2 and 5 kW PEM fuel cells. The alkaline electrolyser from Stuart Energy Systems produced hydrogen at 25 bar, and a battery is integrated into the system to reduce the input fluctuation. The total cost of this hybrid renewable – energy hydrogen system is quoted as being in the order of £600,000 (US$ 894,000) (Gammon et al., 2006).

Another demonstration autonomous wind – hydrogen energy system is situated on the island of Unst in the Shetland Isles, 320 km north of mainland Scotland (Gazey et al., 2006). This system supplies both electricity and hydrogen gas for transportation and mobile power generation. The project has provided valuable experience in operating an electrolyser in conjunction with an aerogenerator, and in system design, sizing and operating practice in the real world. Although the electrolyser used was an alkaline electrolyser, it was stated that a PEM electrolyser would be more suitable for the task (Gazey et al., 2006) because:

- A PEM electrolyser can produce high purity hydrogen gas and eliminate post-production gas treatment.
- It can produce higher-pressure hydrogen gas.
- It does not need to circulate or renew its electrolyte periodically.

A large-scale wind – hydrogen energy demonstration system recently built in Patagonia, Argentina, is being used to study hydrogen utilisation options including a refilling station and use for transportation, as well as system design and safety aspects (Aprea, 2008). An installed aerogenerator capacity of 2.4 MW supplies electricity to a Stuart Energy System alkaline electrolyser (KOH) with 1 Nm^3/h of hydrogen production capacity. The product hydrogen is stored at 200 bar.

Recent reports on wind – hydrogen system demonstration projects at the 17th World Hydrogen Energy Conference were presented by Magill (2008) and Ulleberg *et al*. (2008). Magill (2008) reported a wind – hydrogen energy system installed in Mawson, Antarctica, where a research station is located. The project uses three aerogenerators to provide power

to the station and the excess power is stored as hydrogen at 200 bar for later usage for energy generation, cooking and filling weather balloon. The project faced many problems due to its remote location and extreme weather conditions. It was due to be completed in 2005-6 but the delivery of equipment was delayed. In addition, the lack of skilled technicians and hydrogen-related standards prevented system servicing due to safety risks. After a minor explosion, the demonstration system had to be disassembled before any results could be collected. The aerogenerator, PEM electrolyser, hydrogen compressor and hydrogen storage system were installed but not the fuel cell.

Ulleberg *et al*. (2008) reported on a wind – hydrogen energy system installed on the island of Utsira, Norway. The system was commissioned in 2004 to supply energy to 10 households. The system has a 600 kW aerogenerator, alkaline electrolyser, hydrogen compressor, hydrogen storage (200 bar) and a 55 kW hydrogen internal combustion engine. A PEM fuel cell is also available but no tests of this have yet been conducted. The project concluded that autonomous operation for a long period of time needs higher hydrogen production and utilisation efficiency: that is, a more energy efficient electrolyser, a larger hydrogen storage and use of a hydrogen fuel cell instead of an internal combustion engine.

2.2.9 Modelling and simulation studies of individual component and overall system

A number of modelling and simulation studies of wind – hydrogen RAPS systems have been done over the past years covering system sizing, operation, technical performance and economic evaluation. Details. For example, simulations of system control and operation of stand-alone wind – hydrogen energy systems have been carried out by Bechrakis *et al*. (2006), Isherwood *et al*. (2000), Khan and Iqbal (2005), Kolhe *et al*. (2003), Patel and Pryor (2001), Shakya *et al*. (2004), Sharma *et al*. (2001) and Young *et al*. (2007).

Patel and Pryor (2001) conducted a simulation and associated performance monitoring study of a conventional RAPS system (PV/diesel/battery) operating in the Pilbara region of Western Australia. In this study, the experiment and monitoring were conducted first, and

then the simulation model (RAPSIM) was run to allow model validation and refinement. Another interesting simulation study conducted by the same research group at Murdoch University analysed the power transfer between an aerogenerator with a permanent-magnet synchronous generator and a load (Sharma et al., 2001).

Bechrakis *et al*. (2006) analysed a wind – hydrogen RAPS system for supplying electricity to a hotel on the island of Samothrace, off the northeastern coast of Greece. The study used an estimated electricity demand profile for the hotel (Figure 5) and annual wind data as inputs to the simulation. A PEM fuel cell and electrolyser were chosen to provide back-up power and produce hydrogen respectively. It was assumed that the PEM electrolyser produced hydrogen gas at 13 bar (Bechrakis et al., 2006) and hence did not need a separate hydrogen compressor. An economic study suggested that the initial capital cost was around US$ 180,000 and the cost of the electricity generated was no less than US$ 1.05/kWh (Bechrakis et al., 2006). Similarly, Young *et al*. (2007) investigated the feasibility a renewable-hydrogen energy system for two remote locations in Bhutan. The study investigated primary energy sources such as hydro, solar and wind and employed hydrogen as the energy storage. The remoteness of the locations under consideration makes a good case for this type of energy system, where grid and diesel power are equally expensive and technically challenging to be deployed. The system capital cost ranged from approximately around US$180,000 to almost US$550,000 depends on whether it is wind, solar, hydro, or a combination of these (Young et al., 2007). The most expensive system uses PV and the cheapest system an aerogenerator. A case for a demonstration unit is put forward as the next logical step.

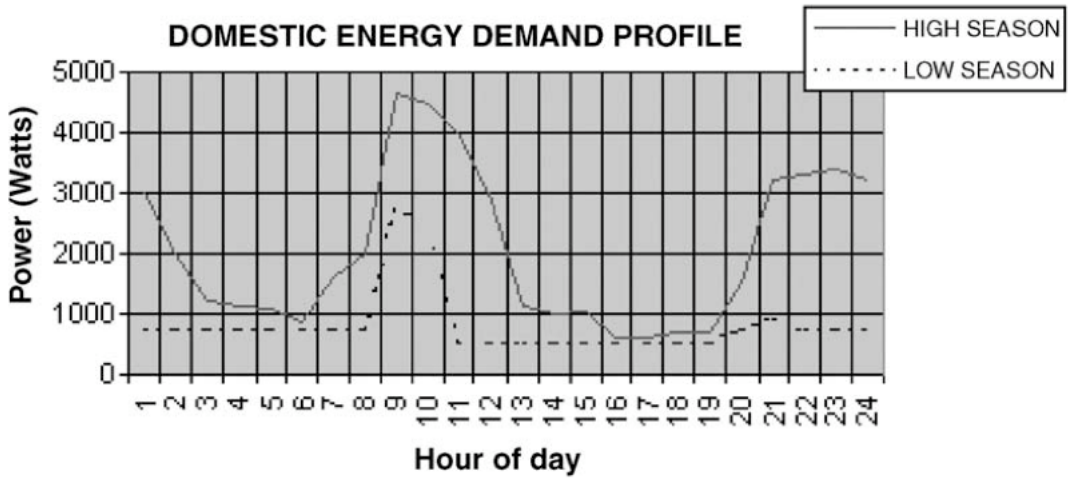

Figure 5: Estimated demand profile of a small hotel in Samothrace island by assuming appliances used and applying seasonal variation (Bechrakis et al., 2006).

Kolhe *et al*. (2003) have developed an analytical model of a combined solar/wind - hydrogen energy system where the PV array and aerogenerator complement each other. The characteristics of the components used are shown in Figure 6. The study focuses on the sizing of components to provide the maximum power delivery.

Component	Specifications
Wind turbine generator	Bergey BWC Excel 10 kW, 3ϕ Permanent Magnet Alternator, VCS-10–48 V DC
Photovoltaic array	Golden Genesis GP 64 module (4S∗4P), 1 kW peak with Charge Controller
Electrolyser	Stuart Alkaline Electrolyser 5 kW with Compressor
Buck converter	Multiphase PWM, HRI made, 5 kW, 36–48 V
Fuel cell	Ballard-Proton Exchange Membrane Fuel Cell (MK5-E), 5 kW, 19–35 V
Boost converter	Multiphase PWM, HRI made, 5 kW, 24–48 V
DC load	12 kW water cooled Dynaload
AC load	3 kW, single phase
Inverter	5 kW, trace engineering
Battery	42.240 kWh
H_2 storage	10 bar, 3.8 m^3 (represents 125 kWh of stored energy [1])

Figure 6: Components used in the study of a RAPS system where aerogenerator and PV are used in the same system (Kolhe et al., 2003).

Khan and Iqbal (2005) developed a dynamic simulation model of a wind – hydrogen energy system, and like the present study employed an AIR 403 aerogenerator as the primary power generator. However, these authors focus on technical issues associated with fluctuations in the aerogenerator voltage and the use of a capacitor to minimise these, rather than optimal coupling of the aerogenerator and electrolyser as in the present study. A PEM fuel cell is modelled, but the electrolyser supplied by Stuart Energy Systems is alkaline not PEM. The simulation aims to study the transient effects and reactions of the system to intermittent and fluctuating wind speed. An interesting finding of this study is shown in Figure 7, which backs up the point made by Nakamura (2002), namely that there is time lag in the response of the aerogenerator in terms of power output to a change in wind speed. Hence, for example, after an increase in wind speed the power output is less than expected on the basis of the instantaneous wind speed (Miland et al., 2006), a feature that will be returned to later in the present thesis.

.

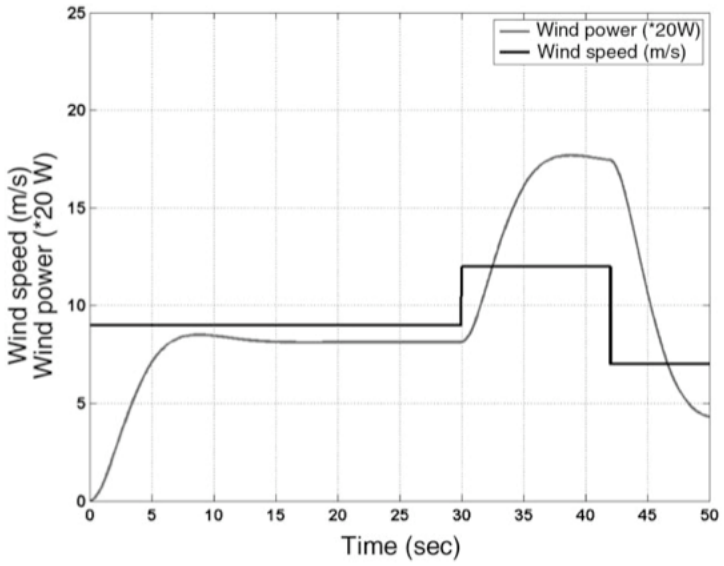

Figure 7: Produced power by an aerogenerator lags behind the changes wind speed, and there is a delay before the turbine can produce power following a sharp increase in wind speed from zero to above the cut-in speed (Khan and Iqbal, 2005).

Simulations of wind – hydrogen energy systems, or ones with the addition of a PV array and hydro-generator, have been steadily improved in their accuracy by modelling the individual components using real data to validate the in-built performance curves.

There have been a number of earlier studies of small aerogenerator with permanent magnet synchronous generators to examine the control process and control electronics to enhance power delivery and stability of voltage and frequency (Boukhezzar and Siguerdidjane, 2005, Beukes and Moor, 2004). But so far as is known to the present author, there has not yet been an analysis of the potential and methodology for directly coupling an aerogenerator with a PEM electrolyser. The present study of direct coupling without any intervening power electronics to determine energy transfer and efficiency therefore presents some useful new findings in this area.

2.3 DIRECT COUPLING OF AEROGENERATOR AND ELECTROLYSER

The present thesis investigates in detail, using both a theoretical simulation and experiment testing, the option of matching the V-I characteristics of a fixed-pitch variable speed aerogenerator and a Proton Exchange Membrane (PEM) electrolyser stack by suitably stacking electrolyser cells in series and parallel, so that the aerogenerator can be directly coupled without any intervening electronics. The rationale is that, if a sufficiently high level of energy transfer is achievable, the significant costs of power electronics can be totally avoided, thus improving the overall economics of wind – hydrogen systems compared to petrol or diesel RAPS systems with batteries.

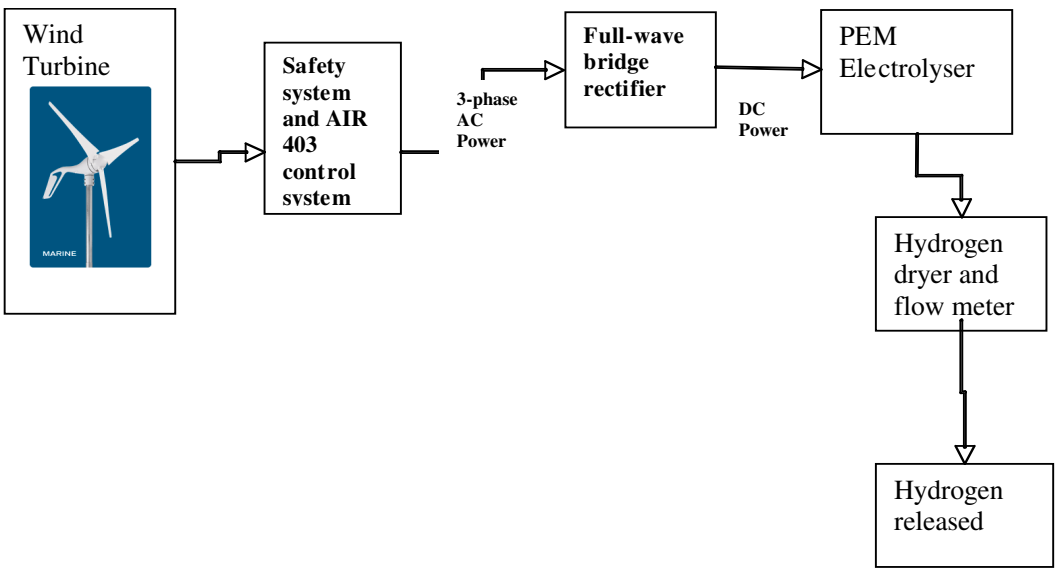

Figure 8: Schematic diagram of a wind – hydrogen energy system employing direct coupling between a suitably matched aerogenerator and electrolyser.

The basic system studied is as shown in Figure 8. In practical systems, it is likely that only the surplus power from the aerogenerator over the load at any given time is transferred to the electrolyser for use in production of hydrogen. However, as a first step in analysing the direct coupling configuration, the simplifying assumption will be made in the present work that all the output of the aerogenerator – and not just the surplus power – is fed to the electrolyser.

The simplified system configuration in which all the power supplied by the aerogenerator is fed to the electrolyser for hydrogen production and subsequent use in the fuel cell to meet all the demand will be the primary one investigated in the present thesis when considering alternative coupling arrangements between the aerogenerator and electrolyser, because it is much easier to analyse both experimentally and theoretically. It is thus an important first step on the path to analysing the more complex configuration in which only the surplus aerogenerator power over the instantaneous load is supplied to the electrolyser.

The extension of the findings from this simplified case to the more realistic case will be discussed later, in Chapter 4 and Chapter 5.

2.4 EFFECT OF INTERMITTENT ELECTRICAL INPUT ON ELECTROLYSER PERFORMANCE

Whether an aerogenerator is coupled to an electrolyser using power electronics incorporating a maximum power point tracker, or by direct coupling as just described, another key question of interest is the effect on the performance of a PEM electrolyser of the continuously varying electrical input. This question has received little attention in the literature to date. Among the studies that have at least partially addressed this issue for PEM electrolysers, Barbir (2005) suggested that gas permeation at low electrolyser current density encountered at low wind speeds could contribute to hydrogen and oxygen mixing due to permeation of hydrogen through the Nafion membrane. The permeation of oxygen through Nafion to mix with hydrogen was found to exist but the rate was very low compared to the case of hydrogen. Another problem referred to by Barbir was that after a period of low operating current, the temperature of the electrolyser cells would remain low, so that if the electrical input from the aerogenerator rose quickly with a rapid increase in

wind speed the cells would output hydrogen at a much higher rate, but at an operating temperature much lower than the optimal one, thus reducing the overall energy efficiency of the electrolyser.

A number of other studies have looked at the effects of variable power input on alkaline electrolysers. Dutton *et al*. (2000) simulated the performance of an alkaline electrolyser with varying wind speed profiles in a wind – hydrogen energy system and found the overall energy efficiency of the electrolyser was 62.7% based on the lower heating value (LHV). It was found that the fluctuation in power input causes the pressure within the cell to fluctuate and reduced the purity of the product gases (Dutton et al., 2000). The test used five sets of wind data input: namely wind speed averaged over 1, 10, 60, 150 and 1200 seconds. Each input set represented a different level of wind speed variability. Hence the electrolyser experienced different levels of input fluctuation. Averaging wind speeds over a longer time interval generates less input fluctuation. The result of the test suggested that there was no significant loss of performance in the alkaline electrolyser in terms of pressure of hydrogen produced, gas purity, and the electrolyte level. However, the longer-term effect of the varying input to the alkaline electrolyser was not explored.

Schiller *et al*. (1998) also investigated the effect of intermittent operation on an alkaline electrolyser. An alkaline electrolyser was used to investigate electrode performance over a test run of 15000 hours. The simulated variable electrical input was from a solar system. No significant degradation of the electrodes was found after a period of operation of 15,000 hours.

Another study of an alkaline electrolyser with variable input was done by Brossard *et al*. (1984) and found similar effects on the electrolyser of a variable electrical input. The electrolyser was subjected to a variable input typical of that from an aerogenerator at an actual site. One effect observed was that the cell temperature under varying input did not reach the temperature attained in the case of a constant input. In addition, the overall energy efficiency of the electrolyser (calculated by using cell voltage) varied with cell temperature, although the Faraday efficiency was not greatly affected.

Faraday efficiency, η_f is expressed as the ratio of the actual hydrogen produced to the theoretical hydrogen production according to the current input of an electrolyser:

$$\eta_f = \frac{h_{actual}}{h_{theory}} = \frac{h_{actual}}{i^{cell}} \times 1000F \qquad \textbf{Equation 1}$$

where h_{actual} is the measured cell hydrogen production rate (mol/s), h_{theory} is the single-cell theoretical hydrogen production rate (mol/s), i^{cell} is current input of a single cell (A=C/s), and F is the Faraday constant, 96 485 C/mol.

A joint project between RMIT University and CSIRO (Clarke et al., 2008) investigated the energy transfer and hydrogen production in a solar – hydrogen system in which a 2.4 kW PV array at RMIT was directly coupled to a 3kW PEM electrolyser built by CSIRO. Investigation of the effects of the intermittent electrical input on the electrolyser performance was one of the main objectives of the study. The testing lasted between September 2007 to January 2008 with a total operational period of 60 days. The energy transfer loss under direct coupling compared to the theoretical maximum achievable was measured to be 25.8 % compared to the 12.4% according to theoretical analysis of the coupling configuration (Clarke et al., 2008). But much of this difference was due to one cell of the 13-cell electrolyser stack degrading prematurely (Clarke et al., 2008). Paul and Andrews (2008a) report on another test of direct coupling using a different PV array and bank of PEM electrolysers using the same experimental set up that found a 24% degradation in the performance of the electrolysers, in terms of the voltage needed to give a specified current density, after an operational period of 467 hours.

The present research project therefore also investigates the effects of intermittent and variable electrical input on the performance of a PEM electrolyser in a wind – hydrogen energy system, in particular one in which the aerogenerator and electrolyser are directly coupled.

2.5 CONCLUSIONS

In the light of this review of previous work, the present research project thus investigates in detail the feasibility of directly coupling the aerogenerator and PEM electrolyser without any intervening power electronics in a wind – hydrogen energy system for RAPS applications.

The key questions addressed are the following:

- How close to the maximum achievable energy transfer and cumulative hydrogen production can be achieved in the direct-coupling configuration?
- What procedure needs to be followed to match the aerogenerator to the PEM electrolyser when they are to be directly coupled?
- What changes to the control system in a wind-hydrogen system are needed in the situation of a directly-coupled aerogenerator and electrolyser?
- What improvement in the unit costs of the power produced on a lifecycle basis can direct coupling yield?
- What effect does the intermittent electrical input from an aerogenerator have on the performance and practical lifetime of a PEM electrolyser.

3 WIND – HYDROGEN ENERGY RAPS SYSTEM SIMULATION

3.1 INTRODUCTION

This chapter presents an overall analysis of a wind – hydrogen energy system for remote area power supply. The wind – hydrogen energy system under investigation is to provide energy to a remote homestead throughout the year without any back-up energy supply, and utilises hydrogen energy storage to be sustainable. An aerogenerator provides primary energy in the form of electricity and any excess over demand is stored in the form of hydrogen gas to be used later at times of lower or no wind. The working principle of the system is similar to that of an aerogenerator-battery system where a battery bank provides the energy storage. The system must provide energy to meet the entire demand of users at all times.

A computer model of the wind – hydrogen energy system based on Microsoft Excel and Visual Basic is described, and used to simulate the system's operation over an annual period in order to study overall system behavior and size individual components. The outputs of the simulation are also used to evaluate the unit costs of the power supplied on a lifecycle cost basis. The use of the model is illustrated by applying it to a case study of supplying the electricity needs of a remote homestead at Kilcunda North, near the coast some 100 km south east of Melbourne. The unit costs of the power supplied are compared with those of conventional RAPS systems such as solar – hydrogen, wind – battery and solar – battery energy systems.

Furthermore this chapter identifies a potential unit energy cost reduction by eliminating the power electronics between the aerogenerator and electrolyser, and hence leads into the next chapter where the direct coupling option is investigated technically.

3.2 SIMULATION MODEL OVERVIEW

The wind – hydrogen energy system simulation model described here is used to study a number of approaches to sizing the main components of such a system, namely the aerogenerator, electrolyser, hydrogen storage, and fuel cell for a given load and annual

wind speed profile. The model is designed for both the academic study of wind-hydrogen energy systems, and potential installers and users of these systems who are interested in component sizing and system economics at their own locations. The simulation program is constructed using familiar user interfaces, and includes many wind data sets for Australian locations and performance data for a number of commercially-available aerogenerators. Users with a good knowledge of Visual Basic may add data such as hourly wind speeds, other aerogenerator performance characteristics and electrical usage profiles to customise the program to their own requirements.

The purpose of the simulation program is to determine a system size and unit costs of electricity supplied for small wind – hydrogen systems for remote homes or similar stand-alone applications. In the system modelled, the aerogenerator supplies electricity directly to the load to the maximum extent possible, as described earlier in Figure 8 (section **Error! Reference source not found.**). When there is surplus wind power over the load, the excess is fed to a PEM electrolyser for producing hydrogen. At times of low wind speed when there is insufficient wind power to meet the load, hydrogen is used from storage to meet the power deficit.

3.3 SIMULATION MODEL INPUT AND OUTPUT DATA

3.3.1 Overview of model

The computer-based model is constructed by using Visual Basic and Microsoft Excel, which allows easy access by other users. Graphical user interfaces such as dialogue boxes allow users to select system components and choices of configuration to define the wind-hydrogen energy system to be modelled and also understand the fundamentals of the system. Moreover, external data sets such as wind speeds, electrical load profiles and aerogenerator characteristics can be input by users for their own purposes. Important formulae describing the performance of each component of the system are described in the following section.

The main inputs to the model are:

- Hourly wind speed data sets for a full year.

- The characteristic curve of the aerogenerator: power output versus wind speed.
- The hourly electrical demand profile to be met over the year.
- The characteristic of the PEM electrolyser: hydrogen production rate versus power input.
- The characteristic of the PEM fuel cell: hydrogen consumption versus power output.
- Lifetimes, and capital and maintenance costs, of all components (aerogenerator, PEM electrolyser and fuel cell, hydrogen storage system, and balance of system).

The input data sets such as hourly wind speed and characteristics of aerogenerators are built into the program. Users can select and run the program to study system sizing of a wind-hydrogen energy system using one of the ten standard commercial aerogenerators (subsection 3.3.3) located at one of the ten sites (subsection 3.3.2) for which wind data are already in the program.

The model then computes the load directly supplied by the aerogenerator, the amount of hydrogen produced and stored, the hydrogen used by the fuel cell and the load supplied by the fuel cell for each of the 8760 hours in a year. The final outputs are:

- The required aerogenerator capacity in kW of electrical output.
- The required electrolyser capacity in kW of electrical input.
- The required hydrogen storage capacity in kg of hydrogen.
- The capital of the system and unit costs of electricity (US$/kWh) of the system.

3.3.2 Wind speed data input

The wind speed data used in this program can be input by users from their own locations. The wind speed data must be averages over an hour. The data should at least cover a year for the analysis to be able to test for seasonal effects. Alternatively, there are ten sets of wind speed data built into the program for specific coastal sites in south-eastern Australia, and one of these can be selected for a trial run using a dialogue box such as that shown in Figure 9.

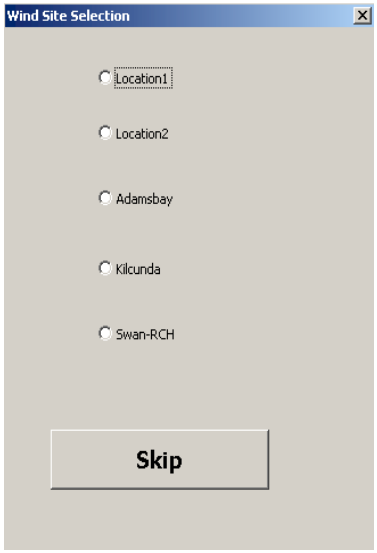

Figure 9: An example of a dialogue box for selecting one of the sites for which hourly wind data are already available in the program. Here only five of the ten sites available are shown.

The hourly wind speed data sets were acquired from a report by Natural Systems Research (1987). This work on which this report is based was jointly funded by the State Electricity Commission of Victoria and the Victorian Solar Energy Council between 1983 and 1984 to study the wind energy resources for electricity production in Victoria. The report has records of wind speeds at ten sites in Victoria, Australia, five on the West coast and other five on the East coast with respect to Melbourne (Figure 10). The hourly average wind speeds were recorded at a height of 10 m at all sites, so they can be extrapolated to the required hub-height of a selected aerogenerator using the standard relationship between wind speed and height above the ground (Patel, 1999).

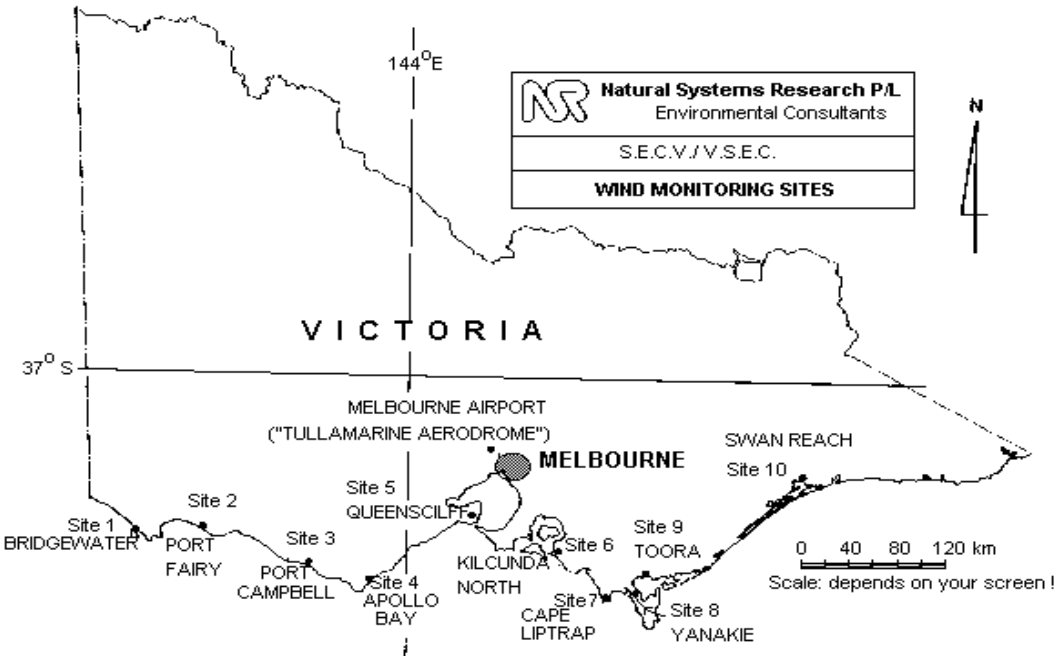

Figure 10: Monitored wind sites in around Melbourne, Victoria, Australia (Natural Systems Research, 1987).

The sites at which the monthly average wind speed exceeded 6 m/s were Toora, Bridgewater, Port Fairy, Apollo Bay, Kilcunda North and Cape Liptrap. On the other hand, the poorest wind site was Swan Reach whose monthly average wind speed was only 3 m/s. With respect to the seasonal variation of the wind, the average wind speed was lowest in May for all other sites except at Apollo Bay where the lowest mean wind speed occurred during March.

The highest average monthly wind speed was experienced in October at all sites except Port Campbell and Apollo Bay where the maximums were in July, and Yanakie and Swan Reach have their maximum during December. This report concluded that, even though Apollo Bay had the highest annual wind energy, Kilcunda North, Toora and Bridgewater would be the better wind sites due to their more consistent wind resource. The report further suggested that the data recorded during these two years were likely to be a good representation of the long-term wind resource.

The available data from Natural Systems Research (1987) are average wind speed over an hour, and hence the term ‘hourly wind speed’ data is employed. The power calculated from an hourly wind speed is therefore an average power over an hour. The power available in the wind (P_{wind}) is the kinetic power of a moving mass of air and can be calculated by:

$$P_{wind} = \frac{1}{2}\rho A v^3 \qquad \textbf{Equation 2}$$

where P_{wind} is power available in the wind (W), ρ is air density (kg/m^3), A is turbine swept area (m^2), and v is wind speed (m/s).

The present analysis uses an average wind speed value over a period of an hour to calculate P_{wind} since no wind speed data for shorter periods are available. P_{wind} is then taken as the average power in the wind over an hour. It should be noted that, if alternatively instantaneous wind speed values were used to calculate power available in the wind at each instant, and then these power values were averaged over an hour to find the average power, the result would be greater than P_{wind}. The discrepancy is a consequence of the difference between the cube of an average wind speed ($\bar{v}^3$) and the average of the cube of the instantaneous wind speeds ($\overline{v^3}$), the latter always being the larger quantity.

3.3.3 Aerogenerator submodel

The power output of an aerogenerator subject to a given incident wind speed is calculated by using its characteristic wind speed – power curve usually provided by the manufacturer. Formulae for the characteristic curves of all aerogenerators available for selection in this program are listed in Table 1. For example, the power output of the AIR 403 aerogenerator per unit swept area in the wind speed range 3.5 – 12 m/s is given by the first formula in the Table 1 and also shown as $P_{gen} = 0.257 \times (v^3) - 1.4117 \times (v^2) + 6.5831 \times (v) - 14.35$ Equation 3.

$$P_{gen} = 0.257 \times (v^3) - 1.4117 \times (v^2) + 6.5831 \times (v) - 14.35 \qquad \textbf{Equation 3}$$

While the second formula in Table 1 ($P_{gen} = 5.5588 \times (v) - 52.146$

Equation 4) is used for the higher range 12 to 20 m/s:

$$P_{gen} = 5.5588 \times (v) - 52.146 \qquad \textbf{Equation 4}$$

where P_{gen} is the power of the aerogenerator (W/m2).

Any wind speed higher than the maximum specified for each aerogenerator is dangerous for the turbine and hence it is assumed no power is produced for wind speeds above this maximum. Since a mean hourly wind speed is used, the resultant power is an average over one hour. In $P_{gen} = 0.257 \times (v^3) - 1.4117 \times (v^2) + 6.5831 \times (v) - 14.35$

Equation 3 and $P_{gen} = 5.5588 \times (v) - 52.146$

Equation 4, the output power is normalised according to unit swept area to allow the program to increase or reduce a turbine beyond its actual size while retaining its characteristic performance, assuming power output remains directly proportional to swept area.

The model assumes that the power output of the selected aerogenerator is fed directly to the load, with any surplus power redirected to the electrolyser for hydrogen production. In the case of a power deficit, the aerogenerator output is complemented by output of the fuel cell drawing on hydrogen from the storage. The amount of surplus or deficit power is calculated by:

Surplus/deficit power = P_{gen} - P_{load} **Equation 5**

where P_{load} is power used by load.

Aerogenerator	Rotor Diameter (m)	Power output (W) formula	Wind speed range (m/s)
AIR 403 (400W)	1.17	$P = (0.257)v^3 - (1.4117)v^2 + (6.5831)v - 14.35$ $P = (5.5588)v - 52.146$	3.5-18 18-20
Westwind 3kW	3.7	$P = (0.0125)v^5 - (0.7742)v^4 + (13.999)v^3 - (75.179)v^2 + (174.89)v - 129.98$	3.5-17
Westwind 5.5kW	5.1	$P = (0.0032)v^6 - (0.1291)v^5 + (1.5435)v^4 - (6.4503)v^3 + (57.309)v^2 - (179.4)v + 133.82$	3.5-17
Bergey 1500W	3	$P = -(0.0029)v^6 + (0.1168)v^5 - (1.8028)v^4 + (12.98)v^3 - (27.577)v^2 - (4.0977)v + 27.366$ $P = (52.04)v^2 - (1776.1)v + 15500$	3.5-15 15-17
AIRX100 (900W)	2.1	$P = (0.0096)v^5 - (0.4831)v^4 + (7.8491)v^3 - (44.189)v^2 + (105.6)v - 81.112$	3.5-20
AIRX200 (1000W)	2.7	$P = (0.0017)v^6 - (0.1418)v^5 + (4.7618)v^4 - (81.839)v^3 + (739.55)v^2 - (3134.6)v + 4978.5$	3.5-20
AIRX500 (3000W)	4.5	$P = -(0.0026)v^6 + (0.1764)v^5 - (4.3812)v^4 + (45.716)v^3 - (166.91)v^2 + (254.76)v - 144.66$	3.5-20
EXCEL-R (7.5kW)	6.7	$P = (0.0999)v^5 - (4.8753)v^4 + (77.383)v^3 - (424.01)v^2 + (930.64)v - 619.62$	3.5-17

Table 1: The ten standard aerogenerators included in the simulation program and the formulae used to represent their characteristic power curves, obtained by curve fitting to the power output graphs provided by manufacturers. Aerogenerators such as AIR 403 and Bergey 1500 need more then one formula to represent their characteristic curve over the full operating wind speed range.

The ten common aerogenerators included in the Visual Basic program – the Westwind 3 kW, Westwind 5.5 kW, Westwind 10 kW, Westwind 20 kW, AIR 403, WHI-100, WHI-200, WHI-500, BWC XL.1 and BWC 1500 – range in capacity from 0.4 to 20 kW output and are considered to be in the small aerogenerator category. These polynomial equations representing power curves of aerogenerators were obtained by curve-fitting in Excel. An aerogenerator's power curve was taken from its product manual and then a power curve was plotted in Excel. The standard Excel curve-fitting function, based on least squares method, was employed and the best-fit formula generated was used to plot a graph. However, a perfect fit was hard to achieve and therefore a middle region of a curve was targeted and given priority for curve fitting.

In the case of model simulation, the polynomial in Table 1 representing AIR 403's power curve was used. It was aware that this would give inflated power output compared to manufacturer's power curve (Figure 19) at region of wind speed above 16 m/s. In addition the wind speed above 16 m/s was rare as shown by Figure 18 and only counted for little more than 200 hours or 2% (between 16 and 18 m/s only, since above 18 m/s, a linear formula was utilised instead). As a result, the application of model to case study at Kilcunda North would gain a valid result within this framework.

For this project the AIR 403 aerogenerator is used because a unit has been available and ready to be installed at RMIT Bundoora East campus for experimental work.

3.3.4 Electrical usage profile

The electrical usage profile over an annual period can be input by users like other input data to the program. The demand data have to be averages over an hour; in other words, the electrical usage is assumed to be constant within an hour. If actual demand data are not available, an approximation of power demand according to the appliances used or by searching for literature data for a similar location and household size may be made.

3.3.5 PEM electrolyser submodel

For the submodel of a single cell electrolyser, the V-I input characteristic of the cell, and its corresponding hydrogen production rate are the two main components. The explanation in this section will start with a single cell then move into calculations of electrolyser cells in stack, using formulae adapted from Ali (2007) and Larminie and Dicks (2003). The voltage applied between the two electrodes of a single-cell electrolyser will initiate current flow, as the chemical reaction to produce hydrogen and oxygen gas by electrolysis process. Considering a single electrolyser cell, the number of electrons flowing in the external circuit to and from the power source directly relates to the number of molecules of water split, and hence to the quantity of hydrogen and oxygen produced. For one hydrogen gas molecule two electrons are required, and the theoretical rate of hydrogen production is calculated from Faraday's first law (

Equation 6) (Ali, 2007):

$$h_{theory} = \frac{i^{cell}}{F \times 2} \qquad \textbf{Equation 6}$$

where h_{theory} is the single-cell theoretical hydrogen production rate (mol/s), i^{cell} is current input of a single cell (A=C/s), and F is the Faraday constant, 96 485 C/mol.

Equation 6 can be rewritten, to give h_{theory} in kg of hydrogen per second, because 1 mol of hydrogen has a mass of approximately 2/1000 kg:

$$h_{theory} = \frac{i^{cell}}{F \times 2} \times \left(\frac{2}{1000} \right) = \frac{i^{cell}}{1000F} \qquad \textbf{Equation 7}$$

In actuality not all electrons contribute to the production of hydrogen gas, so that less hydrogen gas is produced than theoretically expected. The ratio of the actual hydrogen produced to the theoretical hydrogen production according to the current input of an electrolyser is expressed as the Faraday efficiency, η_f :

$$\eta_f = \frac{h_{actual}}{h_{theory}} = \frac{h_{actual}}{i^{cell}} \times 1000F$$ **Equation 8**

The energy stored in the form of hydrogen gas produced ($E_{hydrogen}$) is in practice less than the electrical energy ($E_{electric}$) input into an electrolyser. The overall energy efficiency of an electrolyser cell (η) is the ratio of the energy produced in the form of hydrogen gas to the electrical energy input (Equation 9).
The high heating value (HHV) of hydrogen is used in this thesis (Larminie and Dicks, 2003), which counts all energy stored in hydrogen gas in terms of the maximum heat that can in principle be extracted:

$$\eta = \frac{E_{hydrogen}}{E_{electric}} = \frac{n \times HHV}{i^{cell} \times V^{cell} \times t}$$ **Equation 9**

where n is the number of moles of hydrogen gas produced, V^{cell} is single cell voltage (in volts), and the HHV of hydrogen is 285840 J/mol.

For an electrolyser stack of N cells connected in series and a Faraday efficiency of η_f, the actual hydrogen production rate of a stack (H_{actual}) when a current of i^{cell} amps flows through each cell is:

$$H_{actual} = \frac{N \times \eta_f \times i^{cell}}{1000F}$$ **Equation 10**

For an electrolyser bank comprising M branches each with N series-connected electrolyser cells and the same current i^{cell} amps flowing through each cell, the hydrogen production rate becomes:

$$H_{actual} = M\left(\frac{N \times \eta_f \times i^{cell}}{1000F}\right) = M.N\left(\frac{\eta_f\, i^{cell}}{1000F}\right) \quad \textbf{kg/s} \qquad \textbf{Equation 11}$$

If I is the total current drawn by the electrolyser bank,

$$i^{cell} = I / M$$

In the electrolyser submodel, the standard single-cell characteristic curve is approximated by a straight line with a slope m^{cell} and intercept on the voltage axis at $V^{cell}{}_{cut\text{-}in}$ following the procedure of Ali (2007) (Figure 11).

According to Figure 11, the slope of the straight line is found by:

$$m^{cell} = \frac{i^{cell}_{\max}}{V^{cell}_{\max} - V^{cell}_{cut-in}} \qquad \textbf{Equation 12}$$

where $V^{cell}{}_{max}$ is the maximum allowable cell voltage and $i^{cell}{}_{max}$ is the maximum allowable cell current.

Thus the current can be expressed in term of voltage, cut-in voltage and slope as:

$$i^{cell} = m^{cell}\left(V^{cell} - V^{cell}_{cut-in}\right) \qquad \textbf{Equation 13}$$

and the voltage written as:

$$V^{cell} = \frac{i^{cell}}{m^{cell}} + V^{cell}_{cut-in} \qquad \textbf{Equation 14}$$

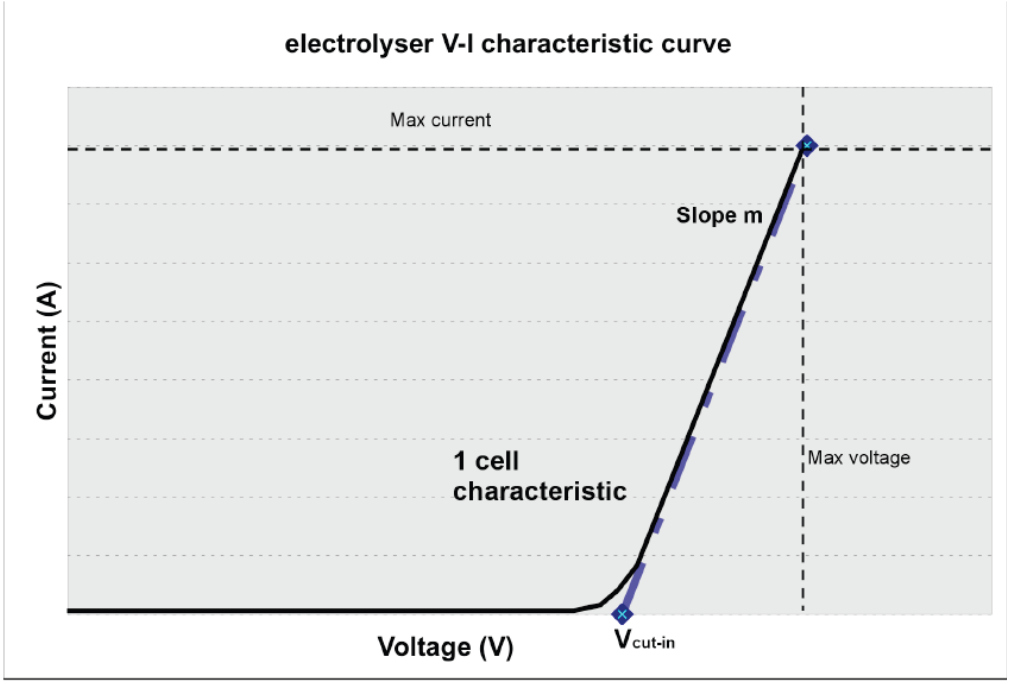

Figure 11: A single-cell electrolyser V-I characteristic from testing (solid line) and the straight-line approximation (broken line) used to represent it in the electrolyser submodel.

The power input of an individual cell (p_{in}) is calculated by using its current and voltage input:

$$p_{in} = i^{cell}.V^{cell} \qquad \textbf{Equation 15}$$

By substituting for V^{cell} from

Equation 14 into

Equation 15 and then solving for the current input i^{cell} the following equation for i^{cell} is obtained:

$$i^{cell} = \frac{-m^{cell}V_{cut-in}^{cell} + \sqrt{\left(m^{cell}V_{cut-in}^{cell}\right)^2 + 4m^{cell}p_{in}}}{2} \qquad \textbf{Equation 16}$$

This equation is particularly useful because the power input is usually known and the resultant current can be used in the determination of hydrogen production. Substituting i^{cell} from Equation 16 into

Equation 8 yields the following equation for the actual hydrogen production rate (h_{actual}) of a single cell:

$$h_{actual} = \frac{\eta_f}{1000F}\left(\frac{-m^{cell}V_{cut-in}^{cell} + \sqrt{\left(m^{cell}V_{cut-in}^{cell}\right)^2 + 4m^{cell}p_{in}}}{2}\right) \quad \textbf{kg/s} \qquad \textbf{Equation 17}$$

For an electrolyser bank, where individual cells are connected in series to form a branch and a number of branches connected in parallel, the power input equation can be written in terms of the single cell current and voltage as follows:

$$P_{in} = (i^{cell}.M).(V^{cell}.N) = I.V \qquad \textbf{Equation 18}$$

where the product of i^{cell} and M is the total current (I) of the electrolyser bank and the product of V^{cell} and N is the overall voltage (V) across the bank.

The cell current can be written in terms of the power input to the bank (P_{in}) as follows:

$$i^{cell} = \frac{-m^{cell}V_{cut-in}^{cell} + \sqrt{\left(m^{cell}V_{cut-in}^{cell}\right)^2 + \frac{4m^{cell}P_{in}}{NM}}}{2} \qquad \textbf{Equation 19}$$

The hydrogen production rate of a stack can then expressed using Equation 11 and Equation 19 as follows:

$$H_{actual} = \frac{\eta_f . N . M}{1000F}\left(\frac{-m^{cell}V_{cut-in}^{cell} + \sqrt{\left(m^{cell}V_{cut-in}^{cell}\right)^2 + \frac{4m^{cell}P_{in}}{NM}}}{2}\right) \quad \textbf{Equation 20}$$

Apart from the equations governing the working of the electrolyser that are input into the program, the electrolyser size in kW capacity is also specified by users at the start as prompted by a dialogue box. There are two conditions for electrolyser sizing used in the simulation to study the effects of component sizing, namely:

- Unconstrained electrolyser capacity, where the capacity is sufficient to allow input of the maximum excess wind power over demand at all times. In this case, users can input any size that is sufficiently larger than the aerogenerator capacity, but in the economic analysis it is important to set the electrolyser size to the minimum needed to take all the surplus wind power over demand.
- Constrained electrolyser capacity, where the capacity is set so that not all excess wind power can be input. To examine the effect of this constraint, users may start with an electrolyser that has the same size in kW as the aerogenerator and then reduce its size progressively.

3.3.6 Storage system submodel

There are a number of hydrogen storage systems being developed to improve their volumetric and mass densities and lower unit costs (Ali, 2007, Gambini et al., 2008, Landucci et al., 2008, Mori and Hirose, 2008). In this study, the hydrogen will simply be assumed to be stored at relatively low pressure in gaseous form so that there are no significant parasitic energy losses for compression. The idealised assumption of a 100% roundtrip energy efficiency into and out of storage – that is, assuming zero leakage or other losses – will be made. Clearly then the predicted performance and unit costs of the system will be superior to some extent to that expected from an actual system. It is planned in future work to include potential losses in the storage system in the modelling and hence investigate how significant their effect on overall system performance and economics is likely to be.

The capacity of the required hydrogen storage system in a particular case can be determined or set by the simulation model according to two different conditions:

- The unconstrained storage condition, in which the model ensures there is just enough capacity to store all the hydrogen produced over the course of year, allowing for continued use of hydrogen from storage to meet the demand via the fuel cell.
- The constrained storage condition, where the capacity is preset at some value less than that necessary in the unconstrained condition, so at any time the storage is filled, hydrogen production from excess wind power is stopped.

The unconstrained storage condition allows the aerogenerator and hence the electrolyser to be of the minimum capacities possible subject to meeting the final electrical demand throughout the year. The reason for this outcome is in simple terms that all the wind energy produced by the aerogenerator is made use of either, as first priority, to supply the demand directly, or as second priority, to produce hydrogen for storage that can be used to meet demand via the fuel cell at times of low or zero wind speed. In terms of overall efficiency of converting available wind energy into electrical energy consumed, this condition will always be preferable to constrained storage, since at times in the latter case excess wind power is wasted since the storage will be full. A wind – hydrogen energy system with a large energy storage can afford to have a relatively small aerogenerator and electrolyser because the energy stored can supply power when the wind cannot. The same system with constrained storage capacity has to rely more heavily on direct supply of power from the aerogenerator, even at times of lower wind speed; hence the aerogenerator installed must be larger.

The simulation model works by successively increasing the size of the installed aerogenerator until the amount of hydrogen in storage at the beginning of the year is the same as that at the end, and hence a sustainable system size has been obtained. If the aerogenerator size is too small, the variation of the amount of hydrogen stored is like that shown in Figure 12, where the hydrogen stored declines sharply into the negative zone, indicating immediately that the rate of hydrogen production, and hence aerogenerator size has to be increased.

For a standalone energy system to function sustainably the hydrogen storage must not go below zero. If this occurs during the calculation, two solutions could be applied: increasing aerogenerator size or raising initial hydrogen storage. The program is designed to detect the conditions at which the storage is below zero. Then firstly it determines the negative hydrogen amount in kilogram, which would be used to add hydrogen to the initial hydrogen storage in the case of unconstrained storage or if the storage has not yet reached its set limit. Secondly, if necessary the program increases the aerogenerator size and the simulation is rerun.

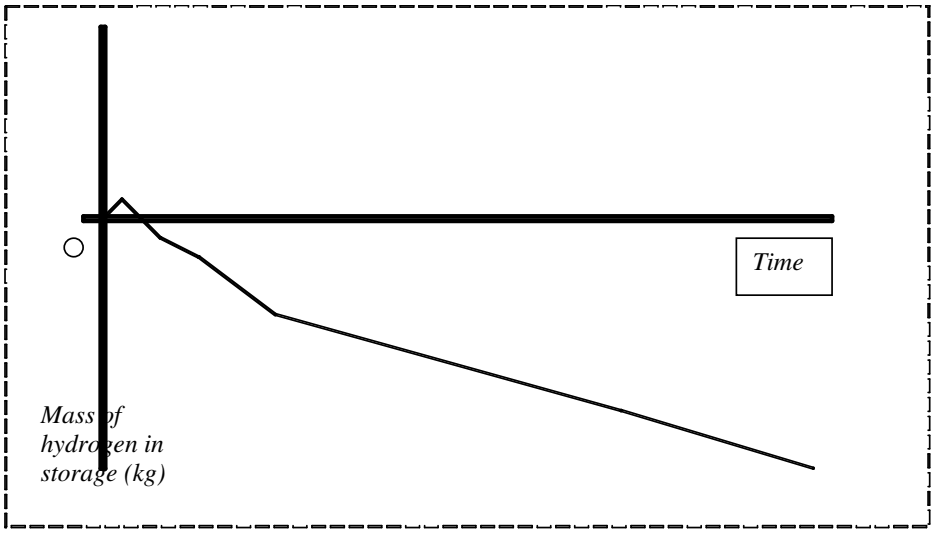

Figure 12: Hydrogen storage level variation over time with an aerogenerator that is too small. The program allows for negative hydrogen storage in the calculation due to energy demand.

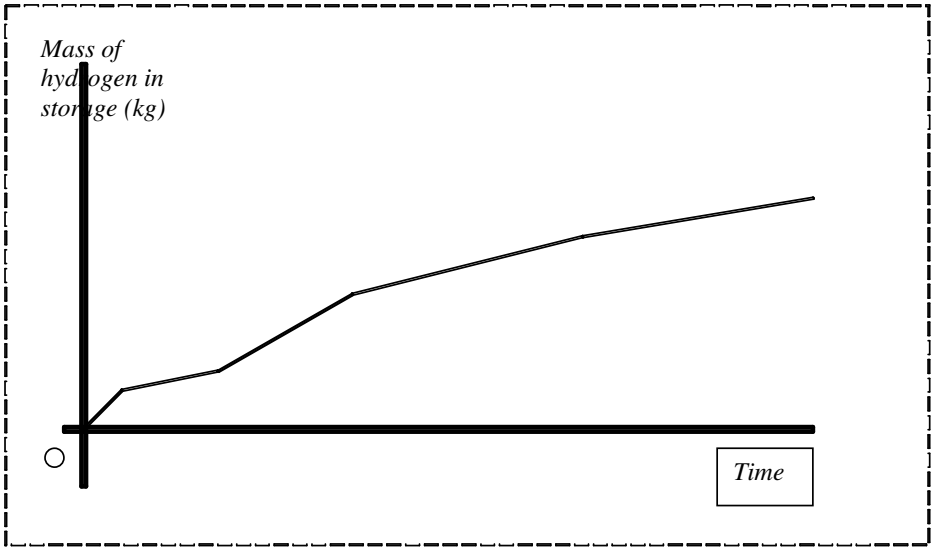

Figure 13: Hydrogen level increases from zero at the start of the year and continues to rise without falling due to an over-sized aerogenerator.

The opposite case of an over-sized aerogenerator in a wind-hydrogen system is illustrated in Figure 13, wherein the hydrogen storage level keeps increasing toward the end of the year, when it is much higher than at the beginning. An optimally sized aerogenerator will lead to a variation of hydrogen in the storage, assuming this is unconstrained, as shown in Figure 14, where the level of hydrogen storage at the end of the year is equal to (or in practice just slightly more than) that of the start of the year,

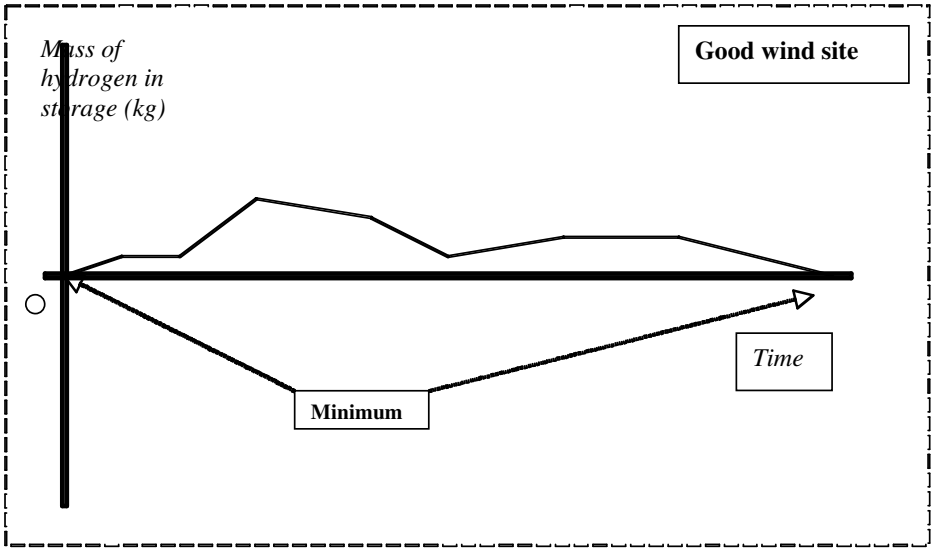

Figure 14: An example of the variation in hydrogen storage level over the year when the aerogenerator is correctly sized. The system uses up all the hydrogen energy stored as a result of having optimally sized components.

An example of the variation of hydrogen in the storage under the constrained storage condition for a correctly sized aerogenerator is shown in Figure 15. In this case, the aerogenerator will need to be larger than in the unconstrained storage condition since the amount of stored hydrogen energy supplied to the final demand via the fuel cell will be less. It can be seen that the storage under the constrained condition is actually full for some of the year, and starts and ends the year full.

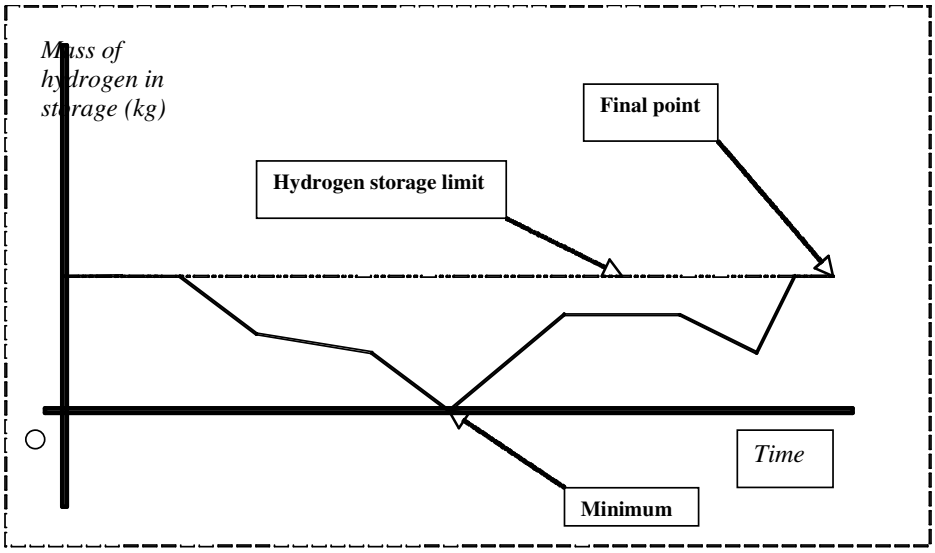

Figure 15: An example of the variation of hydrogen in the storage under the constrained storage condition for a correctly sized aerogenerator. The aerogenerator required will be larger than for the unconstrained storage condition, so that it produces just enough power during the year to restore the hydrogen level to its starting point (storage full) ready for the next year.

The effects of these two storage conditions on the other component sizes, system performance, and unit costs of power supplied will be illustrated further and quantitatively in the case study presented later in subsections 3.5.5 and 3.5.6.

3.3.7 Fuel cell submodel

The fuel cell in the wind – hydrogen energy system provides electrical power by consuming hydrogen gas drawn from the hydrogen storage unit. The water-splitting reaction used in an electrolyser works in the opposite direction in the fuel cell, as hydrogen and oxygen from the air are recombined to form water once again, plus electrical energy and heat. For every molecule of hydrogen gas that takes part in the electrochemical reaction, two electrons are released and pass through the external circuit that includes the load to be supplied.

Considering a single cell fuel cell, where one mole of hydrogen gas is used up and therefore 2 moles, $2N_A$, of electrons are released, where N_A is Avogadro's number. If the electrical charge of an electron is –e, then the total electrical charge for a cell, q, flowing to the external circuit per mole of hydrogen consumed is:

$$q = -e.2N_A = -2F$$ **Equation 21**

where F is Faraday's constant.

For a potential difference across the cell of V^{cell} the work done (W) per mole of hydrogen gas consumed is given:

$$W = e.2N_A.V^{cell} = 2V^{cell}F \quad \textbf{J}$$ **Equation 22**

The maximum energy liberated by a chemical reaction is limited by the enthalpy of formation of the products, Δh_f . In this analysis the HHV for the energy content of hydrogen is used. If all the energy in the input hydrogen could be converted to electrical work, the cell voltage would be given by:

$$V^{cell} = \frac{\Delta h_f}{2F} = \frac{285.84 \times 1000}{2 \times 96485} = 1.48 \text{ V at 25°C}$$ **Equation 23**

In practice the maximum practically achievable electrical work is given by the Gibbs free energy, Δg_f = -237.2 kJ/mol, which is less than Δh_f, so that that the maximum cell voltage is given by Equation 24 (Larminie and Dicks, 2003):

$$V^{cell} = \frac{\Delta g_f}{2F} = \frac{237.2 \times 1000}{2 \times 96485} = 1.23 \text{ V at 25°C}$$ **Equation 24**

Consider a fuel cell stack and let $H_{consumption}$ be the total hydrogen consumption rate (kg/s) for the stack, that is, the rate of hydrogen input. Then the power input to the fuel cell in terms of the energy content of hydrogen is:

$$P_{input} = H_{consumption} \times \frac{1}{2} \Delta h_f .1000 \quad \textbf{W} \qquad \textbf{Equation 25}$$

Given that 1 mole = 2 g of hydrogen.

If the hydrogen fuel utilisation (μ_f) coefficient is defined as:

$$\mu_f = \frac{Hydrogen\_used}{Hydrogen\_input} \qquad \textbf{Equation 26}$$

Then by Faraday's law, the total current (I) flowing in the external circuit is:

$$I = \mu_f .H_{consumption} .\frac{1}{2}.1000.2F \quad \textbf{A}$$
$$I = \mu_f .H_{consumption} .1000.F \qquad \textbf{Equation 27}$$

Alternatively the hydrogen consumption rate can be expressed in terms of cell current:

$$H_{consumption} = \frac{1}{\mu_f} \frac{I}{1000F} \quad \textbf{kg/s} \qquad \textbf{Equation 28}$$

Then power delivered at voltage V:

$$P_{output} = V.I$$
$$P_{output} = V.\mu_f .H_{consumption} .1000.F \qquad \textbf{Equation 29}$$

Hence the energy efficiency of a fuel cell (based on HHV) is given by:

$$\eta_{fuelcell} = \frac{P_{output}}{P_{input}}$$

$$\eta_{fuelcell} = \frac{\mu_f . V^{cell}}{1.48}$$

Equation 30

A typical relationship between cell voltage and current for a PEM fuel cell, that is, its V-I polarisation curve, is shown in Figure 16. This curve is the average polarisation curve per cell measured experimentally by Ali (2007) for a 10 W BCS PEM fuel cell stack (comprising ten cells in total). In the present model, the polarisation curve for an individual fuel cell is assumed to be a straight line with a slope and intercept so that it closely fits an actual curve over the typical operating range of the fuel cell.

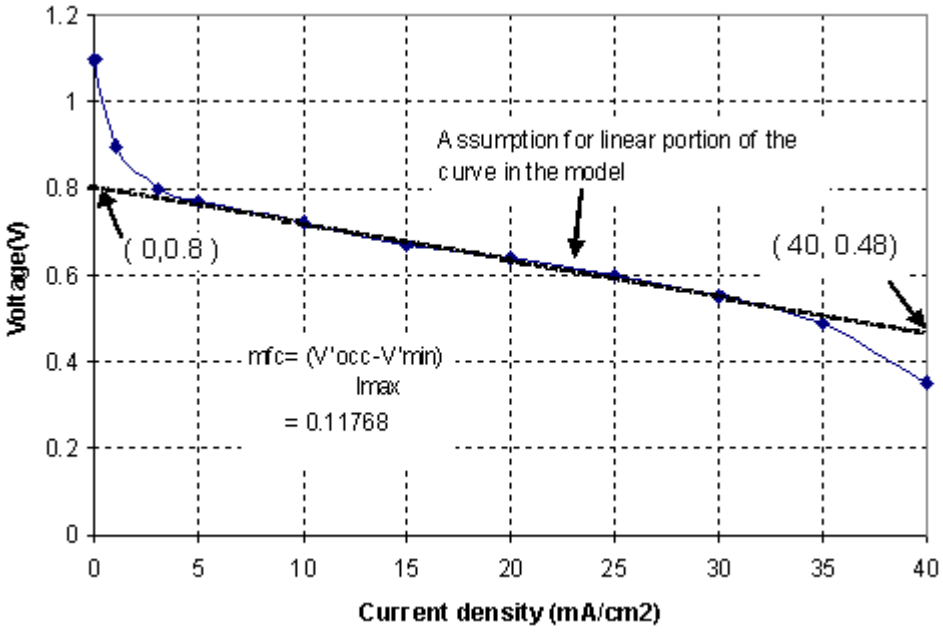

Figure 16: Polarisation curve of a single cell of a BCS fuel cell from experiment. A straight-line approximation is used through out the analysis of fuel cell submodel for ease of calculation (Ali, 2007).

Considering a single cell fuel cell, the power output of a cell is:

$$p_{output} = i^{cell} . V^{cell}$$

Equation 31

The instantaneous voltage (V^{cell}) formula can be written in terms of the cell's open circuit voltage ($V^{cell}_{cut\text{-}in}$), the slope of the approximated straight line (m^{cell}) and current i^{cell} as follows:

$$V^{cell} = V^{cell}_{cut-in} - m^{cell}.i^{cell} \quad \textbf{Equation 32}$$

Substituting for V^{cell} from Equation 32 into Equation 31, the power output equation becomes:

$$p_{output} = i^{cell}.(V^{cell}_{cut-in} - m^{cell}.i^{cell}) \quad \textbf{Equation 33}$$

Solving for cell current i^{cell} in terms of power output, open circuit voltage and slope yields:

$$i^{cell} = \frac{V^{cell}_{cut-in} \pm \sqrt{{V^{cell}_{cut-in}}^2 - 4m^{cell}p_{output}}}{2m^{cell}} \quad \textbf{Equation 34}$$

Only the negative root is used in the following analysis since it is the only solution that is physically valid.

For a fuel cell stack where N cells are connected in series to form a branch and M branches are connected in parallel to complete a stack configuration, the power output of a stack becomes:

$$P_{output} = (i^{cell}.M).(V^{cell}.N) = I.V$$

where $i^{cell}.M$ is equal to the total current output (I) of the stack and $V^{cell}.N$ is equal to the voltage output (V).

Cell current i^{cell} can be written in terms of cell open circuit voltage, cell slope, stack power output, number of cells in series and number of branches in parallel as follows:

$$i^{cell} = \frac{V_{cut-in}^{cell} - \sqrt{V_{cut-in}^{cell\ 2} - \frac{4m^{cell}P_{output}}{MN}}}{2m^{cell}} \qquad \textbf{Equation 35}$$

The hydrogen production rate ($H_{consumption}$) for any given power output of a fuel cell stack can then be found by substituting for i^{cell} from

Equation 35 into Equation 28 to give:

$$H_{consumption} = \frac{1}{\mu_f.1000F} \times \left(\frac{V_{cut-in}^{cell} - \sqrt{V_{cut-in}^{cell\ 2} - \frac{4m^{cell}P_{output}}{MN}}}{2m^{cell}} \right) \qquad \textbf{Equation 36}$$

The fuel cell submodel used in the present version of the wind-hydrogen system model is based on the 10-cell BCS fuel cell with a polarisation curve as described above. The rated power output of this fuel cell stack is 10-12 W at an operating pressure of 20.7 kPag and maximum operating temperature of 70°C. The electrode area of this unit is 10 cm^2 per cell. The open circuit voltage of the unit is 9.2 V, and hence 0.92 V on average for each cell. The voltage at which the maximum operating current (1 A) is drawn is 0.6 V for each cell. It is, however, a simple task to adapt the model to represent other fuel cells with different polarisation curves.

A more detailed explanation of the derivation of the formulae on which the model is based can be found in Ali (2007) and Larminie and Dicks (2003).

3.4 PROGRAM CONSTRUCTION

3.4.1 Introduction

The tasks performed by the simulation program to calculate power from the wind through to power to end users and energy storage in the form of hydrogen are shown in the flow chart in Figure 17. At the start of each simulation, the program will ask users to input data sets and use them throughout the entire run. The initial tasks are:

- Input the aerogenerator power curve provided by users or selected from built-in data sets to calculate power captured for each wind speed.
- Input an hourly wind data set over an annual period provided by users or selected from built-in data sets to calculate the wind power available.
- Input a hourly energy usage profile, which will be used for every day of the year provided by users.

The preferred condition – unconstrained or constrained hydrogen storage capacity – for sizing the hydrogen storage for the run is selected. The electrolyser size may be specified in the case of constrained electrolyser capacity. The program then assumes a turbine swept area of 1 m^2 to start off the simulation in the first iteration. The power available in the wind, the power captured by the aerogenerator, and hence the wind power surplus/deficit over the demand are calculated for each hourly wind data point and the corresponding hourly load, that is, for 8760 hours in total. The electrolyser, hydrogen storage and fuel cell submodels are then used to determine for each hour:

- The hydrogen production rate by the electrolyser
- The hydrogen delivered to the hydrogen storage
- The hydrogen usage rate by the fuel cell
- The hydrogen used from the hydrogen storage
- The net hydrogen inventory in the hydrogen storage.

It is essential for a stand-alone wind – hydrogen energy RAPS system to be able to meet the demand continuously throughout a year, and be self-sustaining through the seasons so that after each year's operation the hydrogen remaining in the storage is the same as at the beginning of the year. Hence the system can proceed to meet the next year's demand as it

did the year before. It is the variation through the year of the amount of hydrogen in the storage that is the key factor in ensuring this sustainability of operation from year to year. The basic conditions of the hydrogen storage to be met are thus:

- The amount of hydrogen in the storage must not go negative at any time during the simulation of a year's operation.
- The amount of hydrogen in storage at the start of the year must be equal or less than the amount in storage at the end, so that the net inputs to storage at times of high winds must counterbalance the net outputs at times of low or no wind.
- The program must ensure the storage limit (if set) is never exceeded.

Each iteration is thus a calculation for the whole year, proceeding stepwise hour by hour through the year, with one size of turbine swept area. If hydrogen gas in the storage at the end of the year is lower than the amount at the start, the program will increase the turbine swept area by a preset increment and restart the next iteration. Iterations continue until the required hydrogen storage condition is satisfied.

Initially, it is assumed the amount of hydrogen in storage at the start of the year is zero. Hence, once the basic hydrogen storage condition has been met – zero or slightly positive hydrogen in storage at the end of the year too – the hydrogen storage level may still go negative at some time during the year due to low wind speeds. The model then adds the minimum amount of hydrogen needed in the storage at the start of the year to avoid the inventory ever going negative. In this way the total magnitude of the storage capacity can then be found from the maximum amount in storage during the year.

Finally, the program will display the results for the particular run, including:

- Aerogenerator size (in kW)
- Electrolyser size (maximum kW electrical input)
- Hydrogen storage capacity (kg)
- Fuel cell size (maximum kW of power delivered)
- Hydrogen inventory in the form of a graph showing the variation in the level of hydrogen gas over the entire year.

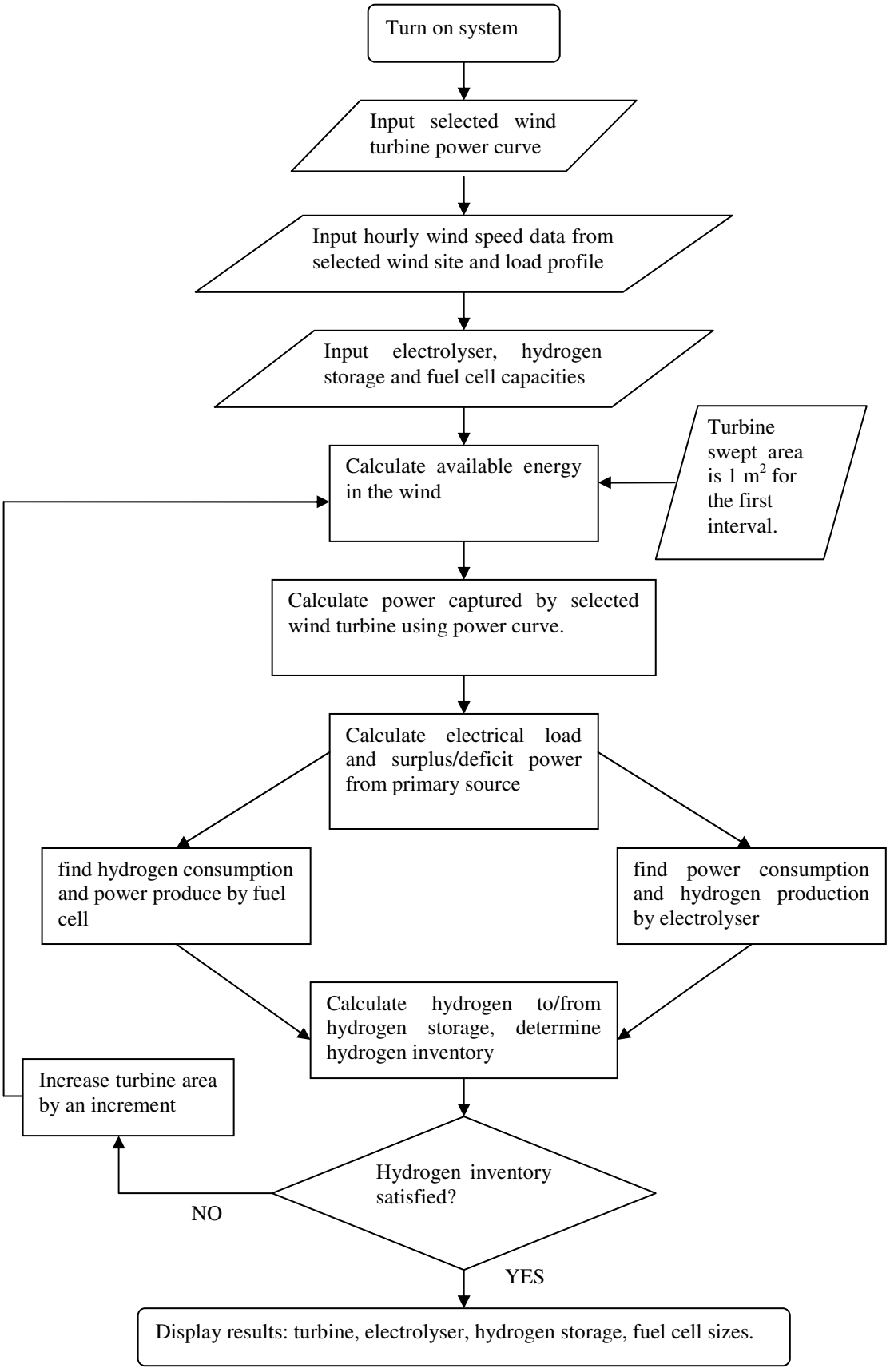

Figure 17: Flow chart showing the calculation steps in the wind-hydrogen energy system simulation program to satisfy the energy demand on a sustainable basis from year to year.

The fuel cell capacity is usually set to ensure the fuel cell can meet the peak power demand, so that this demand can be met even if there is no wind. Therefore this capacity is determined directly by the input load profile.

The electrolyser size in the standard form of the model is determined by the maximum excess wind power over the demand, so that all this excess can be used to produce hydrogen. Hence the electrolyser size is found once the aerogenerator size to meet the load sustainably is determined at the end of the iterative process. In other words, electrolyser size depends on aerogenerator size. Another condition that can be investigated, however, is to limit the electrolyser size at the beginning of a run, to see if a lower unit cost of power supplied results. Under the condition of a constrained electrolyser size, preset at the beginning of a run, the required aerogenerator size will depend on this preset electrolyser size. An example of applying this condition will be provided in the case study described in section **Error! Reference source not found.**.

Under the unconstrained storage condition, the storage capacity required will depend on the aerogenerator size. Under constrained storage, the reverse dependence occurs. The model in its present form finds the storage capacity, and aerogenerator size, such that the hydrogen inventory in the storage is exactly zero at its minimum. In practice, however, the aerogenerator, electrolyser and storage capacity would need to be increased above these theoretically minimum values so that there is some margin of contingency for unexpected events, variability in the wind regime, load profiles from year to year and system performance below that predicted. The level of surplus hydrogen needed to provide a specified high level of supply security has not been addressed in the present study, and is a topic requiring further detailed investigation in the future.

3.4.2 Factors influencing model accuracy and application

3.4.2.1 Step size and accuracy of the modelling

There are a number of factors that can affect the results of the simulation. The first is the selected step size for the increment of wind turbine swept area from one iteration to the next, which directly affects the speed and accuracy of the program. The larger the increment, the faster the program will run, but the less accurate the final result will be. The

value used in the following the case study is 0.1 m^2, but some variation in this value may be necessary to find the optimal value in other cases (see Appendix A).

3.4.2.2 Air density

The ambient air temperature and pressure affect air density and hence the power available in the wind. The relationship between dry air density, pressure and temperature is:

$$\rho = \frac{P}{RT} \qquad \text{kg/m}^3 \qquad \textbf{Equation 37}$$

where P is pressure (Pa), R is the specific gas constant of air (286.9 J/K.kg) and T is temperature (K) (Logan, 1999).

The default air density value used in the program is constant and equal to the annual average for Victoria (ρ=1.225 kg/m^3) (Natural Systems Research, 1987). According to Natural Systems Research (1987), the density of air can vary by some 20% over the range of temperature and pressure likely to be experienced along the coast of Victoria, Australia. The minimum air density in coastal Victoria is likely to be 1.1 kg/m^3 at a pressure of 98 kPa and a temperature of 30°C, which from equation 32 would result in a 10% lower power output for a given wind speed compared to that for the average air density. The maximum is likely to be 1.3 kg/m^3 at a pressure of 103.5 kPa and a temperature of 0°C, which would lead to a 6% higher power compared to the average. This variation in air density affects the power available in the wind and hence the results of the simulation.

3.4.2.3 Simulation of different hub height

Wind speed varies with height above the ground in a way depending on the surface characteristics. The wind speed v_2 at height h_2 can be estimated from the wind speed v_1 at height h_1 using the relationship:

$$v_2 = v_1\left(\frac{h_2}{h_1}\right)^{\alpha}$$ **Equation 38**

where α is the ground surface friction coefficient with a value depending on the local terrain (Patel, 1999). Typical values of α for various types of terrain are given in Table 2 (Patel, 1999).

Hence it is important to use wind speed data in the model that relates to the hub height of the aerogenerator. While meteorological wind data collection is normally done at a standard height of 10 m, aerogenerators are usually installed at greater heights than this. Therefore it is usually necessary to convert meteorological (or other) wind speed data to that for the specified hub height before these data are input into program using equation 34 as appropriate.

Terrain type	**Friction coefficient (α)**
Lake, ocean and smooth hard ground	0.1
Foot high grass on level ground	0.15
Tall crops, hedges and shrubs	0.2
Wood country with many trees	0.25
Small town with some trees and shrubs	0.3
City area with tall building	0.4

Table 2: Values of wind friction coefficient vary with types of terrain (Patel, 1999).

3.5 APPLICATION OF MODEL TO CASE STUDY AT KILCUNDA NORTH

3.5.1 Introduction to case study

The use of the simulation model will now be illustrated by applying it to a case study of a small wind – hydrogen system with a 400 W aerogenerator supplying the entire electricity needs of a remote homestead at Kilcunda North, near the coast some 100 km south east of Melbourne, and not connected to the main electricity grid. This is one of the sites for which hourly wind speed data at 10 m height are available for an annual period, and are already in the model (subsection 3.3.2). It is assumed that the hub height of the aerogenerator is also 10 m, and the ambient temperature stays constant at 25°C. While strictly the findings from this simulation are valid only for this particular site, they are clearly indicative of wind-hydrogen system performance at sites with similar wind speed regimes.

Initially, the system is studied under the unconstrained storage and unconstrained electrolyser size conditions (as defined in subsections 3.3.5 & 3.3.6). Subsequent runs of the model investigate the combined effects of progressively constraining both the hydrogen storage and the electrolyser size to find the optimal component sizes by using financial analysis.

The simulation results for all the runs conducted for aerogenerator size, electrolyser size and hydrogen storage are summarised in a three-dimensional graph so that if any two of the sizes are preset, the value of the third can be found.

3.5.2 Hourly wind speed data for Kilcunda North

As shown by Figure 18, at the Kilcunda North site over the period from 1 Feb 1985 to 2 Feb 1986 the most frequent hourly wind speeds were in the range 5-9 m/s (occurring for almost 3700 hours per year). The mean annual wind speed was 8.0 m/s with the maximum wind speed being just over 24 m/s. During this period, there were 165 hours of average hourly wind speed that exceeded the AIR 403's regular operating range (that is, wind speed more than 18 m/s).

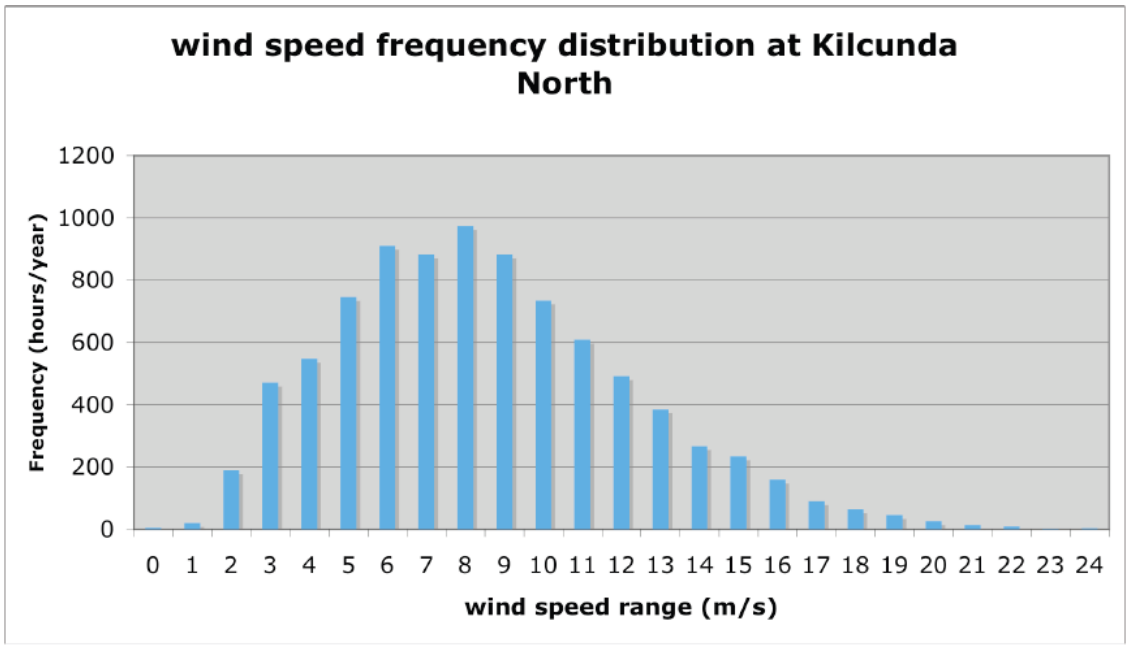

Figure 18: wind-speed frequency distribution for hourly wind data from Kilcunda North, Victoria, Australia from the 1 Feb 1985 to 31 Jan 1986.

3.5.3 Aerogenerator power curve

The AIR 403 aerogenerator was selected as the basis for this case study, and was also used in the experimental investigation of aerogenerator–electrolyser coupling conducted as part of this thesis and reported later in chapter 5. The power–wind-speed characteristic curve for this aerogenerator is shown in Figure 19 as supplied by the manufacturer (Southwest Windpower, 2001). The rated power of the unit is 400 W, which the curve shows can be obtained at a wind speed of about 12.5 m/s (28 mph). The curve shows the output rising to 800 W at a wind speed of 18 m/s. Over 18 m/s power output is limited to just over 100 W and the aerogenerator is shut down at 27 m/s and above. In the simulation model, the entire curve is represented by two equations, as described earlier in Table 1 subsection 3.3.3.

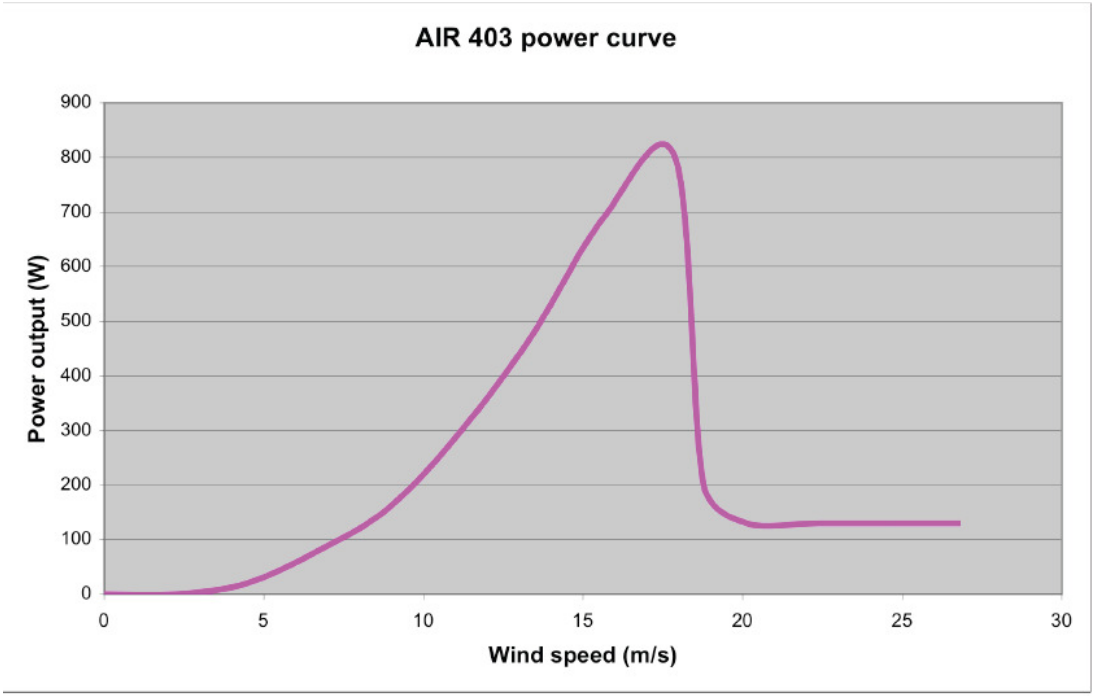

Figure 19: The AIR 403 power output curve provided by its manufacturer (Southwest Windpower, 2001).

3.5.4 Electrical usage profile

The hourly power demand profile over each day for a remote household assumed in the case study is shown by Figure 20, based on a scaled-down profile provided by El Paso Electric (2003). It is further assumed that this daily demand profile stays the same throughout the year. The total daily electricity use assumed is 5.9 kWh/day, which is low by Australian standards and would correspond to a household that does not use electricity for space and water heating, and generally uses power very efficiently for all other applications such as refrigeration, lighting and electronic and other electrical equipment.

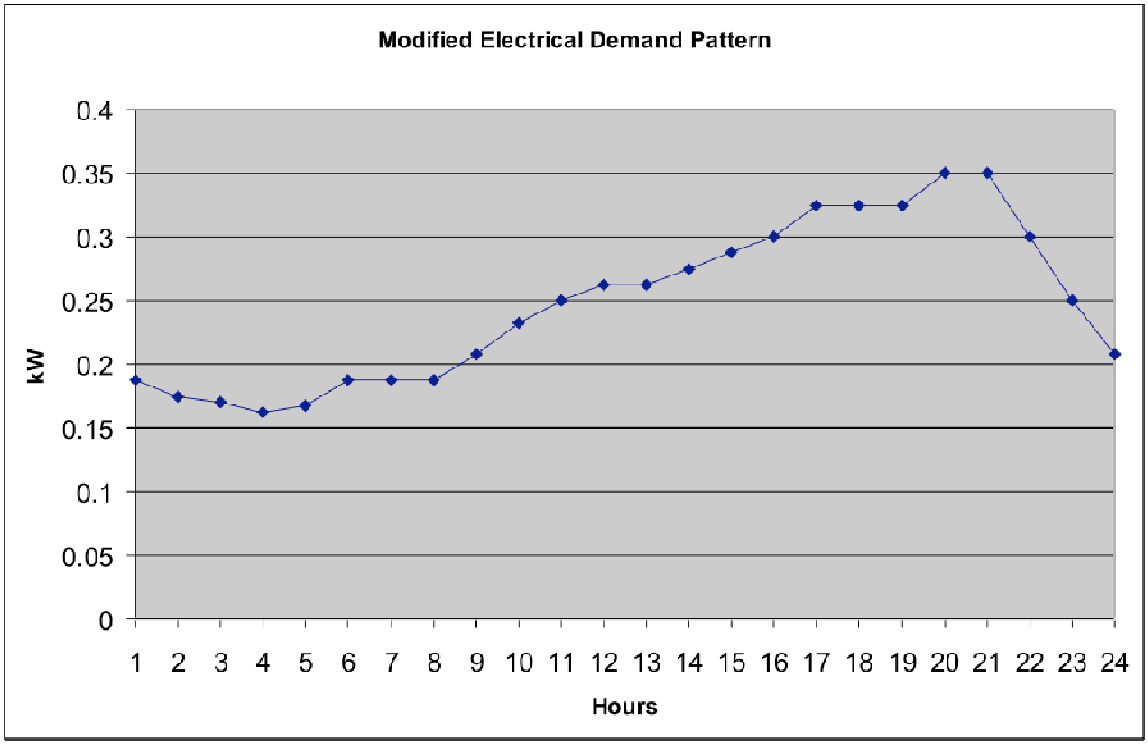

Figure 20 Daily electrical demand profile used in the case study, corresponding to a total demand of just 5.9 kWh/day.

3.5.5 Results for unconstrained storage condition

The simulation model was first used to determine the required capacities of aerogenerator, electrolyser, hydrogen storage and fuel cell to meet the specified hourly load throughout the year under the unconstrained storage condition. The results were as follows:

- aerogenerator capacity – 1.77 kW
- electrolyser capacity – 1.42 kW
- hydrogen storage capacity – 4.8 kg

  When hydrogen compressibility is considered at high pressure, which is common in hydrogen storage tank, Van der Waals formula is used to calculate storage volume (Boles and Cengel, 1998).

  - At 2 bar (absolute) storage pressure, its volume is 29.5 m^3
  - At 11 bar storage pressure, its volume is 5.4 m^3
- fuel cell capacity – 0.35 kW.

The corresponding variation of the mass of hydrogen in storage over the course of a year is shown in Figure 21. The maximum in stored hydrogen of about 4.8 kg occurs in April and

the minimum in November. There is clearly significant storage taking place between the seasons, that is, February-May to August-November. The low season is from June onward until December, where the hydrogen level fluctuates between 0 to 2.5 kg.

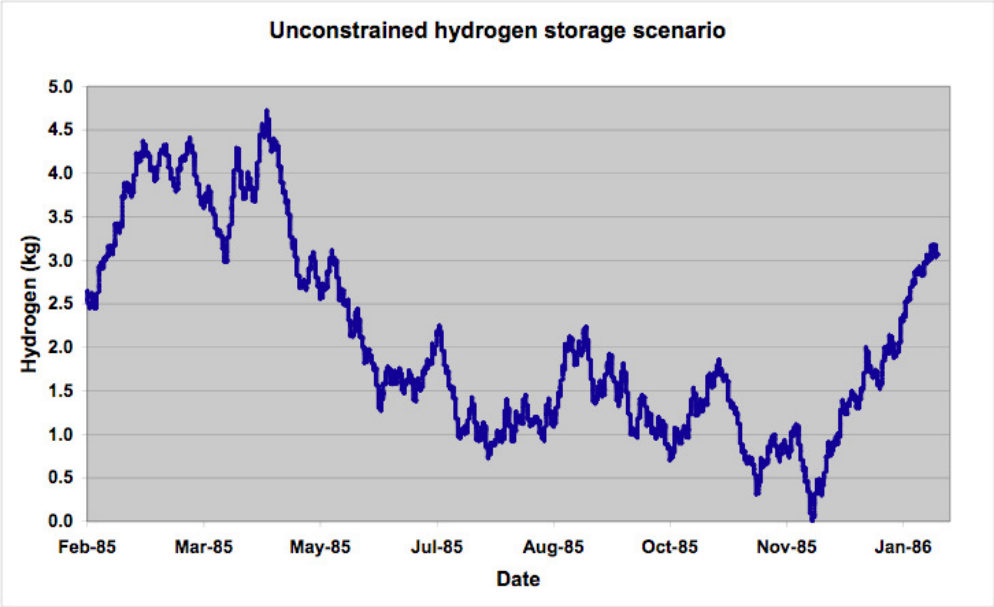

Figure 21: Hydrogen inventory in unconstrained electrolyser and unconstrained storage scenario for Kilcunda North.

3.5.6 Results for constrained storage condition

In the second scenario examined, the hydrogen storage capacity was constrained to 3.0 kg of hydrogen, but the electrolyser was sized to use all the surplus wind power. The results for the minimum component sizes were then as follows:

- aerogenerator capacity – 2.0 kW
- electrolyser capacity – 1.65 kW (unconstrained)
- hydrogen storage capacity – 3 kg (constrained)
    - At 2 bar storage pressure, its volume is 18.5 m^3
    - At 11 bar storage pressure, its volume is 3.4 m^3
- fuel cell capacity – 0.35 kW.

Under this condition, the required aerogenerator size rose from 1.77 kW to 2.0 kW, 13% larger than in the unconstrained storage scenario, since with less storage capacity a higher proportion of the annual load must be met directly from the aerogenerator. The electrolyser size was 1.65 kW to utilise potentially all excess power from aerogenerator, even if at times the storage was full so that no further hydrogen was produced.

The constrained storage is actually full (or very near full) for certain periods during the year, in particular from January to April and from November to January of the following year (Figure 22). The hydrogen inventory reaches its lowest point around June, thereafter rising fairly steadily through to October. The fuel cell capacity remains the same since it is determined directly by the maximum average hourly electrical demand of the household, independently of the other component sizes.

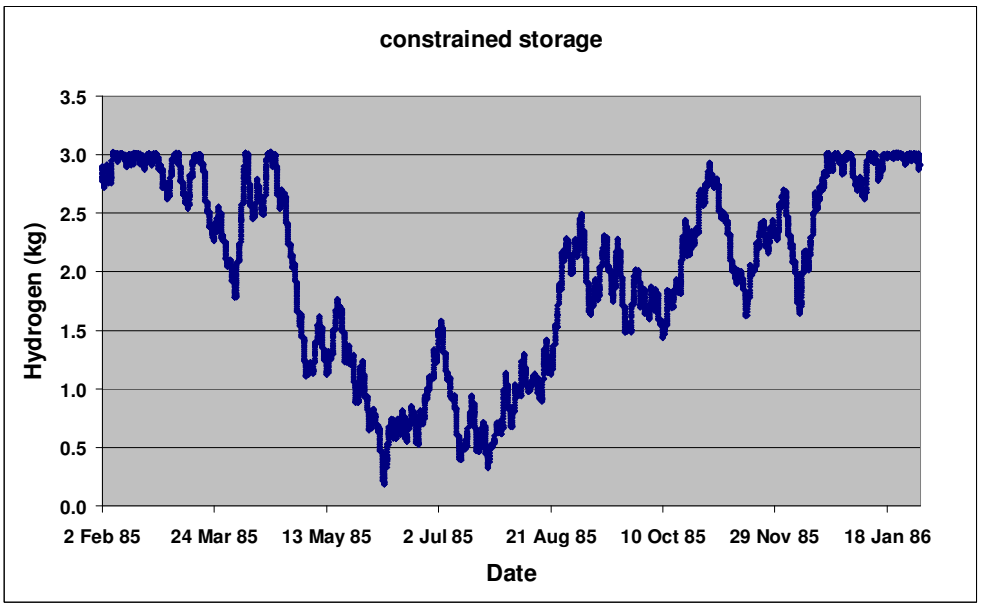

Figure 22: Hydrogen inventory in unconstrained electrolyser and constrained hydrogen storage (3 kg) for Kilcunda North.

3.5.7 Results for constrained electrolyser condition

In another scenario examined using the model, the hydrogen storage capacity was not constrained, but the electrolyser capacity was constrained. The results for the minimum component sizes were as follows:

- wind turbine capacity – 1.9 kW
- electrolyser capacity – 1.3 kW (constrained)

- hydrogen storage capacity – 4 kg (unconstrained)
    - At 2 bar storage pressure, its volume is 24.6 m^3
    - At 11 bar storage pressure, its volume is 4.5 m^3
- fuel cell capacity – 0.35 kW.

The system in this scenario is able to store all the hydrogen produced, but the hydrogen production is sometimes limited by setting the electrolyser capacity at 1.3 kW, which is lower than the surplus of wind power over load at certain times of the year. The aerogenerator capacity is thus greater than it is in the unconstrained storage – unconstrained electrolyser capacity scenario of subsection 3.5.5. As in the other scenarios, there are periods of high hydrogen storage from February to April and around January of the following year (Figure 23), There is also a low hydrogen storage time from May to December. In addition, this scenario obviously has a significantly higher hydrogen level at the end of the period than at the start, which could only be good for the following year. In principle, it would be possible to rerun the model reducing the aerogenerator capacity by a small amount (say 0.01 kW) each time until the hydrogen in storage at the end of the year is very nearly equal to that at the start. However, each run of the model takes considerable time, so that this fine-tuning of the sizing of the aerogenerator has not been done in the present case. The result quoted is in any case correct to one decimal place.

To conduct a simulation for this case it took two hours by using 0.1 increments of aerogenerator area and to fine tune this solution by using 0.01 increments, the computer would have to do 10 rounds of calculation in each 0.1 increment and thus would require 10 times longer. In this case, up to 20 hours are needed to get the desired solution, so that this fine-tuning of the sizing of the aerogenerator has not been done in the present case. The result quoted is in any case correct to one decimal place.

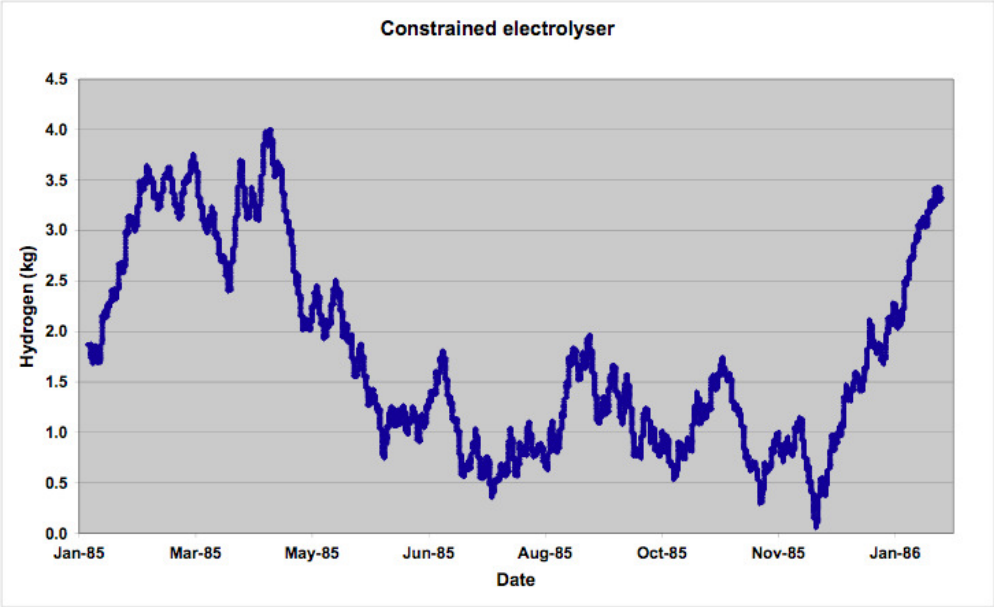

Figure 23: Hydrogen inventory in constrained electrolyser – unconstrained hydrogen storage scenario for Kilcunda North.

3.5.8 General system sizing

A general system sizing chart for a wind-hydrogen system supplying a remote household with the stipulated load at the Kilcunda North location was obtained by running the model for a range of different storage sizes and electrolyser capacities to determine the corresponding minimum aerogenerator capacity to allow the wind-hydrogen energy system to meet the load continuously throughout the year. The system configuration in the unconstrained storage condition where all surplus energy from the aerogenerator is converted to hydrogen is shown as a box on the lower right corner of the graph, corresponding to the smallest aerogenerator (1.77 kW) and largest hydrogen storage (4.8 kg) and electrolyser (1.42 kW) consistent with satisfying the electrical demand at Kilcunda North. The system sizes relating to progressively constrained (that is, reduced) storage capacities, while ensuring the electrolyser is always large enough to allow (potentially) all surplus wind power to be converted into hydrogen (even though this potential is not always realised due to a full storage), are plotted on the lower bounding dotted curve. On this

lower bounding curve, electrolyser size was always set equal to the maximum difference between the aerogenerator output and the load.

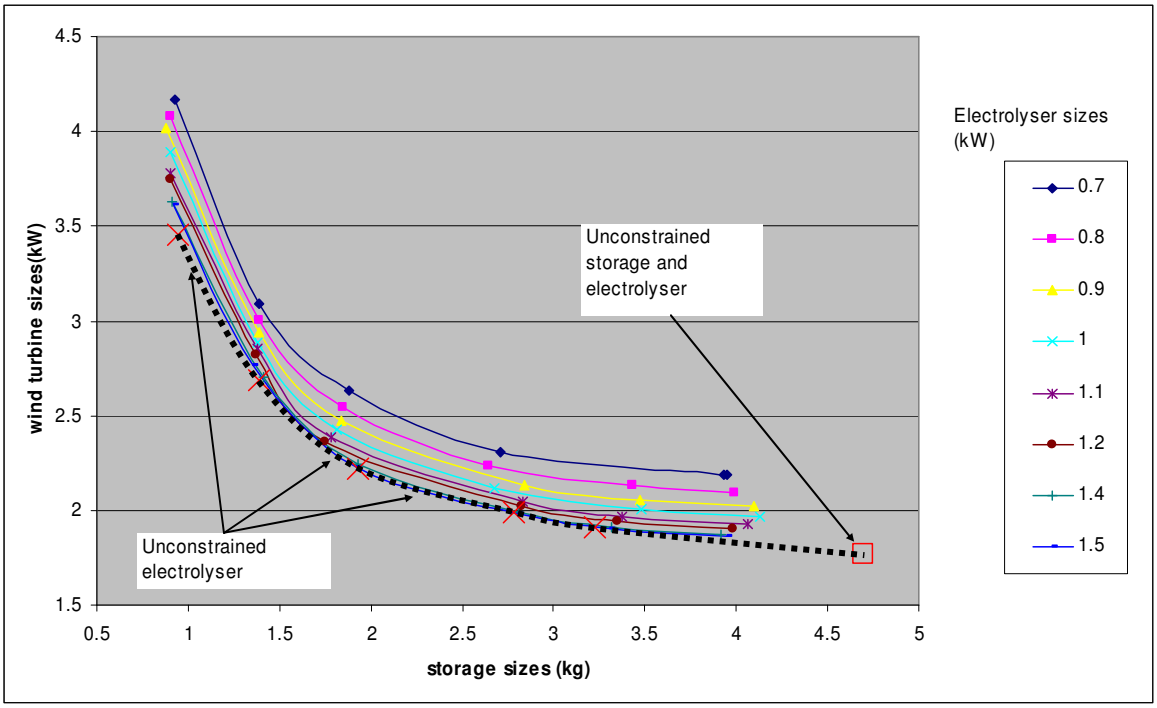

Figure 24: Wind – hydrogen energy system sizing chart for Kilcunda North. The horizontal axis represents hydrogen storage sizes (kg) and the vertical axis represents aerogenerator size (kW). Each curve corresponds to a different electrolyser size.

The other curves correspond to both a constrained storage and constrained electrolyser capacity. For a given constrained electrolyser capacity, the required aerogenerator size increases as the constrained storage capacity progressively decreases. The smaller the storage capacity is, the higher the proportion of the total load met directly by the aerogenerator (rather than from storage via the fuel cell) must be, so that a larger aerogenerator is needed. As the electrolyser capacity is progressively reduced for a given constrained storage capacity, the required aerogenerator size also increases, since overall less hydrogen will be produced and stored, and the aerogenerator must supply a higher proportion of the total load directly.

Overall there is a bounded range of aerogenerator size, storage capacity, and electrolyser size combinations consistent with meeting the load. In this case study, the smallest practical storage capacity is found to be around 1 kg of hydrogen, for which a range of paired aerogenerator and electrolyser capacities are consistent with meeting the load,

varying from a 3.4 kW aerogenerator and 1.5 kW electrolyser, to a 4.2 kW aerogenerator with a 0.7 kW electrolyser. The required aerogenerator size, however, increases steeply as the minimum possible storage capacity is approached.

3.6 ECONOMIC ANALYSIS

3.6.1 Economic analysis of wind-hydrogen energy system for case study

An economic analysis employing the Net Present Value method over 25 years to determine the unit average costs of power produced by the wind energy hydrogen systems under investigation in the Kilcunda North case study has been conducted. The assumptions of the analysis were as follows:

- Real discount rate: 5%
- Wind turbine and power electronics: capital cost of US$ 900/kW and US$800/kW respectively; lifetime 25 years
- Wind turbine tower: capital cost of US$3000; lifetime 25 years
- PEM electrolyser: capital cost of US$ 3000 per kW; lifetime 20 years
- PEM fuel cell: capital cost of US$ 6000 per kW; lifetime 15 years
- Balance of the system: capital cost of US$ 6000; lifetime 25 years
- Hydrogen storage: capital cost of US$ 2000 per kg of hydrogen; lifetime 25 years
- Maintenance costs: 2% of the equipment capital costs per year

It is considered at the beginning of this cost analysis that it must be comparable to an equivalent system: solar – hydrogen energy system. Comparing wind and solar system aims to establish good relative cost of these two technologies. However, previous cost analysises vary substantially according to system scale, component sizes to component specifications and therefore a good comparison could not be made accurately. Ali (2007) had carried out an analysis on a solar – hydrogen energy system set in south-eastern Australia to supply 5 kWh/day of electricity. Logically, this wind – hydrogen energy system is also based in south-eastern Australia and designed to supply the same amount of electricity. By utilising similar cost structure for all common components in a hydrogen energy system, a conclusion could be made about the relative electricity cost of these two

competing renewable technologies. Hence all cost parameters used in this cost analysis were referred to Ali (2007) except the following items:

- Wind turbine and power electronics' capital costs were the average of the commercially available items.
- Wind turbine tower was an average of ready-made towers available commercially.
- Hydrogen storage's capital cost of US$ 2000 per kg of hydrogen was referred to the most expensive storage option used by Ali (2007) to make this analysis conservative.

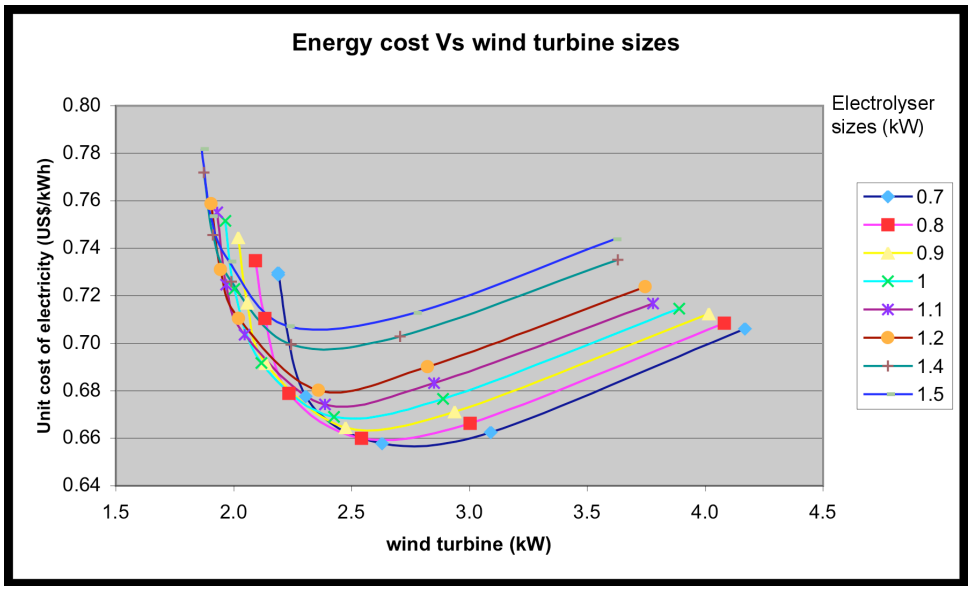

Figure 25: Unit electricity costs for the wind – hydrogen system for varying aerogenerator and electrolyser sizes in kW input.

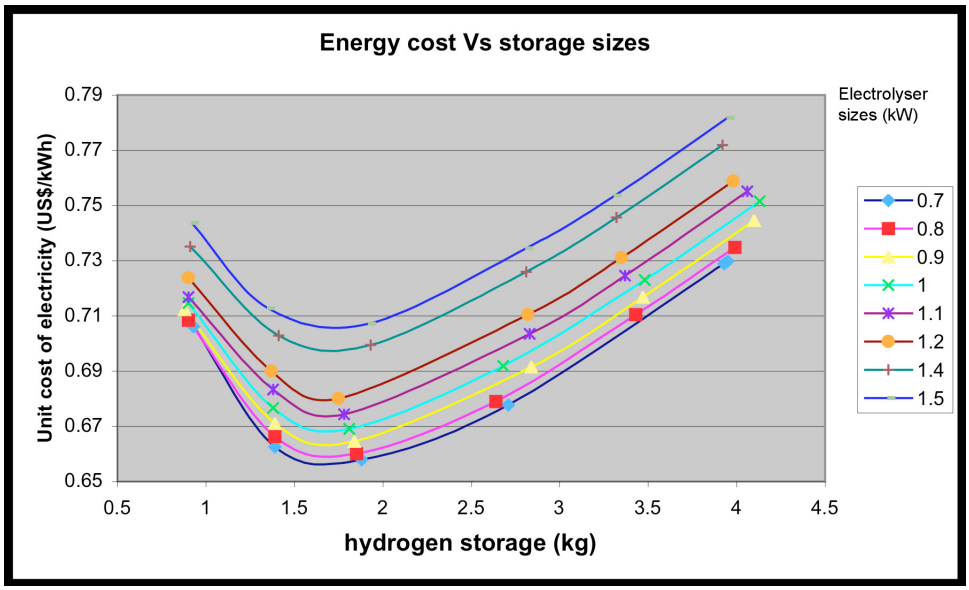

Figure 26: Unit energy costs for the wind – hydrogen system for varying hydrogen storage capacities in kg and electrolyser sizes.

Unit electricity costs are calculated by dividing the present value of the total costs (capital, including equipment replacement, and recurrent) over a 25 year period, and dividing this total by the total amount of electricity supplied over this period.

The results of the analysis are presented in Figure 25 for varying aerogenerator and electrolyser sizes, and for varying storage capacities and electrolyser sizes in Figure 26. It should be noted that each allowable system size comprises a combination of an aerogenerator capacity, a storage capacity, and an electrolyser capacity, that is, a point in a three-dimensional space. Once two of the three variables of an allowed combination are specified, the third is also determined. So each point on a curve in Figure 25 and Figure 26 specifies two variables, and the corresponding third variable can found by using Figure 24.

It can be seen from Figure 25 that, for these assumed unit component costs and a given electrolyser capacity, increasing the size of the electrolyser increases the unit costs of energy delivered. Importantly for each electrolyser size, there is an optimal aerogenerator capacity that minimizes the unit cost of energy. This optimal turbine capacity varies between 2.7 kW with a 0.7 kW electrolyser, and 2.3 kW with a 1.5 electrolyser. For each electrolyser size there is also an optimal storage capacity, in the range 1.5 to 2.0 kg of hydrogen for all electrolyser sizes.

Overall for this Kilcunda North case study, the minimum cost of energy obtainable from the wind hydrogen system modelled is around US$ 0.66 /kWh, corresponding to the following component sizes:

- wind turbine capacity: 2.6 kW
- electrolyser capacity (minimum): 0.7 kW
- hydrogen storage capacity: 1.9 kg
- fuel cell capacity: 0.35 kW

The economic analysis has been repeated with the cost of power electronics (for aerogenerator – electrolyser coupling) omitted and the graph of cost of energy produced versus aerogenerator capacity is shown in Figure 27 and that of unit cost versus hydrogen storage size in Figure 28. Apart from the obvious fact that the capital cost is reduced, in this case by US$ 800/kW, the unit cost of energy produced also drops.

Comparing Figure 25 to Figure 27, the minimum unit cost for a system without power electronics drops from US$ 0.66/kWh to US$ 0.57/kWh (a 14% reduction) and the most economic system would employ a 3.0 kW aerogenerator rather than a 2.6 kW one. Although, the economically optimal electrolyser capacity stays the same, the optimal hydrogen storage is reduced from 1.9 to 1.5 kg of hydrogen.

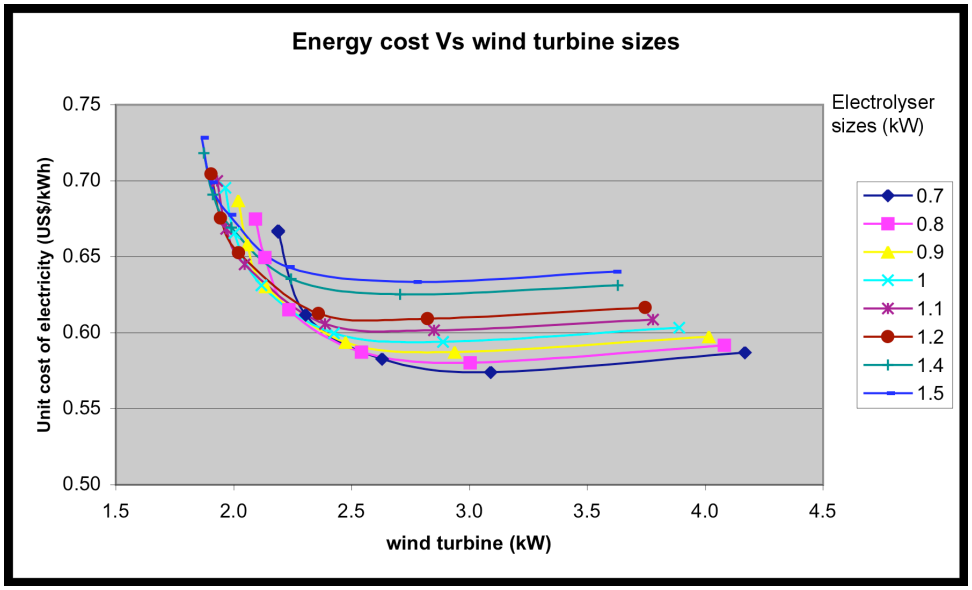

Figure 27: Unit electricity costs for the wind – hydrogen system for varying aerogenerator and electrolyser sizes in kW input, where the cost of power electronics is eliminated.

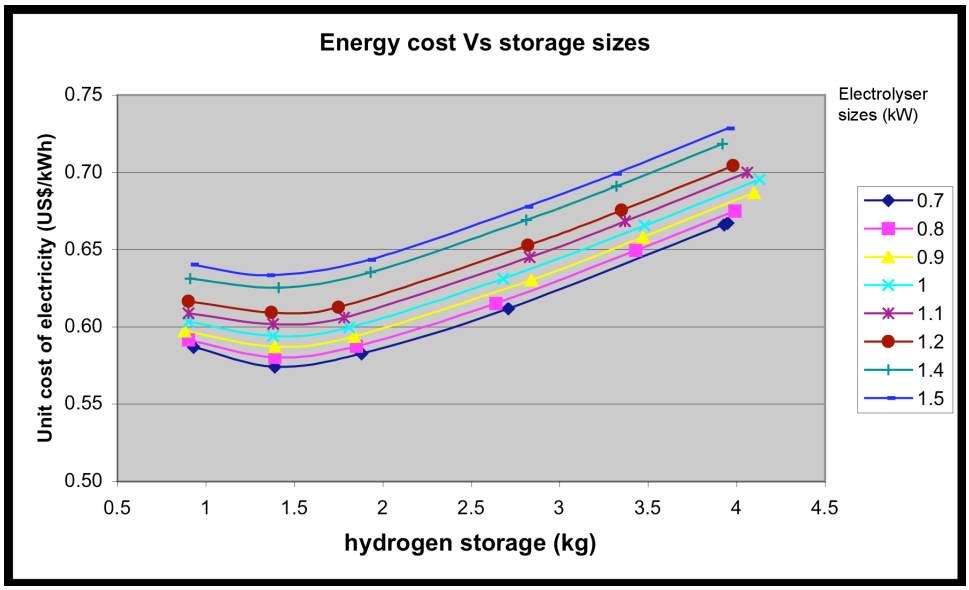

Figure 28: Unit energy costs for the wind – hydrogen system for varying hydrogen storage capacities in kg and electrolyser sizes, where the cost of power electronics is eliminated.

It is determined that the most suitable electrolyser size is 0.7 kW, and the capacity of the fuel cell is then varied to investigate the effect of average hourly peak load on the cost of energy because the fuel cell is sized to supply peak electricity demand. Originally, the average hourly peak load is limited to 0.35 kW according to the load profile discussed (section 3.5.4), but this average hourly peak load is considered to be too low and does not reflex real applications. Therefore the average hourly peak load is increased and they are 0.5, 0.75 and 1 kW. As expected the unit cost of electricity increases with the sizes of fuel cell. It is noticeable that the increase is consistent from 0.5 to 0.75 and 1 kW, the rise is by US$0.05/kWh. As a result, the electricity cost per unit energy of a wind – hydrogen energy with a specified electrolyser capacity and a fixed aerogenerator size will increase proportionally with the fuel cell size or average hourly peak load. And hence it is important for users of an energy system to reduce their average hourly peak load by ways of reduction of consumption or spreading the load.

It should be noted that these unit cost estimates, and the associated minima, are highly dependent on the assumed unit capital and operating costs of system components stated at the beginning of this section. In particular if the unit storage costs were reduced, it would be expected that the optimal system would employ a larger storage capacity, and probably a larger electrolyser capacity while the aerogenerator size would be reduced.

3.6.2 Comparison of costs with competing systems

Wind – hydrogen energy systems competes against PV – hydrogen, and other conventional RAPS systems such as wind – battery, PV – battery and diesel generators.

According to Ali (2007), whose financial analysis uses similar assumptions as in the present analysis, the unit cost of energy for PV – hydrogen energy system at a location similar to the one studied here (that is, southern Victoria, Australia) is US$ 2.5/kWh. Hence on these assumptions the PV – hydrogen system is almost four times more expensive than the wind – hydrogen system (power electronics included). However, at sites with lower wind speeds and higher solar irradiance the differential could be very different. According to Ali (2007) the PV – battery system has a slightly higher unit cost than its hydrogen equivalent. The PV – battery system produces electricity at US$ 2.8/kWh, whereas a similar system with the addition of a diesel generator set reduces the energy cost to US$ 2.3/kWh. Furthermore, a diesel – battery system would generate electricity at a cost of US$ 1.9/kWh. However, 2007 diesel prices were used in these estimates, and the expected real price increases in diesel since then and in the future are likely to increase the unit cost of power from the diesel systems substantially.

A study by Shakya *et al.* (2004) whose PV – hydrogen RAPS system uses similar components to the one studied in the present work but was designed to provide 69 kWh of energy per day found a unit energy unit cost of US$ 1.94 /kWh (AUD 2.52/kWh) for a 25-year operating life.

The cost competitiveness of wind – hydrogen energy systems for RAPS are clearly highly sensitive to the assumptions made. Costing of items that are not yet mass produced such as PEM electrolysers, fuel cells and hydrogen storages are subjected to changes in the future, most probably in the direction of lowered costs. However, the analysis conducted here, albeit preliminary, shows that wind-hydrogen systems are already approaching economic viability at a good wind site.

3.7 CONCLUSIONS

The wind–hydrogen system simulation model presented in this chapter has been found to be a useful tool to study the effects of component sizes on the unit costs of the electricity supplied of the system. A customised Visual Basic program has been constructed to carry out the calculations, where data input sets for various components are available for others to use. Users can conveniently select data from dialog boxes presented in sequence as the program progresses.

The simulation model has been applied to a case study of a wind-hydrogen system supplying the electricity demand of a remote household at for coastal site near Melbourne to serve as an example of component and system sizing, and the relationships between component sizes that stem from the need to satisfy the energy requirement continually throughout the year. For example, if the hydrogen storage capacity is reduced, the aerogenerator and electrolyser must be upsized. The exact results obtained from any run of the model are strictly applicable only to the site used, given that the wind speed data are unique to that site. However, the results may be indicative of the situation for other sites with a similar wind speed regime over the year.

The model has also been used to find the average unit cost of electricity delivered on a lifecycle basis by the wind-hydrogen system for given input assumptions about the unit capital costs of the system's components. The effects of component sizes on unit costs have been examined, and economically optimal combinations of sizes found. The optimal system found gave a unit cost of power of US$ 0.66/kWh. If the power electronics could be eliminated this cost reduces by 14% to US$ 0.57/kWh. This unit cost is very competitive against that for a PV-battery system at the same location (~US$ 2.8/kWh) or a diesel – battery system (~US$ 1.9/kWh).

However, the economic analysis of wind-hydrogen energy systems conducted is clearly very sensitive to the assumptions made about component costs and lifetimes. Some items are not commercially available as yet, so that there are inherent uncertainties in the costing. In addition, the competitiveness of such systems is very site dependent, and the case study presented here has been for a coastal site with a relatively high annual mean wind speed of 8 m/s.

4 THEORETICAL INVESTIGATION OF DIRECT COUPLING OF A FIXED-PITCH VARIABLE SPEED AEROGENERATOR AND PEM ELECTROLYSER

4.1 INTRODUCTION

This chapter presents a theoretical investigation of direct coupling of a fixed-pitch variable-speed aerogenerator to a PEM electrolyser stack using a steady-state model, that is, one in which it is assumed the aerogenerator attains its maximum electrical output at any given wind speed. The theory of direct coupling to achieve near optimal energy transfer by matching the V-I characteristic curves of the aerogenerator and electrolyser are explained. The theory is applied to a case study of a small aerogenerator (an AIR 403 400 W unit) at a particular site (Kilcunda North on the coast near Melbourne) coupled to a particular PEM electrolyser.

The conventional method of coupling an aerogenerator to a load is to use an electronic unit to match the voltage and impedance characteristics of both components. The power electronics used in RAPS systems in the market today are primarily designed for conventional wind-battery or solar-battery energy systems. Some units may be adapted for use in coupling an aerogenerator to an electrolyser, but there is no equipment built specifically for this purpose available currently. Some manufacturers of existing interfacing units provide options for adjusting the voltage and current output over a wide range. However, using these units in wind – hydrogen systems obviously will incur costs and some inefficiencies depending on the units concerned.

These interfacing units basically need to convert variable AC power input from an aerogenerator to stable DC power. The DC voltage and current output from the unit must be within ranges that suit the particular electrolyser unit (Figure 11, section 3.3.5). The units consume power and generate heat, so the conversion of input power to output power is always less than 100%. Most such units have energy efficiency in the range 80-95%. For example, the rated efficiency of the Xantrex XW hybrid inverter/charger at low load is up to 95% (Xantrex Technology Inc., 2008). At high load it can be expected that the energy efficiency would be lower than this figure.

Another function that can be provided by interfacing power electronics is that of maximum power point tracking. In principle, an aerogenerator must be loaded at a certain power in order to work at its maximum efficiency and hence maximum output power a given wind speed. This means that ideally the load needs to vary as wind speed changes to generate maximum power at every wind speed. This apparatus is not a readily available item in the market unlike the case for solar panel systems, though some progress has been made by National Renewable Energy Laboratory (NREL) in the USA towards development of a commercial maximum power point tracker for a small aerogenerator (Corbus et al., 1999).

Simulations of maximum power point tracking techniques have been done by many researchers, such as Miland *et al*. (2006) and Beukes and Moore (2004). The tracking device requires an instantaneous wind speed to be measured and then the appropriate load is calculated by relying on the aerogenerator's maximum power curve. The load is automatically adjusted according to the output of this calculation. There are two methods of determining wind speeds suggested: anemometer output and electrical output frequency (Beukes and Moor, 2004):

- An anemometer can be used to measure wind speed at an instant then a maximum power point tracker will determine V-I combination from a look-up table program into the system.
- An electrical output frequency can be related to rotor RPM (synchronous generators) and thus maximum power for that RPM can be found from its generator characteristic.

A combined inverter/charger from Xantrex suitable for a wind-hydrogen energy system can cost US$ 500-800/rated kW (Infinigi, 2008, Gogreensolar, 2008, Alter systems, 2008). The present research project has not involved any independent experiments to test the performance of available interfacing electronic units. Information on their performance and costs has come from published academic and product literature.

What the present project does focus on is the possibility of directly coupling the aerogenerator and electrolyser in a wind – hydrogen energy system. The costs of the interfacing electronics, and their energy conversion losses, would thus be avoided. But the question to be answered is the degree to which the energy transfer and hydrogen production under direct coupling can approach the maximum achievable through

maximum power point tracking over the full range of operational wind speeds of the aerogenerator.

In direct coupling clearly the DC voltage and current output from the aerogenerator after rectification must match the corresponding ranges of the electrolyser. In addition, to achieve maximum power transfer between these two components, the maximum power curve of the aerogenerator plotted on a V-I graph over the range of operational wind speeds must ideally be identical to the V-I input characteristic of the electrolyser.

4.2 THEORETICAL INVESTIGATION OF DIRECT COUPLING IN STEADY STATE USING OPTIMAL MATCHING OF V-I CHARACTERISTIC CURVES: STEADY STATE MODEL

4.2.1 Electrolyser V-I characteristic curve

If an aerogenerator is to be directly coupled to a PEM electrolyser, ideally the V-I characteristic curve of the electrolyser needs to track the V-I curve of the aerogenerator over all operating wind speeds. The V-I curve of a typical single PEM cell is shown in Figure 29, labelled the '1 cell characteristic'. The current is effectively zero until the applied voltage reaches the cut-in value of about 1.5 V, and then rises linearly with increasing voltage up to its maximum value of 4 A at 2 V for this particular cell. Normally, a number of cells are connected together to form a stack. Hence in practice the V-I curve of an electrolyser stack may be altered by changing the series and parallel configuration in which the individual cells are connected.

As two single cells are stacked in series the cut-in and maximum operating voltages increase linearly with the number of cells, the slope of the V-I curve decreases, while the maximum current stays the same (see '2 cells in series connection' in Figure 29). As two cells are connected in parallel, the current for a given voltage doubles, the cut-in and maximum voltages stay the same, and the slope of the V-I curve increases. The curve is thus in effect stretched out along the current axis (see '2 cells in parallel connection' in Figure 29).

Hence in general the ways that the V-I curve of an electrolyser stack based on a particular basic cell can be altered are as follows:

- Connecting cells in series increases the cut-in and maximum operating voltages in direct proportion to the number of cells, and steadily decreases the slope of the curve, while the maximum current stays the same
- Connecting cells in parallel increases the current for a given voltage (including the maximum current) in direct proportion to the number of cells, and steadily increases the slope of the curve, while the cut-in and maximum voltages stay the same

By varying the series-parallel connection configurations of the basic PEM cells the cut-in voltages, V-I curve slopes, and voltage and current limits of an electrolyser stack can be altered in an effort to match the maximum-power V-I curve of an aerogenerator over the range of operational wind speeds as closely as possible.

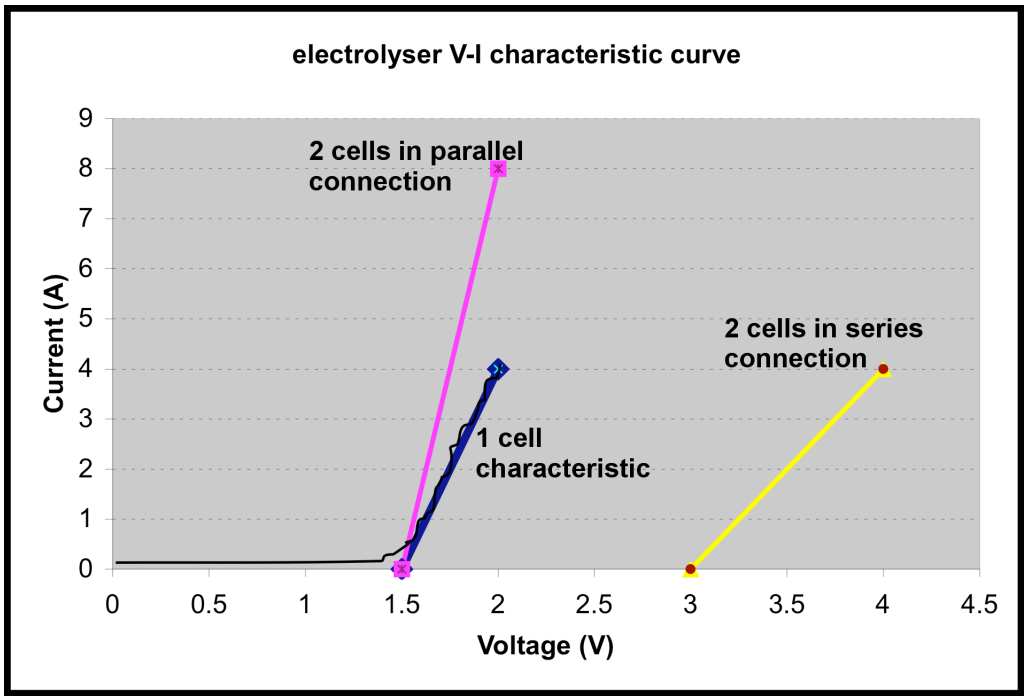

Figure 29: The effects of varying series–parallel connection configurations of PEM electrolyser cells on the V-I characteristic curve of the stack. Connecting two cells in series doubles the cut-in and maximum voltages, whereas parallel connection of two cells doubles the current for a given voltage, including the maximum current.

4.2.2 Aerogenerator V-I characteristic curve

A fixed-pitch variable-speed aerogenerator has a V-I characteristic curve for each wind speed that is unique to its construction. The output voltage and current at a given wind speed depend among other factors on the number of poles and coil windings of the electrical generator. At the same wind speed, a generator can produce high voltage but low current, while another design of the electromagnets will produce high current and low voltage. The influence of the number of poles on the rotor of the generator on the V-I curves for a given wind speed is shown in Figure 30, where the load resistance is varied to give each characteristic curve. It can be seen that as the number of poles increases, the voltage increases and the current decreases for a given load.

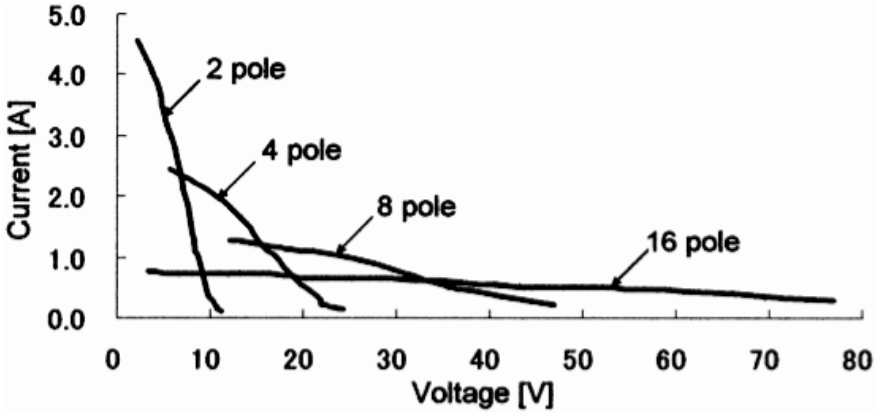

Figure 30: V-I curves of permanent magnet generators with various pole numbers connected to a aerogenerator operating at a constant wind speed (Kazuto et al., 2008).

At a constant wind speed, the aerogenerator can be operating at any point along its V-I characteristic corresponding to that wind speed with the particular point depending on the load applied. However, there is only one V-I combination – that is, point on the characteristic – that will yield the maximum power output at that wind speed. This point is called the maximum power point (MPP), and is shown in Figure 31. The maximum power curve (MPC) for the aerogenerator can then be constructed by linking the maximum power points on the set of characteristic curves for each wind speed.

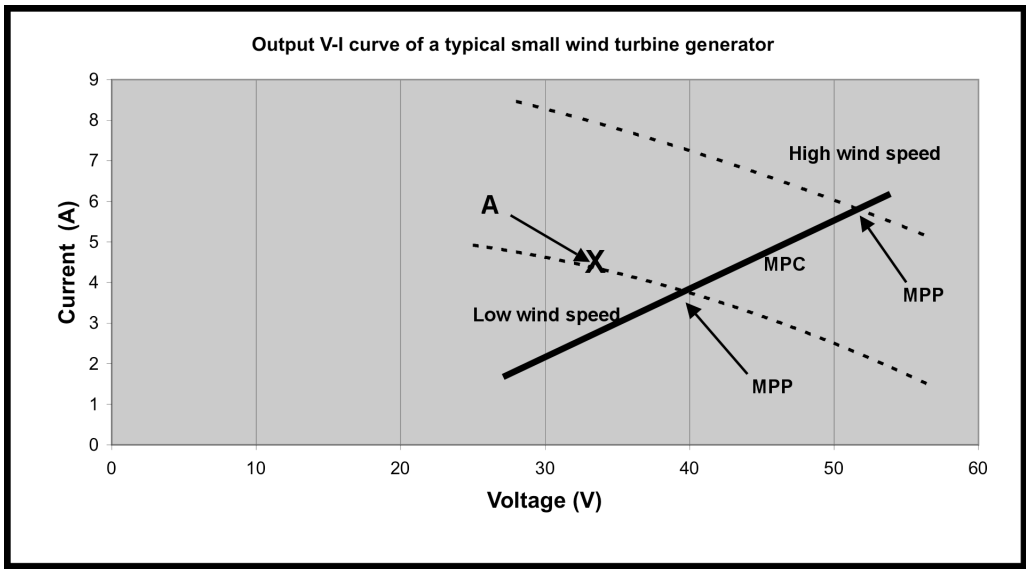

Figure 31: Simplified V-I characteristic curves at a high and low wind speed for a small fixed-pitch variable-speed aerogenerator derived from figure 34. At high wind speed, the product VI, that is, the power output, is higher than that at the low wind speed. At each wind speed, the load can be varied to change V and I to find the maximum power point (MPP).

If a load is connected to a generator and draws a combination of voltage and current as indicated at point A in Figure 31, then the load is not able to extract the maximum power from that generator. The power transfer loss $P_{transloss}$ is calculated by:

$$P_{transloss} = P_{MPP} - P_A \qquad \textbf{Equation 39}$$

where $P_{MPP} = V_{MPP} \,.\, I_{MPP}$, the power production at the maximum power point for the lower wind speed, and $P_A = V_A \,.\, I_A$ is the power production at point A.

The power transfer efficiency (η_{trans}) between the aerogenerator and the connected load at this particular point without considering any other losses is given by:

$$\eta_{trans} = \frac{P_A}{P_{MPP}} \qquad \textbf{Equation 40}$$

There are several ways a V-I curve of an aerogenerator can be altered:

- Changing the permanent magnet of the electrical generator
- Changing the configuration and number of turns in the coils of the stator winding
- Changing of number of poles of the stator windings

It has not been possible in the experimental program of the present project to explore the possibility of altering the electrical generator to change the V-I characteristics of the overall aerogenerator due to limitations of time and technical resources. However, in general, it is certainly worthwhile in future work to consider such options and design an aerogenerator to match a particular electrolyser stack. In principle a better match between the V-I characteristics of the aerogenerator and electrolyser can be found if both characteristics can be varied.

4.2.3 Direct coupling a fixed-pitch wind aerogenerator and PEM electrolyser

In direct coupling the aim is to find a series-parallel stacking configuration of individual electrolyser cells (or small stacks of these if they are already assembled in units) that yields an overall V-I curve (Figure 29) that tracks the MPC of a given aerogenerator as closely as possible (Figure 31). It is clearly desirable to have an electrolyser V-I curve that tracks the MPC of the aerogenerator at all operating wind speeds, although this is not always possible. In practice the aim is therefore to match the two V-I curves as closely as possible taking into account the wind frequency distribution and the power output at each wind speed.

Once a load is connected to a fixed-pitch aerogenerator, the working voltage and current will follow the V-I characteristic curve for the prevailing wind speed, assuming the steady state output of the aerogenerator has been attained. As a result, the system will have a $P_{transloss}$ at this wind speed if the V-I point, set by the electrolyser characteristic, does not sit on the MPC of the aerogenerator. The MPC of an aerogenerator and two alternative V-I characteristic curves of a PEM electrolyser (A and B) are shown in Figure 32. If the aerogenerator is directly coupled to electrolyser A, line A and the MPC diverge increasingly as wind speed increases, so the power loss compared to the maximum achievable (at MPP operation) increases too. At lower wind speeds line A and the MPP are closer together so the power loss is much less. When directly coupled to electrolyser B,

however, line B and the MPP are not so far apart at higher wind speeds, so the power transfer efficiency at these speeds will be better than in case A. In practice the wind speed at any site is variable so it is necessary to know the wind speed frequency distribution and work out the total energy transfer over an annual period, taking into account the power transfer efficiency at each wind speed, to determine the best electrolyser configuration from the point of view of annual energy transfer from the aerogenerator.

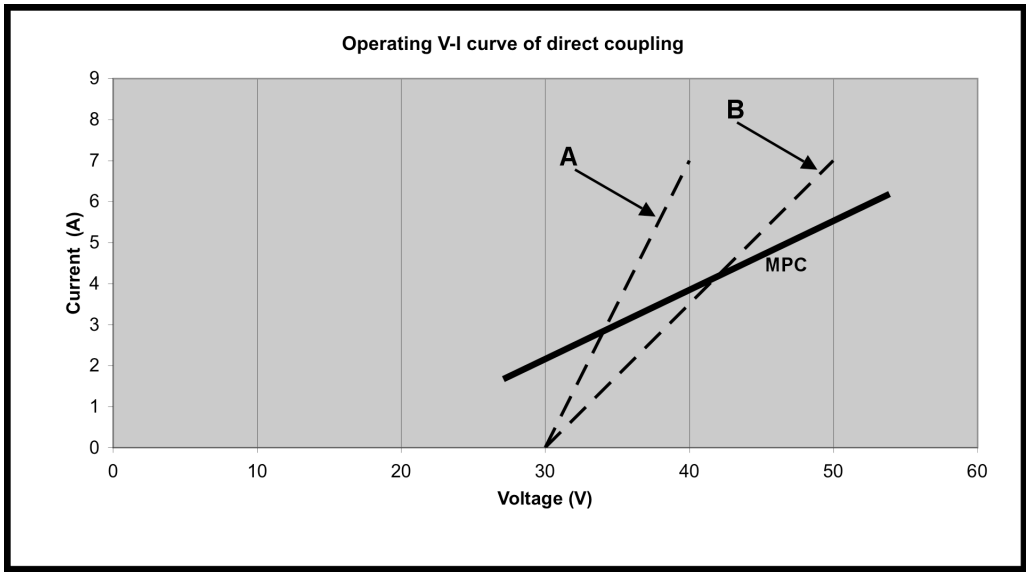

Figure 32: Operating V-I curves of an aerogenerator with maximum power curve MPC direct coupled to two different electrolyser stacks (with characteristic curves A and B). The energy transfer between the aerogenerator and electrolyser will for stack A be more efficient in the low wind speed range, while that for electrolyser stack B will be better in the high wind speed range.

4.2.4 Wind speed frequency distribution

The main aim of direct coupling in a wind – hydrogen energy system is to maximise energy transfer between an aerogenerator and an electrolyser stack that produces hydrogen. There is generally a close relationship between the annual energy transfer and the total annual hydrogen production of the electrolyser, as explained in Paul (2009).

Hence the maximum rate of hydrogen production generally occurs close to the condition for the maximum energy transfer. The aim then is to find the optimal matching between the MPP of the aerogenerator and the V-I characteristic of the electrolyser that maximises the total energy transfer over a period of a year when the aerogenerator is operated at a

particular site with a known wind speed frequency distribution. The best series-parallel electrolyser configuration is thus likely to be site dependent, since over a year the occurrence or frequency of a wind speed in a given wind speed range will vary from site to site, and hence the amount of energy transfer in this range will also vary.

To find the energy transfer for an aerogenerator directly coupled to a given electrolyser (that is, with a particular series-parallel cell-connection configuration and hence V-I characteristic), it is first necessary to find the annual wind speed frequency distribution for the site. By counting the number of occurrences or frequency of measured wind speeds within a series of defined ranges over a period of a year, a wind speed frequency distribution can be drawn, as shown in Figure 33.

The total energy transfer between the aerogenerator over a year will be a product of the rate of energy transfer (power) when a wind speed is in a particular range and the total combined time the wind speed is in this range.

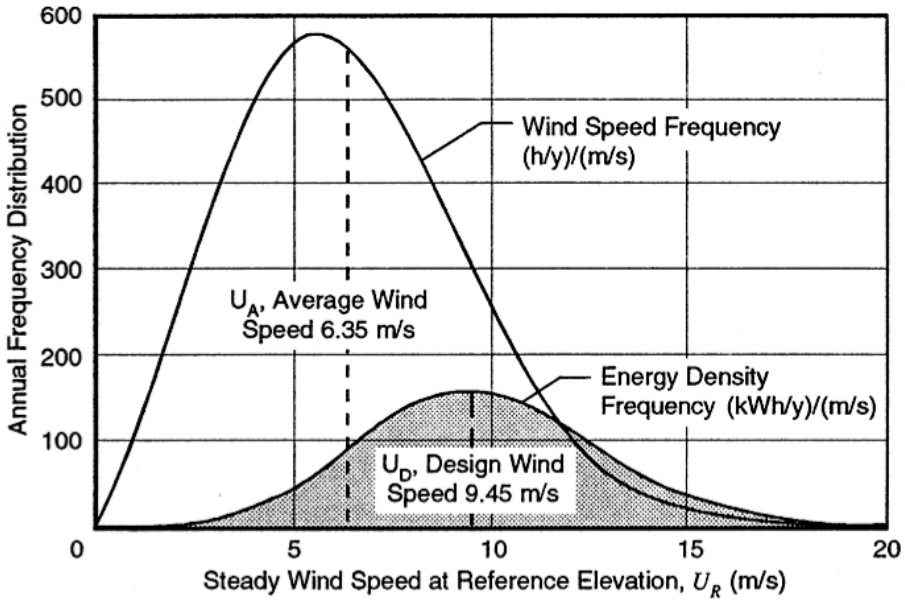

Figure 33: A typical wind speed frequency distribution (Mukund, 1999). In this case, most of the time wind speeds are around 5-6 m/s. High wind speeds above 10 m/s provide more instantaneous power but occur less frequently than the wind speeds clustered about the annual mean.

The difference between the power transfer under perfect maximum power point matching ($P_{MPP}(v_i)$) and power transfer ($P_{elec}(v_i)$) that occurs for the V-I curve of a particular series-parallel stacking configuration of an electrolyser cells at a given wind speed range (v_i) is $P_{transloss}(v_i)$ and can be calculated by Equation 41. Over a period of a year, the loss compared to the ideal MPP matching condition, $E_{transloss}$, is given by Equation 42. Moreover, the actual total energy transfer over a year, E_{trans}, is given by Equation 43.

$$P_{transloss}(v_i) = P_{MPP}(v_i) - P_{elec}(v_i) \quad \textbf{Equation 41}$$

$$E_{transloss} = \sum_{i=1}^{N} \{[(P_{MPP}(v_i) - P_{elec}(v_i))] \times t \times f_i\} \quad \textbf{Equation 42}$$

$$E_{trans} = \sum_{i=1}^{N} \{P_{elec}(v_i)\} \times t \times f_i\} \quad \textbf{Equation 43}$$

where:

$P_{transloss}$ = instantaneous power (W) transfer loss

$E_{transloss}$ = accumulated energy (J) transfer loss over a year

E_{trans} = accumulated energy (J) transfer over a year

P_{MPP} = power (W) production at MPC line at that wind speed

P_{elec} = power (W) production at electrolyser V-I curve at that wind speed

v_i = mean wind speed (m/s) in wind speed range i.

N = total number of ranges of wind speeds

t = time interval (s) over which each wind speed measurement is made, and during which the wind speed is assumed to be constant at the measured value

f_i = frequency of wind speed readings within wind speed range i over a year, that is, the total number of intervals (each of duration t) during which the wind speed is v_i.

A single mean value of v_i is used for each wind speed range even though this range has a finite width, that is, the 'bin size' used in obtaining the annual frequency distribution. However, care needs to be taken in choosing the bin size since if it is too large the mean wind speed in each range may not accurately represent the data and errors in the calculated energy transfers will thus result.

The best electrolyser stack for direct coupling to the aerogenerator at the site examined will be the one with the lowest $E_{transloss}$ over an annual period. Hence this procedure is repeated for each trial series-parallel electrolyser configuration until the minimum value (or an acceptably low value) of $E_{transloss}$ is found.

4.3 APPLICATION OF THEORETICAL ANALYSIS OF DIRECT COUPLING TO A CASE STUDY

4.3.1 The Kilcunda North case study

The procedure just described for direct coupling between an aerogenerator and electrolyser with matching of their V-I characteristic curves will now be applied to a case study to determine energy transfer and energy transfer efficiency over a range of steady wind speeds. This case study will illustrate the calculations and steps involved to determine the best component and system set up. The case study is based on an aerogenerator with similar performance characteristics to an AIR 403 400 W aerogenerator located at Kilcunda North, a site on the ocean coast some 120 km south east of Melbourne, as used in the earlier case study in which the wind – hydrogen system simulation model was applied to sizing a system to supply a remote household (section **Error! Reference source not found.**) (Janon and Andrews, 2006), for which hourly wind speed data are available for an annual period. The electrolyser used is a PEM type by h-tec, model StaXX 7 rated at 50 W maximum input electrical power.

4.3.2 AIR 403 aerogenerator V-I characteristic curve data input

The AIR 403 aerogenerator is in the 'micro aerogenerator' capacity category with rated electrical output of 400 W at a wind speed of 12.5 m/s, although it is capable of producing more than 800 W at 17.5 m/s (see Figure 19 in section 3.5.3) (Southwest Windpower, 2001). It has three fixed-pitch blades made of composite materials. Since there is no pitch control, the rotational speed of the AIR 403's rotor will change according to the wind speed if unloaded. The electrical generator is a synchronous permanent-magnet type, where the permanent magnets are on the rotor.

The standard AIR 403 aerogenerator is designed for battery charging (Southwest Windpower, 2001). An electronic system used to convert the primary 3-phase electrical output to a regulated DC output voltage of 24 V is built into the body of the unit. This system will automatically detect the battery voltage and determine whether the rotor should turn or not. If the battery voltage is low and the wind speed is above the cut-in speed of 3.5 m/s, the system will let the rotor turn in the wind and generate power, (Southwest Windpower, 2001). Once the battery is full, the system will automatically brake the rotor and stop further charging.

In the present experiment, a DC output from the aerogenerator is required, but one that directly corresponds to the rotational speed of the aerogenerator at any given wind speed, and is not modified by the electronic system installed specifically for battery charging. From technical perspective, AC output direct from aerogenerator's coils is required and then it can be rectified to DC output. Hence the standard AIR 403 aerogenerator had to be modified for use in this experiment for direct coupling to a PEM electrolyser bank. The main modifications made in order to obtain 3-phase AC output directly from the generator without any internal voltage-current conditioning were as follows:

- The built-in rectification and control system was removed.
- The slip rings (on the yaw bearing) and wiring were modified in order to get the 3-phase output directly from the generator coils, so that it could be transferred by a 3-phase cable out from the aerogenerator
- The generator coils were connected in the star ('Y') configuration and wired to the slip rings.

A detailed description of the modifications made to the standard AIR 403 machine is provided in Appendix B.

In order to calculate the energy transfer from the aerogenerator to a PEM electrolyser with a particular V-I curve using the theoretical approach just described, it is necessary to have the V-I characteristic curve of the aerogenerator for each wind speed under a range of loads. Such a family of curves was not available from the manufacturers of the AIR403 unit, so it was necessary, before mounting the machine at its outside location, to obtain these data by direct experimental measurement in a wind tunnel. RMIT University's wind tunnel at its Bundoora East Campus was used for this purpose. Each measurement on the aerogenerator was performed at a constant wind speed allowing time for a steady equilibrium output to be attained. A resistive load was applied to each phase. During the experiment wind speed in the wind tunnel was set at a constant wind speed then the resistance was varied. The AC output voltage and current are recorded. The AC voltage and current values were then converted to their equivalent rectified DC outputs, with zero loss in the rectifier is assumed, and then plotted as a V-I curve.

Because the wind speed readings were not round numbers, interpolation was made to find voltages and currents at rounded wind speeds to produce AIR 403 V-I characteristic curves. It was learnt that the wind speeds displayed by the control panel was 5% lower than the actual wind speed reaching the wind turbine (Haryanto, 2000). The wind speed actually experienced by the aerogenerator in the wind tunnel was thus higher than that recorded by a factor of about 1.05, which means that the error from the wind tunnel test is from the wind speed reading only, not the voltage and current reading. Finally, the raw wind speed readings were adjusted according to this reading error then the AC/DC conversion was made and at the end the interpolation was made to construct the AIR 403 V-I characteristic curves (figure C3). One such V-I curve was obtained for each wind speed. The complete family of V-I curves for the range of operational wind speeds (4 – 12.5 m/s) of the modified AIR 403 aerogenerator is shown in Figure 34.

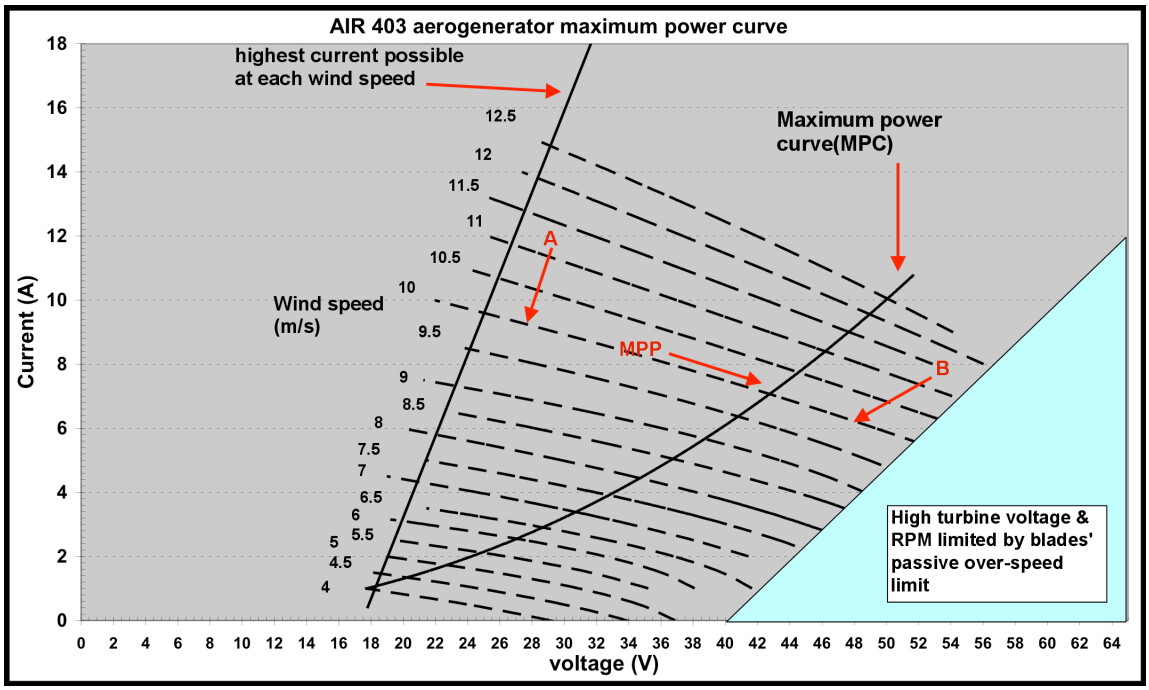

Figure 34: AIR 403 aerogenerator V-I characteristic curve as measured in the RMIT wind tunnel with the estimated 5% wind speed reading error taken into accounted. To obtain maximum power from the AIR 403 machine, the correct V-I combinations are required as shown by the maximum power curve, MPC.

The solid line on the left indicates the generator's current output limit. Any attempt to draw more current by reducing load resistance will overload and potentially damage the generator. The boundary of the blue area on the right indicates the maximum voltage output of the aerogenerator due to blade design rather than generator limitation. To approach this limit at any prescribed wind speed, the generator output current needs to be lowered. The RPM of the aerogenerator will increase until it reaches the "flutter" point, at which considerable noise is made, and the blades become less aerodynamically efficient. This point is a designed feature of the blades to prevent damage due to overspeeding during high wind speeds, or if the aerogenerator is left underloaded at moderate wind speeds.

At a constant wind speed of 10 m/s, for example, the resistive load can be varied to change the V-I values and hence the power delivered by the aerogenerator to the load from 27 V at 9.5 A (256 W) at point A, to 47.5 V at 6.2 A at point B (295 W). By varying the load resistance, the operating point can be moved along the V-I curve until the maximum power point is found, in this case at 43 V and 7 A (301 W). The continuous line passing through

the MPP shows the maximum power points for each of the wind speeds for this generator. The aerogenerator thus generates at maximum 50 V at 10 A (500 W) at a wind speed of 12.5 m/s, falling to 18.5 V at 1 A (18.5 W) at just above its cut-in wind speed of 4 m/s.

If, for example, the aerogenerator is working at point A, the power transfer loss ($P_{transloss}$) is calculated using Equation 41:

$P_{transloss} = 301\text{-}256 = 45$ W.

The power transfer efficiency is calculated using Equation 40:

$\eta_{trans} = 256 \div 301 = 0.85 = 85\%$.

4.3.3 Wind speed frequency distribution at Kilcunda North

At Kilcunda North, hourly wind speed data used were gathered between the 1st of February 1985 to the 2nd of February 1986 by Natural System Research (1987). The corresponding annual wind-speed frequency distribution for this period is presented in the form of a histogram (see Figure 18 section 3.5.2). There was a high incidence of wind speeds within the 5 to 10 m/s range, which suits the AIR 403 operating range. Moreover, it is crucial for the electrolyser's V-I curve to match the maximum power curve in the predominant wind speed range of 5-10 m/s rather than at higher wind speeds because of the much lower frequency of occurrence of the latter.

4.3.4 h-tec PEM electrolyser V-I characteristic curve data input

The PEM electrolyser under investigation in this case study is the h-tec StaXX 7 unit, which has seven identical cells connected in series. Each cell has an effective membrane area of 16 cm^2. The allowable voltage range per cell is 1.5-2.0 V at 4 amps maximum. The manufacturer also suggests 32 Ncm^3/min of hydrogen production (Wasserstoff-Energie-System, 2007).

The average experimentally-measured V-I characteristic of a single cell (Figure 35) within the 7-cell stack is used in the present case study, that is, the characteristic obtained by measuring stack (and hence individual cell) current, and dividing the measured stack voltage by 7. The cut-in voltage is almost 1.5 V and the maximum voltage reached is just under 2 V at a projected current of 4 A.

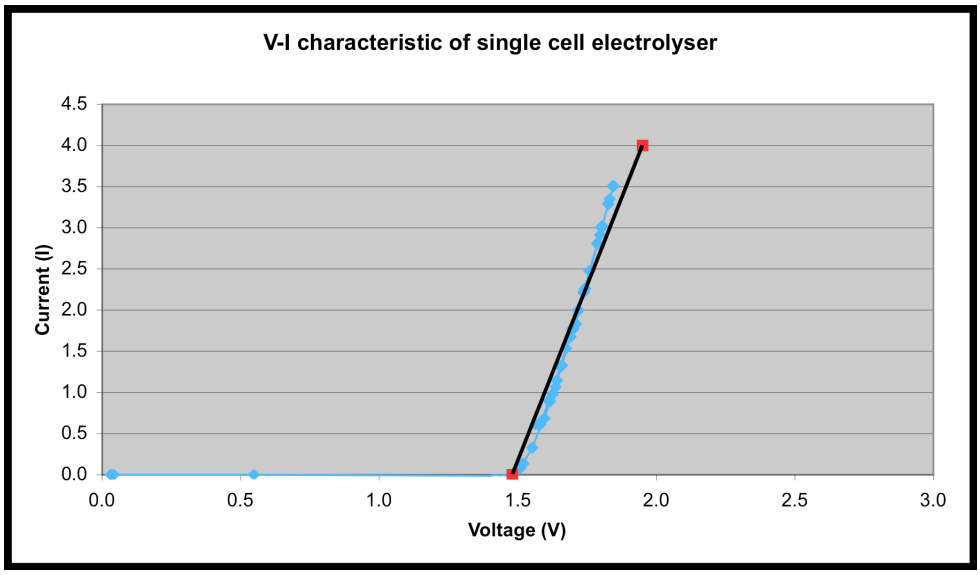

Figure 35: Experimental V-I characteristic of a single cell electrolyser taken from a new h-tec PEM electrolyser StaXX 7. The solid line represents the straight line approximation used (Paul, 2009).

This approach allows electrolyser configurations with a number of series cells other than a multiple of 7. For example, if it is suitable to have 16 cells in series make up a stack, the V-I characteristic according to subsection 4.2.1 is as shown by Figure 36.

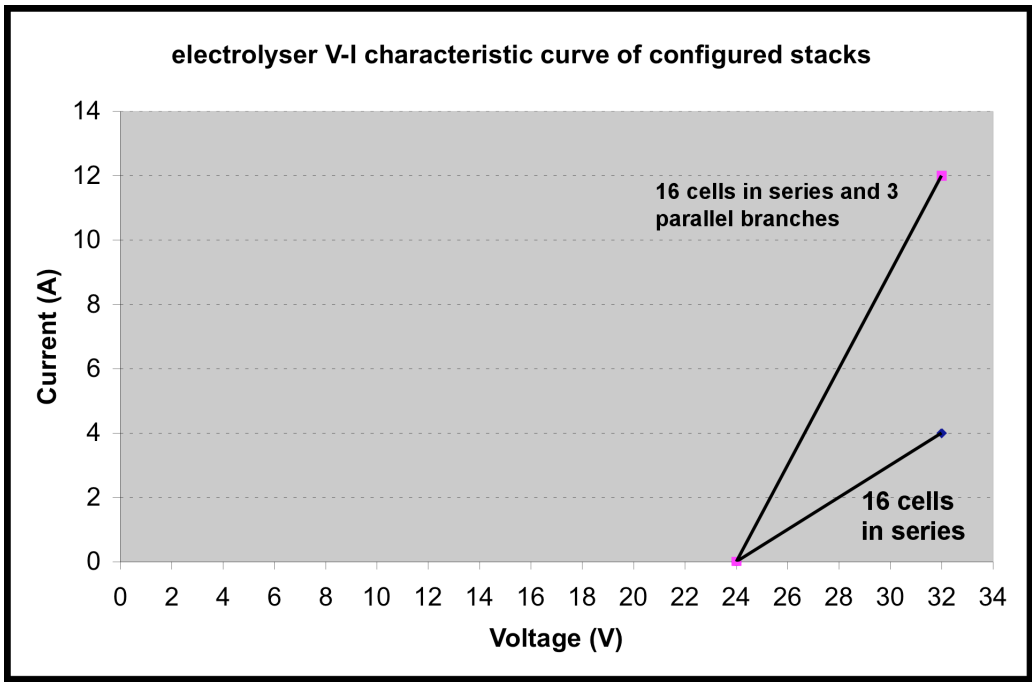

Figure 36: Electrolyser V-I characteristic of electrolyser banks comprising 16 single cells in series, or three branches in parallel with each branch having 16 cells in series.

For a 16 cells in series electrolyser configuration, the key voltage and current specifications of the electrolyser branch are:

- Cut-in voltage = 1.5 * 16 = 24 V
- Maximum voltage = 2 * 16 = 32 V
- Maximum current = 4 A

By using three branches connected in parallel, the maximum total current is multiplied by 3 (12 A) but the voltages stay the same compared to the previous configuration.

4.3.5 Energy transfer

Twelve of the possible series-parallel electrolyser configurations have been analysed in the case study for their total annual energy transfer between aerogenerator and electrolyser, the annual energy loss compared to that obtainable under maximum power point operation at all times, and percentage of this loss compared to the maximum achievable energy transfer, using the procedure described in section 4.2.4. The results are shown in Table 3. The energy transfer (E_{trans}) over a year in Kilcunda North under perfect MPP operation is 1243 kWh. The best performing electrolyser configuration is the one that can theoretically

transfer total energy closest to the MPP operation: that is, yielding the smallest energy transfer loss.

Electrolyser bank series-parallel configurations	Energy losses over a year (kWh)	% loss
16 cells series and 3 branches in parallel	110	8.8
17 cells series and 3 branches in parallel	85	6.8
18 cells series and 3 branches in parallel	66	5.3
19 cells series and 3 branches in parallel	53	4.3
20 cells series and 3 branches in parallel	45	3.6
21 cells series and 3 branches in parallel	42	3.4
22 cells series and 3 branches in parallel	45	3.6
23 cells series and 3 branches in parallel	54	4.3
24 cells series and 3 branches in parallel	66	5.3
25 cells series and 3 branches in parallel	82	6.6
26 cells series and 3 branches in parallel	100	8.1
27 cells series and 3 branches in parallel	124	10.0

Table 3: The annual energy transfer losses compared to maximum power point operation at all times of a number of series-parallel electrolyser configurations in the Kilcunda North case study. The maximum achievable energy transfer for all these cases is 1243 kWh/y.

Three of the twelve configurations analysed are shown in Figure 37, including the best of twelve in terms of energy transfer. The configuration with 3 branches in parallel and each branch with 16 cells in series departs substantially from the MPP line, and has a calculated energy loss compared to MPP operation of 8.8%, that is, unacceptably high. The configuration with 3 branches in parallel and each branch with 27 cells in series stays left of the MPP line, and yields a similar annual energy loss of 10.0%. According to Table 3, the configuration with 21 cells in series and 3 branches in parallel has the least energy transfer loss annually. This electrolyser configuration has a predicted energy loss of 42 kWh/y, given its predicted energy transfer of 1201 kWh/y; that is, the energy transfer is only 3.4% lower than the maximum achievable under MPP operation.

Given that DC – DC voltage converters and maximum power point trackers typically have losses of 5 – 10%, the direct coupling option under these assumptions promises at least as high an overall energy transfer, but without the cost of the electronic conversion equipment.

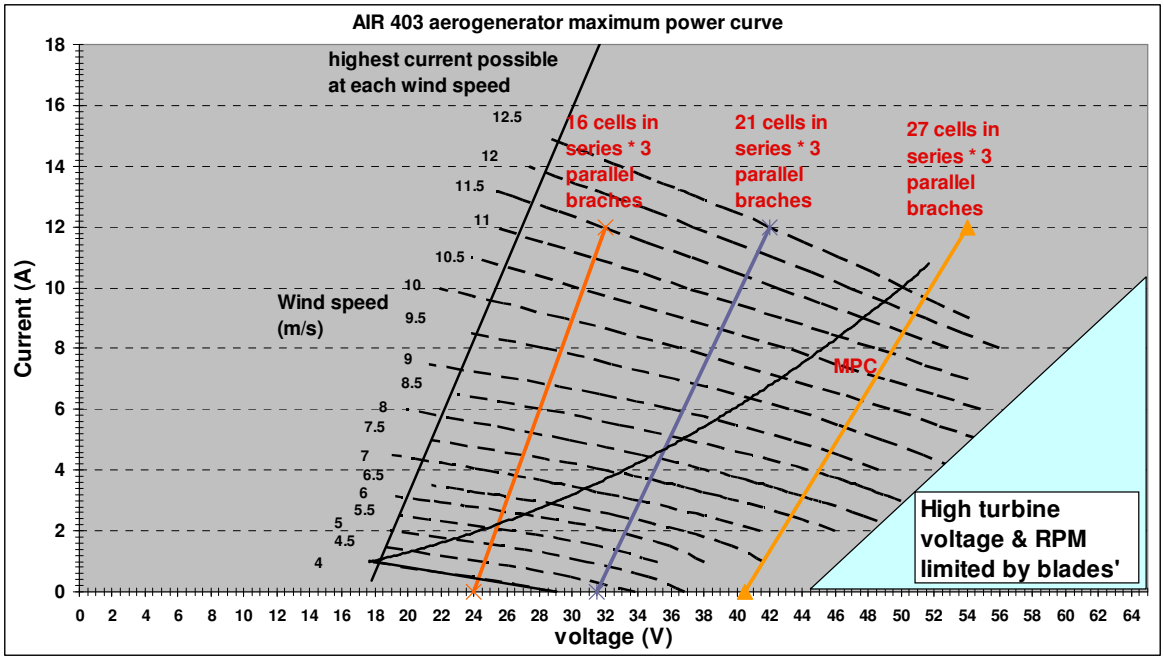

Figure 37: V-I characteristic curves of three of the electrolyser configurations analysed, and their location relative to the MPC of the AIR 403. The configuration that yields the highest energy transfer under direct coupling is 3 branches in parallel and each branch with 21 cells in series.

Even though an electrolyser stack with two branches in parallel has a slope closer to the MPC it will not be able to operate at high wind speed, say >12m/s, because of it low max current – 8 amp. In this study, the next configuration is one cell more than the last (in one branch). The number of cells in one branch determines the minimum and maximum voltages and therefore each configuration shifts from left to right. Since one cell is the minimum possible, the total of 12 configurations covers all operational areas of the graph in figure 37.

In the experiment of direct coupling at RMIT University, electrolyser cells available were not sufficient to test electrolyser with three branches in parallel. Therefore, two branches in parallel were used instead.

4.4 CONCLUSIONS

A procedure for matching the MPP curve of an aerogenerator to the V-I curve of an electrolyser bank by varying the series-parallel connection configurations of individual electrolyser cells has been described. The energy transfer between aerogenerator and electrolyser under the direct coupling condition, compared to the maximum potentially achievable by operating at the MPP of the aerogenerator at all times, has been analysed theoretically. This analysis has been applied to a case study of an AIR403 (400 W) aerogenerator coupled to banks of PEM electrolyser cells with various series-parallel connection configurations for the wind conditions at a coastal site in Victoria (Kilcunda North). For this case study it has been found that the annual energy loss for the best electrolyser configuration is less than 4% of that achievable under perfect MPP operation. This loss is less than that typically found for DC – DC voltage converters and maximum power point trackers (5 – 10%) so that the direct coupling option appears promising as a way to reduce system costs without any energy penalty.

However, a fundamental assumption of the analysis conducted in this chapter has been that the aerogenerator performs during each time interval at the maximum power output for the mean wind speed during the interval, as measured under steady state conditions in a wind tunnel. In other words, this analysis of direct coupling between an aerogenerator and electrolyser is carried out within a steady state frame work.

The assumptions for this analysis are thus that:

- Wind speed is constant throughout each interval.
- The wind speed does not change so rapidly between intervals that the aerogenerator does not have sufficient time to reach its equilibrium rotational speed for the prevailing wind speed in each interval.

These conditions are most likely to be met at sites where wind speeds are relatively constant and turbulence is very low. Their applicability in the case of the AIR403 aerogenerator located at a site at RMIT University's Bundoora East campus will be investigated experimentally in chapter 5.

5 EXPERIMENTAL TESTING OF THE DIRECT COUPLING APPROACH

5.1 AIMS OF EXPERIMENTAL PROGRAM

An experimental investigation of the energy transfer and hydrogen production of an AIR 403 aerogenerator directly coupled to a bank of h-tec PEM electrolysers was conducted to test the viability of this approach in practice and compare the results obtained with theoretical calculations conducted using the method described in chapter 4. The present chapter describes the experimental rig and the results obtained. The experimental results for energy transfer and hydrogen production are shown.

Specifically the aims of the experiment conducted were to:

- Design, construct and operate an experimental direct-coupled aerogenerator – electrolyser system
- Design, construct and gain operational experience with an automated control system, hydrogen handling equipment, and overall safety regimen for this system
- Measure the energy transfer between the aerogenerator and electrolyser and hydrogen production over an extended period
- Investigate any degradation in the performance of the PEM electrolyser due to usage over time, and the variable and intermittent electrical input from the aerogenerator.

5.2 EXPERIMENTAL EQUIPMENT

5.2.1 Overview of experimental rig

The main components of the experimental rig are (Figure 38):

- The AIR403 aerogenerator, anemometer and wind vane
- A full-wave bridge rectifier
- The bank of h-tec PEM electrolysers
- A water deioniser

- A thermostatically controlled water heater
- An electronic load to take any excess wind power from the aerogenerator over what can be input to the electrolyser bank
- Hydrogen drying, flow rate sensors, and detection equipment
- The hydrogen experimental cabinet with constant air inflow and hydrogen and air exhaust to atmosphere
- System safety and control equipment, including the control system for the aerogenerator and electrolysers, hydrogen sensors, and automatic shutdown in the event of any present safety parameters being exceeded
- Data collection system.

The hydrogen produced was dried before passing through the hydrogen mass flow sensor for measurement, and then exhausted to the atmosphere in the exit vent of the hydrogen experimental cabinet. The experimental rig thus contained many of the components found in an overall wind – hydrogen energy system, with the exception of any hydrogen storage, a fuel cell, and final load.

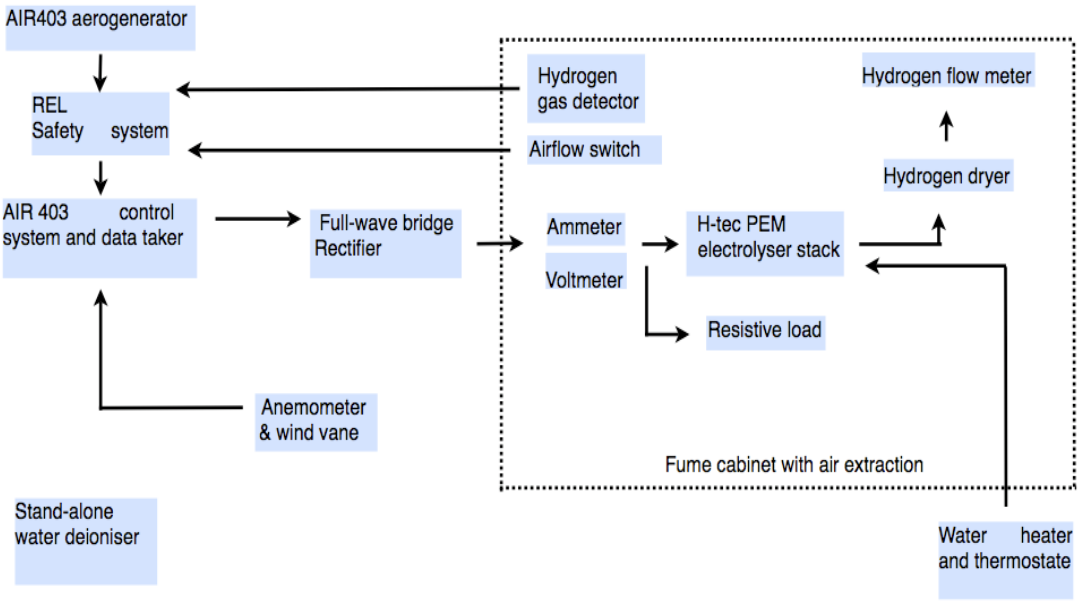

Figure 38: A schematic of the experimental aerogenerator – electrolyser rig.

The rig was designed to allow autonomous data collection with unattended operation over an extended period. The variables recorded at regular intervals were:

- Wind speed
- Wind direction
- Electrical voltage applied to electrolyser bank (that is, after rectification)
- Current flowing through electolyser
- Deionised water supply temperature
- The ambient temperature outside near the aerogenerator
- Electrolyser cell temperatures
- Hydrogen gas production rate.

5.2.2 AIR 403 aerogenerator

After measurements made of the AIR 403 aerogenerator under the steady-state conditions in the wind tunnel (Appendix C), the modified AIR 403 aerogenerator was installed on top of Building 253 at RMIT University's Bundoora East Campus (Figure 39). At this location, the aerogenerator has clear access to the prevailing winds from the south west and north. Budget limitations meant that the height of the tower had to be limited, so that in the actual installation the hub of the aerogenerator was only 3.5 m above the roof of the building, whereas clearly a greater clearance would have been desirable from the point of view of minimising boundary effects and turbulence. Overall the aerogenerator hub was 15.5 m above ground level. The tower was designed and built specifically for this purpose to accommodate the aerogenerator and wind measuring equipment, namely an anemometer and wind vane. The three-phase ac power and data cables run to the Renewable Energy Laboratory (REL) nearby.

The AC power enters the REL safety system first before the AC terminals can be used. It is designed so that there must be an air flow in the hydrogen experimental cabinet before the AC power is available at the terminals. In the direct coupling experiment, the AC power then goes into the AIR 403 control system before it is rectified to DC power by a rectifier.

Figure 39: The AIR 403 aerogenerator, anemometer and wind vane installed on Building 253, at RMIT Bundoora East campus. Power line and data cables run into the Renewable Energy Laboratory.

The location of the installed AIR 403 wind turbine used in this project is on RMIT University's East Campus, where there are buildings and houses. The building roof on which the tower was mounted offered an increase in elevation to put the turbine above the surrounding tree lines. However, it is realized that turbulence generated by the building walls may affect the wind speed coming into the turbine, given its relatively small tower. This is not to mention the turbulence coming off from the surrounding structures and tree lines. The installation was not ideal, but was the best available in terms of practicality and financial resources, including:

- Hydrogen generation rig safety and security: the safety and security of the hydrogen experimental rig is more difficult to ensure outside the campus.
- Limited fund allocation.
- Permission for an off-site installation: a extensive paper work and funds would have been required to install this system in another area outside the campus.

Moreover, it was not the priority of this study to generate maximum power, in which case, a good wind regime would have been essential. But it is designed to perform energy conversion, where its efficiency is examined. Therefore, while the turbulence may have limited the power and hydrogen production from the rig, it did not change the basic relationship and mechanism between electrical power production and hydrogen generation that this study has focused upon.

5.2.3 PEM electrolyser bank and hydrogen handling system

A schematic diagram showing the electrolyser bank, water feed system, hydrogen drier, hydrogen mass flow sensor and the hydrogen exhaust system is shown in Figure 40. There are three h-tec PEM electrolysers electrically connected in series to form a branch and two branches are connected in parallel. These electrolysers (number 1, 2, 3, 4, 7 and 9) comprise the experimental group. The control group of electrolysers (number 5 and 6) are not electrically connected to others, although they utilise the same plumbing system.

The temperature-controlled water is supplied from a container and is delivered via tubing shown dotted lines in Figure 40. The water feed tube goes to every electrolyser (but the connection to electrolysers 1, 7 and 5 are not shown in the diagram for the convenience of viewing). Moreover, hydrogen gas is collected by tubing from every electrolyser and then fed into the hydrogen drying system and hydrogen flow-meter before final release within the exhaust duct of the hydrogen experimental cabinet. (Likewise, hydrogen tubing from electrolysers 4, 9 and 6 is omitted to maintain the clarity of the diagram.)

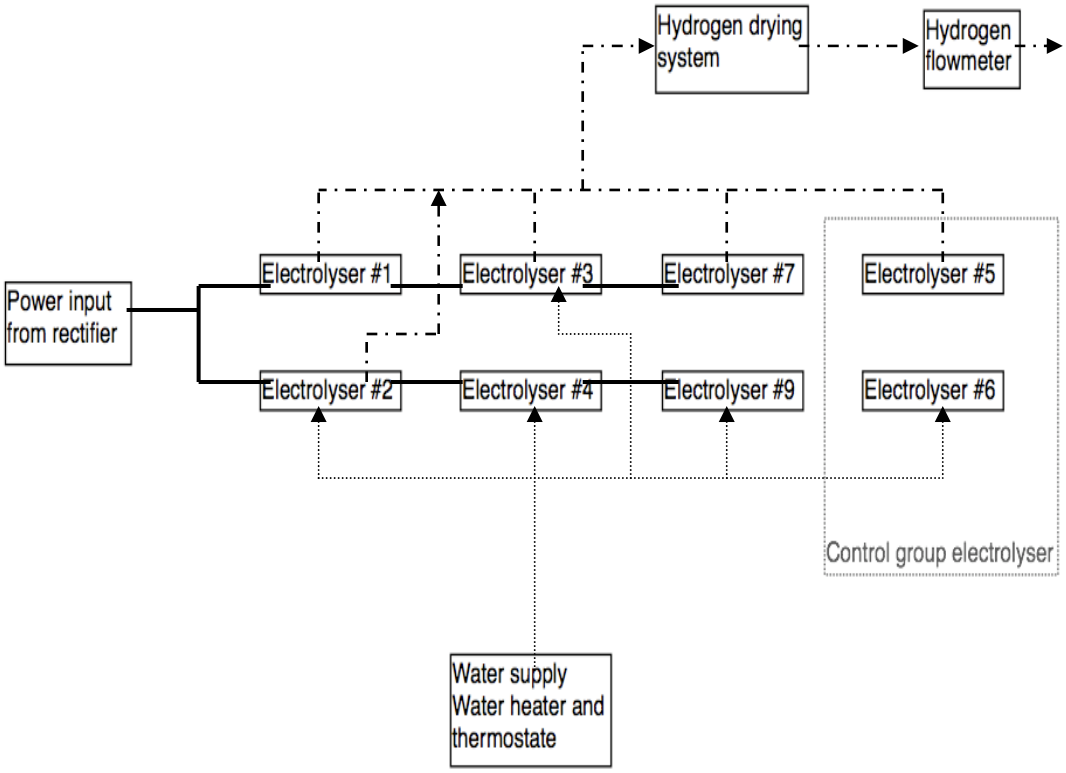

Figure 40: Schematic diagram sowing the experimental group of electrolysers (numbers 1, 2, 3, 4, 7 and 9) and the control group (numbers 5 and 6). The thick solid line shows the electrical connections, the dashed line the hydrogen routes, and the dotted line the water supply line. The hydrogen line from electrolysers 4, 9 and 6, and the water line to all the electrolysers other than number 3) are omitted to maintain the clarity of the diagram.

The electrolysers used in this experiment are h-tec StaxXX7 electrolysers (Figure 41), each unit comprising seven cells connected in series and each cell having an effective area of 16 cm^2. This stack has an operating range of 10.5-14 V at 4 A maximum and can generate hydrogen at up to 230 Ncm^3/min (Wasserstoff-Energie-System, 2007).

A theoretical analysis of the energy transfer between aerogenerator and electrolyser under direct coupling over this period using the actual wind speed distribution has been conducted using the procedure presented in chapter 4 for a number of possible electrolyser configurations. The best electrolyser configuration in terms of total energy transfer found in this case is 3 parallel branches, each branch containing 17 cells in series. However, as a result of the number and types of available electrolyser stacks, the actual trial employed the electrolyser configuration with two parallel branches, with each branch containing three h-tec electrolyser stacks in series, that is, a total of 21 cells in series (Figure 42). Three h-tec

StaXX 7 electrolyser were connected in series to form one branch, and then two of these branches connected in parallel to form the overall electrolyser bank. Within a branch the three electrolysers are electrically connected in series while a fourth electrolyser (a control group unit) is electrically isolated but utilises the same plumbing (Figure 43).

Hydrogen gas produced by the electrolysers, together with the water that accumulates on the hydrogen sides of the electrolyser cells due to electroosmotic drag of water molecules through the membranes by hydrogen ions (Weber et al., 2003), are piped to an outlet manifold (Figure 44). The manifold is positioned on an incline so that the lighter hydrogen gas rises to the top of the manifold while the water flows downwards to the water collector. The hydrogen then flows through a dryer where water vapour is removed, and a filter to remove any particles from the gas dryer, prior to entering the hydrogen mass flow rate meter (Figure 45). During operation, hydrogen gas is produced intermittently at near atmospheric pressure. To prevent back flow of air into the electrolysers during periods of low output, the hydrogen exiting the mass flow meter is introduced into the bottom of a tank partly filled with water (Figure 46). The hydrogen collecting in the upper part of this tank is then conveyed to the outlet duct of the hydrogen experimental cabinet and thus exhausted to the atmosphere by the action of the continually running extraction fan on top of the hydrogen experimental cabinet.

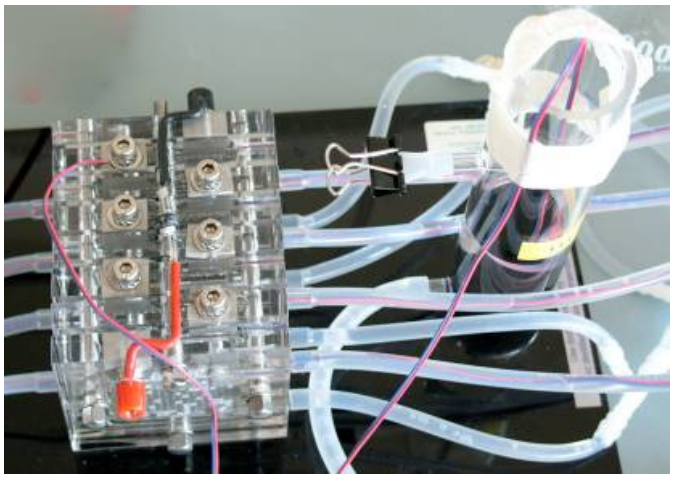

Figure 41: A 50 Watt h-tec electrolyser model StaxXX 7. A stack has seven single cells electrically connected in series.

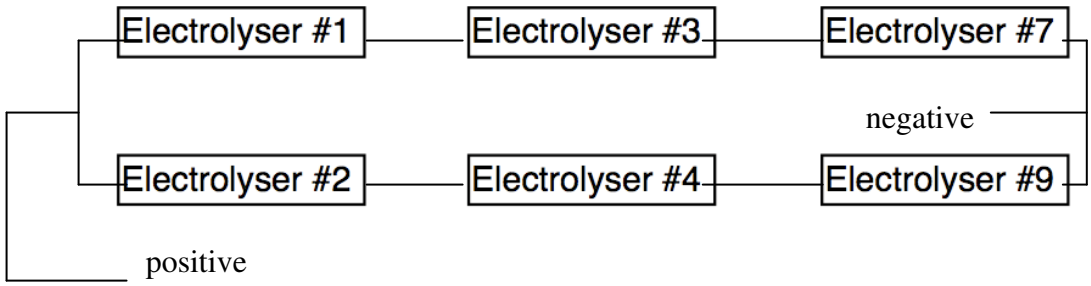

Figure 42: Schematic diagram of electrolyser electrical connection, where three h-tec electrolysers are connected in series to form a branch and two branches are connected in parallel to complete the bank.

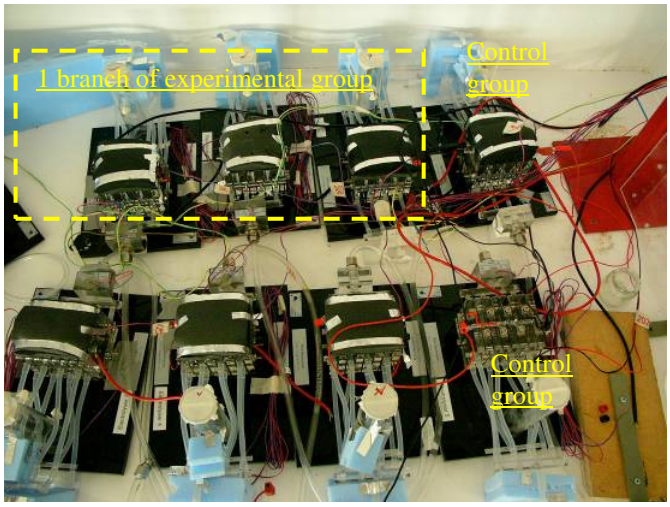

Figure 43: Four StaXX7 electrolysers sharing water and gas plumbing, but only three cells are electrically connected in series to form a branch in the series-prallel connection configuration employed in the actual experiment. The fourth electrolyser has a separate electrical connection and serves as a control unit for performance comparison purposes in the overall experiment.

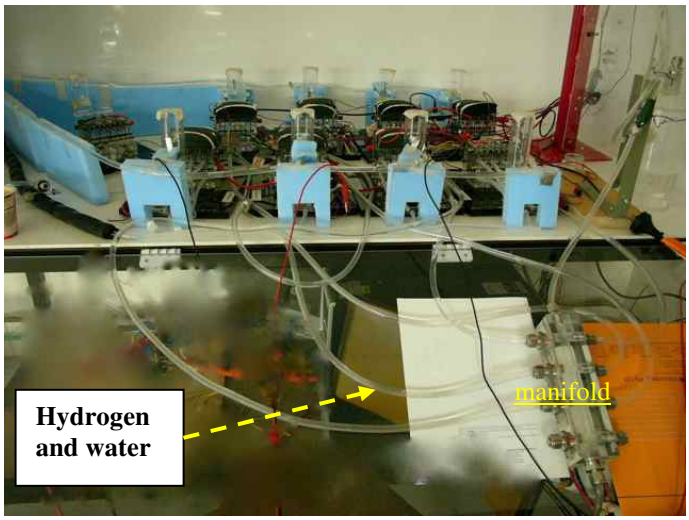

Figure 44: Electrolyser outlets that bring product hydrogen and water run into the manifold, where water is separated from hydrogen gas.

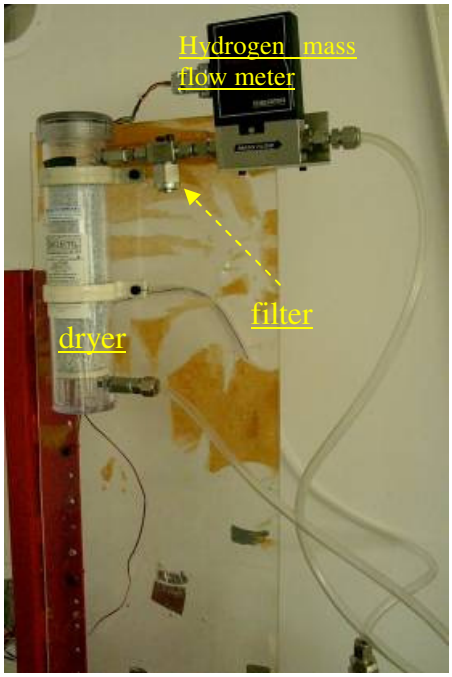

Figure 45: Hydrogen gas from the manifold goes to hydrogen dryer, filter and mass flow rate meter.

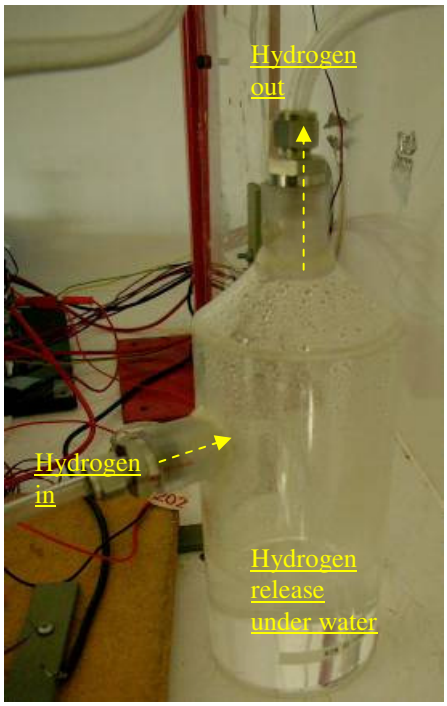

Figure 46: Hydrogen non-return tank where hydrogen gas from the hydrogen mass flow meter is released under water and proceeds to the upper part of the tank and hence to the exhaust outlet of the hydrogen experimental cabinet.

5.2.4 Hydrogen safety system and hydrogen experimental cabinet

The experiment involves production of hydrogen gas and relatively high current flows, so that ensuring safety of operators and equipment is imperative. A number of active and passive safety systems were put in place to deal with the identified risks.

A hydrogen experimental cabinet – a modified form of fume cupboard – has been designed and installed at the Renewable Energy Laboratory at RMIT University's Bundoora East campus specifically the purpose of safe conduct of experiments of this kind involving hydrogen (Figure 47). Details of the design of this cabinet and its associated safety features are provided in Paul (2009). The key feature for safe operation is to ensure that, if hydrogen gas is generated in the course of an experiment and enters the general space of the cabinet, an adequate amount of fresh air is circulated within the cabinet to keep the hydrogen concentration well below the flammable limit. The hydrogen experimental cabinet or hydrogen experimental cabinet employs a pressure switch in the exhaust duct to sense air flow. Power supply from aerogenerators or solar panels to the electrolysers under test inside the cabinet is allowed only when there is an air flow that causes a pressure drop

in the exhaust duct. Hence if the extraction fan did fail during an experiment, the safety system will immediately detect that there is no pressure drop and cut off power to the electrolysers.

In addition, if the hydrogen concentration as detected by the hydrogen detector at the top of the cabinet (Figure 48) is higher than a preset level as a result of leakage or inadequate air flow, the safety system will once again cut off power to the electrolysers immediately and an audible alarm is set off. There is an additional hydrogen detector on the ceiling of the laboratory outside the cabinet that functions in the same way.

Before the experiment is started, the air inside all tanks and tubes of the rig must be removed to avoid mixing with the hydrogen produced. The technique used to remove this air, without reliance on any vacuum pumps or gas purging equipment, was to fill up all tanks and tubes with water prior to starting the experiment. When the electrolysers are turned on, the generated hydrogen was then used to push the water out.

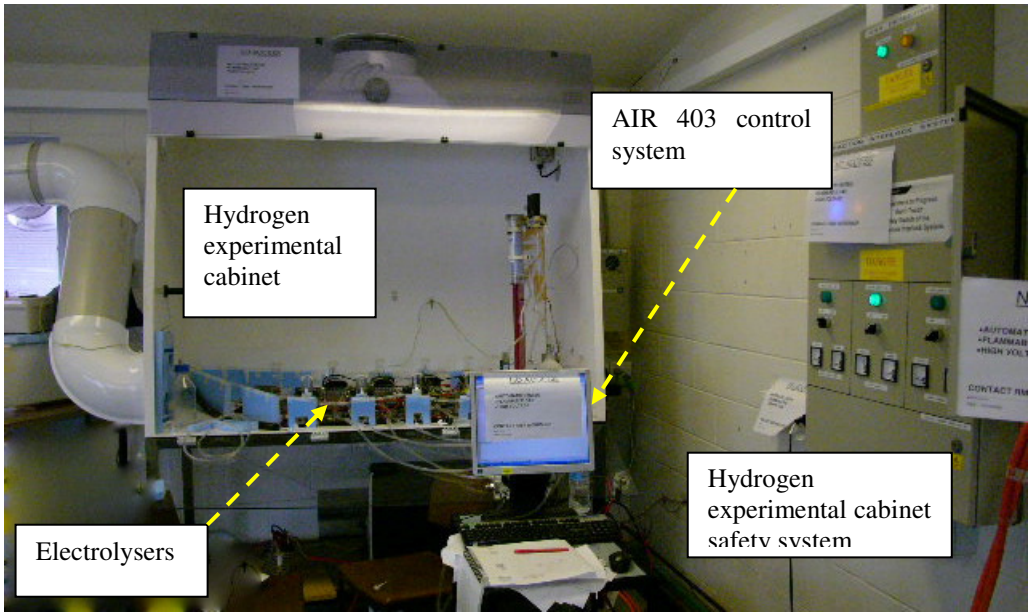

Figure 47: Safety system and experimental rig installed inside the hydrogen experimental cabinet. The safety system ensure that there is an air flow inside the hydrogen experimental cabinet before electrical power is provided to electrolysers.

Figure 48: Hydrogen gas detector inside the hydrogen experimental cabinet is connected to the safety system.

5.2.5 Operational control and data monitoring system

The purpose of the operational control system is to regulate the operation of the aerogenerator using input data on wind speed, and current and voltage conditions at the electrolyser, with an override to ensure that no power from the aerogenerator can be fed to the electrolysers unless the exhaust fan of the hydrogen experimental cabinet is producing the required air flow in the exhaust duct. The data collection and recording system is used to record the overall results of the experiment over an extended period of time. The overall system has been designed for autonomous unattended operation so that an experiment can continue uninterrupted without any intervention from an operator for an extended period.

The AIR 403 control system used in this experiment is located in the Renewable Energy Laboratory, RMIT Bundoora East campus, and is made up of a number of devices that replace the original control system in the unit purchased from the manufacturer. Specifically the functions of the control system are:

- Monitoring and recording of wind speed and wind direction.
- Turning on/off the AIR 403 aerogenerator at appropriate wind speeds.
- Recording a set of parameters during the experiment.
- Preventing excess current input into the electrolysers
- Preventing excess voltage input into the electrolysers
- Returning the system to off position in the event of power failure, or unsafe conditions (such as exhaust fan not working, or hydrogen leaks detected).

An Agilent data acquisition unit is connected to a desktop computer (PC) where the custom designed program for the present project is run. The Agilent reads wind speed data from anemometer and sends it to the computer for the program to use in making a decision. If the decision made is to turn on the AIR 403, then the PC will send a command to the Agilent to power-up the contactors. The program also actively monitors values that may be damaging to other equipment – such as high wind speed, high current, high voltage – and can take actions to prevent overloading. Moreover, there are a few passive measures to safeguard the system such as fuses and contactors that need power to operate. For example, use of a normally close (N/C) contactor for the turbine brake offers protection against power failure, because the brake is always on unless power is supplied and will remain so if all power failed.

The data processing system is a software program custom designed for the present project using a Visual Basic/VISACOM platform as a means of communicating between the computer and the data acquisition unit. The system acquires and processes data, and then makes decision according to conditions and logic to control all the hardware in the experimental rig. The data processing unit performs two levels of control: supervisory control and safety (overriding) control.

Supervisory control is a set of logics designed to control operational functions in normal operation and is divided into states as follows:

a. *Stand-by state*: the turbine is on electromagnetic brake (all generator coils are shorted), while the control system is continuously measuring the wind speed and compare against predetermined operational wind speeds. In this state the master contactor (C) shown in Figure 49 is powered, readying power to all other contactors.
b. *Start-up state*: the data processing unit establishes that wind speed is in the operational range, and powers up the normally closed (N/C) contactor (A), as shown in Figure 49 and Figure 50. The aerogenerator is now free to spin.
c. *Loaded state*: the turbine is connected to the load by powering the normally open (N/O) contactor (B) (Figure 49 and Figure 50). This condition requires that the output voltage after rectification of the turbine before loading is in the safe range in regard to the load. In the case of an electrolyser the maximum allowed voltage input is crucial. In this state, the DC voltage and

current are continuously monitored over defined intervals to prevent overloading.

d. *Shut-down state*: all power to the contactors is cut off, and the data processing unit will reset itself to 'stand-by state' in the following round of data reading. Shut-down state state is activated by:
    i. High wind speed detected. The wind speed data is continuously monitored. Once the wind speed exceeds a set value, it triggers the alarm and power to the master contactor is cut off. This action shuts down the aerogenerator, while the data processing unit in the computer processes data. At this point the program detects 'alarm trigger' (Figure 49). The program sequence is returned to 'stand-by state'.
    ii. Low wind speed detected. If the anemometer reads a lower wind speed than the preset minimum value, the aerogenerator is still allow to spin and all contactors are powered until the data processing unit detects that wind speed averaged over 5 seconds is below the present minimum value. This averaging procedure helps prevent the system shutting down in a sudden drop in wind speed and keeps up the turbine's rotational momentum.
    iii. High DC voltage or current detected. To prevent overloading of electrolyser and other loads, this function is programmed into the Agilent at the start of the program. Th Agilent's internal alram uses a purpose-built 'alarm trigger' to cut power to the master contactor (C).

Safety (overriding) control is a set of software logic-based operations designed to assume overall system system control and perform functions in dangerous conditions to bring the system to a safe state. These operations are as follows:

a. *Excess DC voltage and current detection.* This is an isolated excess voltage and current detection system. It comprises a 24 V DC monitoring relay (Omron K8AB-AS-DC24) and its power supply unit. If at times of high wind speed, the AIR 403 control system was not responding and did not bring itself into *shut-down state,* the relay will detect voltage or current exceeding the allowable levels (set at slightly lower than that of the fuses

capacity) and then cut power to the master contactor (C). Thus the aerogenerator is shorted and will stop.

b. *Excess DC current detection*. The DC current going into the electrolysers must not exceed a certain present value (corresponding to the particular series-parallel configuration selected), which is regulated by fuses if all other systems have failed. When these fuses are blown, the aerogenerator will be unload and start to free spin. At high wind, this is not recommended, although it is not dangerous.

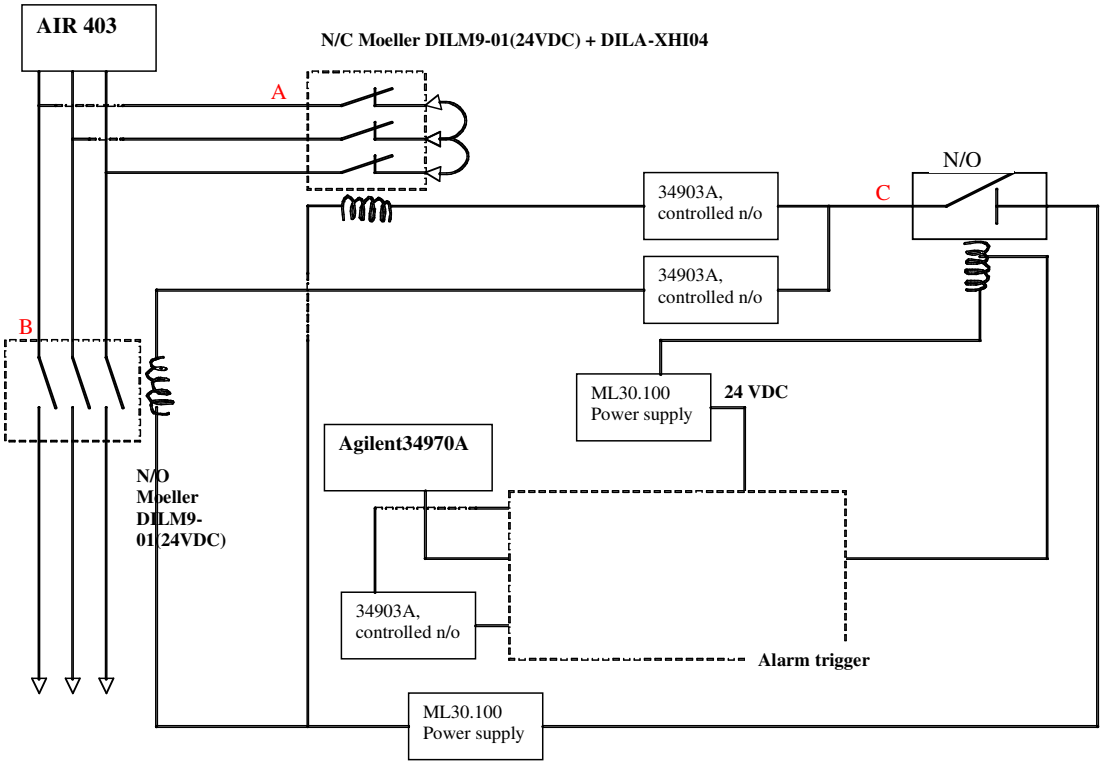

Figure 49: AIR 403 control system schematic diagram with contactors positioned to control the AIR 403 (A), turn on produced power (B), master power to all contactor (C) and alarm trigger.

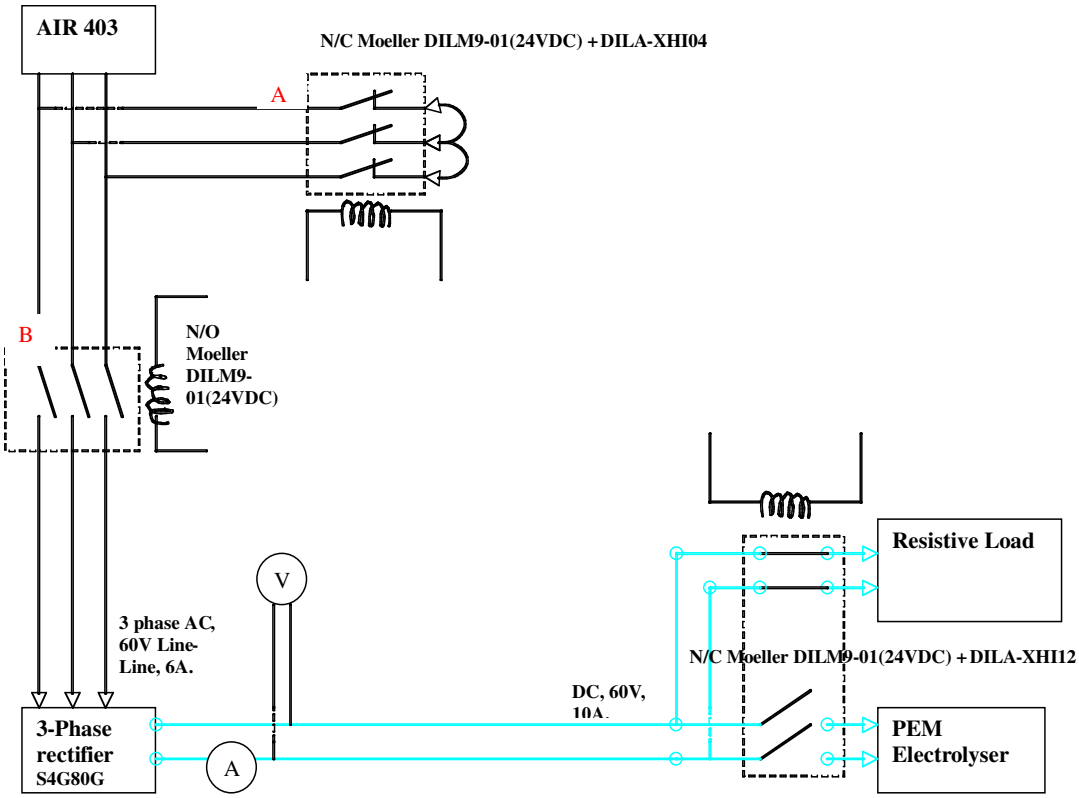

Figure 50: AIR 403 control system schematic diagram without showing the alarm diagram. The system shows the power route from the AIR 403 to rectifier and then load, where it can be switched from resistive load to electrolysers by another contactor.

The data acquisition system consists of all the apparatus necessary to measure parameters and send data for the PC for processing and storage. This apparatus includes the Agilent 34970A data taker equipped with 20 channels, multiplexers and switching unit (Figure 51), thermocouples, current shunts, voltmeter, ammeter, anemometer, wind vane and hydrogen flowmeter.

Figure 51: Agilent 34970A data acquisistion unit, which takes data from all transducers and sends this information to the PC. It also take commands from the PC to control the contactor unit.

The contactor unit is made up of all the contactors (that is, switches) operated by the PC via the Agilent 34970A such as to turn on or off, and load or unload the turbine, together with the alarm trigger (Figure 52). This unit was constructed using standard electrical equipment available off the shelf.

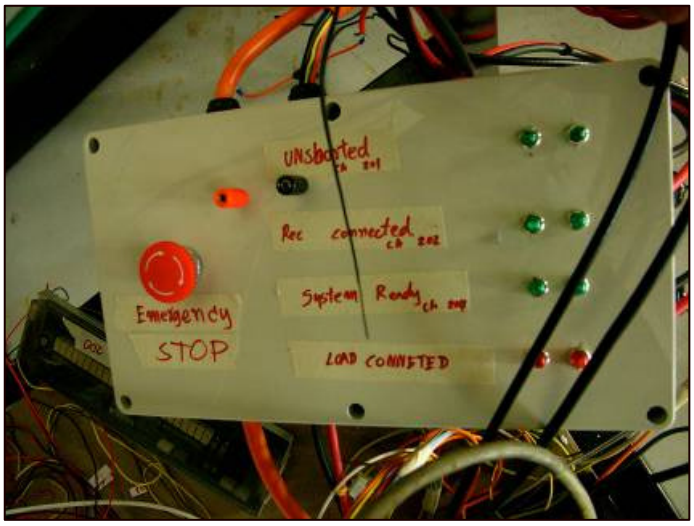

Figure 52: Contactors, power supply and other hardware of the AIR 403 control system integrated into a single unit with emergency stop button and indicator lights.

The AIR 403 control system must be able to bring the turbine to a halt under a number of failure modes to guard against damage to personnel and equipment, especially during high wind speeds.

If there is a power failure in the laboratory, the overall operational control system, which includes the data processing unit, data acquisition unit and other sensors, will stop working. In this event, the system is set so that all contactors return to their initial (shut-off) state, which means the aerogenerator's coils are shorted and the turbine is brought to a stop, so the system is safe.

If the anemometer fails and gives a reading of zero volts in high wind during the loaded state, the aerogenerator will keep producing more and more current until it exceeds the maximum current limit. At this point, all the contactors are switched to the off position, and the aerogenerator is shorted and stops. The data processing system will detect that the

wind speed reading is zero during the following interval and goes into shut-down state. Because of the faulty anemometer, the system will stay in this state in definitely.

If the anemometer gives a reading of zero volts in low wind during the loaded state, the aerogenerator will keep producing power to the electrolysers as before. However, by the next interval, the data processing unit will notice zero wind speed reading and will inititate the shut-down state.

Electrical failure of contactors A and B will bring the device back to the original position or stand-by state. The contactors are rated in number of cycles with industrial standards and will take many years to fail. In addition, the failure of the contactor C does not lead to dangerous situation because other contactors will not be powered and the turbine generator remains shorted. Therefore, the failure of the contactors does not pose any danger to the system.

Failure of the the data acquisition and processing systems in the worst-case scenario will allow the voltage and current to rise and may overload the system during high wind speed period. But then the safety (overriding) control, containing items that are hardwired and separate from the AIR 403 control system, will take over and shut down the aerogenerator and overall system.

5.3 EXPERIMENTAL METHOD

The bank of electrolysers with the selected series-parallel connection configuration was directly coupled to the aerogenerator, and the performance of the system over an extended period of time was measured using the experimental rig described in the previous section.

Six h-tec PEM electrolysers were used in the primary bank tested in the direct coupling experiment, with two branches, each with three h-tec electrolysers linked in series, connected in parallel (section 5.2.3). Thus, given that each h-tec electrolyser is a stack of seven individual cells connected in series, the overall configuration used was two branches connected in parallel, each branch containing 21 individual cells connected in series.

This electrolyser bank was assembled from four h-tec electrolyser that had been used previously (electrolyser number 1-5) in a different research project, and two such electrolysers that were completely new (electrolyser number 6, 7 and 9). The location of the used and new electrolysers in the overall bank is shown in Figure 40. These electrolysers in experimental group (electrolyser number 1, 2, 3, 4, 7 and 9) were subjected to the varying input from the aerogenerator over the study period.

In addition, electrolysers in the control group (numbers 5 and 6) were subjected to constant electrical input. These two h-tec PEM electrolysers, one used and one new, were used for control purposes, and subjected to a constant voltage and current input over a period such that the total energy input was the same as that into the experimental electrolyser bank subjected to the varying voltage input from the aerognerator. The V-I curves of all eight electrolysers were measured individually before and after the experiment. In this way, any differences in the rate of degradation of performance between the electrolysers subjected to the variable input and those subjected to the constant input were able to be measured.

To control for other variables, every effort was made to ensure that each electrolyser in the experimental electrolyser bank was provided with identical inputs in terms of:

- Water supply quality, temperature and pressure
- Ambient temperature
- Hydrogen gas outlet pressure

Input water temperature in this experiment was controlled at 30°C by a thermostatically-controlled water heater. This water was heated and delivered to electrolyser cell by tubes. The water consumption rate is slow and the water level in the reservoir drops slowly, so that the pressure of the water reaching the electrolyser stayed relatively constant. However, atmospheric pressure and pressure within electrolyser cell were not controlled nor monitored and they fluctuate over time. Their effects are neglected.

The atmospheric pressure will vary depends on weather conditions (the RMIT University location is close to sea level) and this is directly related to the internal pressure of electrolyser cells since the hydrogen gas produced is released to the atmosphere. The pressure within the cell will also be increased to overcome pressure drop from series of components that hydrogen gas has to flow through, as seen in section 5.2.3. However, this

type of electrolyser was used to compress hydrogen (to slightly above atmospheric) into a hydrogen storage unit during the experiments done earlier by Ali (2007).

The variables measured and recorded in each interval (1 second) over the study period were :

- Wind speed
- Input current and voltage to the electrolyser bank
- Hydrogen production rate
- Electrolyser cell temperature
- Atmospheric temperature.

Electrical current and voltage input of electrolysers from the aerogenerator were monitored continuously, and the average power in each interval calculated and recorded as well. The voltage is monitored closely because it must not exceed the voltage limit of the electrolysers and it also can be used to estimate the turbine RPM. Likewise, the current input also must not exceed the electrolyser limit.

Electrical current and voltage inputs were measured separately at each of the two branches of electrolysers. The difference between them was marginal. The average values of voltage and current were derived from them, and then used to calculate electrical input power to the electrolysers.

The hydrogen flow rate is measured using the mass flow meter. The mass flow meter works by letting a portion of gas pass through a tube, where the moving gas is heated. The coil of the Resistance Temperature Detector (RTD) is coiled around this tube, and transfers a given constant amount of heat into the gas. The moving gas carries away the heat and changes the resistance in the coil in proportion to the temperature difference. Since it is the gas molecules that carry the heat, the mass flow rate can be calculated and is independent of temperature and pressure changes.

At all times there was hydrogen gas in the tubes. If the system is not operating due to the lack of wind power, the hydrogen is then sealed within the system from the electrolysers to the outlet by the hydrogen non-return tank. At the moment when electrical power is available to the electrolysers, hydrogen gas is generated and pushed through tubes. The amount of hydrogen produced by the electrolysers and the hydrogen that is going through

the mass flow meter is the same amount, and this occur with minimal lag due to the existing hydrogen gas within the tubes. The same cannot be true in a case where the tubes are empty and the hydrogen gas has to travel from the electrolyser along the tubes to the mass flow meter.

The hydrogen mass flow meter used was a Smart-Trak2® Model 100 by Sierra Instrument. The respond time as stated by the manufacturer is 300 millisecond time constant (sierra instrument, 2009). The response time is approximately a third of the measurement time interval (1 second). Therefore the measurements were made when the instrument had reacted to the change in mass flow rate and hence acceptable.

Electrolyser cell temperature is taken as the temperature of two cells in the middle of the seven-cell h-tec electrolyser and was measured using a type-T thermocouple. The thermocouple is insulated and attached by thin tape to the electrical conductors of two adjacent cells (Figure 53). Only one sensor for the two middle cells of a seven-cell electrolyser stack was used and only the thermocouple area was thermally insulated to improve measurement accuracy. As a result, the temperature measured is an averaged temperature of these two middle cells, whose heat is allow to dissipate into the surroundings and product gases and liquid.

Supply water temperature was measured at the water reservoir located next to the hydrogen experimental cabinet. The difference in temperature between this point and that at the electrolyser inlets was assumed to be negligibly small. With the supply temperature controlled, the water inlet temperature would in any case have been held reasonably constant. The ambient temperature is measured both inside the hydrogen experimental cabinet and outside the building.

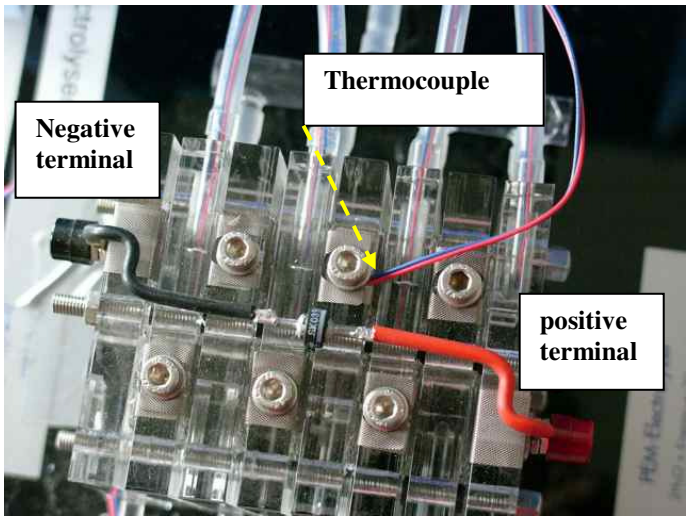

Figure 53: Type-T thermocouple with insulated tip is placed on metal electrical conductor between two cells and secured with a bolt to measure cell temperature, which would be the average of two cell.

5.4 RESULTS

5.4.1 Study period

The AIR 403 control system was turned on from 25/04/2008 to 14/06/2008 and the aerogenerator directly coupled to the PEM electrolyser bank during this period. This period included some testing and maintenance, which were carried out on days with low wind speed and hence no energy transfer. Over the entire period, there were only 12 days in which wind speeds were higher than the cut-in wind speed for the aerogenerator, and hence caused the system to go into the 'start-up state' and recording of wind speed every second. The accumulated time of hydrogen production was 76 hours, less than 12 days because for the system to generate hydrogen the wind speed has both to exceed cut-in wind speed and the aerogenerator has to produce a voltage exceeding the electrolyser cut-in voltage (after rectification). The AIR 403 control system took data from all transducers on average every second and stored the data in an Excel spreadsheet for later analysis.

The measured wind speed frequency distribution over this study period is shown in Figure 54, with the interval over which each wind speed is recorded being one second. It can be seen that for close to 65% of the time over this period, the wind speed was less than 3.5 m/s, the cut-in wind speed of the AIR 403 aerogenerator, so that the unit was not operational.

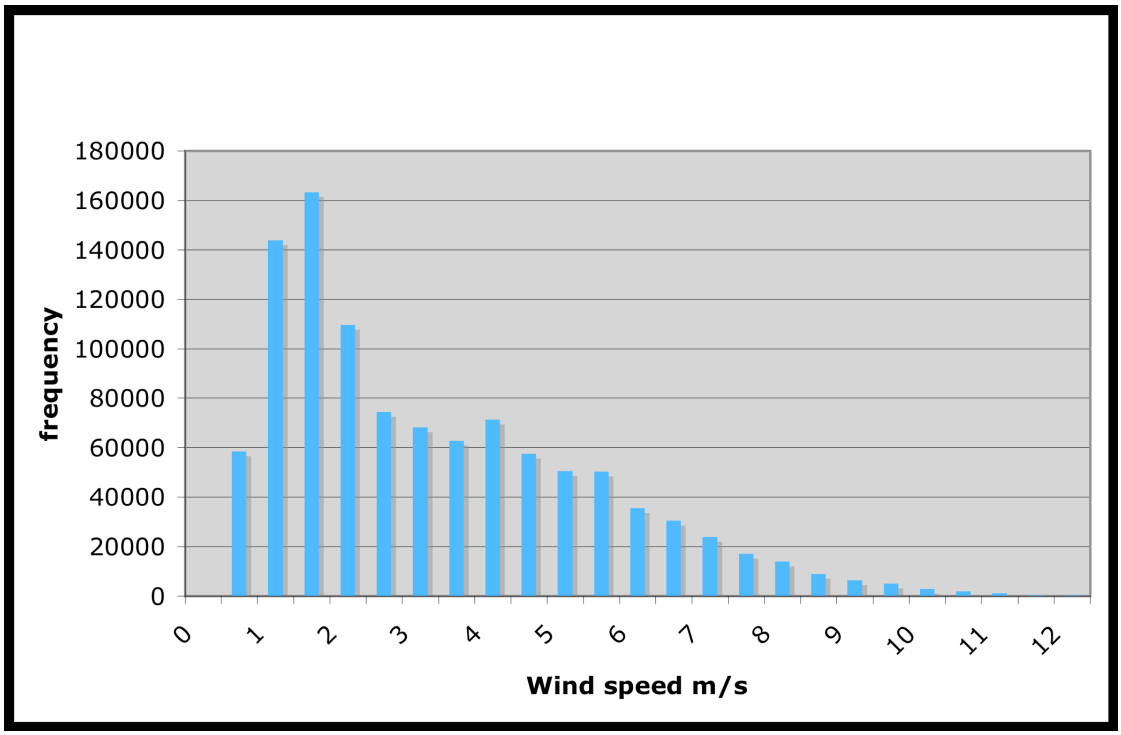

Figure 54: Wind speed frequency distribution at RMIT Bundoora East over the trial period 25/04/2008 – 14/06/2008. The frequency refers to the number of intervals of 1 second during which the wind speed was in each of the ranges shown. The ranges are each of 0.5 m/s width, that is, 0 – <0.5 m/s, 0.5 - <1 m/s and so on up to 11 – 11.5 m/s.

5.4.2 Energy transfer and hydrogen production

5.4.2.1 Total energy transferred

The electrolyser configuration used in the direct coupling experiment had 21 cells electrically connected in series and 2 branches in parallel, made from six h-tec StaXX 7 electrolysers as explained earlier in section 5.2.3. The total measured electrical energy transferred for the entire experimental period from the aerogenerator to the electrolyser bank was 1.53 kWh (or approximately 0.255 kWh per individual electrolyser stack).

5.4.2.2 Hydrogen gas production and efficiencies

The total hydrogen gas produced over the experimental period was 27.6 g, which is the equivalent of 1.1 kWh of energy (HHV).

The Faraday efficiency for each electrolyser stack was calculated from the experimental data from an average of 50 data points, that is, as an average over each successive period of 50 seconds. The instantaneous value of Faraday efficiency could have been be calculated but would not be accurate because it takes a short time for the hydrogen gas flow rate to change as a result of a change in the electrical input to the electrolysers.

The reaction time to electrical input of the electrolysers was observed and can be categorized as "instant". The electron that flow into an electrolyser will be transported through conductors to electrode then into electrolyte – this process has no time lag. However, the step that form hydrogen gas molecule does have very small time lag in itself but because it was not possible to time the period between the electrical input and the hydrogen generation due to its rapidity.

Electrolyser number 5 and 6 are control group electrolyser. Only electrolyser number 5 was used in a previous experiment by another researcher. As a result, the control group comprised new and used electrolysers of the same model.

Two Faraday efficiency experiments were carried out on each electrolyser where electrical DC voltage and current were applied. One experiment varied current input from 0 to 3.8 amps, whereas the other applied a constant 13.0 volts and 3.85 amps. The hydrogen production rate was measured by the same equipment as in the main rig: Agilent 34970A data acquisition unit, thermocouples, current shunt, hydrogen mass flow meter. Practically, nothing was moved from the main experimental rig, but each electrolyser was isolated.

The temperature of an electrode at the middle of an electrolyser stack was continuously sampled. Only the area close to the thermocouple was insulated. The current input was used to calculate the total charge input into the electrolyser, which intern used to determine the theoretical hydrogen production. The measured hydrogen production in mass is always less than the theoretical value and hence the Faraday efficiency.

The average Faraday efficiency of the electrolyser bank over the full period of its operation was 85%, that is, moderately high. The Faraday efficiency of each electrolyser varied from less than 10% at very low current, to 94% at maximum current. The variation of Faraday efficiency with current for two of the electrolyser stacks used is presented in Figure 55.

Another experiment was conducted on one h-tec electrolyser stack (number 6) to investigate whether the cell temperature affects Faraday efficiency significantly (figure 56).. It can be seen that the Faraday efficiency stayed in a narrow band just above 90% throughout this rise in temperature. Thus it can be concluded that the cell temperature of the h-tec PEM electrolyser did not significantly affect its Faraday efficiency.

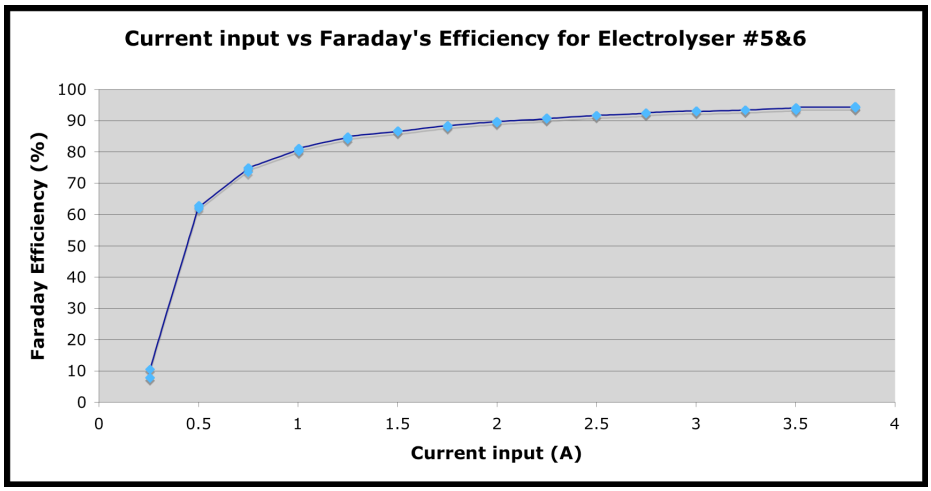

Figure 55: Variation of Faraday efficiency of electrolyser stacks 5 & 6 with current input

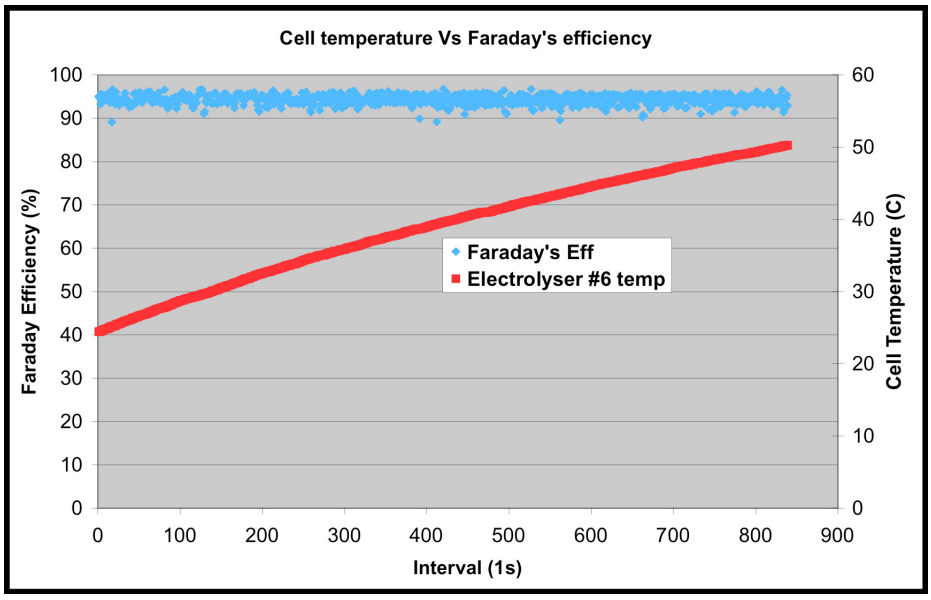

Figure 56: Faraday efficiency (electrolyser #6) was not significantly affected by cell temperature at constant current input.

For the entire period of the direct coupling experiment, the electrically measured energy input of electrolyser stack was 1.53 kWh. This amount of energy is used in the electrolysis process and essentially produces hydrogen gas. The measured energy produced in the form of hydrogen gas from electrolyser stack was 1.1 kWh (HHV). Therefore the experimentally measured efficiency of electrolyser stack was 72%.

5.4.3 Electrolyser performance and degradation

5.4.3.1 Experimental method of direct couping to study electrolyser degradation due to intermittent and variable electrical input from aerogenerator.

The V-I characteristic curves of the electrolysers both in the experimental group and control group were measured before the experiment to provide a benchmark against which any performance degradation during the experiment could be identified. The control group was subjected to a constant electrical input up to the same total kWh as input to the experimental group from the aerogenerator over the full experimental period. After the experiment, the V-I characteristic curves of all the electrolysers were remeasured.

Electrolysers1-5 had previously been used in an earlier experiment in another project in which they were directly coupled to a PV array and each subjected to an average energy input of 7.96 kWh over a period of 1 month (Paul, 2009). Electrolysers 6, 7 and 9 were new at the start of the present experiment. The V-I characteristic of electrolyser 5 will thus be compared to those of electrolysers 1-4 since they have been used for the same total energy input. The V-I characteristic of electrolyser 6 will be compared to those of electrolysers 7 and 9 for the same reason. Because the latter electrolysers were directly coupled to the aerogenerator and subjected to a variable and intermittent electrical input, the comparison with the control group electrolyser shows any degradation due to this variable and input, rather than simply the time of use.

The V-I curve of each electrolyser was measured in an experiment, where DC voltage was applied by using a DC power supply, as the voltage was increased in steps, the current input was monitored. The experimental set up was the same as in section 5.4.2.2, where each electrolyser was isolated and all equipment was as the main experiment and the equipment accuracy can be seen in section 5.2.5. The set up of voltage and current

measurement offered very accurate data and this was also helped by the use of the same equipment set up at both V-I test before and after the direct coupling experiment.

5.4.3.2 Energy input to control group electrolysers

From the experimental results, the total energy input is 1.53 kWh for the six electrolysers in the experimental group. The average energy input was thus 255 Wh per electrolyser. Therefore electrolysers 5 and 6 in the control group were connected in parallel and received a constant power input of 46.7 W (3.83 Amps at 12.2 V), that is, 23.4 W each, for a period of 10.9 hours so that the energy input per electrolyser was again 255 Wh as for the electrolysers in the experimental group.

Electrical power input into each branch was monitored separately (see comment 4 above or section 5.3): current and voltage inputs. The difference between power inputs at each electrolyser branch is negligible as suggested by experimental results. Because electrolysers in each branch are connected in series and hence the current passes through each of them is the same. Therefore only the difference in voltage drop across each electrolyser will contribute to the power input of each electrolyser. The voltage drop across an electrolyser was not measured. However, degradation test (section 5.4.3.3) showed that the power inputs of all electrolysers are between 53 and 56 W. The difference is 5.6% of the smallest power input.

5.4.3.3 Degradation of previously used electrolysers

As mentioned earlier, electrolysers 1-5 were used in an earlier PV direct-coupling experiment and hence may have suffered performance degradation due to a combination of straight time of usage, and the variable power input

The results here show that electrolyser 5 had the largest degradation in the previous experiment (Figure 61) as measured by the changed gradient of its V-I curve. Hence after the PV experiment, a higher applied voltage was required to produce the same current. For example, 12.98 V applied to electrolyser 5 yielded a current of 3.5 A before the PV direct coupling experiment, whereas after 13.76 V was required to give the same current, that is,

a 6.0% voltage increase. Thus the power input increased by 2.7 W for the same hydrogen production rate. The performance of electrolysers 1, 2 and 3 only degraded slightly (Figure 57, Figure 58 and Figure 59), while electrolyser 4 (Figure 60) did not show any sign of degradation, as a result of the PV experiment.

After the PV direct-coupling experiment, electrolysers 1-4 were used in the aerogenerator direct-coupling experiment each to a total of 255 Wh energy input, whereas electrolyser 5 was used for constant input of 255 Wh. Electrolyser 5 did not show any further degradation as a result of this constant power input (Figure 61). The other electrolysers used in the wind experiment showed recognisable degradation after the experiment (Figure 58, Figure 59 and Figure 60) except for electrolyser 1, where the result suggested performance improvement after direct coupling wind – hydrogen energy system (Figure 57). This unexpected behavious is discussed later in section 5.5.

For illustration, electrolyser 2 required 13.19 V voltage before the PV experiment to produce a current of 3.5A (that is, a power input of 46.2W), while after the PV experiment this voltage increased to 13.44 V (47.0 W power input). After the aeorgenerator direct-coupling experiment the voltoage to produce 3.5 A rose again to 13.8 V (power input 48.3 W) (Figure 58). This degradation means that to produce the same amount of hydrogen at 3.5 A the power input to electrolyser 2 had to be increased by 1.3 W (2.8%) after the aerogenerator direct coupling experiment compared to before. The V-I curves of electrolyser 3 show a similar trend (Figure 59).

Thus this degradation is likely to be due to the intermittent and variable power input only, rather than simply time of usage.

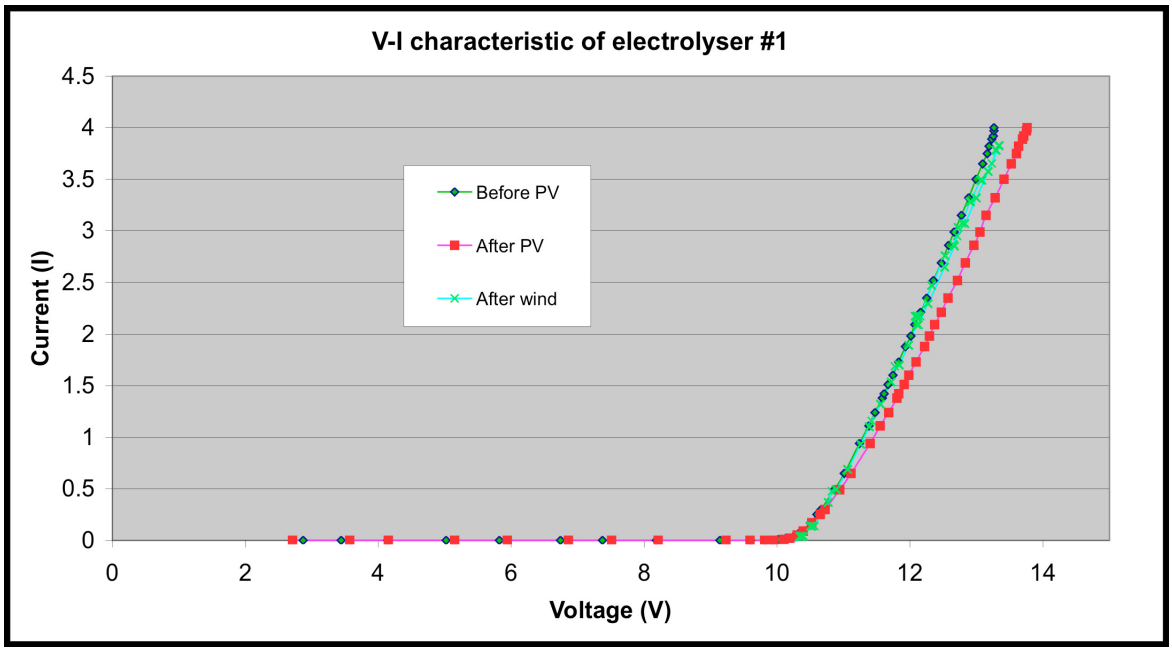

Figure 57: V-I curve plots for electrolyser 1 before a previous PV direct-coupling experiment, after the PV experiment (that is, at the start of the present wind direct coupling experiment), and after the wind experiment coupling. The V-I curve shows an unexpected improvement of performance after the wind direct coupling experiment.

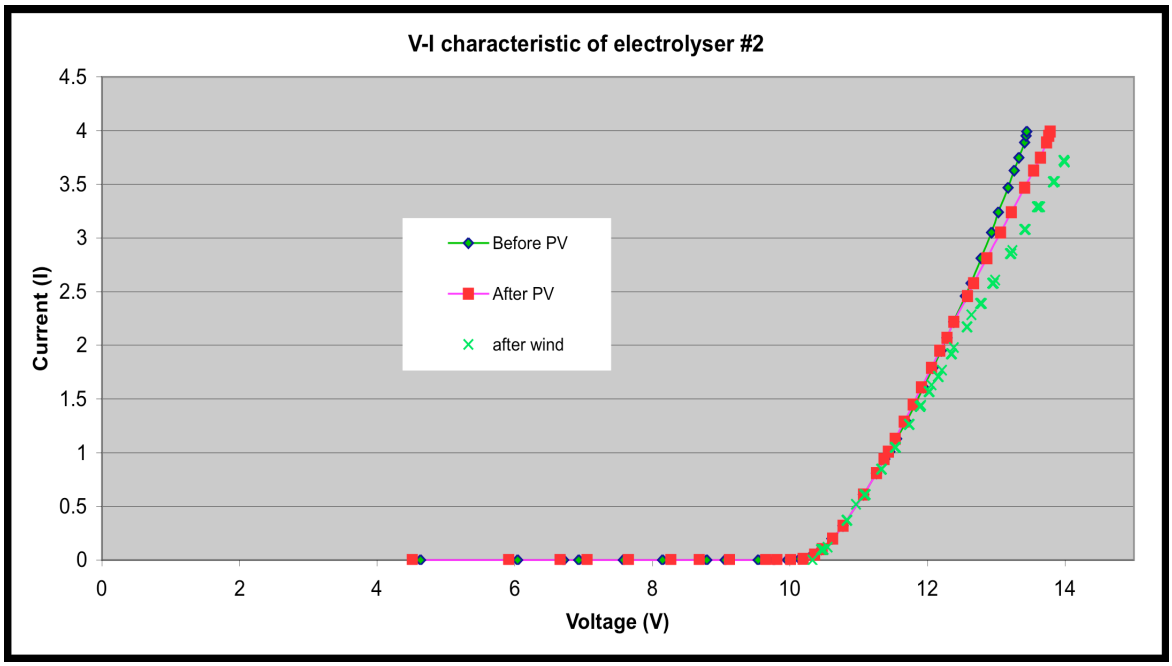

Figure 58: V-I curve plots for electrolyser 2 before a previous PV direct-coupling experiment, after the PV experiment (that is, at the start of the present wind direct coupling experiment, and after the wind experiment coupling. This electrolyser shows moderate further degradation due to the wind experiment.

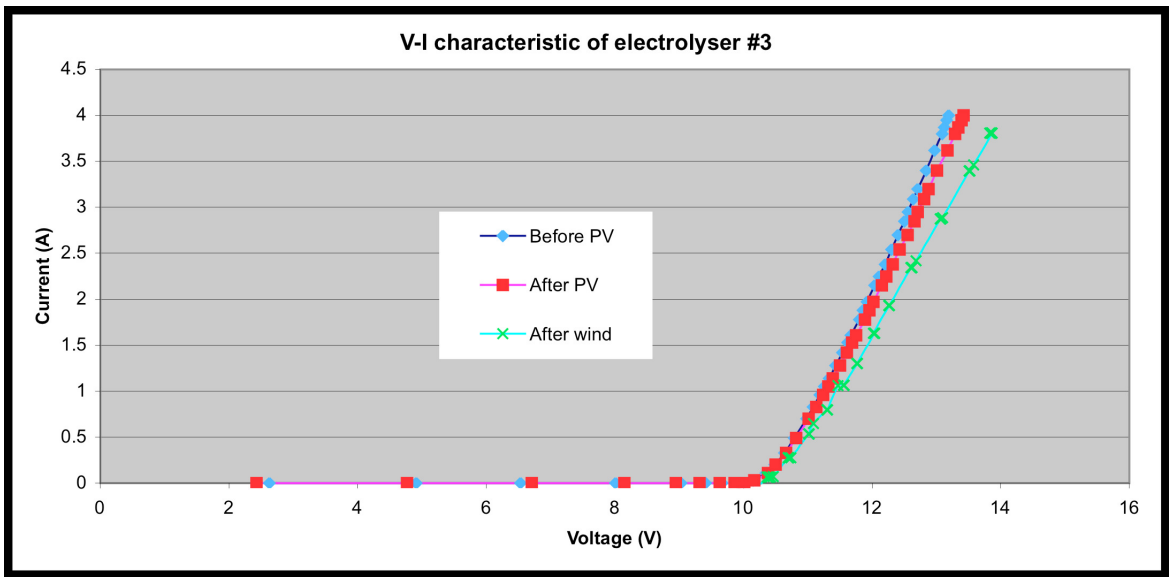

Figure 59: V-I curve plots for electrolyser 3 before a previous PV direct-coupling experiment, after the PV experiment (that is, at the start of the present wind direct coupling experiment, and after the wind experiment coupling. This electrolyser shows significant degradation due to the aerogenerator direct-coupling experiment.

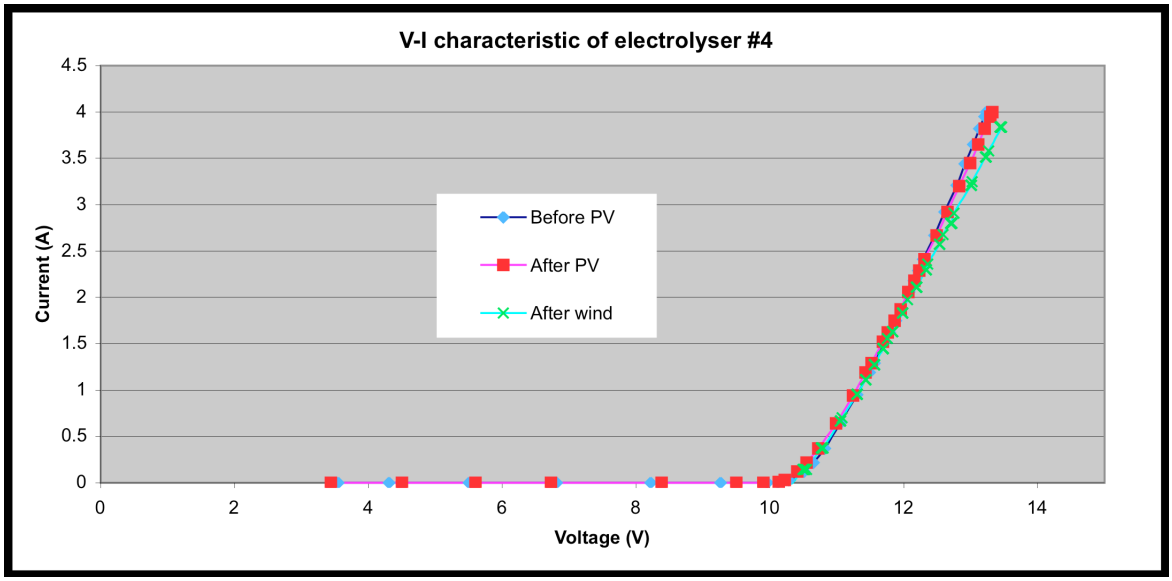

Figure 60: V-I curve plots for electrolyser 4 before a previous PV direct-coupling experiment, after the PV experiment (that is, at the start of the present wind direct coupling experiment, and after the wind experiment coupling. This electrolyser shows only a slight degradation due to the aerogenerator direct-coupling experiment.

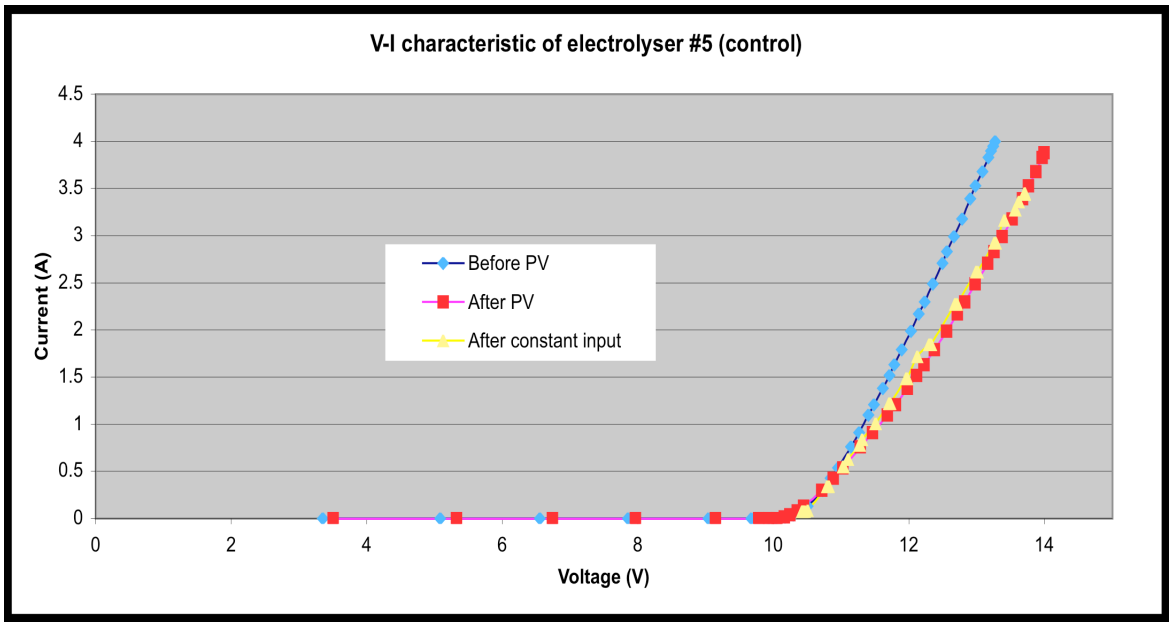

Figure 61: V-I curve plots for electrolyser 5 (control group/previously used electrolyser) before a previous PV direct-coupling experiment, after the PV experiment, and after a constant electrical input. This electrolyser shows significant degradation due to the PV direct coupling experiment but very little further degradation after the constant power input.

5.4.3.4 Degradation of new electrolysers

Electrolysers 6, 7 and 9 were purchased new for this project. Electrolysers 7 and 9 were used in the aerogenerator direct coupling experiment and were therefore exposed to an intermittent and variable electrical input. Electrolyser 6 was used as a control and subjected to a constant electrical input equivalent to the total energy input to the electrolysers in the experimental group over the study period.

By examination of their V-I characteristic curves before and after the experiment in Figure 62, Figure 63 and Figure 64, recognisable degradation occurred only in electrolyser 7. For the latter electrolyser (Figure 62), 12.7 V was needed to produce a current of 3.5 A prior to the experiment (that is 44.45 W), while 13.0 V was needed for the same current after the experiment, that is, a 2.4% voltage increase, and a power input increase of 1.05 W (2.4%).

A comparison between a sample of used and new electrolysers was made. In this case, electrolyser number 2 will be compared to number 7. Firstly, the amounts of degradation due to aerogenerator direct coupling of both electrolysers are similar: electrolyser number

2 has power input increased by 2.8%, while it is 2.4% for the other. The voltage of electrolyser number 2 increased by 2.6%, similar to the 2.4% for electrolyser number 7 at the current of 3.5 A.

However, the energy inputs of the electrolysers are much different. The electrolyser number 2 received 7.96 kWh and the addition of 255 Wh (0.255 kWh), whereas the electrolyser number 7 only received 255 Wh.

It is appearent that the new electrolyser received very little energy and this may have caused the non-uniform result of degradation. The amount of energy input may not have allowed some electrolysers sufficient time for degradation of performance to develop. In addition, each electrolyser is slightly different due to manufacturing processes. Therefore the result from each electrolyser in this group is slightly different.

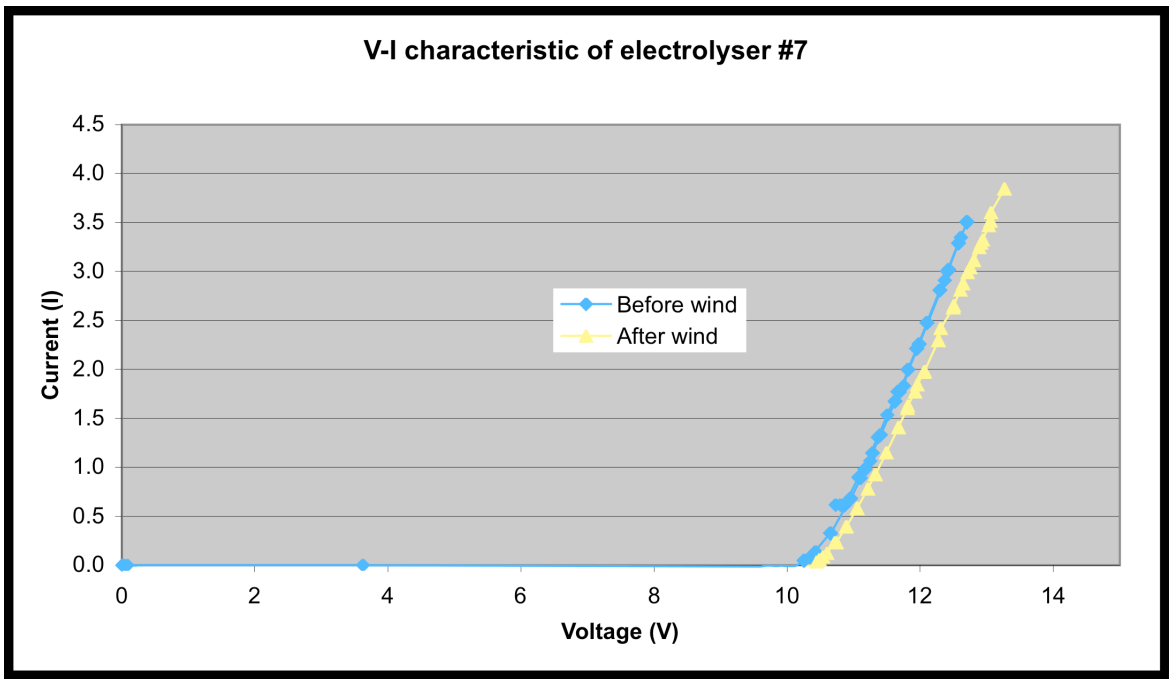

Figure 62: V-I curve plots of electrolyser 7 before and after aerogenerator direct-coupling experiment. A slight degradation due to the wind experiment is evident.

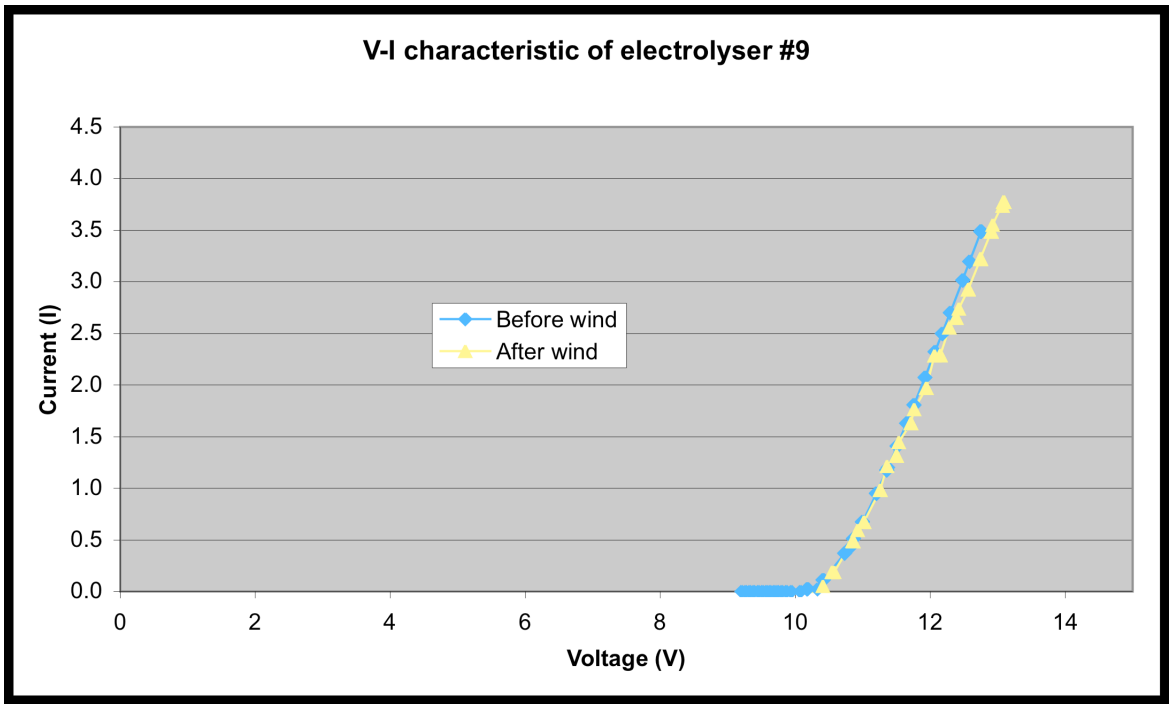

Figure 63: V-I curve plots of electrolyser 9 before and after the aerogenerator direct-coupling experiment. This electrolyser does not show any obvious degradation due to the wind experiment.

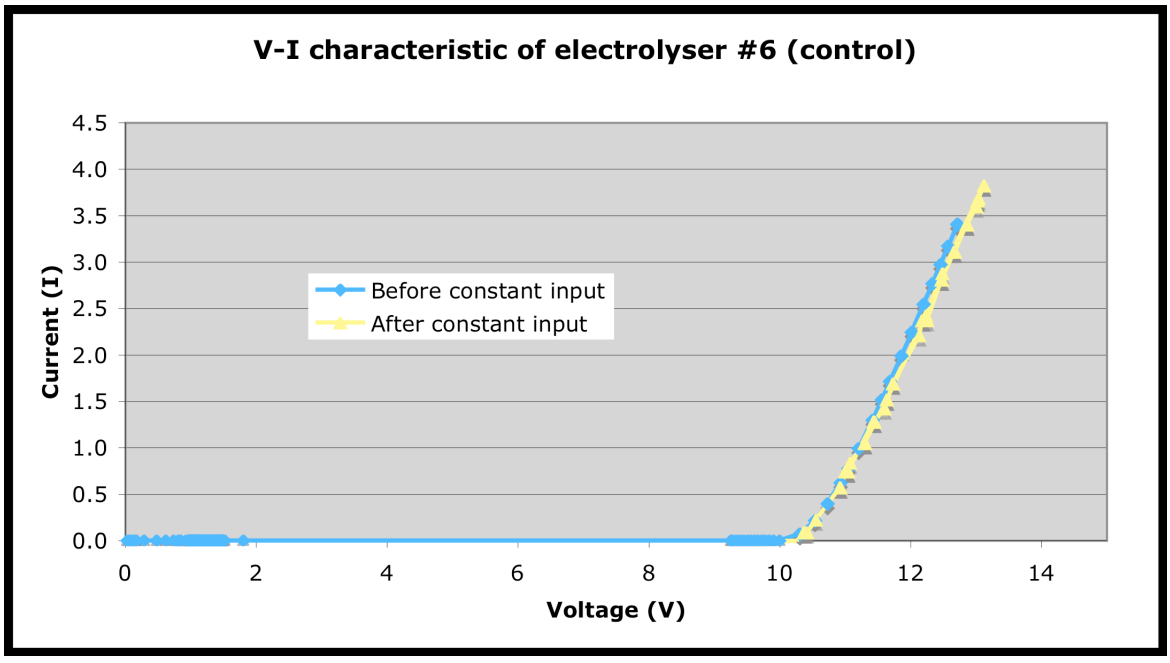

Figure 64: V-I curve plots of electrolyser 6 (control group/new electrolyser) before and after the aerogenerator direct-coupling experiment. This electrolyser does not shows any obvious degradation due to the wind experiment.

5.5 DISCUSSION

During the entire period of the experiment, days with low wind speed were used for maintenance and system checks, so that wind data are not available. There are days with reasonable wind speed; however, on many occasions, the system started but it could not produce sufficient voltage to generate hydrogen gas. There are a several days with good wind speed, which bring the experimental rig into action and hydrogen is produced and measured. The autonomous control system worked well without human intervention.

The wind speed data from this experiment will be used as input in theoretical analysis of direct coupling and the result of ths experiment is then used to validate the theoretical result. The electrolyser bank configuration was decided on the basis of electrolyser availability. Therefore the theoretical analysis must use the same electrolyser configuration. There were five used electrolysers, of which four were used in the experiment as experimental group and one electrolyser was kept as the control; used electrolysers will be campared to used electrolyser. Likewise, there were three new electrolysers, of which one was kept for the control group. As a result there were six electrolysers in the experimental group.

The measured degradation of electrolyser number 2,3,4 and 7 that occurred due to direct coupling to the aerogenerator is similar in magnitude to the degradation as a result of the earlier PV direct coupling experiment (Paul, 2009). But the energy input in the experiment was much less. The total energy input for each electrolyser from PV direct coupling is 31 times that in the aerogenerator direct coupling experiment. The form of degradation that occurred in this experiment will be more apparent in new electrolysers if more time is provided.

The result from electrolyser 1 suggested that the electrolyer performance decreased after PV direct coupling experiment (Paul, 2009) but only to improve after aerogenerator direct coupling experiment. This particular result is in contradiction with others. A more thorough investigation is certainly needed of this result, which is unexpected since generally performance would be likely to decrease rather than increase with additional usage. However, this further testing could not be achieved within the time frame of the current project.

Other used electrolysers that showed signs of degradation were electrolysers 2, 3 and 4, although the degradation of electrolyser 4 was small compared to the other two. This difference in effect may be due to the manufacturing processes of the electolyser themselves. On the other hand, only one of two new electrolysers showed recognisible degradation: electrolyser 7.

This variability in the degree of degradation from electrolyser to electrolyser in both the experimental and control groups indicates that additional experiments involving a larger number of electrolysers are needed before any firmer conclusions can be drawn. In addition, the degradation in performance needs to be measured at regular intervals over a longer period of usage, both with constant power input and variable power input, to gain a better understanding of the practical lifetime of the electrolysers. A number of different designs of PEM electrolyser also need to be tested under similar conditions to see whether the degree of degradation differs from design to design.

5.6 CONCLUSION

An experimental rig to investigate quantitatively the direct coupling of an AIR 403 aerogenerator to a bank of h-tec PEM electrolysers has been constructed at RMIT University Bundoora East campus. The rig and its safe operation are controlled by a specially designed and constructed control system. The software is constructed using Visual Basic/Visacom. The complete rig is designed for autonomous operation in which the system control is exercised by the control system using contactors and switches and real-time experimental and process data. The electrolysers and hydrogen handling unit were installed in a specially-designed hydrogen experiment cabinet with a safety system set up so that power from the aerogenerator can only be fed to the electrolysers if air is being extracted from the cabinet by an exhause fan. Moreover, installed hydrogen detectors ensure that power input is terminated if hydrogen gas concentration reaches a present value well below the flammable limit. The control system that operates the experimental rig also monitors the wind speed, voltage and current, and makes sure they are all within safety limits.

An experiment in which the AIR403 aerognerator was directly coupled to a bank of PEM electrolysers was run successfully over a period of 51 days. The measured total enegy transfer from the aerogenerator to the electrolyser bank over the srtudy period was 1.53 kWh. The total hydrogen produced was 27.6 g, which is the equivalent of 1.1 kWh of energy (HHV). These results will be compared in chapter 6 with predictions using the theoretical analysis of direct coupling presented in chapter 4.

Some degradation in the performance of electrolysers as a result of the intermittent and variable electrical input from the aerogenerator was observed, over and above any degradation simply due the period of usage. For example, for some previously used electrolysers, the power input to obtain near the maximum current (and hence hydrogen production) rose by as much as 2.8% between the beginning and end of the direct coupling experiment.

However, the degradation in performance of the new electrolysers varied from one unit to another so that no general conclusions can be drawn.

While a great deal of further testing is required to establish just how much PEM electrolysers of various types and previous usage degrade under sustained variable power input, the results here do suggest that ways to minimise electrolyser degradation in wind – hydrogen energy systems is an important issue requiring further investigation in the future.

6 COMPARISON OF EXPERIMENTAL RESULTS FOR DIRECT COUPLING WITH A THEORETICAL ANALYSIS

6.1 INTRODUCTION

In the previous chapter, the results of an experimental trial of directly coupling an AIR403 aerogenerator to a matched PEM electrolyser bank at RMIT University's Bundoora East campus were reported. The present chapter applies the theoretical analysis of direct coupling described in chapter 4, based on the steady-state aerogenerator performance as measured in the wind tunnel experiment described in chapter 5, to the conditions prevailing during this direct-coupling trial. The experimental results for energy transfer are then compared with the theoretical prediction.

6.2 THEORETICAL ANALYSIS OF DIRECT COUPLNG – BUNDOORA EAST TRIAL

As described in chapter 5, the experimental trial of the AIR 403 aerogenerator directly coupled to a bank of PEM electrolysers was conducted at RMIT Bundoora East over the period from 25/04/2008 to 14/06/2008.

A theoretical analysis of the energy transfer between aerogenerator and electrolyser under direct coupling over this period using the actual wind speed distribution (as presented in Figure 54 in chapter 5) has been conducted using the procedure presented in chapter 4 for a number of possible electrolyser configurations. The results obtained are shown in Table 4. The best electrolyser configuration in terms of total energy transfer found in this case is 3 parallel branches, each branch containing 17 cells in series. This configuration was estimated to result in only a 6.42% energy transfer loss compared to the maximum theoretically achievable.

However, in the actual trial based on h-tec seven-cell electrolyser stacks, the configuration employed comprised 2 parallel branches, with each branch containing three h-tec electrolyser stacks in series, that is, a total of 21 cells in series (see section 5.2.3). With this

configuration it is estimated that the total energy transfer over the study period is 4.81 kWh, compared to a maximum achievable of 6.0 kWh if the maximum power point operation could have been maintained at all times; that is, the energy transfer loss is 19.8% of the total energy transfer (Table 4). The operating V-I curve of this configuration is shown in relation to the maximum power point curve of the aerogenerator (MPC) in Figure 65.

Theoretical energy transfer (kWh)				**Experimental energy transfer (kWh)**
Maximum power curve (MPC)	*Maximum power curve (MPC):after rectification*	*Configuration tested:before rectification*	*Configuration tested:after rectification*	
6.67	6.0	5.34	4.81	1.53

Table 4: Theoretically-estimated energy transfer between aerogenerator and electrolyser bank (2 parallel branches) in a direct-coupling experiment based on the actual wind frequency distribution over the period of the experiment conducted at RMIT Bundoora East (25/04/2008 to 14/06/2008).

However, a rectifier efficiency must be appied to this theoretical estimate of energy transfer under direct coupling need to be made before any comparison is made with the experimentally-measured energy transfer reported in chapter 5. The power transfer efficiency of the rectifier is estimated to be 90%. Hence the theoretical power must be further multiplied by a factor of 0.9.

In addition, the wind speed frequency distribution was obtained from an anemometer that was not located in exactly the same place as the rotor of the aerogenerator, so it is likely that there was some disparity between the recorded wind speed and the actual wind speed experienced by the aerogenerator in any given interval during the study period. It has not been possible due to time constraints to conduct a separate experiment in the course of the research program for this PhD project to measure the magnitude of this difference in wind speeds under a range of conditions, in particular wind directions and wind speed magnitudes. Here then it will simply be noted that a correction still needs to be made for this effect, but that it cannot be made at this time due to lack of experimental data.

For the correction factors that have been estimated, the theoretically estimated power ($P_{theoretical}$) at a given recorded wind speed thus needs to be corrected as follows:

$$P_{corrected} = 0.9\ P_{theoretical}$$

Therefore, the correction factor can be substituted into

Equation 43 (chapter 4) and hence the theoretical estimated energy transfer becomes:

$$E_{corrected} = \sum_{1}^{N}\{(0.9).P_{elec}(v_i)\}\times t\times f\} = (0.9)\sum_{1}^{N}\{P_{elec}(v_i)\}\times t\times f\} = (0.9)E_{trans}$$

where $E_{corrected}$ is the theoretical estimated energy transfer after application of correction factor and P_{elec} is $P_{theoretical}$.

The theoretical estimated energy transfer of direct coupling between the AIR 403 aerogenerator and h-tec PEM electrolyser with the configuration comprising two parallel branches, each branch containing 21 cells in series, is thus:

$$E_{corrected} = (0.9)E_{trans} = 0.9\times 5.34 = 4.81 \quad \text{kWh}$$

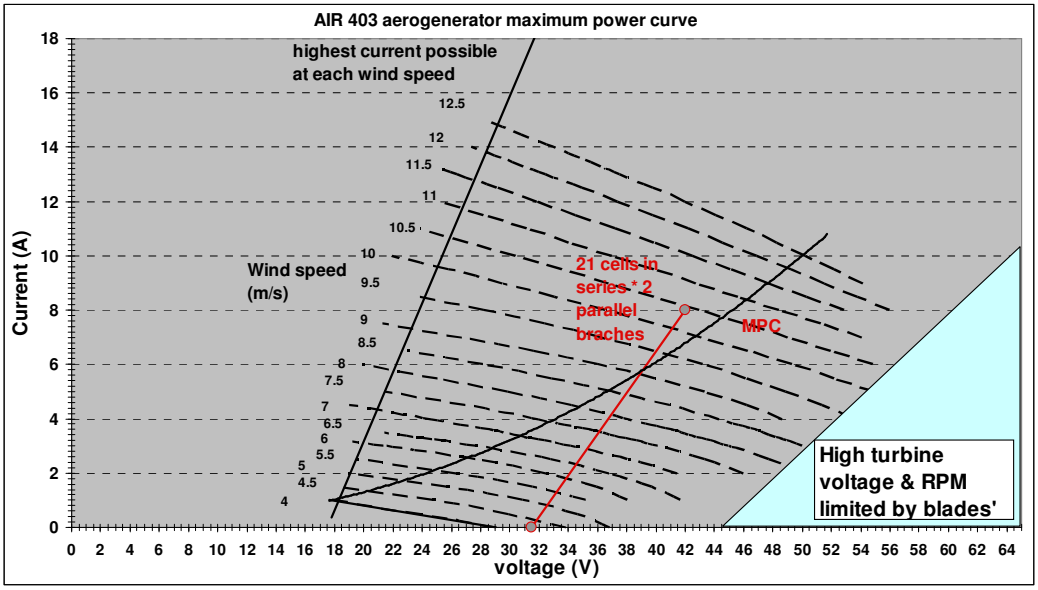

Figure 65: The V-I operating curve of the electrolyser configuration used in the direct-coupling trial (2 parallel branches each with 21 cells in series) compared to the maimum power point curve of the AIR403 aerogenerator.

6.3 COMPARISON OF THEORETICAL RESULTS FOR DIRECT COUPLING WITH THEORETICAL PREDICTIONS

The experimental result of energy transfer with direct coupling between the AIR 403 aerogenerator and h-tec PEM electrolyser is compared to the theoretical estimated energy transfer in Table 4. The theoretical estimated energy transfer is 4.81 kWh compared to the experimental result of only 1.53 kWh. Although the effect of the expected disparity between the recorded wind speed and the actual wind speed experienced by the aerogenerator has not been considered, the discrepancy between the two energy transfer results is large enough to suggest that other factors also merit further investigation.

It can firstly be observed from Figure 66 that the experimentally-measured V-I curve for the directly-coupled aerogenerator – electrolyser system (labelled "operating point of AIR 403") tracked the expected curve based on the analysis of the electrolyser reasonably closely, showing only a small deviation as wind speeds climbed.

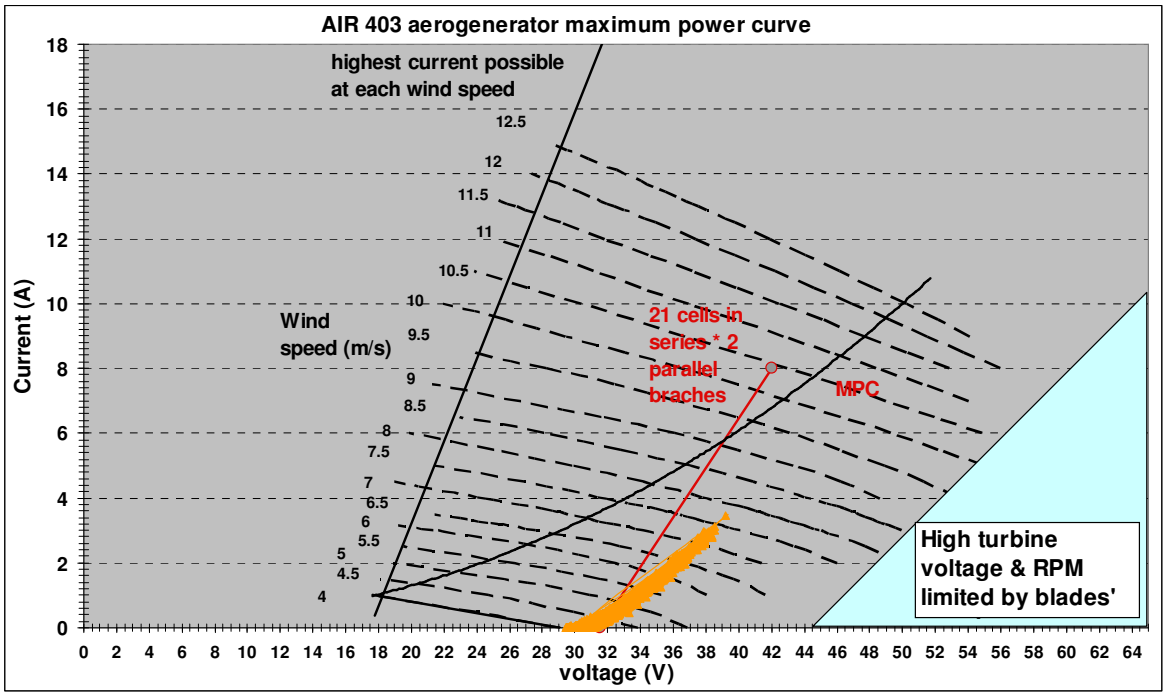

Figure 66: AIR 403 aerogenerator operated as expected and output current and voltage close to V-I characteristic of the electrolyser stack.

However, a comparison of the experimental data on actual power generated by the aerogenerator with theoretically estimated power using the measured wind speed over relatively short time periods reveals that the actual power fell well short of that expected (Figure 67).

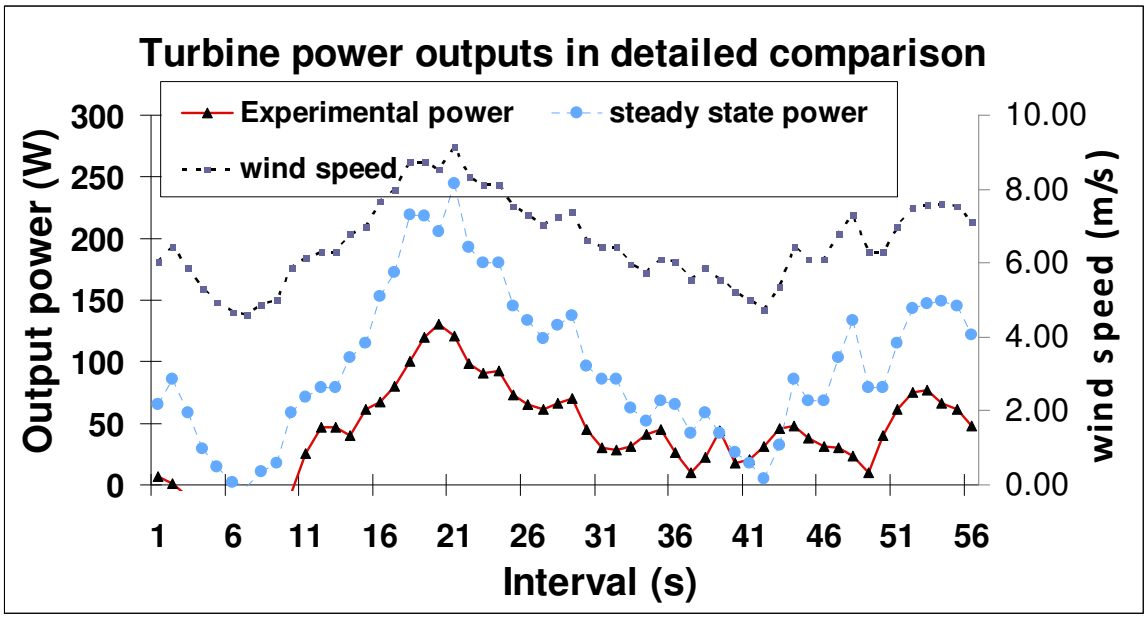

Figure 67: Actual power transferred between the aerogenerator and electrolyser stack measured from the experiment compared with the theoretical power transferred calculated from the measured wind speed.

According to Figure 67, during the experiment from the start up to the 11th interval the wind speed is above the cut-in wind speed of 3.5 m/s and the system is turned on. The theoretical steady state power transferred is positive (see section 4.2.2). However, the actual power is zero. Between the interval 11th and 26th, the theoretical power jumps rapidly to 250 W due to increasing wind speed to 8 m/s whereas the actual power is positive and rises to only 130 W. Although the actual power graph does have a similar profile over the period, its magnitude reaches only approximately half the theoretical estimate.

From more extensive examination of the data over the whole experimental period, two observations can be made:

- There are many times when theoretical power is positive and the actual power is zero.
- The actual power graph usually has the same profile as the theoretical power but has a much lower magnitude.

As mentioned above the magnitude of the effect of any disparity between anemometer wind speed readings and actual hub height wind speed remains unknown at this stage. Nevertheless there would appear to be some evidence from the power data collected that the dynamic response of the aerogenerator subject to varying wind speeds may be significantly different to the response calculated from the measured wind speed in each interval assuming the steady state output of the aerogenerator has always been attained. This finding is supported by similar result of work by Wood and Wright (2004).

Hence the following dynamic factors are likely to require consideration:

- In the experiment, the aerogenerator needs time to change from a stationary state to the minimum angular velocity at which it actually produces power, whereas the theoretical calculation assumes in effect an immediate response.
- In the experiment, the fluctuating wind speed may not allow the angular velocity of the aerogenerator to rise to its steady-state angular velocity, whereas the theoretical calculation assumes immediate attainment of the steady state corresponding to the given wind speed in each interval and thus overestimates the power production. The steady state analysis thus does not take account of the aerogenerator's moment of inertia.

To obtain a closer fit between experimental data and theoretical estimates it is thus likely that a dynamic model of the aerogenerator's response in a variable wind situation is required. The dynamic system model needs to take into account the finite time needed for the turbine to pick up angular velocity from a stationary state, and to respond to rapid changes in wind speed, due to its moment of inertia.

6.4 CONCLUSION

The comparison between the theoretically-estimated energy transfer and the experimental energy transfer between a directly-coupled aerogenerator and PEM electrolyser bank at RMIT University over a period of 51 days has revealed that the steady-state model covered in chapter 4 appears to overestimate the overall energy transfer by as much as three times. The theoretical estimated energy transfer is 4.81 kWh compared to the experimental result of 1.53 kWh. However, it must be noted that the potentially significant effect of any differences between the wind speed as measured by the anemometer and the wind speed experienced by the aerogenerator has not yet been able to be quantified and properly taken into account in this comparison.

Despite this missing information, a close examination of the wind power production data provides some evidence that that the steady-state theoretical model of the aerogenerator employed may overestimate the energy transfer to the electrolyser in intermittent and variable winds because it does not take account of the finite time required for the aerogenerator to respond to the change in wind speed and reach its steady state for any given wind speed. Some preliminary work on the construction and application of a dynamic model of the AIR 403 aerogenerator direct coupled to a bank of h-tec PEM electrolysers has thus been conducted, and is covered in the next chapter.

7 DYNAMIC ANALYSIS OF AEROGENERATOR – ELECTROLYSER SYSTEM

7.1 INTRODUCTION

In the earlier analysis of the energy transfer achievable between a fixed-pitch variable-speed aerogenerator directly coupled to a PEM electrolyser it was assumed that the aerogenerator achieved its steady-state (maximum) output for each wind speed and load. The experimental test of this theoretical approach for an AIR 403 aerogenerator and a suitably-matched PEM electrolyser stack reported in chapters 5 and 6 has revealed a significantly lower energy transfer over the period of the test than that predicted. It was observed that the aerogenerator in the experimental test frequently did not attain the power output expected at the given wind speed on the basis of wind tunnel measurements even after accounting for the wind speed measurement error referred to in Chapter 4. The power output attained in the wind tunnel at each wind speed was of course the steady state value, after allowing sufficient time for the aerogenerator to reach a constant maximum power output. The discrepancy between the energy transfer estimated on the basis of the steady state analysis and the actual experimental result was substantial, although the effect of a possible difference between anemometer wind readings and those actually experienced at the hub of the aerogenerator is still uncertain.

Another possible explanation of this discrepancy is that in a real outside situation where the wind speed is fluctuating at times quite rapidly, there is insufficient time for the aerogenerator to reach its steady-state output at the wind speed measured in a particular small interval. In other words, the dynamic response of the aerogenerator lags significantly behind that expected on the basis of a steady-state analysis for each wind speed measurement as conducted in a wind tunnel. In the present chapter, a preliminary attempt is made to develop a basic theoretical model of the dynamic response of an aerogenerator to varying wind speeds in each successive interval between measurements when directly coupled to a PEM electrolyser load. The model is founded upon an equation relating the net torque on the turbine – generator rotor assembly at a given wind speed to the angular acceleration of this rotating assembly. This equation is then used to calculate the change in angular velocity of the assembly over each interval of wind speed, and hence plot the changes in angular velocity over successive intervals. The variation over time of voltage

generated by the system, which is directly related to the angular velocity of the turbine-rotor assembly, can thus be estimated, and hence the total energy transferred to the electrolsyer over a specified period of multiple intervals.

7.2 PREVIOUS WORK ON THE DYNAMIC RESPONSE OF AEROGENERATORS IN VARYING WIND SPEEDS

The aerogenerator with no pitch adjustment mechanism or other mean of controlling its RPM would produce electrical output whose profile is dictated by changing wind speeds. It is these turbines with permanent magnet synchronous generator (PMSG) that are widely used in RAPS, and their dynamic response has been studied by Wood and Wright (2004). An experiment was carried out on a small PMSG aerogenerator, with a 1 m blade length and a rated power of 600 W, to study its starting behavior. It was found experimentally that the time it takes the turbine to change from being stationary to 250 rpm and generating power varies from 11 to 55 s depending on the profile of the wind speed variation over the period, as shown in Figure 68 & Figure 69. When the wind speed increased from under 6 to above 11 m/s, the turbine started to spin increasingly fast and reached 250 rpm after just over 11 s. However, when the wind speed stayed relatively low at between 3-6 m/s, the aerogenerator took 55 s to reach 250 rpm (Figure 69). The analysis attempted to predict turbine RPM by employing three methods and are validated by experimental results. The first method (curve a in Figure 68 and Figure 69) used lift coefficient (C_l) and drag coefficient (C_d) data vs angle of attack (α) to calculate induced torque. The second method (curve b in Figure 68 and Figure 69) used lift and drag coefficient obtained from approximation, where $C_l = 2\sin\alpha\cos\alpha$ and $C_d = 2\sin^2\alpha$. Lastly, the third method (curve c) obtained the lift and drag coefficient from the average of the first and second methods. As seen in Figure 68 the first method overestimates the RPM slightly compared to the experimental values, whereas the second method underestimates the RPM and yields a greater lag in the response compared to the actual. The third method, on the other hand, is able to track the experimental result closely. The result shown in Figure 69 displays a similar trend but the departures of method a and b from the experimental data are far greater.

The study pointed out that, if wind speeds during the starting time are used to calculate aerogenerator power output, then the analysis would overestimate the energy transfer from a aerogenerator during the process of starting, particularly if the turbines experience low or unsteady winds (Wood and Wright, 2004).

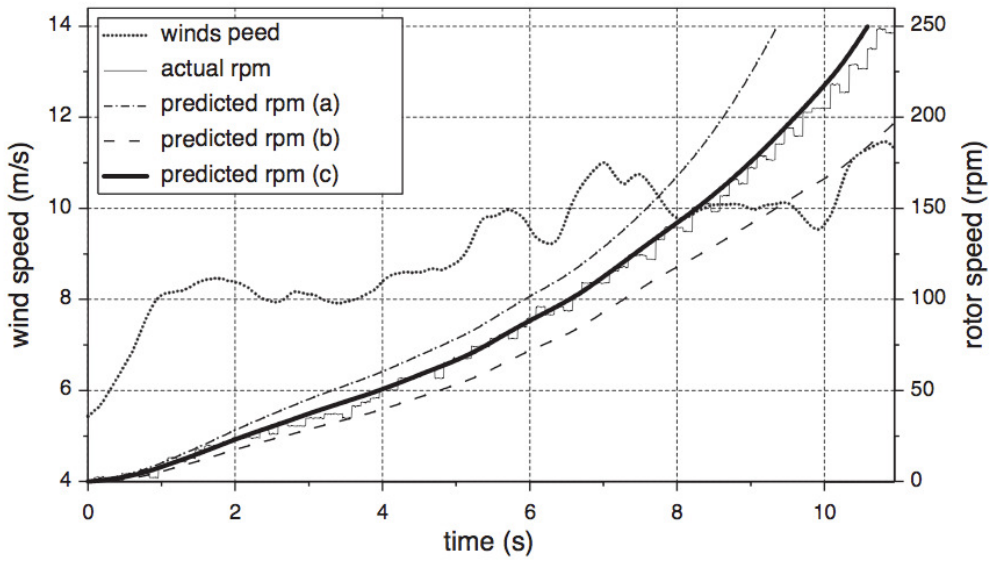

Figure 68: Starting behavior of a small aerogenerator similar in construction to the AIR 403 at high wind speed (Wood and Wright (2004). The diagram indicates the time it takes for this aerogenerator to accelerate to its RPM where electrical power is generated for a wind speed increasing from 5.5 m/s to over 11 m/s. The prediction methods a, b and c are explained in the text. Method a overestimates whereas method b underestimates the RPM. On the other hand, method c tracks the experimental result well.

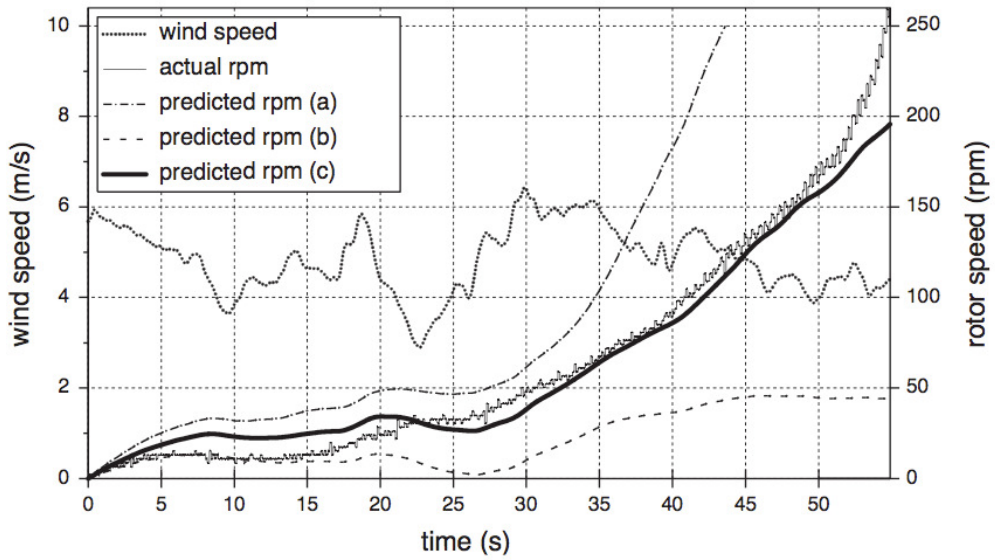

Figure 69: Starting behavior of a small aerogenerator similar in construction to the AIR 403 subjected to relatively low wind speeds in the range 3 – 6 m/s indicates much longer time is taken in this case compared to that shown in Figure 68 for the turbine to reach the rotational speed (250 rpm) where electrical power is generated (Wood and Wright (2004). The method a overestimates whereas the method b underestimates the RPM by large margins as the RPM increases. On the other hand, the method c tracks the experimental result well.

7.3 THEORY INCORPORATING DYNAMIC EFFECTS

7.3.1 Theoretical investigation of direct coupling in the dynamic state

A dynamic simulation of direct coupling of an aerogenerator to a PEM electrolyser is thus needed in order to investigate the dynamic response of the system in highly variable wind speeds and hence predict the power transfer between these two components more accurately.

The main components of the aerogenerator – electrolyser system and the corresponding power inputs and outputs, and energy efficiencies, are shown schematically in Figure 70. The theoretical analysis of each component taking into account dynamic effects is presented in the following subsections. This analysis is then used to construct a simulation model based on Visual Basic and Excel.

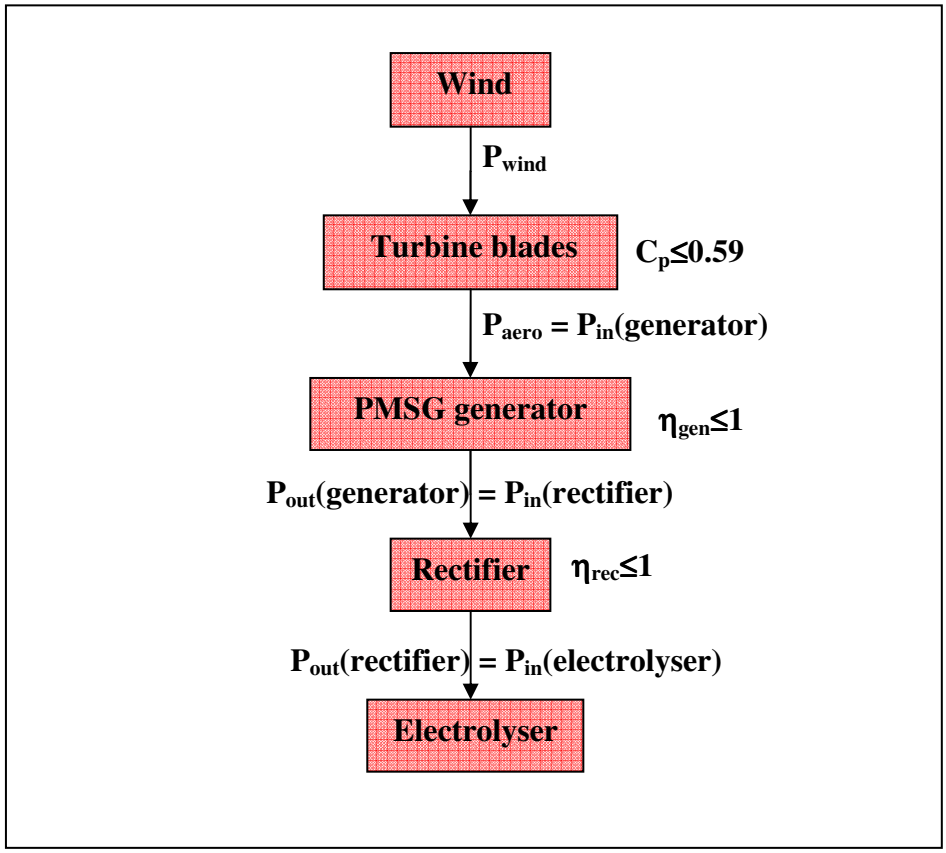

Figure 70 Power transfer and corresponding efficiencies (η) for the main components in the dynamic simulation model starting from power available in the wind (P_{wind}) to the power input to the electrolyser.

7.3.2 Governing equation

In the case under consideration, the aerogenerator is directly coupled to the generator with a common axle and bearings, so the governing equation relating the angular velocity of the aerogenerator (and hence of the rotor of the generator) to the net torque (T_{net}) on the system is:

$$T_{net} = J\frac{d^2\theta(t)}{dt^2} = J\frac{d\omega}{dt} \qquad \textbf{Equation 44}$$

where J is the combined moment of inertia of the rotor and generator rotor assembly, comprising:

- the moment of inertia of the blades

- the moment of inertia of the rotor hub
- the moment of inertia of the rotor of the generator
- the moment of inertia of the axle and any other rotating parts connected to it.
-

θ is the angular displacement of the rotor from some fixed reference point, and $\omega = d\theta/dt$.

At any instant, T_{net} is the difference between the aerodynamic torque generated by the turbine, T_{aero}, and the total mechanical braking torque T_{mec} exerted by the generator rotor on the turbine, as in Equation 45:

$$T_{net} = T_{aero} - T_{mec} \quad \textbf{Equation 45}$$

In the static case, as assumed in the wind tunnel measurements of performance, T_{net} is zero, and the angular velocity of the turbine at the given wind speed remains constant. But in the dynamic case now being considered, there is in general a difference between T_{aero} and T_{net} so that there will be an angular acceleration/deceleration of the turbine and its angular velocity ω will change over time. In order to find the variation of ω with time it is therefore necessary to find expressions for both T_{aero} and T_{net} and then solve equation Equation 44 either analytically or by a numerical method.

7.3.3 The aerogenerator

The aerogenerator blades of a small aerogenerator with a fixed pitch are designed to work in a prescribed wind speed range, typically from 3.5 to 18 m/s. The efficiency of the turbine in extracting the kinetic energy from the wind depends on the aerofoil profile. This efficiency is normally defined as the power coefficient, C_p, as in Equation 46:

$$C_p = \frac{Power\_extracted}{Power\_available}$$ **Equation 46**

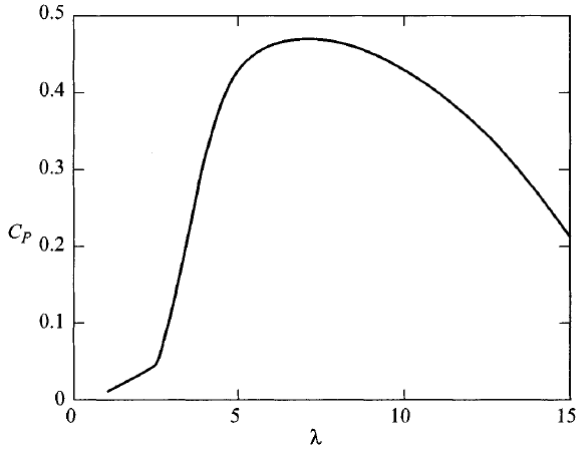

Figure 71: Example of turbine power coefficient (C_p) vs tip speed ratio (λ) of a typical aerogenerator.

The theoretical maximum power coefficient, C_p, is approximately 0.59 and is termed the Betz limit (Burton et al., 2001). The performance of a aerogenerator is conveniently described by a graph of the power coefficient, C_p, versus tip speed ratio (λ), that is, the ratio between the speed of the tip of the rotor and the wind speed (Figure 71). It can be seen from this graph that C_p, and hence the power extracted by the turbine from the wind, depends directly on λ, increasing at first steeply with increasing λ, then reaching a maximum and falling off as λ increases further. Hence for a given wind speed there is an optimal value of λ at which the power extracted by the turbine is maximised, while as λ increases or decreases from this optimal point the power falls. Therefore, the $C_p - \lambda$ graph of a turbine allows the instantaneous power extracted from the wind at any given wind speed and angular velocity (or RPM) of the rotor – and hence value of λ – to be calculated as follows (Burton et al., 2001, Boukhezzar and Siguerdidjane, 2005).

The total power available in the wind at a wind speed of v (m/s) incident on a aerogenerator with a radius of R (m) is given by

Equation 47:

$$P_{wind} = \frac{1}{2}\rho\pi R^2 v^3$$ **Equation 47**

where ρ is the air density (kg/m^3).

From the definition of the coefficient of performance, C_p, the aerodynamic power captured by the aerogenerator, P_{aero}, is given by

Equation 48:

$$P_{aero} = \frac{1}{2}\rho\pi R^2 C_p(\lambda,\beta) v^3$$ **Equation 48**

where the tip speed ratio (λ) is given by

Equation 49:

$$\lambda = \frac{\omega R}{v}$$ **Equation 49**

where ω is the angular velocity of the rotor (rad/s), and β the pitch angle of the rotor blades.

For a aerogenerator of the kind under consideration in this study, the pitch of the rotor blades cannot be actively changed; hence the dependence of C_p on the pitch angle term, β, can be dropped from the formula. The aerodynamic torque T_{aero} induced on the turbine by the moving air can now be found using the relationship given in

Equation 50. In addition, the torque coefficient, C_q, can be related to C_p as shown by

Equation 51, and then substituted into

Equation 48 &

Equation 50 for T_{aero} as done in

Equation 52.

$$T_{aero} = \frac{P_{aero}}{\omega}$$ **Equation 50**

$$C_q(\lambda) = \frac{C_p(\lambda)}{\lambda}$$ **Equation 51**

$$T_{aero} = \frac{1}{2}\rho\pi R^3 C_q(\lambda) v^2$$ **Equation 52**

7.3.4 The electrical generator

The electrical generator in the AIR 403 aerogenerator receives mechanical power transferred through mechanical linkages from P_{aero} via the applied torque T_{aero} and converts it into electrical power. The generator exerts an opposing torque T_{mec} to the torque from the turbine T_{aero}. In general T_{aero} is not equal to T_{mec} and the rotating system will change in angular velocity. If the loss in mechanical linkages is included in the generator efficiency given by the manufacturer, then electrical power output of the generator is given by Equation 53, and the mechanical torque T_{mec} is as given in Equation 54.

$$P_{in}(generator) = \frac{P_{out}(generator)}{\eta_{gen}}$$ **Equation 53**

where $P_{in}(generator)$ is the generator power input (W) and $P_{out}(generator)$ is the generator power output (W).

$$T_{mec} = \frac{P_{in}(generator)}{\omega}$$ **Equation 54**

where the generator efficiency, η_{gen}, includes resistive losses, frictional losses in bearings (which incorporates losses in bearings of the aerogenerator since the same bearing is employed), and core loss (due to eddy currents in the stator) (Boldea, 2006). In this analysis, it is assumed that the generator efficiency is constant throughout its power output range. In addition, since the AIR 403 does operate at its maximum power in the experiments conducted, the rise in losses due to saturation effects is likely to be minimal.

The electromotive force developed (*EMF*) in each phase of a three-phase PMSG has a general relationship as shown in

Equation 55 (Boldea, 2006):

$$EMF = \sum_{i=1}^{N/3} W \times B \times l \times u \qquad \textbf{Equation 55}$$

where W is the number of turns of copper per coil in the winding, B is the average flux density (Tesla) produced by permanent magnet, u is the peripheral speed in m/s, l is the stack length (m), and N is the number of stator slots.

This relationship excludes core loss. The physical construction of a generator – such as copper in the winding, permanent magnet, stack length and number of stator slots – dominates the produced voltage and are fixed by it design. Therefore the voltage output depends primarily on the peripheral speed, which directly relates to ω or RPM. The theoretical voltage output is sinusoidal.

The *EMF* can be re written in the form of ω as in

Equation 56.

$$EMF = \left| \sum_{i=1}^{N/3} (W \times B \times l \times \omega R) \right| \qquad \textbf{Equation 56}$$

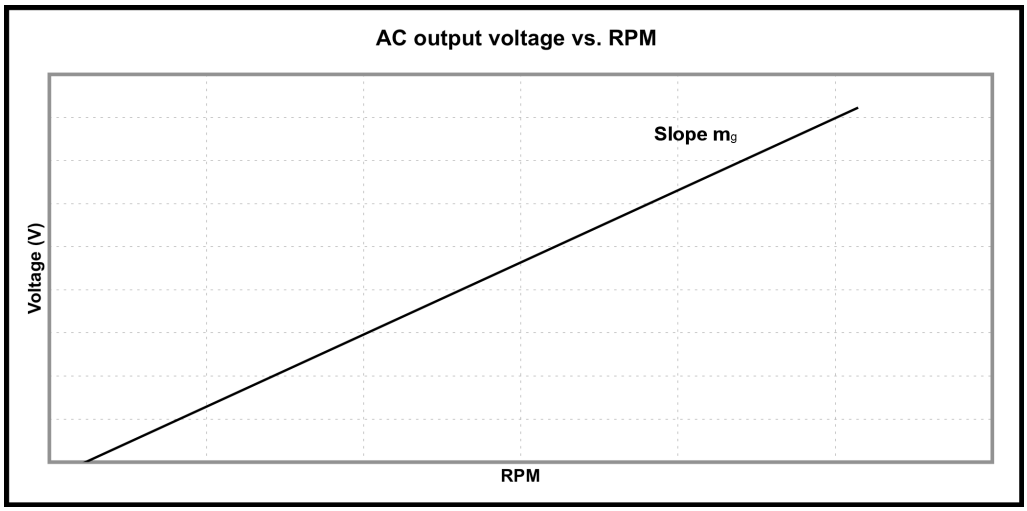

Figure 72: A straight-line approximation of voltage output and RPM relationship of a PMSG generator. This graph suggests that the RPM must be above a value where the EMF is just overcome the internal voltage drop and output useful voltage.

Alternatively, the voltage output (single phase, phase to neutral voltage) vs. generator RPM can also be found experimentally. As shown by Figure 72, it is linear relationship and cuts the voltage axis at point C_g. The RPM need to be above a certain value for the generator to output any useful voltage. This is because it has to overcome internal voltage drop due to internal resistance. The relationship is described by

$$V_a = V_b = V_c = m_g(\frac{60}{2\pi}\omega) + C_g$$ Equation 57:

$$V_a = V_b = V_c = m_g(\frac{60}{2\pi}\omega) + C_g$$ **Equation 57**

where V_a, V_b and V_c are phase-to-neutral voltage output of a generator, $\omega = \frac{RPM \times 2\pi}{60}$ (rad/s), m_g is graph slope and C_g is a constant.

The theoretical three-phase AC voltage inputs to the rectifier are equal to the voltage outputs of the generator assuming zero loss in the transmission line between these two components. Alternatively, if a relationship between generator speed, ω, and voltage

output is available from the manufacturer of an aerogenerator, then it can be used directly in place of $V_a = V_b = V_c = m_g(\frac{60}{2\pi}\omega) + C_g$

Equation 57. The relationship obtained in this project by experiment for the AIR403 aerogenerator is a straight-line relationship of the form illustrated by

$$V_a = V_b = V_c = m_g(\frac{60}{2\pi}\omega) + C_g \qquad \text{Equation 57.}$$

7.3.5 The rectifier

The rectifier used in the present experiment to convert the three-phase AC power output of the generator into DC power for inputting into the electrolyser is a full-wave diode type (Figure 73). According to the theory of such rectifiers, the voltages input V_a, V_b and V_c are converted by the rectifier to a DC voltage (V_o) and DC current (I_o) as shown in Equation 58 and Equation 59 respectively (Luo and Ye, 2004):

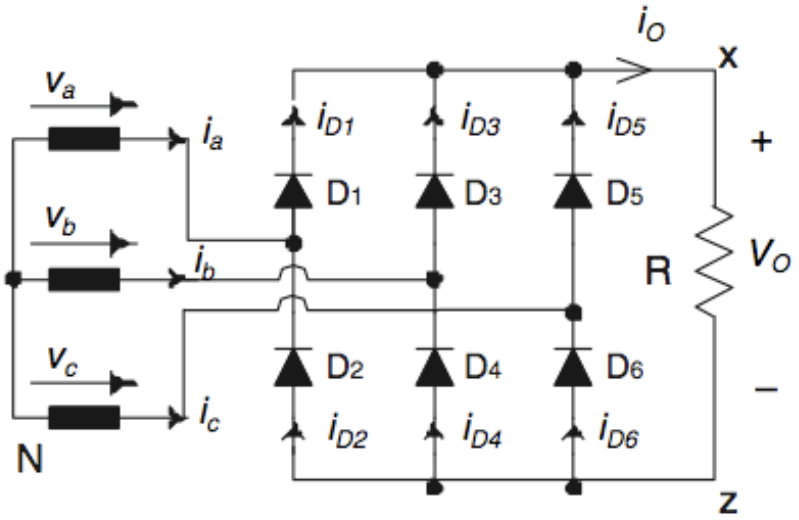

Figure 73: Circuit diagram of a 3-phase full-bridge rectifier, where the AC voltage inputs are V_a, V_b and V_c and V_o is the DC voltage output. The current are designated similarly, where i_O is the current output (Luo and Ye, 2004).

$$V_O = \frac{3\sqrt{6}}{\pi} V_{ac} = 2.34 V_{ac}$$ **Equation 58**

$$I_o = \frac{2.34 V_{ac}}{R}$$ **Equation 59**

where V_{ac} is the RMS value of the AC input voltages V_a, V_b and V_c; that is, $V_{ac} = (1/\sqrt{2})\ V_a$, and $V_a = V_b = V_c$.

The average DC power supplied by the rectifier P_{dc} is thus given by

Equation 60:

$$P_{dc} = V_o \times I_o$$ **Equation 60**

The rectifier energy efficiency, η_{rec}, can be determined by an experiment or obtained from the manufacturer. In this project, the efficiency is obtained from an experiment and using the relationship

$$\eta_{rec} = \frac{P_{out}(rectifier)}{P_{in}(rectifier)}$$ **Equation 61**

where $P_{in}(rectifier)$ is power input of rectifier (W) and $P_{out}(rectifier)$ is power output of rectifier (W).

The three-phase AC voltage produced by the aerogenerator can thus be converted into an average DC voltage as provided at the output of the rectifier. The voltage conversion according to Equation 58 is the theoretical

conversion and assumes zero loss. However, in practice there will be some loss in the conversion process. The energy efficiency of the rectifier can be found from the manufacturer or by testing, and then applied in Equation 62:

$$P_{in}(rectifier) = \frac{P_{out}(rectifier)}{\eta_{rec}} = P_{out}(generator) \qquad \textbf{Equation 62}$$

Alternatively, the voltage conversion characteristic of a rectifier can be obtained from an experiment, which has the advantage of giving actual voltage conversion values directly, including the effect of the rectifier's inefficiency. For an ideal rectifier, the AC voltage input would be converted into DC output by a linear relationship, which passes through the origin. However, the actual conversion, as shown indicatively in Figure 74, is not 100% efficient and the input voltage must initially exceed a certain minimum value before any useful output voltage is obtained. Typically the AC voltage input and DC voltage output are linearly related, as shown in Figure 7 with slope m_r and intercept on the input voltage axis of C_r.

The conversion formula described this linear relationship between AC voltage and DC voltage can be written as Equation 63:

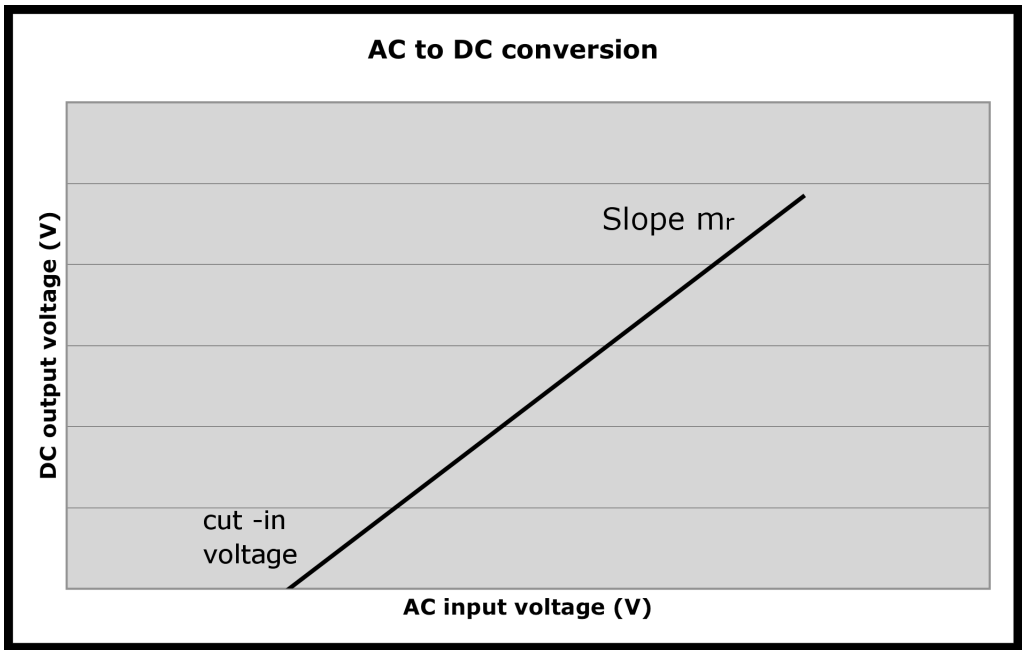

Figure 74: Figure 74: A straight-line approximation of AC voltage input and DC voltage output of a rectifier derived from the diode characteristic (Walters, 2008). The graph has a slope mr and cuts the vertical-axis at point Cr. The graph suggests that the input must be at a certain value to overcome internal loss and supply a useful DC voltage.

$$V_o = m_r V_a + C_r \qquad \textbf{Equation 63}$$

where $V_a = V_b = V_c$.

7.3.6 The PEM electrolyser

When the rectified output of the aerogenerator is directly connected to the PEM electrolyser, the resulting voltage and current combination will be a point on the V-I characteristic of the electrolyser. As explained in section 3.3.5 and 6.2, the latter characteristic is approximately a straight line, so that the relationship between I_{dc} and V_{dc} will be of the form of

Equation 64:

$$I_o = m_e(V_o) + C_e \qquad \textbf{Equation 64}$$

where m_e is the slope of the electrolyser characteristic, and C_e is the intercept of the characteristic on the current axis.

7.3.7 Net torque

The rate of change in angular velocity of the mechanically-connected turbine and generator is dictated by the net torque, T_{net} (

Equation 45). T_{net} will determine whether the system accelerates or decelerates. A positive T_{net} value means the aerodynamic torque is larger than mechanical torque and the angular velocity will be increased; a negative T_{net} value means the aerodynamic torque is less than mechanical torque and the angular velocity will be decreased.

The mechanical torque produced by the generator is obtained in term of P_{in}*(electrolyser)* by substituting Equation 53 and Equation 62 into Equation 54 to get Equation 65:

$$T_{mec} = \frac{P_{in}(electrolyser)}{\eta_{gen} \times \eta_{rec} \times \omega} \qquad \textbf{Equation 65}$$

The resultant torque T_{net} is then found using Equation 45, together with Equation 50 and Equation 65:

$$T_{net} = \left(\frac{P_{aero}}{\omega} \right) - \left(\frac{P_{in}(electrolyser)}{\eta_{gen} \times \eta_{rec} \times \omega} \right)$$

$$T_{net} = \left(\frac{\frac{1}{2}\rho\pi R^2 C_p(\lambda) v^3}{\omega} \right) - \left(\frac{P_{in}(electrolyser)}{\eta_{gen} \times \eta_{rec} \times \omega} \right)$$ **Equation 66**

7.3.8 Change in angular velocity due to net torque

As mentioned earlier in subsection 7.3.7, T_{net} determine whether the turbine-generator system accelerates or decelerates, in other words, change angular velocity (ω). In addition, the rate at which it changes angular velocity depends on the inertia of the rotating system (J). The general equation governs the movement of a rotating system is

Equation 67:

$$T_{net} = J\frac{d\omega}{dt}$$ **Equation 67**

T_{net} given by equation

Equation 67 is in general a function of ω so it is usually necessary to solve this equation for ω approximately for small intervals of time, Δt, using

Equation 68:

$$\Delta\omega = \frac{T_{net}\Delta t}{J}$$ **Equation 68**

Hence if we know the starting value of ω and an average value of T_{net} over successive small intervals of time, Δt, it is possible to use this equation to find the approximate variation of ω over time using the incremental relationship as stated by

Equation 69:

$$\omega_{n+1} = \omega_n + \Delta\omega_n$$ **Equation 69**

where the subscripts refer to number of time intervals from the starting point, that is, $t = n \Delta t$.

7.3.9 Algorithm of dynamic model

The dynamic analysis of the directly-coupled aerogenerator system is carried out using the theoretical analysis presented in the foregoing subsections and the algorithm presented in the form of a flow chart in (Figure 70). Theoretically, the net torque must be derived from aerodynamic input torque and the opposing generator input torque. This net torque is used to determine the change in angular velocity of the turbine-generator system in each time interval. The calculated angular velocity in each interval is used to estimate the voltage and hence current input to the electrolyser.

The program uses an experimentally-measured DC voltage input to electrolyser as the starting value to calculate the initial angular velocity of the generator at the start of a simulation. The DC voltage is firstly converted into the corresponding AC voltage (V_a, V_b and V_c) by the voltage conversion characteristic of the rectifier. Then using the RPM and voltage output relationship for the electrical generator, the angular velocity of the rotor is found. The angular velocity and measured instantaneous wind speed are then used to find the instantaneous tip speed ratio. The power captured (P_{aero}) by the turbine can be found by using turbine' $C_p - \lambda$ relationship. The DC voltage is used once more in the V-I characteristic of the electrolyser to determine the current input (I_{dc}) and thus the power input is calculated (P_{in}*(electrolyser)*).

The net torque (T_{net}) is the resultant of aerodynamic torque and counter generator torque, which are obtained from P_{aero} and P_{in}*(electrolyser)* respectively. T_{net} is then used to find the angular velocity of the generator in the next time interval. The predicted DC voltage is calculated from the new angular velocity. The calculation continues interval by interval until the end of the time period under consideration has been reached. The flow chart

illustrating the calculation process using the algorithm outlined in the Visual Basic simulation program for dynamic simulation of direct coupling of the AIR 403 aerogenerator and h-tec PEM electrolyser is in **Figure 75**.

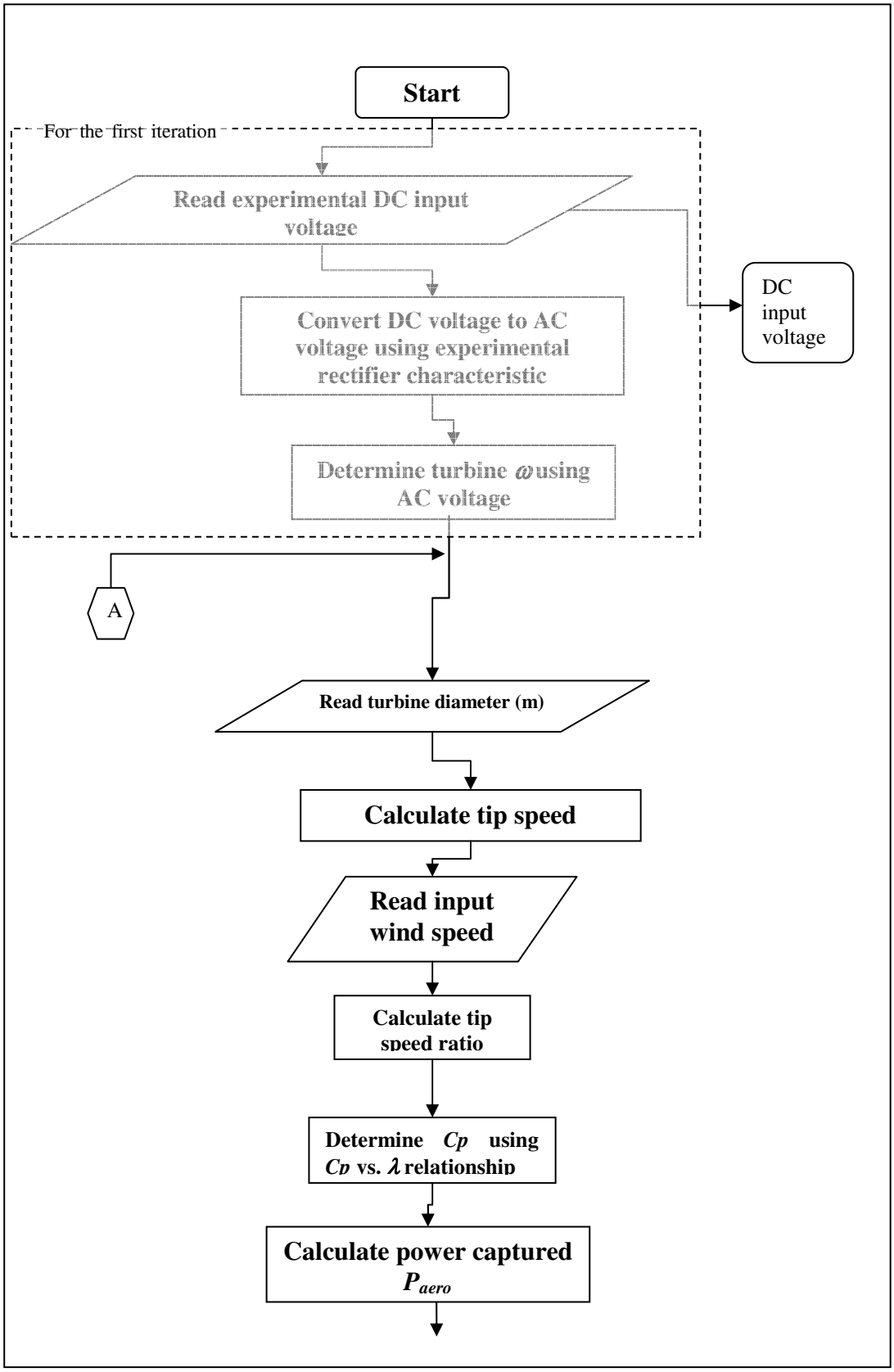
Start
For the first iteration
Read experimental DC input voltage
DC input voltage
Convert DC voltage to AC voltage using experimental rectifier characteristic
Determine turbine ω using AC voltage
A
Read turbine diameter (m)
Calculate tip speed
Read input wind speed
Calculate tip speed ratio
Determine Cp using Cp vs. λ relationship
Calculate power captured
P aero

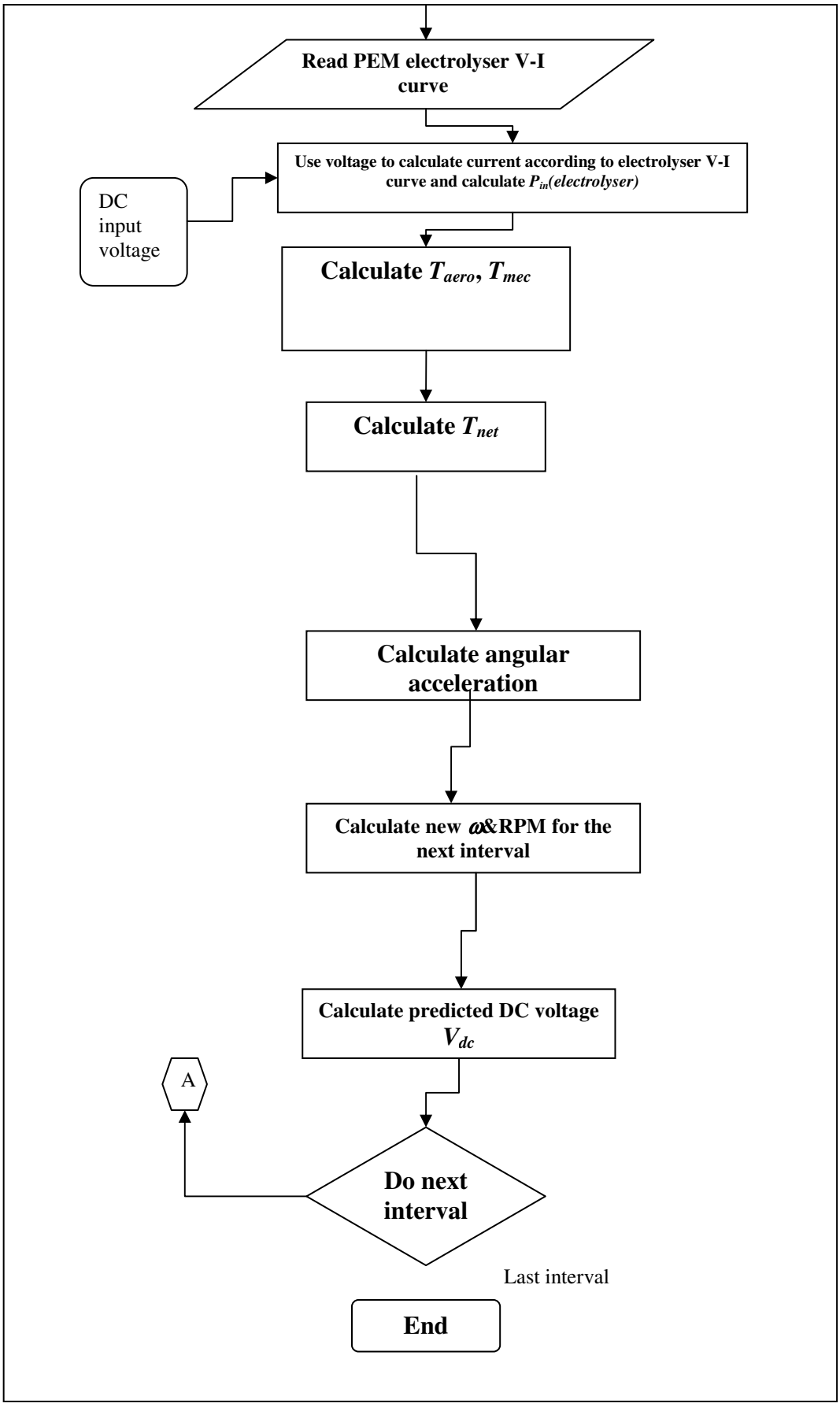

Figure 75: Flow chart of calculation process in dynamic simulation program of direct coupling.

7.4 NUMERICAL SIMULATION OF AIR 403 AEROGENERATOR USING DYNAMIC MODEL

7.4.1 Dynamic model

A program has been developed based on the foregoing algorithm, and using Visual Basic and Microsoft Excel for ease of use and data visualisation, to carry out a dynamic simulation of the AIR403 aerogenerator directly coupled to a PEM electrolyser bank, as in the experiment conducted and reported in chapter 5. The aim of the simulation is to investigate the departures from the performance of the aerogenerator as predicted by a steady-state model, and that actually observed in the experiment, as identified in chapter 6.

7.4.2 Input data

The principal input data required by the dynamic model are the following:

- Aerogenerator characteristic performance data:
  - The $C_p - \lambda$ relationship for the turbine blades
  - The relationship between the AC voltage output and the angular velocity, and overall energy efficiency of the permanent magnet synchronous three-phase AC generator:
  - The physical dimensions and materials of the turbine and generator rotor, to enable calculation of the moment of inertia of this assembly
- The voltage input to voltage output characteristics of the three-phase full-wave bridge rectifier
- The V-I characteristic curve of the PEM electrolyser bank.
- Wind speed in each interval over the study period of the direct coupling experiment performed.

The program then calculates for each interval the DC voltage output applied to the electrolyser bank, and hence the power transfer from the aerogenerator to the electrolyser.

7.4.3 AIR 403 blade characteristic

The C_p – λ relationship for the AIR 403 aerogenerator (Jones et al., 2000) given by its manufacturer is shown in Figure 76. At different Reynolds numbers for the air flow, the blades of the AIR 403 perform differently. For ease of numerical calculation, the four curves in Figure 76 corresponding to different Reynolds numbers were averaged into a single curve, as presented in Figure 77.

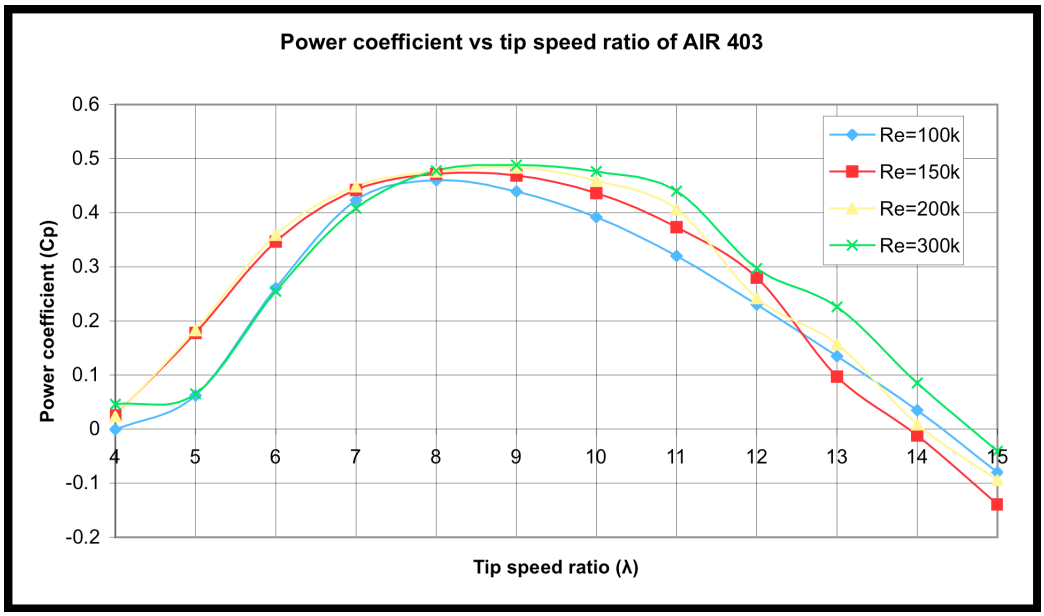

Figure 76: C_p – λ relationship provided by the manufacturer of the AIR 403 aerogenerator. The relationship varies slightly with various Reynolds numbers for the air flow.

The graph provided by the manufacturer did not show C_p values for $\lambda < 4$, and thus cannot be applied to the start-up of the aerogenerator from a stationary state when $\lambda = 0$. To overcome this problem, the assumption has been made that C_p increases linearly from close to zero at $\lambda = 0$ to its mean value as given in Figure 76 at $\lambda = 4$. C_p must be just above zero at $\lambda = 0$ otherwise the turbine would not start turning at all.

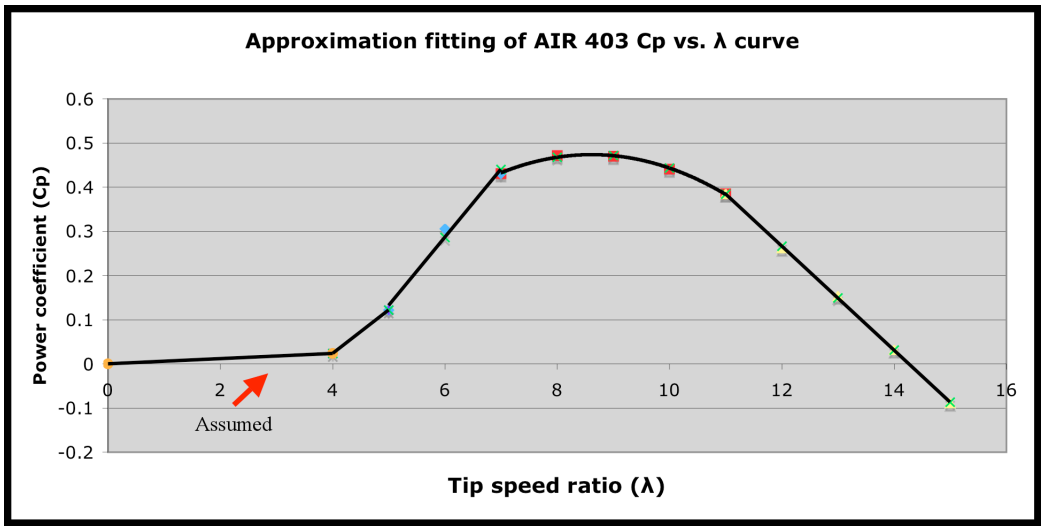

Figure 77: Averaged C_p – λ relationship for the AIR 403 aerogenerator, with an assumed linear increase in C_p from near zero in the $\lambda < 4$ region (see arrow).

7.4.4 Angular velocity vs. AC output voltage relationship from wind tunnel experiment of AIR 403 aerogenerator

Data sets for the relationship between wind speed, power output, voltage, current and angular velocity were obtained from the wind tunnel experiment reported in section 4.3.2 and Appendix C. The RPM – voltage output relationship is of central interest, which forms part of the generator's characteristics. The following relationship was found from the data for the AIR 403 aerogenerator as shown in Figure 78:

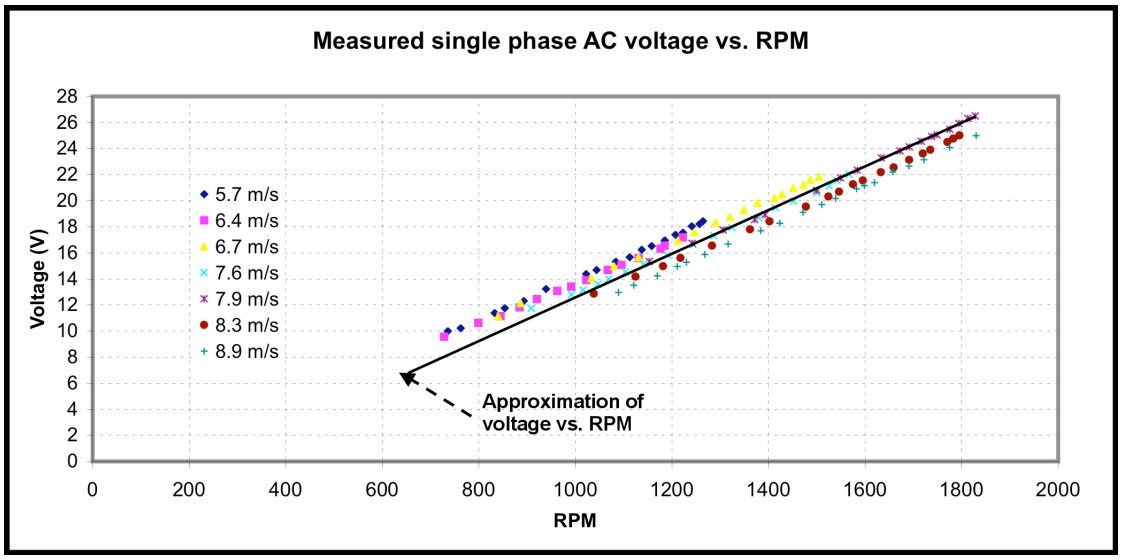

Figure 78: Relationship between the single-phase AC voltage output and measured RPM for the Air 403 aerogenerator obtained from the earlier wind tunnel experiment. Different dot shapes represent measurements for different wind speeds as indicate in the legend.

According to Figure 78, the single-phase (line-to-neutral) AC voltage output at given angular velocity is almost constant regardless of the wind speed and generator power output. The best straight line fit to the experimental data points matches these closely, with maximum deviations in the order of ±2 V. For example, in the case of wind speed of 6.4 m/s, at 800 RPM the actual voltage is 10.5 whereas the approximated voltage is 9.5 V. The line does not pass through the origin because in the actual experiment the turbine has to spin up to an RPM until voltage output is measurable. It is because the EMF has to overcome the internal voltage drop.

The RPM – voltage graph in Figure 78 was obtained by measuring rotor RPM directly and the voltage across each of three resistive loads connected to each phase output of the generator. Hence the voltage measured already includes the effects of energy losses in the generator, and is lower than the theoretical maximum. Moreover the relationship is not affected by wind speed measurements in the wind tunnel. Because regardless of how the particular RPM of the turbine is achieved, the voltage output will correspond to this RPM as:

$$V_a = V_b = V_c = \left((0.0167) \times (\frac{2\pi}{60} \omega) \right) - 4.161$$ **Equation 70**

where $\omega = \frac{RPM \times 2\pi}{60}$ (rad/s).

7.4.5 AIR 403 generator

According to the manufacturer, the overall energy efficiency of the generator of the AIR 403 (η_{gen}) is typically 64% (Jones et al., 2000). In the present simulation this efficiency is assumed to be constant throughout the power output range, and independent of rotor RPM. Substituting this assumed generator efficiency into

Equation 53 yields:

$$P_{in}(generator) = \frac{P_{out}(generator)}{\eta_{gen}} = \frac{P_{out}(generator)}{0.64}$$ **Equation 71**

7.4.6 AIR 403 physical parameters

The combined moment of inertia of all the rotating parts of the AIR 403 – namely the blades, hub, and rotor and shaft of the electrical generator (Figure 79) – was calculated from the dimensions and masses of these components. The specifications given by the manufacturer are:

- Blade moment of inertia (J_{blade}, single blade) = 0.0217 kg m^2
- Blade mass = 0.18 kg
- Distance from centre hub to the centre G of a blade = 0.095 m
- Hub mass (M_{hub}) = 0.27 kg
- Rotor mass = 0.939 kg

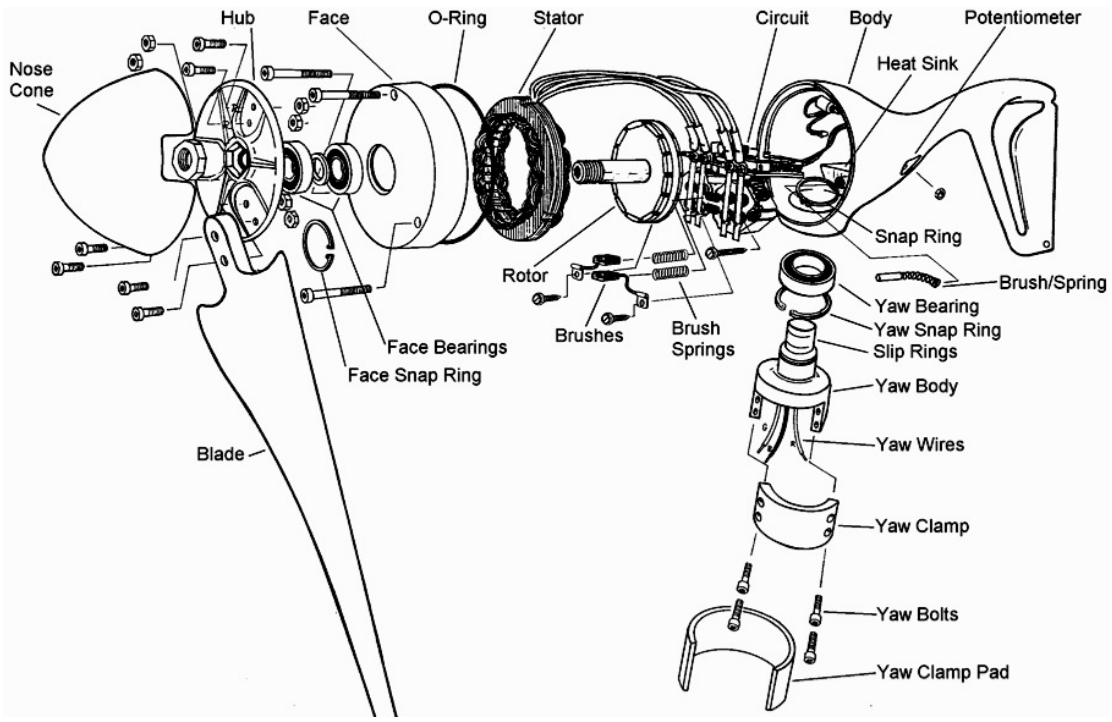

Figure 79: Exploded view of AIR 403 aerogenerator showing the hub, a blade and rotor (Southwest Windpower, 2001).

It was assumed that the hub is a solid disk with the diameter of 0.129 m and a thickness of 0.011m (Jones et al., 2000). Its moment of inertial is then:

$$J_{hub} = \frac{M_{hub} R_{hub}^{\ 2}}{2} \qquad \textbf{Equation 72}$$

where J_{hub} is moment of inertia of the hub, R_{hub} is hub radius. Hence

$$J_{hub} = \frac{0.27 \times (\frac{0.129}{2})^2}{2}$$

$J_{hub} = 0.0006$ kg m^2

The rotor was taken to be a solid disk with a shaft attached from the centre of the disk, with dimensions:

- Disk radius (R_{disk}) = 0.040 m
- Disk thickness = 0.013 m
- Shaft length from the face of the disk = 0.057 m
- Shaft radius (R_{shaft}) = 0.009 m
- Stainless steel density (ρ_s) = 8000 kg/m^3

The moment of inertia of this component is then given by:

$$J_{rotor} = \frac{\rho_s V_{shaft} R_{shaft}^{\ 2}}{2} + \frac{\rho_s V_{disk} R_{disk}^{\ 2}}{2}$$

where J_{rotor} is moment of inertia of rotor assembly, V_{shaft} is the volume of the shaft (m^3), V_{disk} is the volume of the disk (m^3)

Hence J_{rotor} = 0.0005 kg m^2.

Hence the combined moment of inertia (J) of the rotating assembly in the AIR 403 is given by:

$$\boldsymbol{J} = 3(\boldsymbol{J}_{blade}) + \boldsymbol{J}_{hub} + \boldsymbol{J}_{rotor}$$

$$= 3(0.0217) + 0.0006 + 0.0005$$
$$= 0.066 \text{ kg m}^2$$

7.4.7 Rectifier performance and efficiency

The efficiency of the rectifier is calculated using $\eta_{rec} = \frac{P_{out}(rectifier)}{P_{in}(rectifier)}$ Equation 61, and the theoretical DC power using Equation 60. The average power transfer

efficiency (η_{rec}) of the S4G80G rectifier used in the experiment was found from the data obtained to be 0.9.

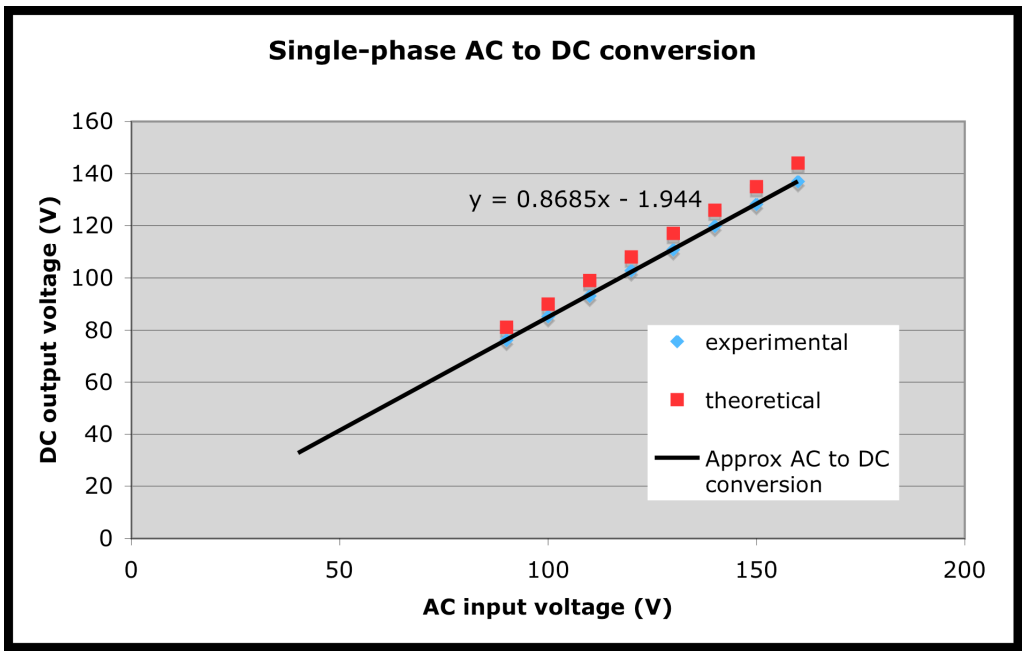

Figure 80: Single-phase AC voltage input to DC voltage output conversion relationship of the S4G80G rectifier obtained from the experiment.

Instead of using Equation 58 & Equation 59 to determine the voltage and current and then apply the rectifier efficiency, the AC to DC conversion relationship given in Equation 73, which was derived from the graph in Figure 80, was used. This formula converts AC voltage to DC voltage (or vice versa) with the rectifier efficiency and voltage drop due to diodes included because it comes from an experimental result. The use of this experimental data in this simulation program enables easy and realistic calculation within the rectifier submodel:

$$V_o = (0.8685)V_a - 1.944 \qquad \textbf{Equation 73}$$

It appears that the best-fit line for AC to DC conversion does not pass through the origin, so that V_a has to exceed 2.24 V before the rectifier gives any output. This form of relationship is not unexpected because diodes need an initial starting voltage.

7.4.8 Electrolyser characteristic

The current output from the rectifier depends on the V-I characteristic of the electrolyser connected to it as the load. For the h-tec PEM electrolyser bank used, the relationship between current and applied DC voltages is:

$$I_o = (0.8063) \times (V_o) - 25.543 \qquad \textbf{Equation 74}$$

7.5 APPLICATION OF DYNAMIC MODEL TO EXPERIMENTAL RESULTS FROM RMIT BUNDOORA CASE STUDY

The dynamic model described in the previous sections has been applied to the results of the experiment reported in chapter 5 in which an AIR 403 aerogenerator was directly coupled to a PEM electrolyser bank for a period of 51 days, and the energy transferred between the aerogenerator and electrolyser measured.

Wind speed data gathered during the direct coupling experiment over each interval during a period of the experiment have been input into the dynamic model and the model used to predict the output DC voltage applied to the electrolyser, and hence the energy transferred. The period simulated was a more limited period than the full experiment, being from 11:05 am of the 30/05/2008 until 9:50 am of the 04/06/2008, that is, 4 days, 23 hours in total. The frequency distribution of the wind speeds over this period is shown in Figure 81. The electrolyser used in the model was configured in same way as the actual electrolyser bank used in the experiment, that is, 2 branches connected in parallel with each branch containing 21 cells connected in series.

The DC voltages applied to the electrolyser as measured in the experiment (triangular dots) are compared over intervals of a second with the corresponding predictions by the dynamic

simulation (square dots) in Figure 82 over a selected period of just over a minute. The dynamic simulation results on average track the experimental results closely, while showing some additional short-term variations. Another two plots of extracted results (Figure 83 and Figure 84) show a similar performance of the dynamic-state simulation in predicting the voltage output. There is, however, an occasional exaggerated predicted voltage, as for example between intervals 882 and 902 in Figure 84, where the data significantly fluctuate over and under the experimental voltage.

The oscillation of dynamic simulation results is likely to be a result of the time step. At a close comparison of dynamic simulation results and experimental results this effect appears prominent. Investigating this effect further will require extra time and computing power. However, the overall power profile, hence voltage profile, was of the greater interest. Therefore, the effect of time step is not addressed in the present thesis.

A comparison of the model predictions and experimental results for a 20-minute period of the simulation is shown in Figure 85. The overall agreement between the simulated voltage and actual voltage is once again quite close, on average within ±8%, while the predicted voltage shows greater short-term variability. One reason for the lesser variation in the measured voltage is that at times when the actual voltage output applied to the electrolysers by the aerogenerator is lower than electrolyser bank cut-in voltage (approximately 30.9 V), the voltage recorded across the electrolyser stays near the cut-in voltage because of the inherent capacitance of the electrolyser. This effect explains the flat portions of the experimental voltage curve, all just over 30 V. No account is taken of the capacitance of the electrolyser in the model, so the simulated voltage continues to fall below 30 V during these periods.

The simulation model estimated that the total energy transferred between aerogenerator and electrolyser over the period studied is 95 kJ (0.027 kWh), while the actual energy transfer as measured in the experiment was 104 kJ (0.029 kWh). The dynamic model's prediction of energy transfer is thus within 10% of the experimentally-measured value. This estimate is a considerable improvement on the corresponding estimate using the steady state model for the same period of 122 kJ (0.034 kWh), which is over 17% greater than the actual measured value.

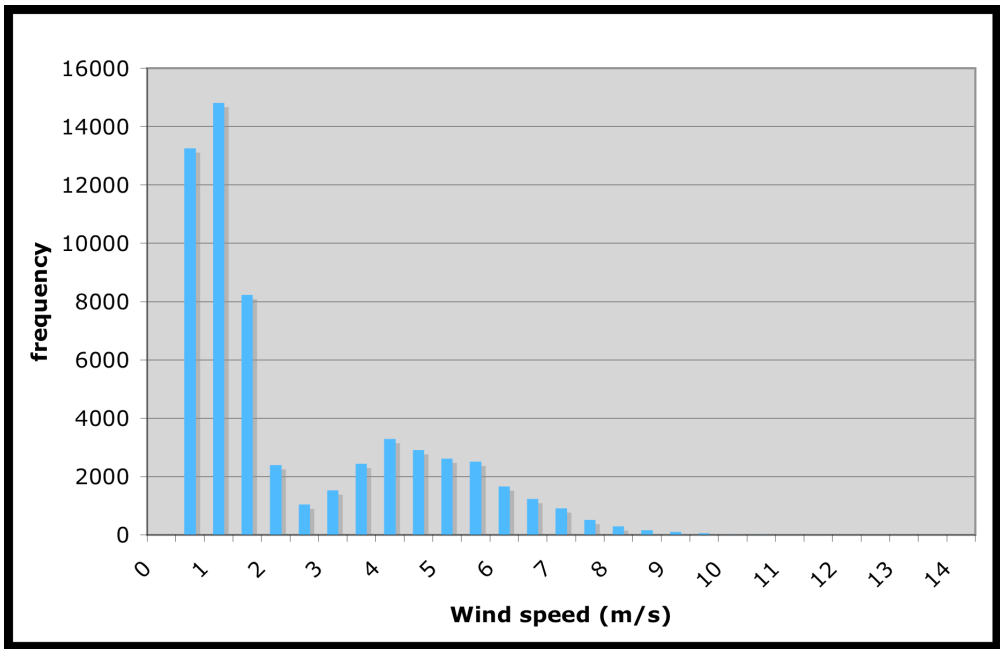

Figure 81 Wind speed frequency distribution of direct coupling experiment during the period of 11:05 am of the 30/05/2008 until 9:50 am of the 04/06/2008.

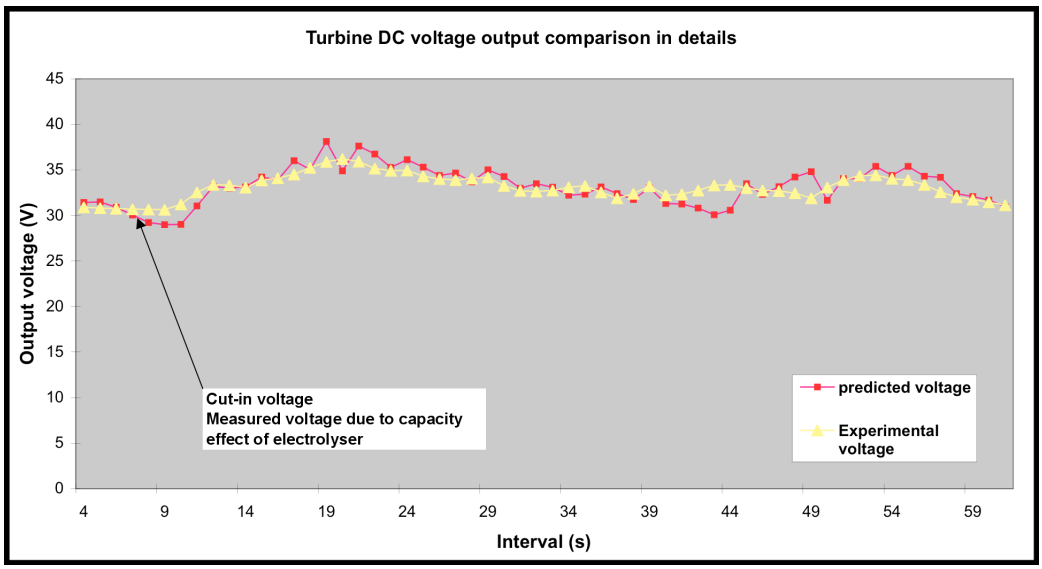

Figure 82: DC voltage output comparison between experimental and predicted voltage by dynamic modeling between intervals 1 and 65.

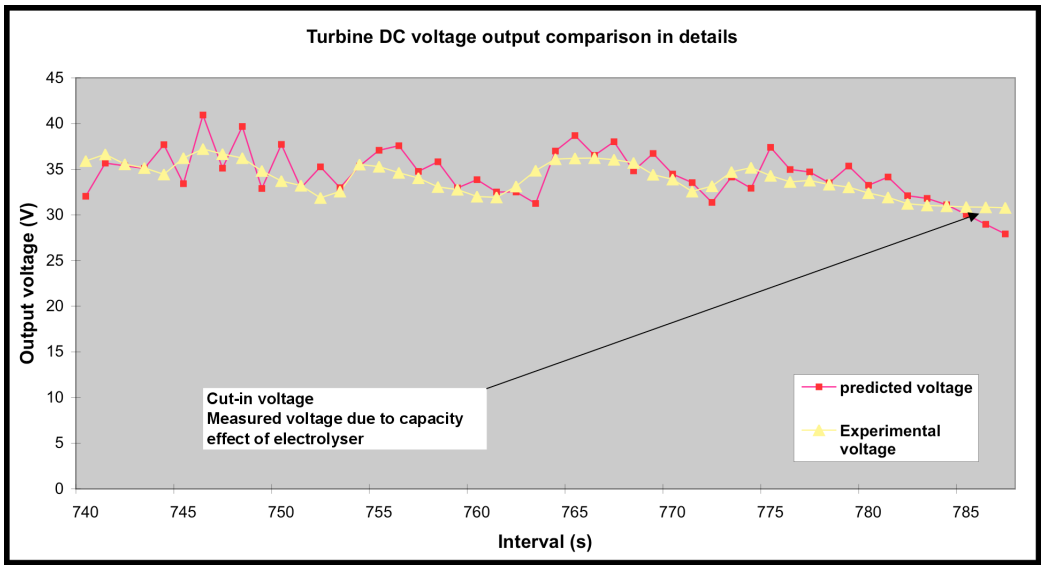

Figure 83: DC voltage output comparison between experimental and predicted voltage by dynamic modeling between intervals 740 and 795.

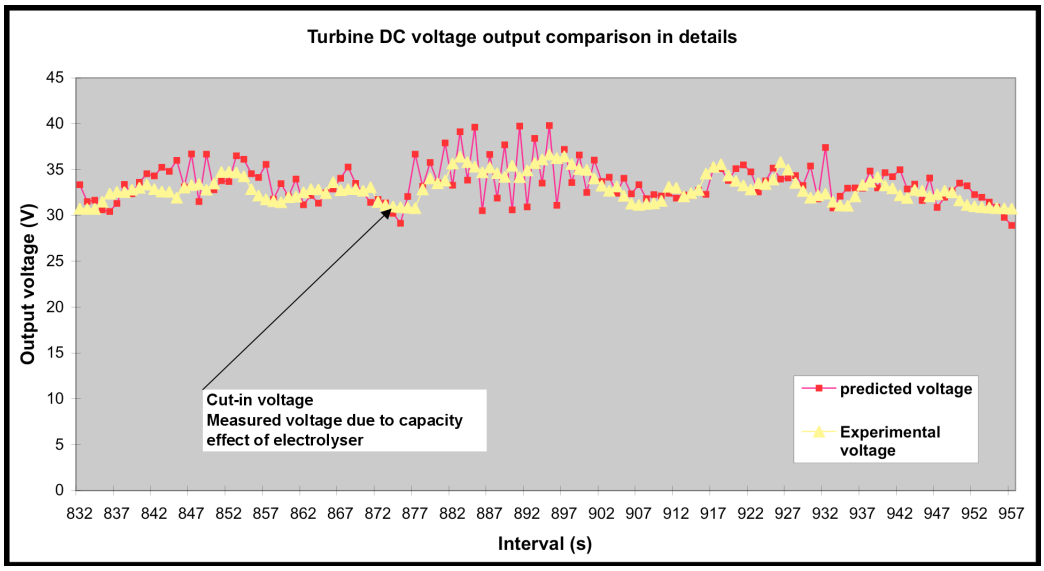

Figure 84: DC voltage output comparison between experimental and predicted voltage by dynamic modeling between intervals 832 and 960.

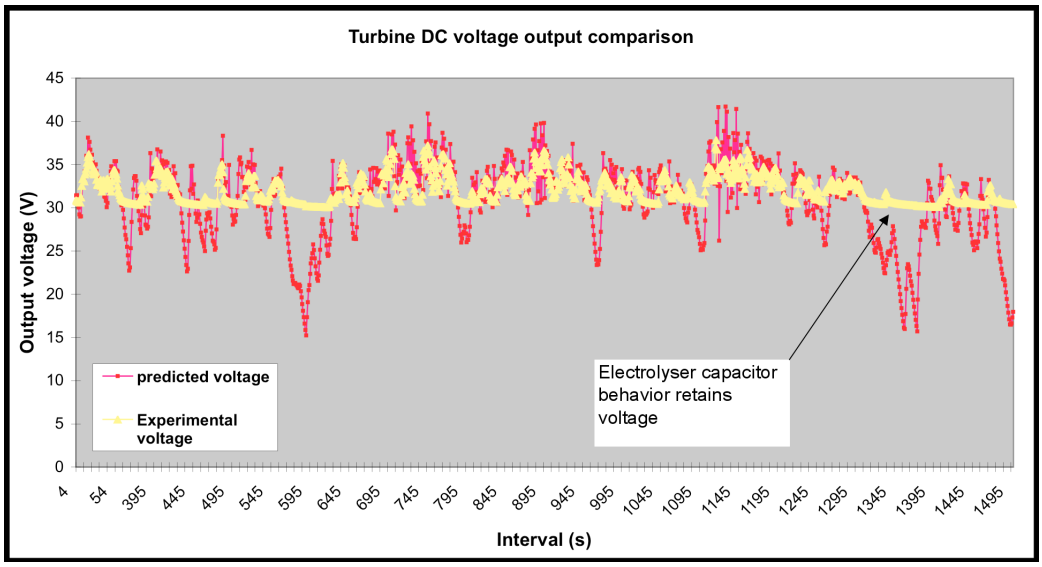

Figure 85: DC voltage output comparison between experimental and predicted voltage by dynamic modelling during the period from 11:05 am of the 30/05/2008 until 9:50 am of the 04/06/2008.

The dynamic-state simulation model of direct coupling of the AIR 403aerogenerator and h-tec PEM electrolyser has thus shown some initial promise in predicting the voltage input of the electrolyser and hence the energy transfer over a period with intermittent and variable wind speeds more accurately than the steady state model used earlier did. However, the predictions of the dynamic model still show some occasional significant fluctuations about the experimental data, and the comparisons between model predictions and experimental values conducted here of limited duration and number. The dynamic simulation program therefore needs further analysis, improvement, and testing against experimental values before it can be regarded as validated.

7.6 CONCLUSION

The construction and calculation algorithm of a dynamic simulation program to model an aerogenerator directly coupled to a PEM electrolyser bank have been described. The characteristics of all the main components of the model are explained including their performance and efficiency.

The program has been used to predict the power and energy transfer between an AIR 403 aerogenerator directly coupled to a bank of PEM electrolyser using wind speed data from the direct coupling experiment conducted at RMIT University and reported in Chapter 5.

The period simulated was a limited one of 4 days, 23 hours selected from the 51 days of the entire experiment. The DC voltages applied to the electrolyser as measured in the experiment were compared to the dynamic simulation results. The dynamic simulation results on average track the experimental results closely, while showing some additional short-term variations. The simulation model estimated that the total energy transferred between aerogenerator and electrolyser over the period studied was 96 kJ, while the actual energy transfer as measured in the experiment was 104 kJ (0.029 kWh). This estimate is a considerable improvement on the corresponding estimate using the steady state model for the same period of 122 kJ (0.034 kWh). The prediction of the dynamic model for cumulative energy transfer over the study period is much closer (within 10%) of the actual experimentally-measured energy transfer than the corresponding prediction using the steady state model over the same period (overestimate by 17%).

It should be noted here that the comparison of energy transfer calculated by the dynamic and steady state models has been conducted over a much shorter period than the the entire experimental period. Over the full period, the steady-state model overestimates the energy transfer by a factor ofthree, whereas over this more limited period it only overestimates by 17%. Hence clearly further comparisons between model predictions are neded over much longer periods before any firm conclusions can be drawn

The predictions of the dynamic model also show occasional significant fluctuations about the experimental data, and the comparisons with experimental values conducted here have been of limited duration and number. Consequently, further analysis, improvement and testing against experimental values are required to validate the dynamic simulation program proposed here.

The experimental and theoretical work conducted in this thesis, however, strongly suggests that in an area where the wind speed is highly variable, dynamic effects do need to be considered in estimation of power transfer between an aerogenerator and electrolyser, so that a dynamic model of the direct-coupled system is needed.

8 CONCLUSIONS AND RECOMMENDATIONS

8.1 THIS CHAPTER

In this final chapter, the research questions set for this thesis in chapter 1 are addressed drawing upon all the theoretical and experimental investigations conducted in the course of the research program conducted. Some more general conclusions are then drawn, and recommendations made relating to the future development of wind – hydrogen energy systems for remote applications. The thesis concludes with a short epilogue.

8.2 RESPONSES TO RESEARCH QUESTIONS

8.2.1 What are the optimal design parameters of a wind – hydrogen system to meet a given remote area electrical demand in terms of lowest unit cost of energy on a lifecycle basis?

The overall analysis of a wind – hydrogen energy system was conducted at the start of the project to evaluate and study system and component sizing. A specially-designed and constructed Visual Basic program has been used to simulate a working wind – hydrogen energy system employing a fixed-pitch variable speed aerogenerator, a PEM electrolyser and PEM fuel cell (chapter 3). The main inputs to the program are hourly wind speed data, the aerogenerator power curve, the electrolyser and fuel cell characteristics, and the hourly load profile to be supplied. The main outputs from the program are a graph of hydrogen in storage throughout the year, and the required sizes of the aerogenerator, electrolyser, hydrogen storage, and fuel cell to enable the load to be met throughout the year, and sustainably from year to year.

A wind – hydrogen energy system designed to deliver power to a remote homestead has technical parameters such as aerogenerator, electrolyser, hydrogen storage and fuel cell capacities. Because the fuel cell size is determined by power demand it is set directly from the input load profile. The required capacities of the aerogenerator, electrolyser and hydrogen storage, on the other hand, are strongly related to each other.

The wind – hydrogen simulation model developed has been applied in a case study to meet the daily load of 5.9 kWh of a remote household located at a site in Kilcunda North, on the ocean coast just over 100 km south east of Melbourne, with an annual mean wind speed of 8.0 m/s. The model outputs suggest that in general the smallest practical storage capacity is found to be around 1 kg of hydrogen. The required aerogenerator size increases steeply as the smallest practical storage capacity is approached. The aerogenerator capacity should be between 3.4 to 4.2 kW and electrolyser should be between 0.7 to 1.5 kW.

For a case where hydrogen storage is unconstrained, the aerogenerator capacity is 1.77 kW, electrolyser capacity is 1.42 kW, hydrogen storage capacity is 4.8 kg of hydrogen and fuel cell capacity is 0.35 kW. If hydrogen capacity is constrained at 3 kg of hydrogen, the required aerogenerator capacity is 2.0 kW, electrolyser capacity is 1.65 kW and fuel cell capacity is 0.35 kW.

The general relationships between the required capacities of the main components of the system are the following:

- A reduction in hydrogen storage capacity increases the required aerogenerator size. This is because, as the hydrogen storage capacity gets smaller, a higher proportion of the annual load must be met directly by the aerogenerator. The system then relies less on the energy stored..
- A reduction in electrolyser capacity also increases aerogenerator size. This is because the hydrogen production is sometimes limited by as a result of setting the electrolyser capacity below the maximum surplus of wind power over the load. The system thus cannot rely so much on energy storage and the aerogenerator capacity has to be increased to meet more of the final load directly. A larger hydrogen storage does not help the situation since the amount of hydrogen produced has been cut back.

On the basis of the assumptions made about component costs and lifetimes, the most economic system has an average unit cost of electricity supplied over 25 years of US$ 0.66 /kWh, and employs a 2.6 kW aerogenerator, a 0.7 kW electrolyser, 1.9 kg of hydrogen storage, and a 0.35 kW fuel cell.

If the aerogenerator and electrolyser are suitably matched so that they can be directly coupled without electronic interconnection equipment, the unit cost of energy produced is reduced to US$ 0.57 /kWh, that is, 14% cut. In this case the optimal system comprises a 3.0 kW aerogenerator, a 0.7 kW electrolyser, and 1.5 kg of hydrogen storage. Hence it can be seen that direct coupling has the potential to reduce the cost of a wind – hydrogen energy system for RAPS applications significantly.

Moreover, the unit cost of electricity increases with the sizes of fuelcell. It is noticeable that the electricity cost rise is consistent from 0.5 to 0.75 and 1 kW of fuel cell, the rise is by US$0.05/kWh. As a result, the electricity cost per unit energy of a wind – hydrogen energy with a specified electrolyser capacity and a fixed aerogenerator size will increase proportionally with the fuelcell size or peak load. And hence it is important for users of an energy system to reduce their peak load by ways of reduction of consumption or spreading the load.

8.2.2 What matching procedures can be applied to maximise the power transfer efficiency between a fixed-pitch variable-speed aerogenerator directly coupled to a PEM electrolyser, and hence the overall rate of hydrogen production, without using an electronic converter/impedance matching unit?

The matching of the V-I characteristics of an aerogenerator and PEM electrolyser has been utilised to achieve a high power transfer efficiency between a fixed-pitch variable-speed aerogenerator directly coupled to a PEM electrolyser. This matching was done by altering the V-I characteristic of a bank of electrolysers so that it matched as closely as possible the maximum power point curve of the aerogenerator over its range of operating wind speeds. Single electrolyser cells are connected in various series and parallel configurations to form a bank with varying V-I curves. Adding cells in each series-connected branch increases the cut-in and maximum operating voltages, and decreases the slope of the V-I curve, of the bank, while the maximum current stays the same. Adding parallel branches increases the current, and decreases the slope of the V-I curve, while the voltage operating range stays constant. The connection configuration that gave the highest overall energy transfer over an annual period when directly coupled to the aerogenerator is then found using the known

maximum power point curve of the aerogenerator and the annual frequency distribution of wind speeds at a particular site.

A case study of direct coupling for an AIR403 aerogenerator and PEM electrolyser bank at the Kilcunda North site has been conducted. A theoretical investigation of the annual energy transfer for 12 series-parallel configurations for the electrolyser bank, ranging from 16 to 27 cells in series in each branch, and up to three branches connected in parallel, has been carried out. The configuration found to yield the highest annual energy transfer to the electrolyser at this wind site was that 3 parallel branches each containing 21 cells in series. In this case, the predicted total energy transfer was 1201 kWh annually, only 3.4% less than the theoretical maximum energy transfer in which maximum power point tracking was assumed to be present at all times. Given that DC – DC voltage converters and maximum power point trackers typically have losses of 5 – 10%, the direct coupling promises at least as high an overall energy transfer, but without the cost of the electronic conversion equipment.

However, the direct coupling experiment conducted at RMIT University over a period of 51 days as reported in chapter 5 and 6 illustrated that in this particular case the energy transfer loss in direct coupling was greater than that theoretically estimated even after factoring in possible sources error. The theoretically-estimated energy transfer was 4.81 kWh compared to the experimental result of 1.53 kWh. It was thus found that the steady state model covered in chapter 4 appeared to overestimate the overall energy transfer by as much as three times. Close inspection of data revealed that on many occasions the aerogenerator did not generate power while the theoretical prediction suggested that power was generated. Moreover, the intermittent and variable wind speeds hindered the ability of the aerogenerator to develop its maximum expected RPM at each recorded wind speed, so that and much less power was generated than expected on the basis of the steady state response..

This discrepancy between theoretical prediction and experimental result warranted a new theoretical prediction approach, namely a dynamic state analysis. Consequently preliminary steps were taken to develop a dynamic model of the aerogenerator that takes into account the characteristics of its blades, electrical generator and moment of inertia. The dynamic model estimates the turbine RPM and output voltage according to the instantaneous and series of preceding wind speeds.

The dynamic model has been tested in a preliminary way by applying it to a limited period of 4 days, 23 hours selected from the 51 days of the entire experiment. The model estimated that the total energy transferred was 95 kJ, while the actual energy transfer as measured in the experiment was 104 kJ. Estimation using the steady state model for the same period gave 122 kJ (0.034 kWh). The overall energy transfer estimated by the dynamic model was thus within 10% of the experimental value. A great deal of further testing of the model is, however, needed in a range of different cases in order to assess its predictive power and validity more generally.

8.2.3 How are the performance and longevity of the PEM electrolyser affected by the intermittent electrical input from an aerogenerator in the direct-coupled arrangement?

The intermittent and variable wind speed creates highly variable current and voltage input to an electrolyser bank directly coupled to an aerogenerator. The current input affects the Faraday efficiency of the electrolyser. For the h-tec PEM electrolysers used in the direct-coupling experiment conducted in the present project, the Faraday efficiency varied from 80 to 95% for currents in the range of 1 to 4 A, but fell rapidly as the current declines below 1 A, reaching as low as 10% at 0.25 A. Hence with a variable power input and hence variable current, the Faraday efficiency of the electrolyser changes accordingly. However, in the case of the direct-coupling experiment, the average Faraday efficiency of the electrolyser bank over the full period of its operation was measured to be relatively high at 85%.

For the entire period of the direct-coupling experiment, the electrically measured energy input to the electrolyser stack was 1.53 kWh. This amount of energy was used in the electrolysis process and produced hydrogen gas. The measured energy produced in the form of hydrogen gas issuing from the electrolyser bank was 1.1 kWh (HHV). Therefore the experimentally-measured overall energy efficiency of the electrolyser bank was on average 72% over the full period of the experiment.

The experimental group of electrolysers (six stacks) each received a total of 255 Wh variable energy input over the 51-day experimental period. A control group of electrolysers (two stacks) were subjected to very nearly the same total energy input but with their voltage and current held constant over a period of 10.9 hours. V-I curves of all the electrolysers in both groups were measured before and after their exposure to the input power to assess whether their performance had degraded.

The electrolysers in the control group did not show any detectable sign of degradation as determined by comparing their V-I curves before and after being subjected to the constant power input. However, four electrolysers in the experimental group did show some signs of performance degradation after being subject to the variable power input during the direct-coupling experiment. On the contrary, electrolyser number 1 seemed to improve on performance, while the performance of electrolyser number 9 stayed constant.

As an example of one electrolyser whose performance fell after the direct-coupling experiment is the following:

- Before the experiment this electrolyser required 13.44 V to produce a current of 3.5A (that is, a power input of 47.0 W),
- After the experiment the voltage to produce 3.5 A rose to 13.8 V (corresponding to a power input 48.3 W).

This degradation means that to produce the same amount of hydrogen at 3.5 A the power input of the electrolyser had to be increased by 2.8% after the 51 days duration of the aerogenerator direct-coupling experiment compared to before. Since the control group of electrolysers subjected to constant power input showed no detectable degradation in performance, the observed degradation is likely to be due to the intermittent and variable power input only, rather than simply time of usage.

The energy input for each electrolyser compared to a PV direct-coupling experiment conducted prior to this project was very small, in fact only around 3% of the latter over a month. This small energy input may have not been enough for detectable degradation to develop among the new electrolysers. The number of specimens in new electrolyser experimental group was also very small.

The variability in the degree of degradation from electrolyser to electrolyser found in both the experimental and control groups indicates that additional experiments involving a larger number of electrolysers are needed before any firm conclusions can be drawn. The performance degradation also needs to be measured at regular intervals over a longer period of usage than was possible in the experiment conducted in this project, both with constant power input and variable power input, to gain a better understanding of the practical lifetime of the electrolysers. A number of different designs of PEM electrolyser also need to be tested under similar conditions to see whether the degree of degradation differs from design to design. Such information is important since maintenance of the performance of electrolysers over a long lifetime is critical to the viability and market competitiveness of wind – hydrogen energy systems.

8.2.4 How do the unit costs of electricity produced by a wind – hydrogen energy system for RAPS, with a conventional electronic coupling unit and under direct coupling of the aerogenerator and electrolyser, compare with those for other RAPS options.

Wind – hydrogen energy systems must compete for RAPS applications with other energy systems such as wind – battery, PV – hydrogen, PV – battery and diesel generator sets. The most economic system measured by unit energy cost, as reported for the Kilcunda case study, produces electricity at a cost of US$ 0.66 /kWh. By using direct coupling or practically eliminating a power electronic between an aerogenerator and electrolyser the cost of energy produced becomes US$ 0.57 /kWh. These unit costs are already very competitive with those for stand-alone wind – battery energy systems of the equivalent capacity, where unit energy costs are in the order of US$ 0.7/kWh, and diesel-battery systems, with costs at current diesel prices in the order of US$ 1.9/kWh. However, the unit cost estimates for wind-hydrogen energy systems made in the present work assume unit capital costs for the main hydrogen-related components, in particular the electrolyser and fuel cell, that are much lower than the prices of currently-available commercial products. Hence some cost reductions in the latter, as well as longer lifetimes, will still be needed for wind hydrogen systems to achieve competitiveness against conventional RAPS systems.

It is also noteworthy that the aerogenerator in a comparable standalone wind – battery system is significant larger than that in an aerogenerator- hydrogen system, since the hydrogen storage allows much more season-to-season storage. It is further reported that the approximate unit cost of energy for PV – hydrogen energy system is US$ 2.5/kWh (chapter 3), which is almost four times higher than that from the wind – hydrogen energy system investigated in this project (power electronics included) at a good wind site. A PV – battery energy system is estimated to produce electricity at a slightly higher cost (US$ 2.8/kWh), whereas a similar system with the addition of a diesel generator set is estimated to yield a unit electricity cost of US$ 2.3/kWh. Furthermore, a diesel-battery would generate electricity at the cost of US$ 1.9/kWh, already much higher than the estimated cost of a wind-hydrogen system even at current diesel prices, which are likely to rise in real terms in coming years.

8.2.5 What are the most promising opportunities for cost reduction and improving competitiveness of wind – hydrogen energy systems?

There are a number of approaches available to reduce the average unit costs of electricity delivered by a wind – hydrogen energy system on a lifecycle basis:

- Reduction of the capital costs of components. An electrolyser, hydrogen storage and fuel cell are some of the most costly units in a wind – hydrogen energy system. PEM electrolysers and fuel cells are currently manufactured by specialist machining processes using expensive materials such as carbon cloth, polymer membranes, and precious metals. The reduction of prices requires technical development of components and high-volume mass production..
- Extension of the lifetimes of major components while maintaining a high-level of performance. The longevity of components such as the electrolyser and fuel cell is crucial for system economic and practical viability. The longer a component lasts, the lower the unit cost of energy produced. In addition, the performance and efficiency of these components must be maintained over their entire lifetime.
- Improvement in system efficiency while keeping costs constant. Technical development in individual components and improved system design can both improving reduce unit energy costs.
- Elimination of components. Reduction in the system cost by eliminating some components has an instant effect on the financial analysis. As shown by the case

study for Kilcunda North conducted in this project, the use of the direct-coupling methodology presented here to eliminate the power electronics between the aerogenerator and electrolyser could save US$800/kW of the capital cost and result in around a 14% reduction in the unit cost of electricity produced.

8.3 CONCLUSIONS

This research project set out to investigate a wind – hydrogen energy system for RAPS applications.

The review of previous work presented in chapter 2 led to the present research project focusing on the feasibility of directly coupling the aerogenerator and PEM electrolyser without any intervening power electronics in a wind – hydrogen energy system for RAPS applications.

A theoretical analysis of a wind – hydrogen energy system has been carried out and used to construct a simulation program based on Visual Basic/Excel for sizing and costing such a system to meet a specified end-use demand over an annual period (chapter 3). The program uses easy-to-use and intuitive dialogue boxes to guide users through a simulation run. It also has built-in wind data sets for ten coastal sites in Victoria, together with the characteristics of ten common small aerogenerators, so that users can select from these to conduct a case study.

The simulation program was then used for a case study of a wind – hydrogen energy system at Kilcunda North, supplying a daily household load of 5.9 kWh/day (chapter 3). It was found that the system could supply electricity at an average unit lost of US$ 0.66/kWh. If direct coupling is used the energy cost is reduced to US$ 0.57/kWh (a 14% reduction), which would have a 3.0 kW aerogenerator, 0.7 kW electrolyser, hydrogen storage of 1.5 kg of hydrogen and a 0.35 kW fuel cell. The cost reduction can be made instantly by eliminating the power electronic and hence improve its competitveness. Furthermore, this unit power cost for a wind – hydrogen energy system is lower than that estimated for an equivalent PV – hydrogen energy system, and highly competitive with conventional RAPS systems such as diesel generators or PV with battery storage

A methodology was then developed in chapter 4 to maximise the power transfer efficiency between a fixed-pitch variable-speed aerogenerator directly coupled to a PEM electrolyser, and hence the overall rate of hydrogen production, without using an electronic converter/impedance matching unit. The key step in this methodology is to alter the V-I characteristic of a bank of electrolysers by changing the series - parallel connection configuration of the cells so that the characteristic tracks as closely as possible the maximum power point curve of the aerogenerator over its range of operating wind speeds.

The direct coupling technique was then applied to Kilcunda North as a case study. The best electrolyser configuration was determined by maximising the energy transfer between the aerogenerator and electrolyser. In this case the best configuration had 21 cells in series and 3 branches in parallel, The estimated energy transfer was only 3.4% lower than the maximum achievable under constant MPP operation. Such a small loss is less than that typically found for DC – DC voltage converters and maximum power point trackers (5 – 10%), so that on this basis the direct coupling option appears promising as a way to reduce system costs without any energy penalty.

An experimental investigation of the energy transfer and hydrogen production of an AIR 403 aerogenerator directly coupled to a bank of h-tec PEM electrolysers was conducted from 25/04/2008 to 14/06/2008 at RMIT University's Bundoora East campus to test the viability of this approach in practice and compare the results obtained with theoretical calculations conducted using the method just described (chapter 5).

The experimental result for the energy transfer of between the AIR 403 aerogenerator directly coupled to the optimally matched PEM electrolyser bank was 1.53 kWh, which was less than a third of the theoretically-estimated energy transfer of 4.81 kWh. The discrepancy between the two energy transfer results was large enough to suggest that other factors also needed to be investigated.

A close inspection of the variation over time of the aerogenerator output with changes in the wind speed indicated that the dynamic response of the aerogenerator was significantly different to the response calculated from the measured wind speed in each interval assuming the steady state output of the aerogenerator had always been attained (Chapter

6). This observation led to the conclusion that the following dynamic factors were likely to require consideration in the experiment:

- The aerogenerator needs time to change from a stationary state to the minimum angular velocity at which it actually produces power, whereas the theoretical calculation assumes in effect an immediate response.
- The fluctuating wind speed may not allow the angular velocity of the aerogenerator to rise to its steady-state angular velocity, whereas the theoretical calculation assumes immediate attainment of the steady state corresponding to the given wind speed in each interval and thus overestimates the power production. The steady state analysis thus does not take account of aerogenerator's moment of inertia.

To obtain a closer fit between experimental data and theoretical estimates a dynamic model of the aerogenerator's response in a variable wind situation was thus developed (chapter 7). The dynamic system model takes into account the finite time needed for the turbine to pick up angular velocity from a stationary state, and to respond to rapid changes in wind speed, due to its moment of inertia.

The dynamic simulation program was used to predict the power and energy transfer between an AIR 403 aerogenerator directly coupled to a bank of PEM electrolyser using wind speed data from the direct coupling experiment conducted. The period simulated was a limited period of 4 days, 23 hours selected from the 51 days of the entire experiment. The prediction of the dynamic model for cumulative energy transfer over the study period is much closer (within 10%) of the actual experimentally-measured energy transfer than the corresponding prediction using the steady state model (an overestimate by 17%). The dynamic model has thus shown some initial promise in more accurately predicting the energy transfer in a wind – hydrogen energy at sites, where intermittent and variable wind speed is present. However, a great deal of further analysis, improvement, and testing against experimental values are required to check the model's predictive power and validity in more general situations.

The experimental investigation of direct-coupling further revealed that degradation in performance of PEM electrolysers when subjected to a highly variable power input from an aerogenrator is an issue requiring additional detailed study, as discussed earlier (subsection 8.2.3).

From an overall perspective, it is likely to be possible to reduce the cost of a wind – hydrogen energy system and improve its competitiveness among others RAPS systems using direct coupling between an aerogenerator and electrolyser. However, the direct coupling technique as investigated in this thesis raises other questions that must be closely examined, including principally:

- How does the V-I curve matching technique proposed in the present thesis need to be modified when a dynamic model of aerogenerator performance is employed rather than a steady state model?
- Can this matching technique still be used, with suitable modifications, in the preferred system configuration when only the surplus wind power over load is fed to the electrolyser, rather than all the wind power as examined in the present thesis?
- How can the performance and longevity of PEM electrolysers be maintained when subject to the intermittent and variable electrical input from a directly-coupled aerogenerator?

8.4 RECOMMENDATIONS

On the basis of these conclusions and the thesis as a whole, it is recommended that:

- Further research and development is conducted into direct coupling of an aerogenerator and electrolyser in which the aerogenerator V-I curve is altered as well as the electrolyser characteristic to see if even better matching can be obtained. The aerogenerator characteristic can be modified by changing the permanent magnet or windings of the generator coils.
- The system and component sizing simulation model developed as part of the research program for this thesis is improved by:
    - The improvement of each submodel. For example, the net energy losses in the hydrogen storage system should be quantified. Options for storing as compressed gas or in metal hydrides of various kinds could be added.
    - Further automating the procedure for finding component sizes under different conditions, and minimum unit cost configurations.

- Further analysis, improvement, and testing against experimental values are conducted to check the predictive power and validity of the dynamic aerogenerator model in more general situations. The characteristic of the generator used (output voltage vs RPM) should be incorporated directly into the model
- Follow-up theoretical and experimental investigations are carried out into modifying the aerogenerator-electrolyser matching technique proposed in the present thesis for use:
    - with a dynamic model of aerogenerator performance rather than a steady state model
    - in the system configuration when only the surplus wind power over load is fed to the electrolyser, rather than all the wind power as examined here.
- Further research and development in conducted into ways to maintain the performance and longevity of PEM electrolysers when subject to the intermittent and variable electrical input from a directly-coupled aerogenerator.

8.5 EPILOGUE

It has been shown through the work in this project that a wind – hydrogen energy system can at a good wind site soon become competitive with conventional RAPS systems.

The direct coupling technique investigate in this thesis is technically possible and promises significant system and energy cost reductions in wind-hydrogen energy systems. Yet there are a number of outstanding questions still to be answered before the technique is applied commercially.

A wind – hydrogen energy system in general is a way forward in the attempt to cut carbon emissions and minimise global warming and catastrophic climate change. In a good wind location, a wind – hydrogen energy system may well be the first example of the kind of technology that could become commonplace on a much larger scale in a global and truly sustainable hydrogen economy.

APPENDICES

APPENDIX A

STEP SIZE OF THE WIND – HYDROGEN ENERGY SYSTEM MODEL

In the Visual Basic/Excel program constructed to simulate a wind – hydrogen energy system, one aspect affecting its accuracy is the variable called *Step Size*. *Step Size* is the amount by which the overall system sizing model increases the area of an aerogenerator by from one iteration to the next as the program progresses towards finding the minimum size to give sustainable supply on an annual basis. The bigger *Step Size* is, the faster the simulation reaches its solution. However, by getting the solution quicker, the accuracy is reduced. *Step Size* could be 10, 3, or 0.5 m^2 depending on the requirement of the simulation and the resources available such as time and computer power. If accuracy is the priority, the *Step Size* may be decreased. To find out the best value of *Step Size*, four sample models: Kilcunda 3.5, Kilcunda 4.5, Port Campbell 2.5 and Port Campbell 3.5, were subjected to testing with decreasing *Step Size* numbers. The number following the location name denotes the hydrogen storage capacity.

As shown in Figure A1, all four sample models are run 10 times each. The first run uses a *Step Size* value of 0.5 m^2 and then this value was consistently reduced for the consecutive runs to 0.1, followed by 0.075, 0.05, 0.025, 0.01 and 0.005 m^2. For each sample model, all others parameters were kept constant. For example, while the *Step Size* number was reducing from 0.5 to 0.005 m^2 for the Kilcunda 3.5 model, the percentage improvement (% difference with respect to results based on the run with *Step Size* = 0.5 m^2 as the benchmark, though it does not represent the most accurate result it is the first starting point) of the results increased from 0 to 8.5%. The results of runs with *Step Size* between 0.2 to 0.005 m^2 are closely stacked around 8%. Similarly, the sample model Kilcunda 4.5 has the same trend. Moreover, there was no significant difference between the percentages of improvement for Kilcunda 3.5 and Kilcunda 4.5.

More importantly, the percentages of improvement of the results were slightly flat after from the *Step Size* value decreased from 0.2 to 0.005 m^2 for all models except Port

Campbell 2.5 (Figure A2) whose percentage of improvement stabilised from *Step Size* number of 0.075 to 0.005 m^2.

Finally, *Step Size* values, which could be used for most of the models, are between 0.2 and 0.005 m^2. However, a compromise *Step Size* value had to be selected to meet the criteria that it should not be too small to keep simulation time short, but it should still give an accurate result. Therefore, a number of 0.1 m^2 was selected because this number is between 0.2 and 0.005 m^2, yet it would give a reasonable result in some cases such as Port Campbell 2.5. A *Step Size* value any smaller than this would not give significantly more accuracy while more simulation time and computing power are needed.

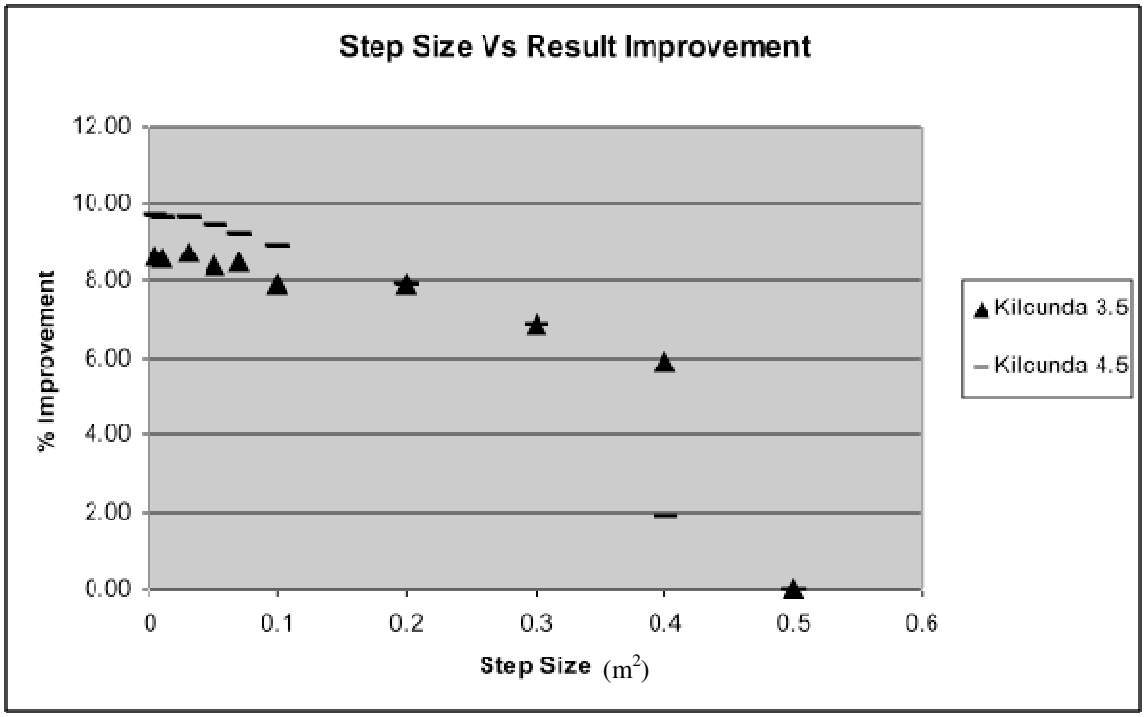

Figure A1: Step Size specified in the overall system sizing model influents the % of improvement of result. Both sample models have similar trends throughout ten runs, where the % of improvement becomes flat after Step Size of 0.2.

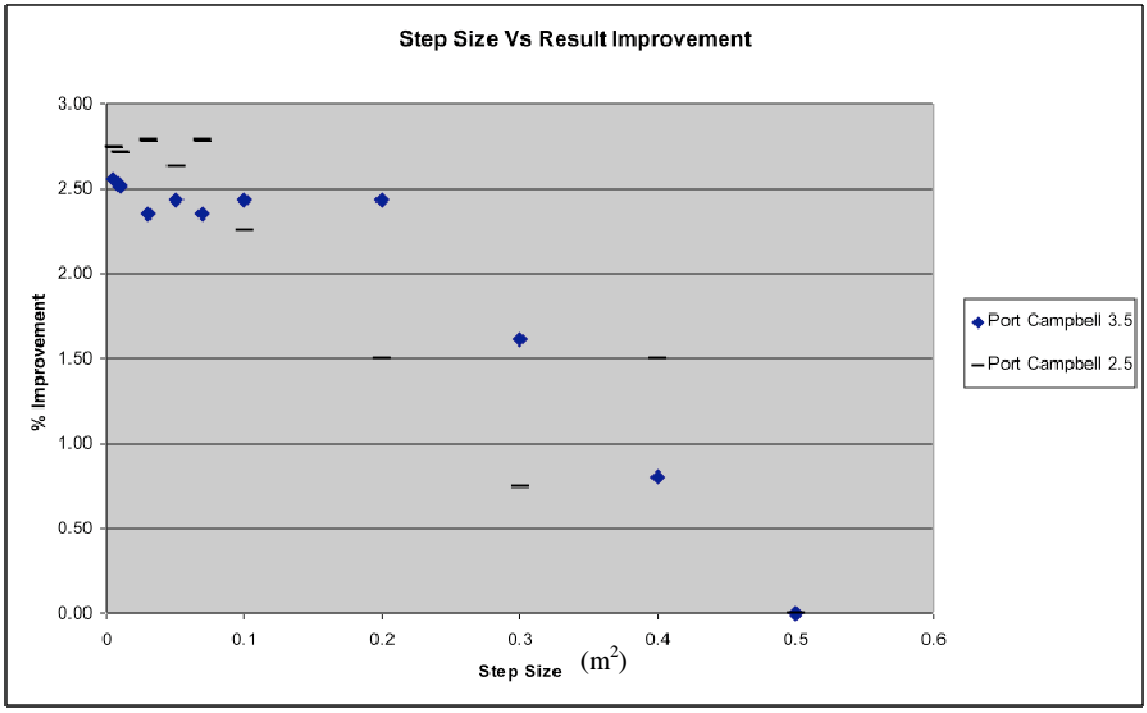

Figure A2: Step Size specified in the overall system sizing model influents the % of improvement of result. Port Campbell 3.5 results become stable at Step Size of 0.2, where Port Campbell 2.5 results become stable at Step Size of 0.1.

APPENDIX B

AIR 403 AEROGENERATOR MODIFICATION: AIR 403 BUILT-IN CONTROL SYSTEM

The AIR 403 aerogenerator is designed for battery charging with its own control system built-in and will sense battery voltage as a prerequisite. As a result, the built-in control system is not suitable for this experiment. The items that needed modification are:

- AIR 403 aerogenerator built-in power electronics
- Copper brushes and holder
- Slip rings (yaw bearing) and wiring
- Generator coils.

The internal electronic unit (Figure B1) was removed and the generator coils of the AIR 403, phase 1, 2, & 3, were connected in star configuration. The brushes connected to the generator coils by wires had been made with copper blocks (Figure B2), which were installed behind the slip rigs (Figure B3).

The old slip rings, which were used for DC power transfer from the aerogenerator, were modified for AC use; ground connection was also re-routed to the turbine body. The three original slip rings were used to transfer DC electricity: positive, negative and ground. An extra groove had to be made on the bottom ring to split it physically into two rings to give the four rings required for the 3-phase AC: phase 1, 2, 3 and ground (Figure B3).

As a result, the modified permanent magnet generator produced AC power, wired out from the aerogenerator into the lab, where a newly designed control system and a rectifier were installed. This arrangement gave the flexibility of choosing from a range of control techniques. After reassembly, the AIR 403 was ready to be tested in wind tunnel.

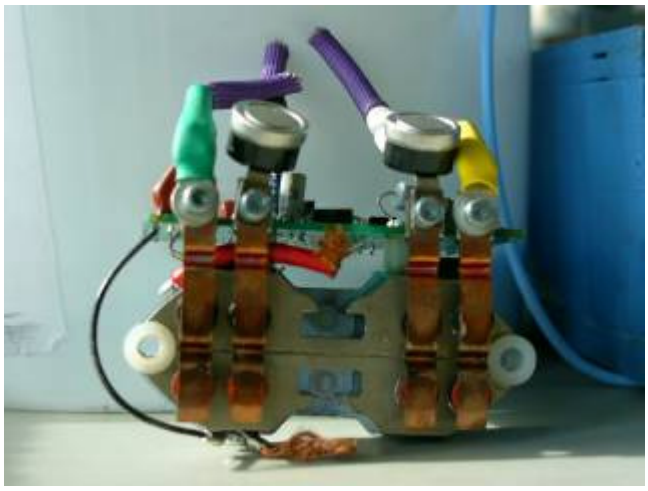

Figure B1: AIR 403 aerogenerator built-in power electronics. The unit contains a rectifier, voltage regulator and battery charger.

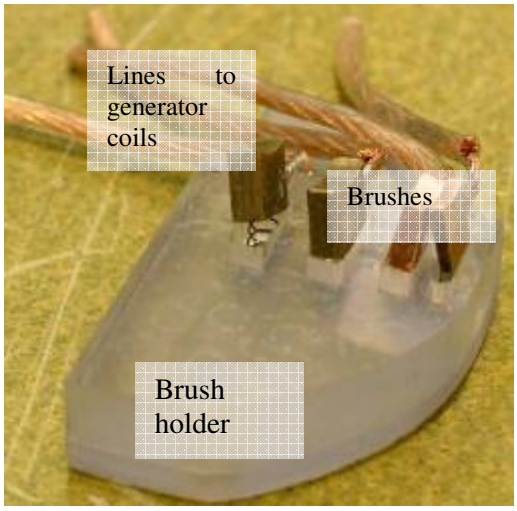

Figure B2: Copper brushes and holder made to accommodate 3-phase AC. Four copper brushes to connect to phase 1,2,3 and ground.

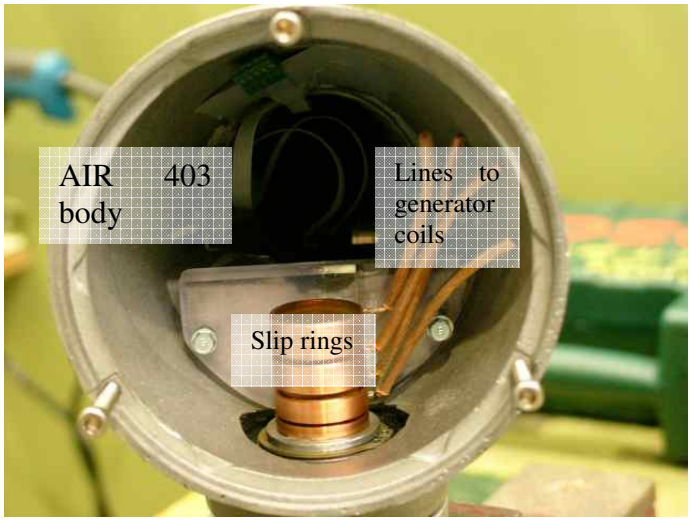

Figure B3: Installed modified slip rings (yaw bearing) and brushes suitable for 3-phase AC. The copper brushes are installed behind the rings and turn relative to the rings when the turbine yaws.

APPENDIX C

AIR 403 3-PHASE AC OUTPUT TESTING IN WIND TUNNEL

C.1 Equipment

The equipment used in to measure the output of the AIR403 aerognerator in the RMIT University wind tunnel, Bundoora East campus was as follows:

- 3 variable resistive loads, each had 10 A and approximately 12 Ω resistance
- 6 digital multimeters
- Digital tachometer
- The AIR 403 aerogenerator

C.2 Experimental procedure

The AIR 403 was positioned into the wind tunnel by a support structure (Figure C1). Then the digital tachometer was attached to the nacelle or body of the turbine. The reflective strip was place at the back of one of the blades, where it would reflect light beam from the tachometer and hence one revolution equal to one reflection.

The 3-phase AC output leads from the turbine were run inside the support tube and along the floor of the wind tunnel then to the resistive loads outside the tunnel. Each load was assigned to each phase, and each had two digital multimeters connected for current and voltage readings (Figure C2). The three coils of the generator were connected in star or Y configuration (Figure C2). A digital ammeters (A) was connected in series with each load and a voltmeter (V) was connected in parallel across each load (R1, R2 & R3).

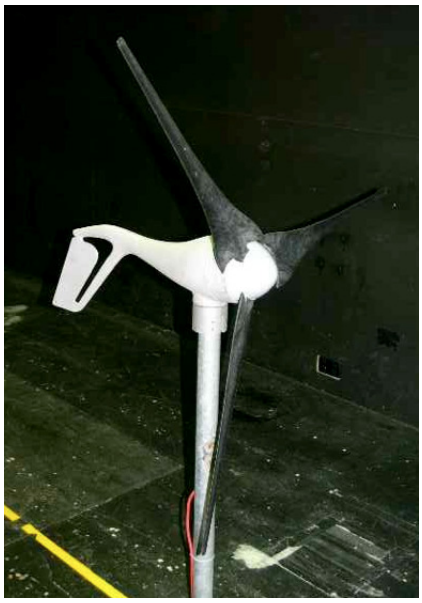

Figure C1: AIR 403 aerogenerator install inside RMIT Industrial Wind Tunnel.

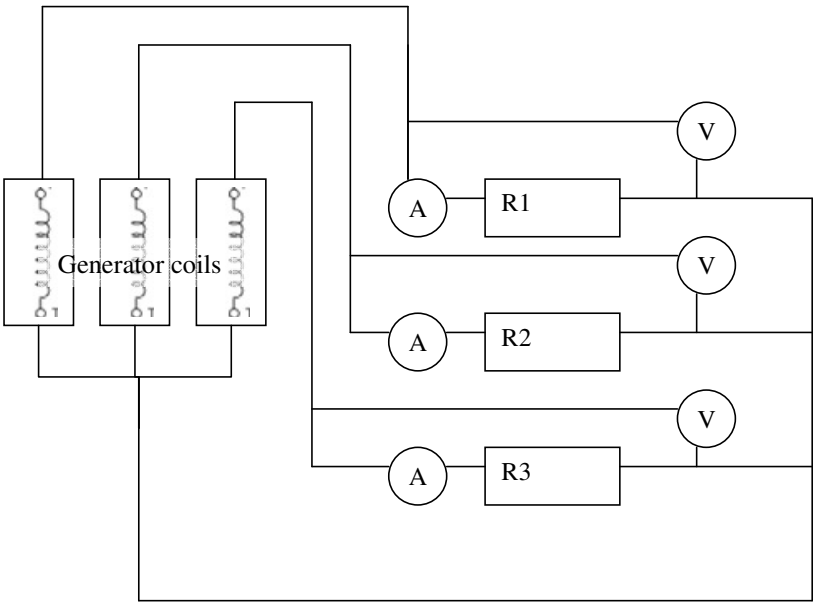

Figure C2: Schematic of AIR 403 coil connection and electrical loading. R1, R2 and R3 are variable resistive load and three generator coils are on the left. Ammeters are labeled as A and voltmeters as V.

Each measurement was made at a constant wind speed. Once a wind speed was set and the aerogenerator was generating power equally at each load, the current, voltage and RPM at each load were recorded. Then the resistances of the loads were consistently reduced until

the aerogenerator running to a halt. The experiment was done for a range of wind speeds from 4-12.5 m/s as the load capacity allowed.

The aerogenerator had to be unloaded at the start of each run to let its RPM rise to a working range, indicated by a rapid sore in voltage, and then load was applied and the system allowed to reach a steady state before readings of voltage and current outputs were recorded for that wind speed.

The measured wind speeds were read from the control panel and recorded. The AC output voltage and current into each resister were measured by digital multimeters. The AC electrical values then converted into DC values in the process of plotting V-I curves, where conversion loss is assumed to be negligible. The model used was a Digitech QM1536, which measures with ±1% accuracy at this AC voltage range. Moreover, the accuracy on AC current measurement is ±2.5%.

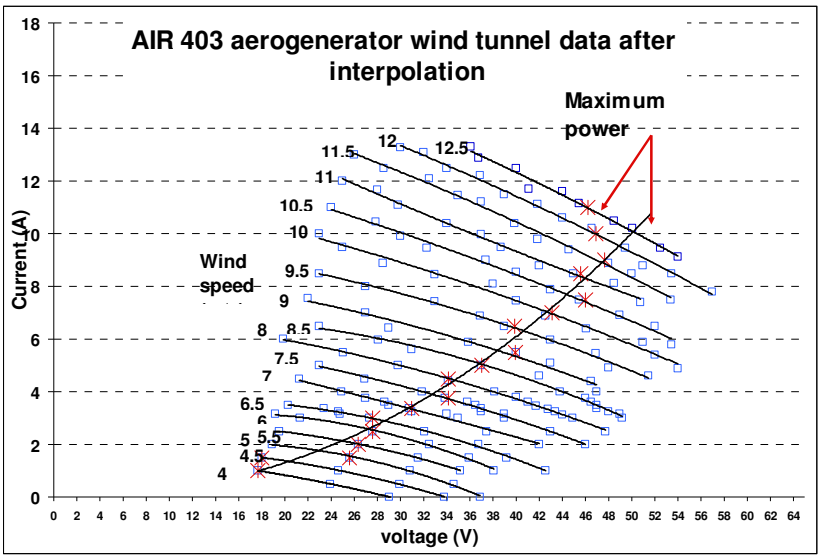

Figure C3: AIR 403 V-I characteristic curves, which have been adjusted by AC/DC conversion, rounded interpolation, and for error in measured wind speeds in the wind tunnel.

APPENDIX D

AIR 403 CONTROL SYSTEM

In the designing the AIR 403 control system, a flowchart was used to determine the logical steps needed to perform tasks required by the system (Figure D1). The flowchart provided a general guide for constructing the program without having to know any program language. The basic tasks performed by the software are taking data, processing data and output commands.

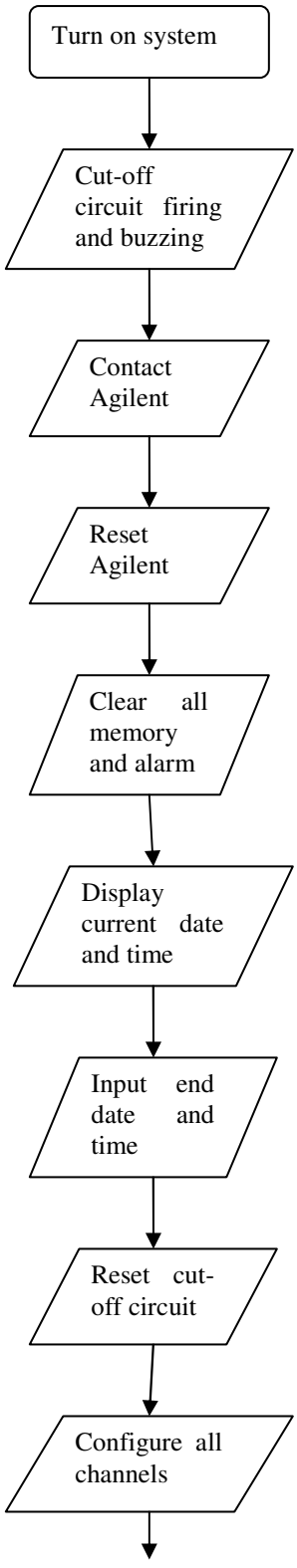
Turn on system
Cut-off circuit firing and buzzing
Contact Agilent
Reset Agilent
Clear all memory and alarm
Display current date and time
Input end date and time
Reset cut-off circuit
Configure all channels

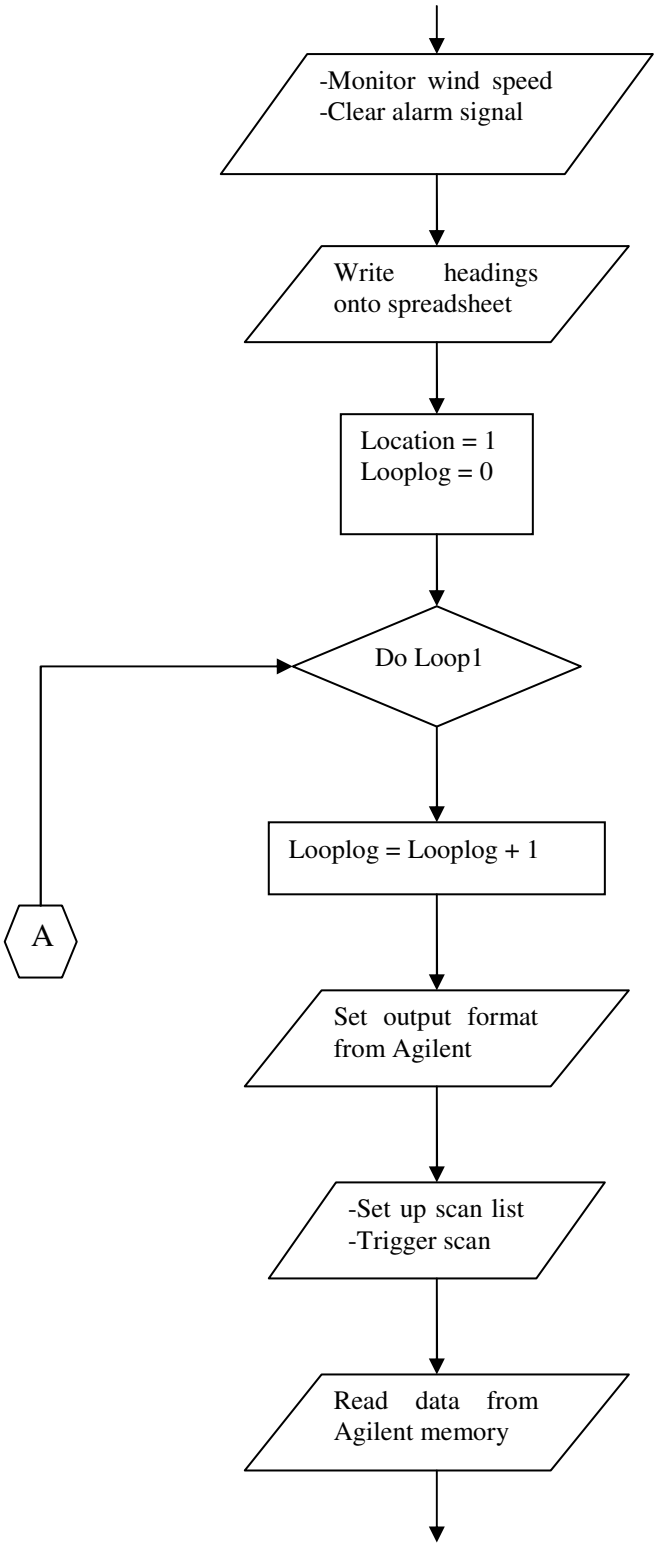
-Monitor wind speed
-Clear alarm signal
Write headings onto spreadsheet
Location = 1
Looplog = 0
Do Loop1
Looplog = Looplog + 1
A
Set output format from Agilent
-Set up scan list
-Trigger scan
Read data from Agilent memory

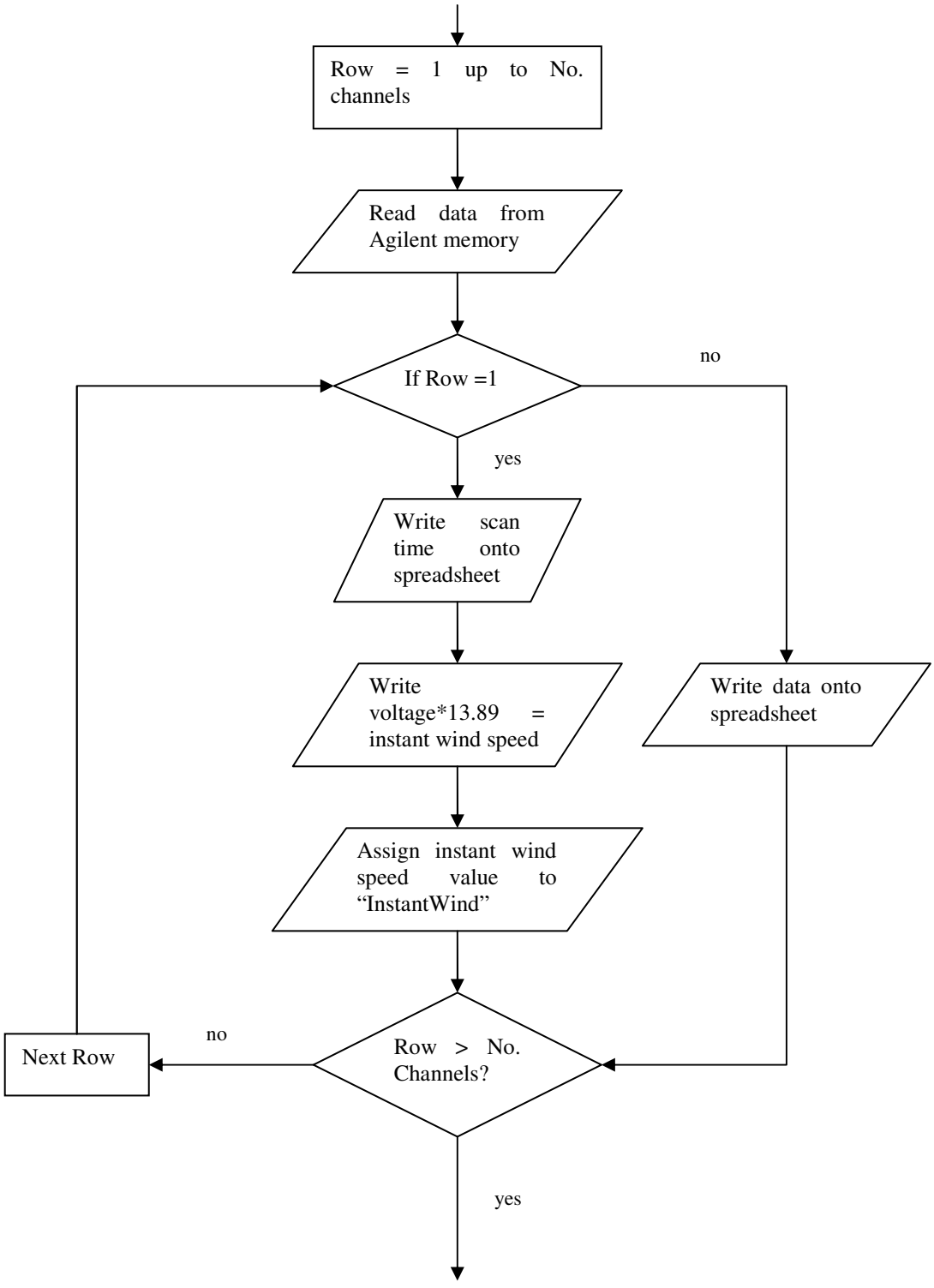
Row = 1 up to No. channels
Read data from Agilent memory
If Row =1
no
yes
Write scan time onto spreadsheet
Write voltage*13.89 = instant wind speed
Write data onto spreadsheet
Assign instant wind speed value to "InstantWind"
Row > No. Channels?
no
Next Row
yes

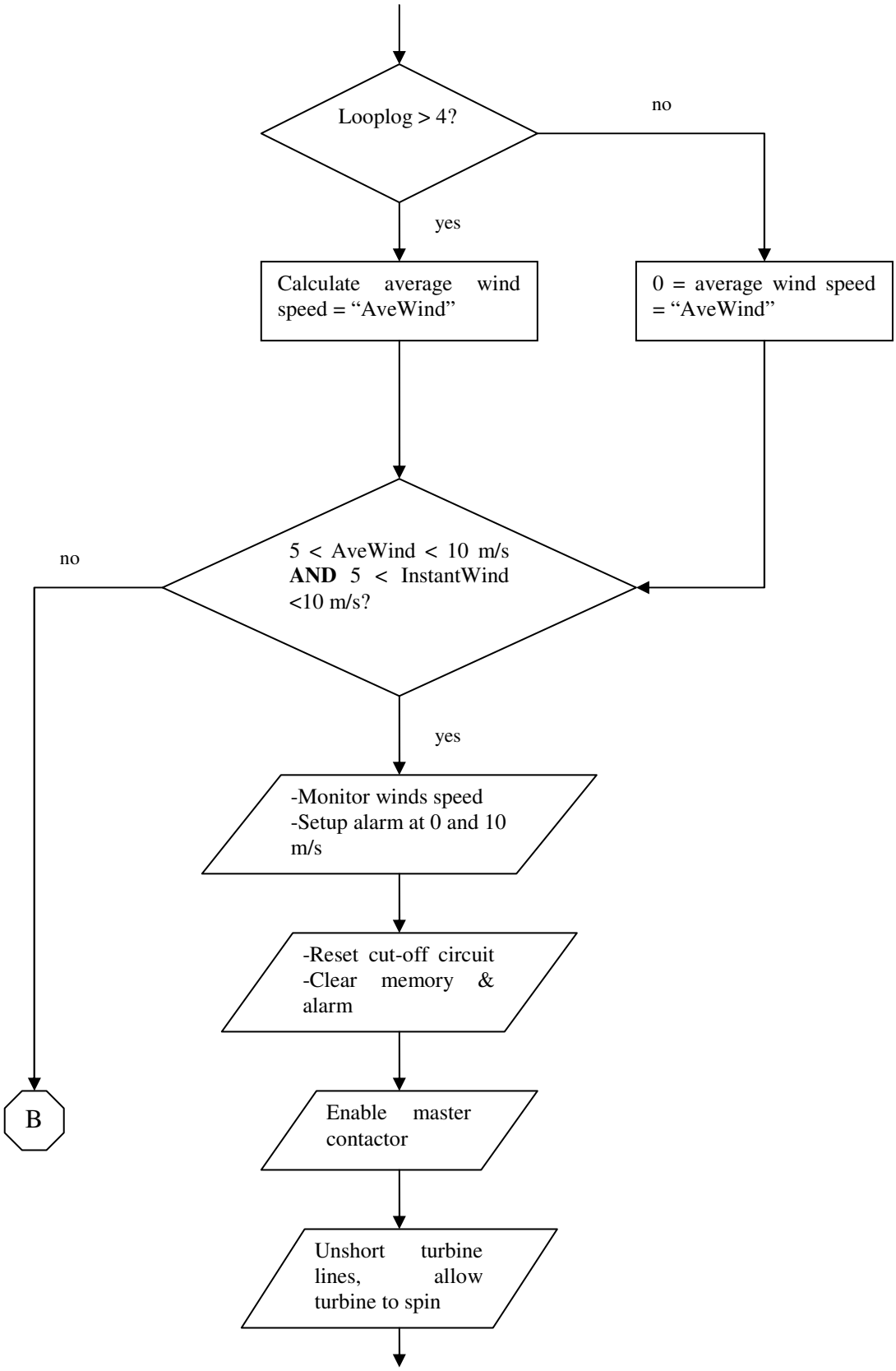
Looplog > 4?
no
yes
Calculate average wind speed = "AveWind"
0 = average wind speed = "AveWind"
5 < AveWind < 10 m/s **AND** 5 < InstantWind <10 m/s?
no
yes
-Monitor winds speed
-Setup alarm at 0 and 10 m/s
-Reset cut-off circuit
-Clear memory & alarm
Enable master contactor
Unshort turbine lines, allow turbine to spin
B

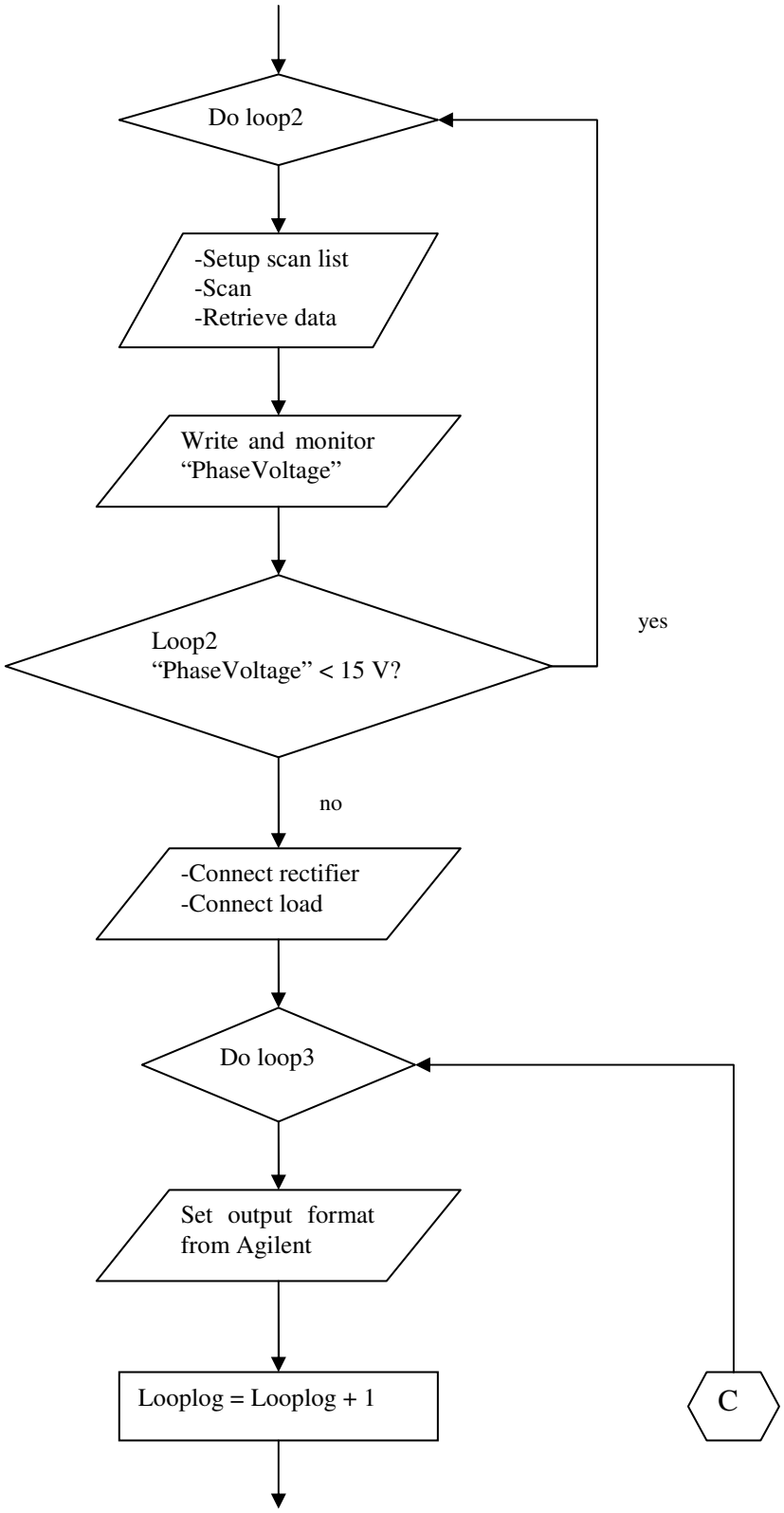
Do loop2
-Setup scan list
-Scan
-Retrieve data
Write and monitor
"PhaseVoltage"
Loop2
"PhaseVoltage" < 15 V?
yes
no
-Connect rectifier
-Connect load
Do loop3
Set output format
from Agilent
Looplog = Looplog + 1
C

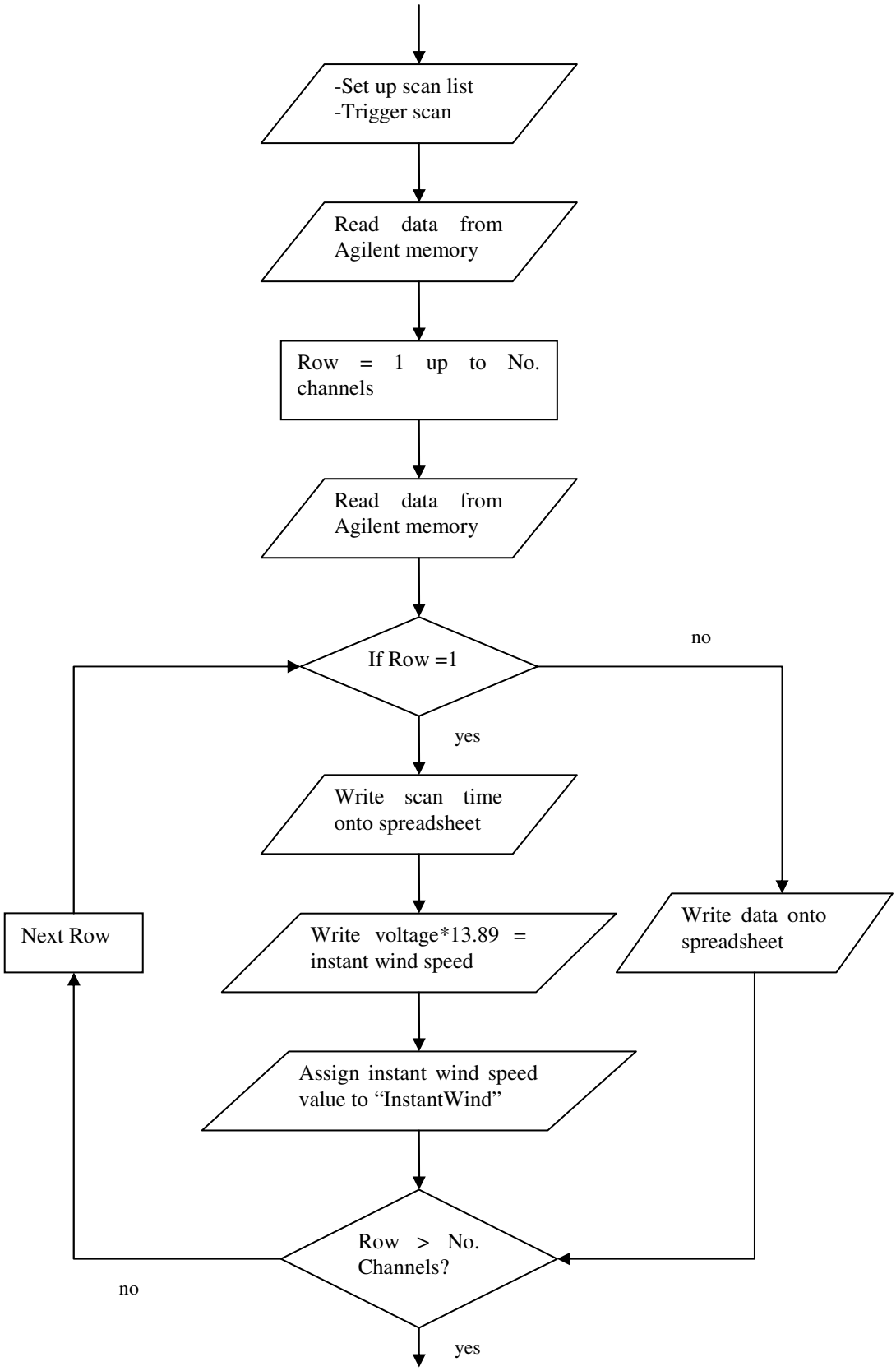
-Set up scan list
-Trigger scan
Read data from Agilent memory
Row = 1 up to No. channels
Read data from Agilent memory
If Row =1
no
yes
Write scan time onto spreadsheet
Write voltage*13.89 = instant wind speed
Assign instant wind speed value to "InstantWind"
Write data onto spreadsheet
Next Row
Row > No. Channels?
no
yes

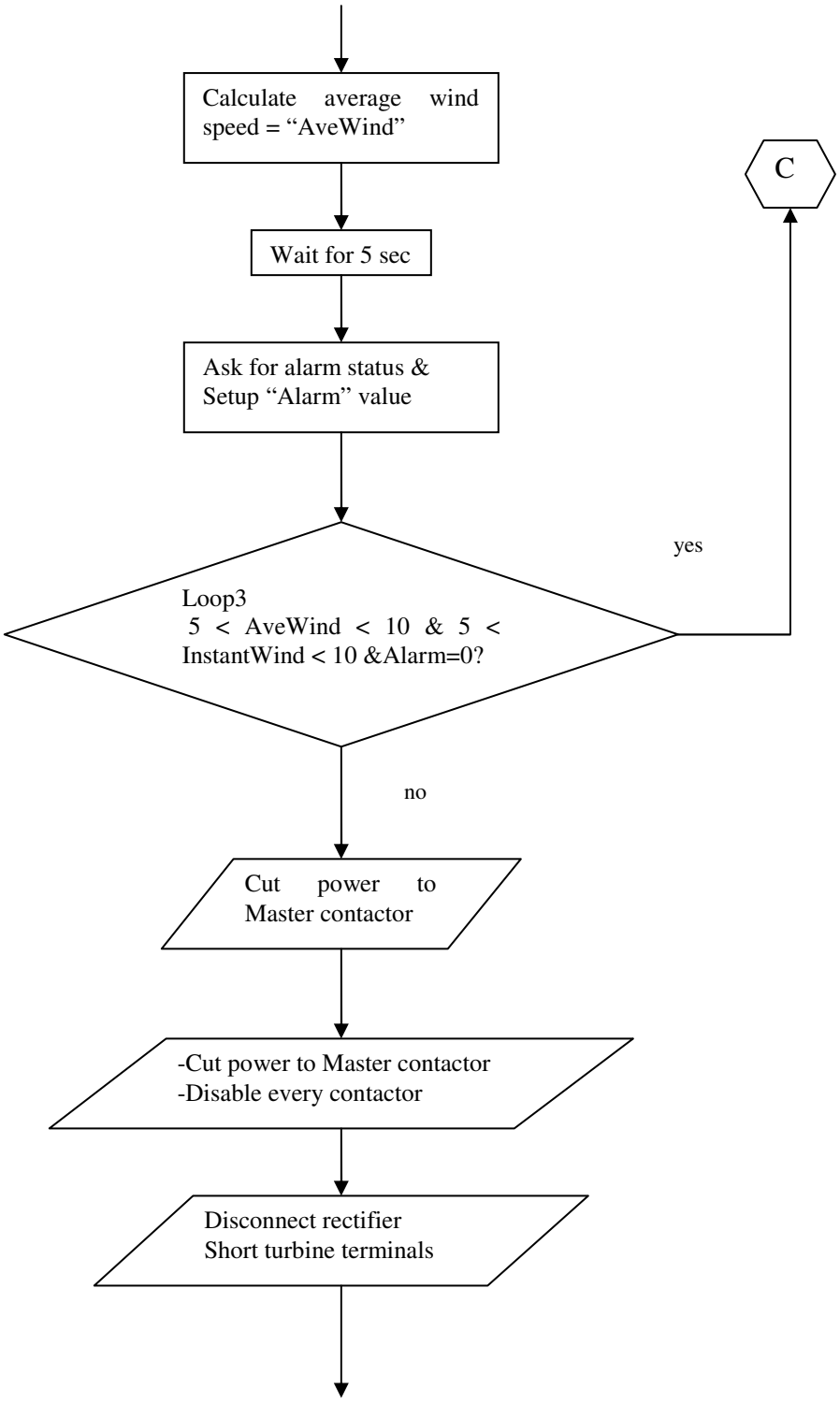
Calculate average wind speed = "AveWind"
Wait for 5 sec
Ask for alarm status & Setup "Alarm" value
Loop3
5 < AveWind < 10 & 5 < InstantWind < 10 &Alarm=0?
yes
C
no
Cut power to Master contactor
-Cut power to Master contactor
-Disable every contactor
Disconnect rectifier
Short turbine terminals

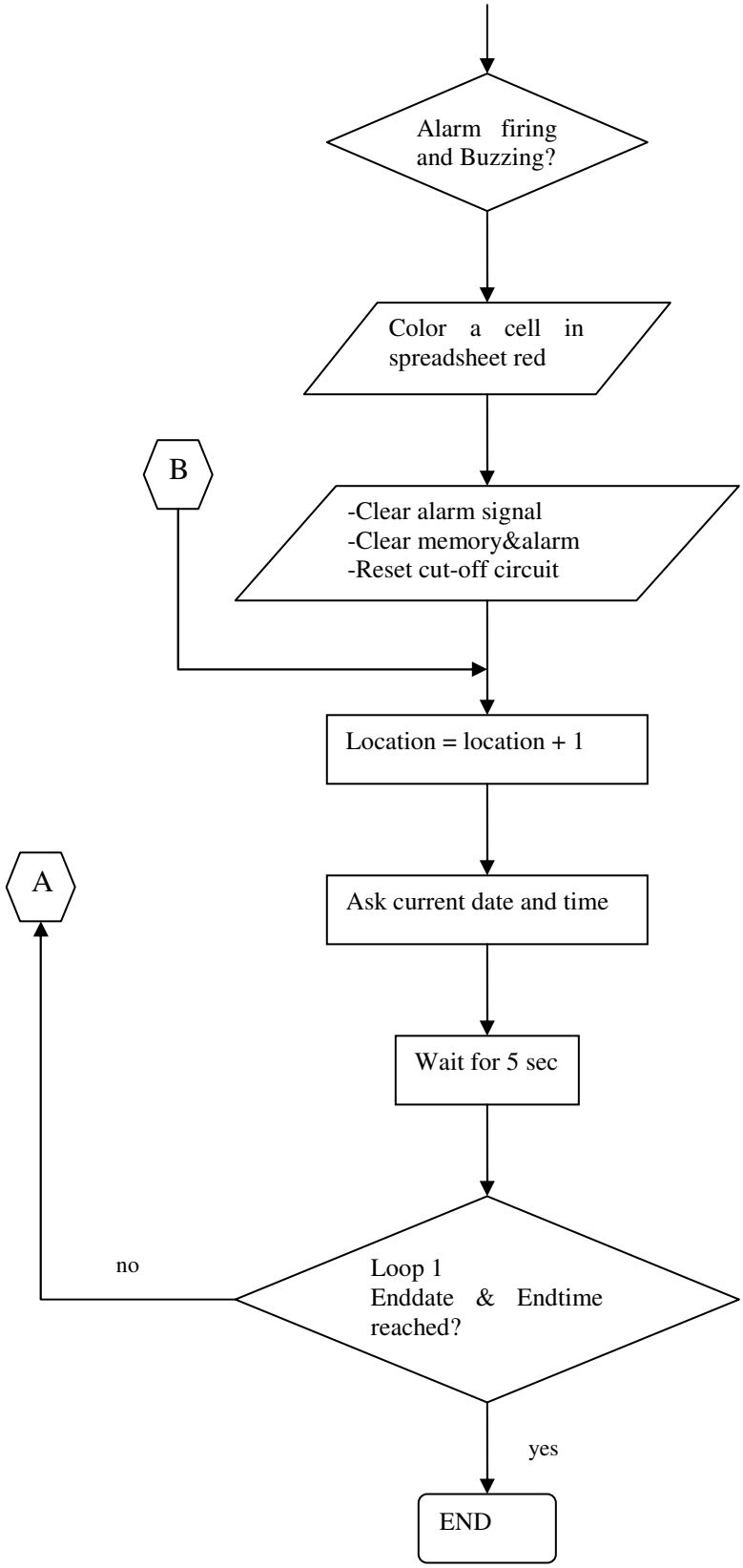

Figure D1: AIR 403 control system flowchart, which determine the logical steps needed to perform tasks required by the system.

REFERENCES

AGBOSSOU, K., CHAHINE, R., HAMELIN, J., LAURENCELLE, F., ANOUAR, A., ST-ARNAUD, J.-M. & BOSE, T. K. (2001) Renewable energy systems based on hydrogen for remote applications. *Journal of Power Sources,* 96**,** 168-172.

ALI, S. M. (2007) Solar-hydrogen systems for remote area power supply. *School of Aerospace, Mechanical and manufacturing Engineering.* Melbourne, RMIT University.

ALI, S. M. & ANDREWS, J. (2006) Low-cost storage options for solar hydrogen systems for remote area power supply. *World hydrogen energy conference.* Lyon France.

ALTER SYSTEMS (2008) Alter systems go green for life. Berkeley CA, USA.

APREA, L. J. (2008) Hydrogen energy demonstration plant in Patagonia: description and safety issues *International Journal of Hydrogen Energy***,** 1-8.

BARBIR, F. (2005) PEM electrolysis for production of hydrogen from renewable energy sources. *Solar Energy,* 78**,** 661-669.

BECHRAKIS, D. A., MCKEOGH, E. J. & GALLAGHER, P. D. (2006) Simulation and operational assessment for a small autonomous wind-hydrogen energy system. *Energy Conversion and Management,* 47**,** 46-59.

BEUKES, H. J. & MOOR, G. D. (2004) Maximum Power Point Trackers for Wind Turbines. *35th Annual IEEE Power Electronics Specialists Conference.* Aachen Germany.

BOCKRIS, O. J. (2002) The origin of ideas on a hydrogn economy and its solution to the dacay of the environment. *International Association for Hydrogen Energy,* 27**,** 731-740.

BOLDEA, I. (Ed.) (2006) *The electric generators handbook, variable speed generators,* NW, CRC press Taylor & Francis.

BOLES, A. M. & CENGEL, A. Y. (1998) *Thermodynamics: An Engineering Approach*, McGraw Hill.

BOUKHEZZAR, B. & SIGUERDIDJANE, H. (2005) Nonlinear control of variable speed wind turbine without wind speed measurement. *44th IEEE Conference on Decision and Control, and the European Control Conference* Seville, Spain.

BROSSARD, L., BELANGER, G. & TRUDEL, G. (1984) Behavior of a 3kW electrolyser under constant and variable input. *International Association for Hydrogen Energy,* 9**,** 67-72.

BURTON, T., SHARPE, D., JENKINS, N. & BOSSANYI, E. (2001) *Wind energy handbook,* West sussex, England, John Wiley & Sons

CLARKE, R. C., GIDDEY, S., CIACCHI, F. T. & BADWAL, S. P. S. (2008) A stand-alone 2 kW PEM electrolyser integrated with a solar PV system for hydrogen generation. *17th world hydrogen energy conference.* Brisbane, Australia.

CORBUS, D., BARING-GOULD, I., DROUILHET, S., GERVORGIAN, V., JIMENEZ, T., NEWCOMB, C. & FLOWERS, L. (1999) Small Wind Turbine Testing and Applications Development. *Windpower '99.* Burlington, Vermont.

DEPARTMENT OF THE ENVIRONMENT WATER HERITAGE AND THE ARTS, A. G. (2008) Remote Area Power Supply (RAPS).

DIVISEK, J. & EMONTS, B. (2003) *Handbook of Fuel Cells* West Sussex, John Wiley & son Ltd.

DOUGHERTY, W., KARTHA, S., RAJAN, C., LAZARUS, M., BAILIE, A., RUNKLE, B. & FENCL, A. (2008) Greenhouse gas reduction benefits and cost of a large-scale transition to hydrogen in the USA. *Energy Policy,* 37**,** 56-67.

DUTTON, A. G., BLEIJS, J. A. M., DIENHART, H., FALCHETTA, M. H., PRISCHICH, D. & RUDDELL, A. J. (2000) Experience in the design, sizing, economics and implementation of autonomous wind-powered hydrogen production systems. *International Journal of Hydrogen Energy,* 25**,** 705-722.

EDWARDS, P. P., KUZNETSOV, V. L., DAVID, W. I. F. & BRANDON, N. P. (2008) Hydrogen and fuel cells: Towards a sustainable energy future. *Energy Policy,* 36**,** 4356-4362.

EL PASO ELECTRIC. (2003) Usage Patterns and Load Profiles.

GAMMON, R., ROY, A., BARTON, J. & LITTLE, M. (2006) Hydrogen and renewables integration. Leicestershire, UK, Centre of renewable energy systems technology (CREST), Loughborough.

GAZEY, R., SALMAN, S. K. & AKLIL-D'HALLUIN, D. D. (2006) A field application experience of integrating hydrogen technology with wind power in a remote island location. *Journal of Power Sources*.

GIPE, P. (1999) *Wind Energy Basic: A Guide to Small and Micro Wind Systems,* Totnes, England, Chelsea Green Publishing Company.

GOGREENSOLAR (2008) Gogreensolar. Los Angeles, USA.

HAMNETT, A. (2003) Thermodynamics and kinetics of fuel cell reactions IN VIELSTICH, W., GASTEIGER, A. H. & LAMM, A. (Eds.) *Handbook of fuel cells.* John Wiley & sons Ltd.

HOFFMANN, P. (2001) *Tomorrow's energy: hydrogen, fuel cells, and the prospects for a cleaner planet,* London, MIT Press.

HOLLADAY, J. D., HU, J., KING, D. L. & WANG, Y. (2008) An overview of hydrogen production technologies. *Catalysis Today*.

HOOGERS, G. (2003) *Fuel cell technologyhandbook*, CRC press.

INFINIGI (2008) Infinite Energy Solution. Palos Verdes Penisula, CA, USA.

IPCC (2007) Climate Change 2007: Synthesis report. Sweden, The Intergovernmantal Panel on Climate Change.

ISHERWOOD, W., SMITH, J. R., ACEVES, S. M., BERRY, G., CLARK, W., JOHNSON, R., DAS, D., GOERING, D. & SEIFERT, R. (2000) Remote power systems with advanced storage technologies for Alaskan villages. *Energy,* 25**,** 1005-1020.

JANON, A. & ANDREWS, J. (2006) Modeling small wind-hydrogen energy systems for coastal sites. *ANZSES national conference 2006: Clean energy? Can do!* Canberra.

JONES, D. A., WOOD, P. & CALLEY, D. (2000) AIR 403 design document.

KAZUTO, Y., YOSHIHIRO, K., YOSHINAO, I., YASUYUKI, G., KATSUHIRO, I. & TESURO, K. (2008) Basic study on pole change generator for micro windmill generation system. *IEEJ Transaction on Power and Energy* 128**,** 201-207.

KHAN, M. J. & IQBAL, M. T. (2005) Dynamics modeling and simulation of a small wind-fuel cell hybrid energy system. *Renewable Energy,* 30**,** 421-439.

KOLHE, M., AGBOSSOU, K., HAMELIN, J. & BOSE, T. K. (2003) Analytical model for predicting the performance of photovoltaic array coupled with a wind turbine in a stand-alone renewable energy system based on hydrogen. *Renewable Energy,* 28**,** 727-742.

LARMINIE, J. & DICKS, A. (2003) *Fuel cell systems explained,* West Sussex, John Wiley & Sons Ltd.

LOGAN, E. (1999) *Thermodynamics: Processes and application,* Arizona, Marcel Dekker.

LUO, F. L. & YE, H. (2004) *Advanced DC/DC converters,* NW, CRC press LLC.

MAGILL, P. (2008) Wind-hydrogen demonstration project, Mawson Antarctica. *17th World Hydrogen Energy Conference.* Brisbane, Australia.

MILAND, H., GLOCKNER, R., TAYLOR, P., AABERG, J. R. & HAGEN, G. (2006) Load control of a wind-hydrogen stand-alone power system. *International Journal of hydrogen Energy,* 31**,** 1215-1235.

MUKUND, R. P. (1999) *Wind and solar power systems,* Newyork, CRC press.

NAKAMURA, T. M., S SANADA, M TAKEDA, Y (2002) Optimum control of IPMSG for wind generation system. *Powerconversion conference.* Osaka, IEEE.

NATURAL SYSTEMS RESEARCH PTY, L. (1987) Wind Monitoring Study Final Report. State Electricity Commission of Victoria, Victoria Solar Energy Council.

NATURAL SYSTEMS RESEARCH. (1987) Wind Monitoring Study Final Report. State Electricity Commission of Victoria, Victoria Solar Energy Council.

PATEL, M. S. & PRYOR, T. L. (2001) Monitored performance data from a hybrid RAPS system and the determination of control set points for simulation studies. *ISES 2001 Solar World Congress.* Adelaide, South Australia.

PATEL, R. M. (1999) *Wind and Solar Power Systems*, CRC Press.

PAUL, B. (2008) Direct coupling of PV panels with PEM electrolysers in solar-hydrogen systems. *School of Aerospace, Mechanical and manufacturing Engineering.* Melbourne, RMIT University.

PAUL, B. (2009) Direct coupling of the Photovotaic array and PEM electrolyser in a solar-hydrogen system for remote area power supply. *School of Aerospace, Mechanical and manufacturing Engineering.* Melbourne, RMIT University.

PAUL, B. & ANDREWS, J. (2008a) Direct coupling of PV panels with PEM electrolysers in solar-hydrogen systems: experimental performance analysis. *17th world hydrogen energy conference.* Brisbane, Australia.

PAUL, B. & ANDREWS, J. (2008b) optimal coupling of PV arrays to PEM electrolysers in solar-hydrogen systems for remote area power supply. *International Association for Hydrogen Energy,* 33**,** 490-498.

SCHILLER, G., HENNE, R., MOHR, P. & PEINECKE, V. (1998) High performance electrodes for an advanced intermittently operated 10-kW alkaline water electrolyser. *International Journal of hydrogen Energy,* 23**,** 761-765.

SHAKYA, B. D., AYE, L. & MUSGRAVE, P. (2004) Technical feasibility and financial analysis of hybrid wind-photovoltaic system with hydrogen storage for Cooma. *International Journal of Hydrogen Energy*.

SHARMA, H., PRYOR, T. & ISLAM, S. (2001) Effect of pitch control and power conditioning on power quality of variable speed wind turbine generators. *AUPEC 2001.* Perth Australia.

SHERIF, S. A., BARBIR, F. & VEZIROGLU, T. N. (2005) Wind energy and the hydrogen economy-review of the technology. *Solar Energy,* 78**,** 647-660.

SOUTHWEST WINDPOWER (2001) *AIR 403 The New 400 Watt Turbine! Owner's Manual Revision D,* Flagstaff, Arizona, USA.

ULLEBERG, O., NAKKEN, T. & ETE, A. (2008) The Utsira wind/h2 demonstration system in Norway: An evaluation of the operation using updated system modeling tools. *17th World Hydrogen Energy Conference.* Brisbane, Australia.

WASSERSTOFF-ENERGIE-SYSTEM (2007) *h-tec Bedienungsanleitung,* Luebeck Germany.

WEBER, A., DARLING, R., MEYERS, J. & NEWMAN, J. (2003) Mass transfer at two-phase and three-phase interfaces. IN VIELSTICH, W., LAMM, A. & GASTEIGER, A. H. (Eds.) *Handbook of fuel cells.* West Sussex, England, John Wiley & Sons.

WOOD, D. H. & WRIGHT, A. K. (2004) The starting and low wind speed behavior of a small horizontal axis wind turbine. *Journal of Wind Engineering and Industrial Aerodynamics* 1265-1279.

XANTREX TECHNOLOGY INC. (2008) Xantrex Technology Inc. - Residential Wind - XW Hybrid Inverter/charger. Burnaby, Bc, Canada.

YOUNG, D. C., MILL, G. A. & WALL, R. (2007) Feasibility of renewable energy storage using hydrogen in remote communities in Bhutan. *International Association for Hydrogen Energy,* 32**,** 997-1009.